Department of Real Estate, Planning and Geoinformatics

GEONAVPOS: Seminar publications on Geodesy, Navigation and Positioning

Octavian Andrei
Martin Vermeer
(Editors)

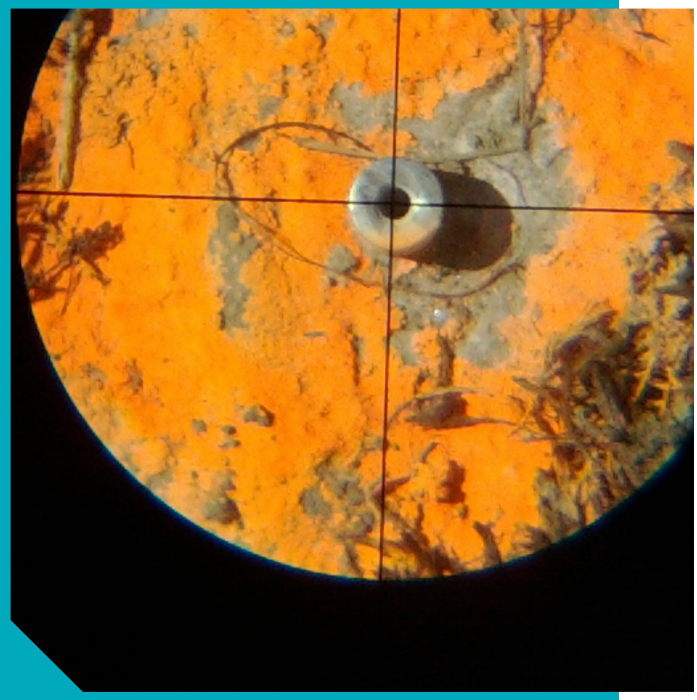

Aalto University

SCIENCE + TECHNOLOGY

COMPILATION

Aalto University publication series
SCIENCE + **TECHNOLOGY** 12/2013

GEONAVPOS: Seminar publications on Geodesy, Navigation and Positioning

Octavian Andrei
Martin Vermeer
(Editors)

Aalto University
School of Engineering
Department of Real Estate, Planning and Geoinformatics
Geoinformatics research group

Aalto University publication series
SCIENCE + **TECHNOLOGY** 12/2013

ISBN 978-952-60-5214-4 (pdf)
ISSN-L 1799-4896
ISSN 1799-4896 (printed)
ISSN 1799-490X (pdf)
http://urn.fi/URN:ISBN:978-952-60-5214-4

Unigrafia Oy
Helsinki 2013

Finland

Preface

In 1880, Friedrich Rober Helmert gave the fundamental definition of geodesy as "*the science of measurement and mapping of the Earth's surface*". As many geodetic observations refer to the Earth's gravity field that also shapes the surface of the Earth, the fundamental definition can be extended by "*including the determination of the Earth's external gravity field*". Based on this extended definition, geodesy focuses on: positioning (geometric geodesy), temporal change (geodynamics), and gravity field (physical geodesy). As a result, the US National Academy of Sciences (1978) named geodesy as part of the geosciences and engineering sciences, including navigation and geomatics.

Nowadays, the advances in Global Navigation Satellite System (GNSS) technology and its impact on geodetic activities may recommend a modern definition of geodesy as "*the science of precise georeferencing and change monitoring on or above the Earth's surface*". Modern geodesy relies on space technology and integrates complex Earth observation systems and modelling of geospatial data at higher accuracy in order to understand and predict how the solid Earth, atmosphere, and oceans work as a system. Modern geodesy applications include precise determination of position and velocity of points on the surface of the Earth, precise determination of the shape and changes of the Earth's ocean and land surfaces, or precise mapping of the spatial and temporal features of the gravity field.

Navigation and geodesy relate both on positioning (location) information. Although a connecting element, positioning also makes the difference between navigation and geodesy. In navigation, the positioning information is required instantaneously or almost instantaneously with a certain latency (real-time). On the other hand, in traditional geodesy the position information is obtained post-mission after post-processing calculations. Usually, these calculations are carried out under the assumption

that the points are fixed or undergo a very slow movement. However, in navigation, the points are variable, therefore time dependent.

At the Department of Real Estate, Planning and Geoinformatics, the above mentioned subjects are covered among the basic courses by the Maa-6.3255 Seminar on Geodesy, Navigation and Positioning offered to both master and doctoral students of Aalto University. The seminar builds on active participation between the theory and practice, using a student-centred approach for teaching. The students can ear 3-6 ECTS credits. One ECTS credit corresponds to 27 hours of work. The workload and the seminar topic is mainly decided by the student based on student's level and field of study. The work can be done individually but working in pairs/groups is possible. The students are responsible for the management and organization of their work. In addition, the seminar work may be organized in collaboration with other research and industrial partners. Staff members are available for consultation and guidance. The seminar course includes written report, oral presentation and opponent activity.

This publication consists of the best 12 student works prepared by the seminar participants (i.e., 24 students) during 2011-2013. Several works cover various topics of modern geodesy, such as space-geodetic techniques (Niko Kareinen), satellite missions (Timo Saari), positioning algorithms (Ville Jussila, Ville Vuokko), sea-level rise (Toni Veikkolainen), and atmospheric and ocean circulation (Esa-Pekka Sundell). In addition, other works cover topics related to navigation, such as navigation technologies (Iiro Kuusisto, Aditya Raju, Henri Turto and Niko Kareinen), or mobile positioning and tracking (Ross Snell, Tuomas Keränen, Tanja Kantola).

Helsinki, May 10, 2013,

Octavian Andrei
PhD, teacher-in-charge

Martin Vermeer
Professor in Geodesy

Contents

Post-glacial rebound: modelling, measurement, significance on society

Toni Veikkolainen

Department of Department of Surveying
Otakaari 1, FIN-02150 Espoo Finland
toni.veikkolainen@aalto.fi

Abstract

Global isostatic adjustment (GIA) means the normalization of the earth's crust after a glacial period. In Finland the land is still rising, fastest in Ostrobothnia and most slowly in the south-east. In the last ice age, the centre of the 3-km thick ice sheet was located in the area of Gulf of Bothnia. In Kvarken region, changes in landscape are easily visible during lifetime. On the northern hemisphere, Canada is another good example of effects of glaciation. The post-glacial rebound has an influence on coordinate values, so it can be monitored with the aid of GPS. Values of gravity also change, and they can be observed both from space and with ground-based systems. Generally, land rises in the area with the strongest ice load, but sinks in the territory that surrounds the former glacier area. However, even the most conservative predictions tell that sea level will rise due to the global warming, and it is important to monitor whether or not it will cancel the effect of GIA.

1 Introduction

According to isostasy, what goes down, must go up, equilibrium as a goal. The principle works very well with the landmasses of our planet. During the last glacial period, large parts of Europe, Russia, Greenland and Americas were laid under the pressure of ice, and sea level was lowered for 120 metres. As continents drowned, mantle material was removed from the region. As the land was released from ice, it began its rise towards its former height. However, due to the viscosity of the mantle, the viscoelastic relaxation phenomenon demands thousands of years to get completed. In Finland we are still in that phase.

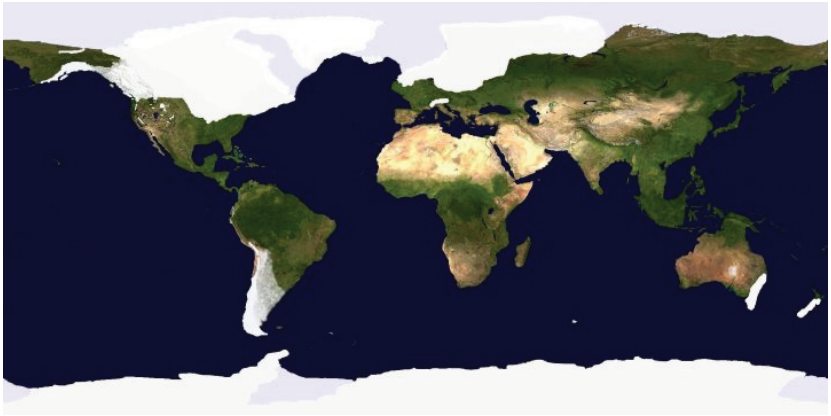

Figure 1. A hypothetical map of Earth during the last glacial maximum, roughly at 16000 BC. Continental ice with white colour, sea ice white [3].

2 Land uplift in Finland

Talking about land uplift is quite simplistic. In reality, the isostatic adjustment involves not only the rising of the landmasses, but also horizontal and even in some areas downward motion, changes in gravity, stress-induced earthquakes and several other effects. Although the Finnish bedrock is very stable, when compared to several other ice-stressed areas, e.g. Iceland, Patagonia, and New Zealand, the three-dimensional character of the phenomenon must be borne in mind. Controlled mainly by the viscosity of the mantle, the effect can be monitored from the changes of Earth's rotation, gravity field, centre of mass and deformation. These refined methods don't have a long history. In the past, merchants just settled for worrying about the seaports becoming landlocked.

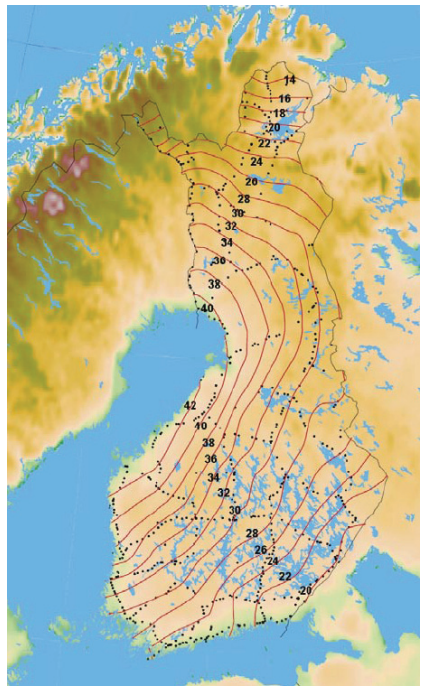

Figure 2. The difference between the Finnish height systems N60 and N2000 [1].

In Finland the most typical example of long-term isostatic uplift can be seen in the valley of the Kokemäenjoki river. In 1365, town of Ulvila was established on the mouth of the river. In 1558, the Duke of Finland ordered that the town must be relocated 7 km to the north, due to the rapidly receding sea. This was the beginning of Pori. It was founded beside a narrow inlet, which was a good natural harbour. But even it was just a temporary location. Presently the harbour of Pori is situated in Mäntyluoto, 20 km north-west of the city centre. Thanks to the high clay mineral content, the land is very fertile and agriculture has a long history there. About 9000 years ago, during the Ancylus lake period of Baltic sea, most parts of western Finland were under a shallow sea. Now these areas have large, flat plains.

Until the rule of Imperial Russia, research of the Finnish land uplift was merely qualitative. There was no precise height system to be maintained. However, things changed due to the activity of the national Road and Water Construction Authority, The first precise levelling took place in years 1892-1910, but it covered only the southern and central parts of the country. After the establishment of Finnish Geodetic Institute, the second one of carried out during 1935-1975. It was nationwide, and the result was a height system N60 with orthometric heights. It took only three years to

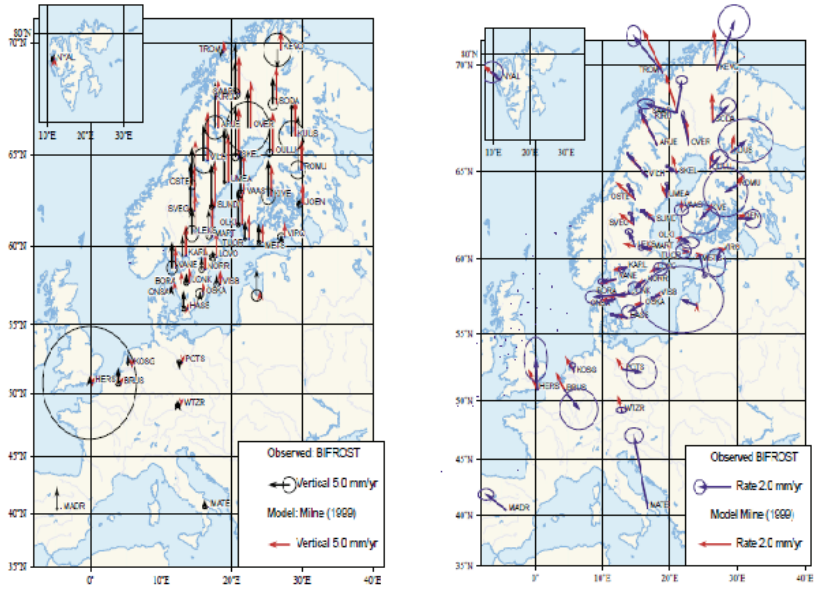

Figure 3. Vertical (left) and horizontal (right) motions as detected by BIFROST stations. Observed values with black arrows and circles of 95 % confidence level (ellipses in the case of horizontal motion, as there are two dimensions). Results by [17] are visible for comparison. The lithosphere was thought of being 71 km thick, and the mantle with a viscosity of 5×10^{20} Pa in above 670 km and 5×10^{21} Pa below that level. Confidence generally grows, as the observation period becomes longer.

start the third levelling, which was finished in 2004.

The third precise levelling was by far the most extensive one. The combined length of the doubly measured lines was even 9158 km, and there were 6092 benchmark values. Ten observers and 800 field assistants were needed during the project. The resulting N2000 model uses normal heights. They were tied to NAP (Normaal Amsterdams Peil), the point zero of the European vertical reference system EVRS2000. National triangulation networks were connected on both sides of the Baltic sea, and each country in the area began using the same geoid model. As normal heights are tied to the quasiqeoid, which is just a computational concept, and orthometric heights to the true geoid, there is a maximum difference of 8 cm between these two heights in Finland. On sea level both heights are the same. Implementing a height system is nevertheless a long and laborious project. It is straightforward to transform numerical data, but old raster maps with height contours can be very tricky. Even some complimentary levellings may be necessary.

Since its establishment in 1978, the Metsähovi research station has been used as a base point in Finnish height determinations, and its most

precise height value in N2000 system was a result of an extensive levelling project carried out by Nordic Geodetic Commission. Differences between Finnish and Swedish systems were only some millimetres after that, but the Swedes had a much denser network. Before levelling campaigns, all knowledge of land uplift was based on tide gauge values, and therefore it was limited to coastal areas. It was not possible to construct uplift maps like that in Figure 2. In fact, tidal forces deform the crust also in Finland, and the effect, about 4 cm in height, is taken into account in both N60 and N2000 systems. It is best visible in north-south direction. Even the Finnish bedrock, which is the oldest and most stable in Europe, is dynamic in a small scale. [20].

Substantial changes in the height of the ground were observed during first and second levellings, and a maps of land uplift was published by [10]. Readjusted results from the same dataset were presented by [25]. Uplift values were determined for roughly one thousand base points, which were common to both levellings. [11] used the first data from the third levelling, from southern Finland only. As the project was close to its end, the new uplift map of the entire country was compiled by [22]. After the introduction of the BIFROST (Baseline Inferences for Fennoscandian Rebound Observations, Sealevel, and Tectonics) project in 1993, satellite data received from stations of Baltic Rim countries has also been utilized. However, nearly all results are from Finland and Sweden, but with some Western European reference values. In Finland, all 13 stations of the permanent FinnRef network take part in BIFROST [24].

Nonetheless, precise levellings have a major weakness. They are a powerful tool in determining differences of land uplift, i.e. they are a relative method. All values must be tied to a fixed point, such as the tide gauge of Hanko with the measured uplift value of 2.63 mm/year [9]. [21] applied this initial value in his model with following parameters:

$y(i,j,k)$	the measured height difference between base points i and j in the levelling
$t(i,j,k)$	time of observation (epoch)
$t0$	epoch for adjustment
$h(i), h(j)$	velocities of land uplift for base points i and j (unknown values)
$h(i,t), h(j,t)$	heights of base points i and j in the adjustment epoch $t0$

(unknown values)

$e(i, j, k)$ observation error

The model was used with heights and land uplift values simultaneously. In the adjustment, a priori accuracies calculated from closure errors were not used. Mean errors were estimated for the area common to all levellings, and values were 2.01 (1st levelling), 0.57 (2nd one) and 0.88 mm$\sqrt{(km)}$ (3rd one). Altogether 1223 observations and 462 base points, all of them on the bedrock, were used. The accuracy of uplift estimates was best in the vicinity of base points, and worst in northern Finland (0.6 mm/year). Prefiltering was made using the open-source GMT program of University of Hawaii [4]. By choosing the base points wisely, local anomalies as well as levelling errors were easy to remove.

In Finnish Geodetic Institute (FGI), GPS time series of different stations are used for calculating velocity vectors, with Metsähovi as a reference. Data is analysed using Bernese software and exact satellite ephemerides published by IGS (International GPS Service for Geodynamics). Orbits are given in ITRF (International Terrestrial Reference Frame) using the epoch of the observation moment. Results of calculations are coordinate differences, with z as the principal component in land uplift studies. [14], found a good correlation with GPS and tide gauge observations. The root mean square misfit between these results was only 0.6 mm/year. When comparisons with results of tide gauges are made, it is reasonable to choose only stations close enough to the sea (e.g. 40 km), so that the uplift between the locations of the tide gauge and the GPS station can be properly modelled. It is mandatory to combine GPS results with results from other studies, since satellite measurements tell nothing about the direction where water flows, as they give only ellipsoidal heights, not orthometric or even normal ones. In Hamina, the mean sea level is a few meters closer to the Earth's centre than in Helsinki [20].

In general, levellings give the land uplift differences with respect to geoid, which isn't actually the same as the local mean sea level obtained from the tide gauge. Lengths of the levelling rods must be known precisely, and in FGI it is done by using a vertical comparator. The scale of rods used in the third precise levelling of Finland was determined three times a year. Presently there is no way to replace tide gauges and levellings in measurements of absolute heights from sea level. In the new geoid model FIN2005, the mean water level of Helsinki harbour is no

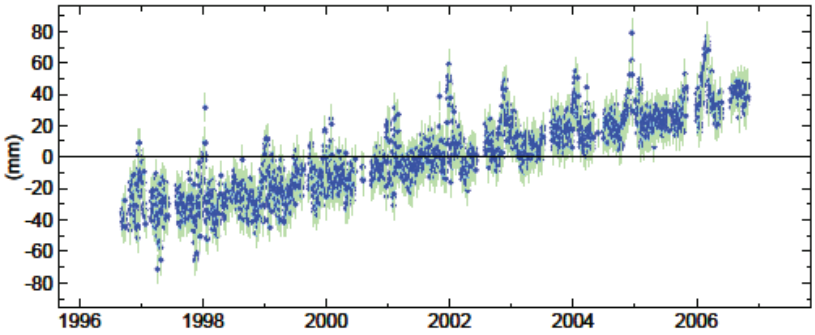

Figure 4. A continuous time series of the vertical movement of Kivetty GPS station, central Finland. The accumulation of snow on the antenna during winter months causes prominent errors, but the linear trend is still very distinct. The change in horizontal coordinates was also monitored, but it was much smaller and the influence of isostatic adjustment cannot be easily extracted from it.

longer used as a reference, but it has been replaced by NLP. Geoid calculations are determined by geopotential numbers (unit m^2/s^2), which are a true physical quantity.

3 A Canadian perspective

With a land area as large as the whole of Europe, Canada was entirely under the influence of continental ice. [8] chose the Northern Cascadia Subduction Zone for research. Apart from the tectonically quiet Fennoscandian and Canadian shields, this area is subject to several plate movements. Changes in sea level tell that the part of the ice sheet that was over the ocean, collapsed in a short time over 12000 years ago. The viscosity of the underlying mantle is about $5 \times 10^{18} Pa \cdot s$ to $5 \times 10^{19} Pa \cdot s$, which is less than viscosities on seismically quiet areas. In the study, a grid model was used, with values of ice thickness for every square of the grid 14000 years ago. Shoreline elevations with respect to distance from the ice outlet were collected, and linear regression models were constructed for Lake Bretz and Lake Russell-Hood close to Seattle. Small uplift velocities mean that monitoring and modelling is not easy.

The crustal displacement caused by the Cordilleran ice sheet was modelled by using a circular disc, with the thickness and duration similar to the average values in the southwestern part of the mountainous area. The vertical displacement grows as a function of distance from the centre of the ice sheet, but not linearly. In case of thick sheets, the curve is very flat-bottomed. In the first test, the mantle viscosity was fixed at $10^{18} Pa \cdot s$,

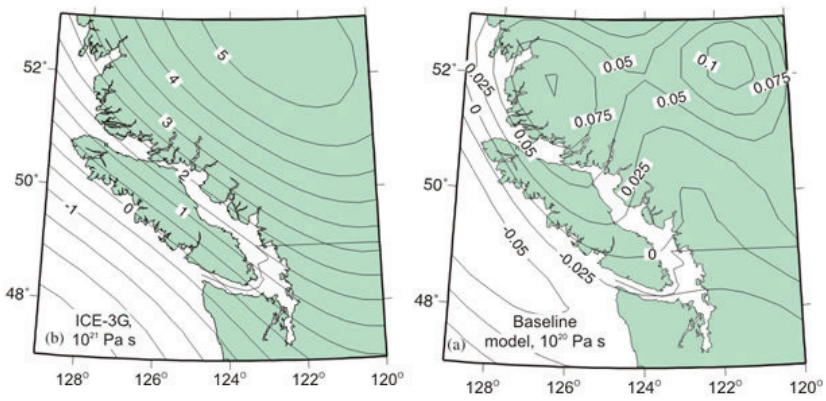

Figure 5. A land uplift map according to the old ICE-3G model [26] and the new model [8] for Vancouver Island and surroundings. Uplift values are in millimetres. In tectonic sense, Juan de Fuca plate is overlain by North America Plate, and Vancouver Island has been torn away from the mainland. The rugged coastline is to some extent similar to that of Norway.

but the crustal thickness was adjusted. In another approach, the crust was 35 km deep, but the viscosity was varied. Change in the relative sea level during the ablation of the ice was as much as 250 meters. As no continuous GPS surveys have been made in the area, the land uplift values shown in 5 are just predictions based on the models.

4 Space geodetic techniques

The interest in global isostatic adjustment (GIA) has grown a lot during the last few years, thanks to the results of the GRACE (Gravity Recovery and Climate Experiment) satellite launched in 2002. In addition, as a result of the POLENET programme of International Polar Year 2007-2009, dozens of GPS measurement stations were set up on Arctic regions, and new networks are planned. In years 2008-2012, the European Cooperation in the field of Scientific and Technical Research (COST) programme produces new models for land uplift, based on GPS, very long baseline interferometry (VLBI), satellite laser ranging (SLR) and Doppler Orbitography and Radiopositioning Integrated by Satellite (DORIS). Results for Antarctica can be seen in Figure 6, and results for Greenland and eastern Canada in Figure 7. [12]

While GIA changes gravity globally and locally, the distribution of ocean water doesn't remain the same, but large changes in ocean flows are likely. The tidal and other deformations of solid Earth, the pressure caused by

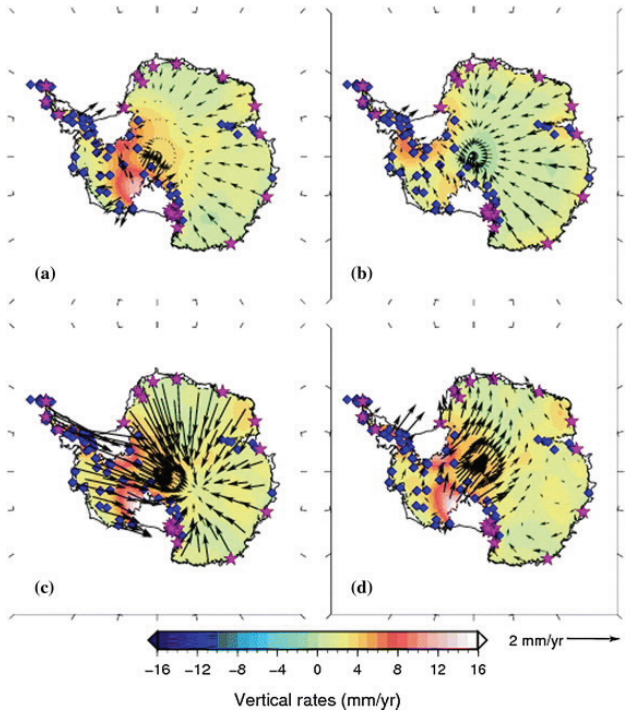

Figure 6. The post-glacial rebound in Antarctica. Parts a and b are based on the same laterally homogeneous model of the crust, but with a different glaciation history (a: ICE-5G, b: IJ05). In parts c and d, ice models are as in a and b, but the heterogeneous composition of the crust has been taken into account. Purple stars indicate locations with continuous GPS measurement sessions, lasting for over 1000 days. Diamond symbols are for shorter campaigns.

ice, and also the relocation of seawater must be included in models, so geodesists need to co-operate with seismologists and marine researchers. The sea level equation was published by [6] and updated by [17]. In case of solid earth and sea floor alike, different rocks react very differently in stress changes, and thus a three-dimensional approach and a rheological model is necessary. As the observational evidence of limits and thickness of ice in different times of the last ice age is often very limited, one-dimensional flat-earth models have been used widely. Moreover, the mass of ice in Antarctica and Greenland has been overestimated in several studies [5, 23].

The ICE5G model by [19] describes the rise of Antarctica. The vertical deformation has been concentrated in the western part of the continent, mainly in the proximity of Siple coast as well as marine ice sheets of Ronne and Filchner. However, horizontal changes are typical of inland areas. The IJ05 model by [7], gave entirely different results. The largest vertical changes are visible near the Antarctic peninsula and on the coast

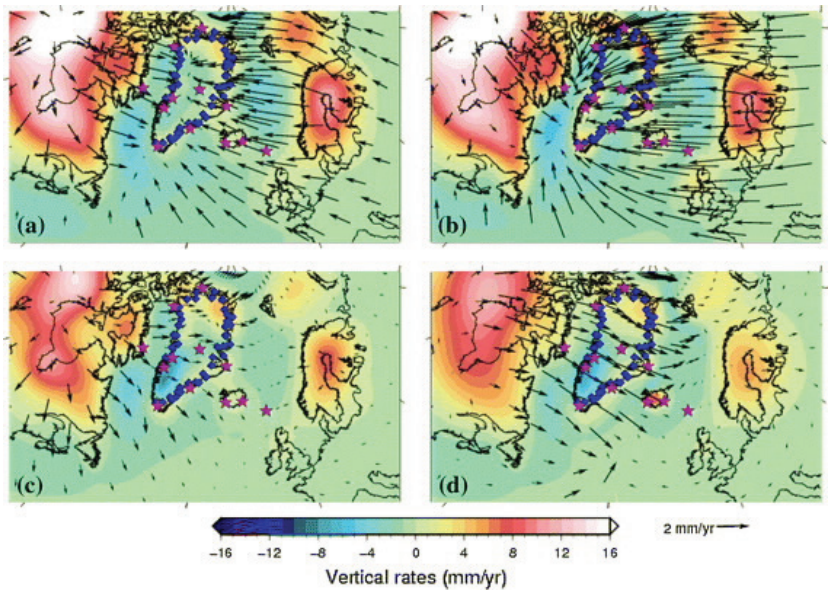

Figure 7. Land uplift in Greenland, central-northern Europe and eastern Canada. Maps a and b were presented by [27], with the crustal model RF3S20. Solutions in c and d are as calculated by [13], using the VM2 model with a simplified approach on viscosity. In b and d, the crust was regarded as laterally heterogeneous, but in a and c not. Stars and diamonds as in Figure 6.

of the opposite side of the continent. However, Antarctica is not laterally homogeneous, but its eastern parts form a Precambrian craton, whereas in the west the crust is thinner and the heat flux much stronger. The convergence of motion vectors towards an area in the middle is stronger in models with a heterogeneous lithosphere. This may be an artefact, since there are large inland areas in middle and eastern Antarctica without any surveys.

Same models were applied to the northern hemisphere, too, and results deviate especially on Canadian and Baltic shields. The theory holds true in the sense that uplift is greatest on areas, where the ice compressed the soil and bedrock most. The horizontal motions in Fennoscandia are best visible in the model with lateral heterogeneities, and the signal is so prominent that it even causes a bias in the results of Greenland. However, results are much more unsure as the number and duration of measurement campaigns has been much worse than that in Antarctica. The uplift of the Hudson Bay area is notable, with vertical velocities as large as 15 mm per year. Nowhere in Europe are rates like this.

In studies of post-glacial rebound, and deformation of crust in general, GPS has become the most-used technique due to its price and mobility.

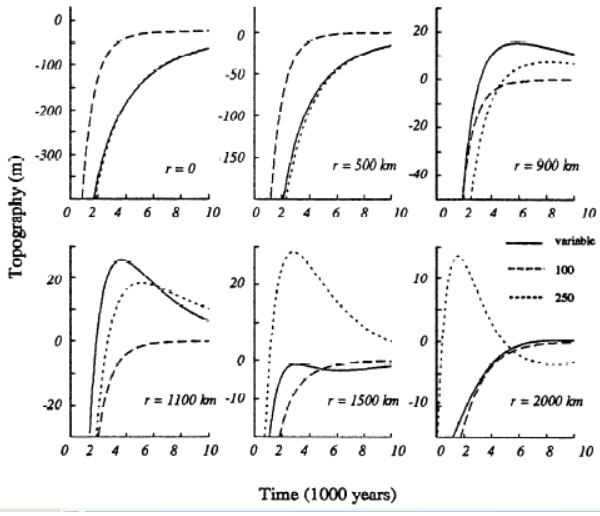

Figure 8. Rebound in several distances measured from the centre of glaciation. Curves are for different thicknesses of the crust (variable, 100 km, 250 km). The tectosphere was fixed at the width of 1000 km. It is the seismically fast region of the lithosphere [16].

For a long time, solar-energy-driven GPS devices were impossible to use on arctic and subarctic areas, but the problem has yet been solved. In Greenland, campaigns have been performed since the mid-1990s, originally only in a few stations as a co-operation project between Denmark and the USA. In Kellyville, which is located on the western edge of the ice, the first results told that the land rises even 5.8 mm per year. In later studies, the velocity was just 1.2 mm per year. Also in Antarctica, numbers have sometimes been unexpected: predicted values have been 2.5 mm per year, measured values only 0.3 mm/year for the same area. Absolute gravity measurements were in favour of the predictions, while GPS values didn't support them. This is not uncommon: in various cases GPS, VLBI and DORIS have given very different outcomes. They cannot be integrated without a precise knowledge about phases of glaciation and deglaciation on different parts of the continent.

It is not easy to extract the uplift caused by the isostatic adjustment from the GPS data, because the signal is sensitive to tropospheric, ionospheric and other delays. In addition, the short-term movement of a temporary or permanent GPS station is controlled by a great deal of factors. In addition to the isostatic adjustment, there are periodic effects, such as tides and difficult-to-predict non-periodic phenomena, such as tectonic deformation. Luckily the areas whose uplift is most extensively studied are

seismically quiet, with the exception of Iceland. The choice of the reference frame has a remarkable influence on the coordinates of the station, and the centre of the mass of Earth has to be known accurately. For this purpose, SLR is almost mandatory [12].

When the isostatic rebound is modelled, both the mantle and the lithosphere can be considered as Newtonian fluids, with their shear rate linearly related to their shear stress. In their theory, [16], tested the idea that the depression in the beginning of the load follows a normal distribution curve. The mantle was considered an infinite half-space, i.e. a box model was applied. With a Maxwell time exceeding 100 years, long wavelength effects were primarily caused by viscous flow. The idea of continental roots is just an application of Bouguer's hypothesis, that under mountainous areas, crust is thicker so that each vertical column of lithosphere has a similar total mass. In the model the continental root was assumed to depress into the mantle by 1 km, slightly more than in Finland, but typical of several ice-affected Canadian areas. In the axisymmetric model the root itself is 2000 km in width, but three different depths were tested: constant 250 km, 100 km and a depth varying in between.

Manga and O'Connell concluded that the relaxation of the lithosphere is strongly dependent on the radial distance measured from the centre of the continental root. The tested radial positions were r = 0 km, 500 km, 900 km, 1100 km, 1500 km and 2000 km, and results are visible in Figure 6. According to them, land will rise very rapidly on boundaries of the glaciated area in the case of a thick lithosphere, but the maximum is reached within a few thousand years, and after that the height will drop. This is just about the readjustment of the mass balance, and the effect can be seen in areas surrounding the Baltic ice sheet. Nonetheless, near the centre of the ice sheet, land goes up and remains there, just as it is happening in the Gulf of Bothnia area. Relaxation is smoother when the distance is small and the crust is thin. For generation of models of mantle, knowledge about GIA processes is essential. For instance, a power-law model has been applied using the coupled Laplace finite-element method and observations of relative sea-levels (RSLs), land uplift rate from GPS and gravity-rate-of-change from GRACE satellite. Traditionally, seismologists have studied the internal structure of the Earth, but they need the knowledge of geodesists, too [28].

5 Case Perämeri and crustal motion

In Finland, the middle and northern parts of Gulf of Bothnia is the most remarkable natural laboratory of post-glacial rebound. Islands in the Finnish Kvarken area are mostly moraine, and their topography is very different from that of the High Coast (Höga Kusten) area in Sweden. That area is located on the opposite side of the sea and it holds the world record of isostatic compensation. It has risen 286 meters in ten thousand years. Nowadays the Bothnian Bay is not more than 147 meters at its deepest point, and the Kvarken area is only 25 meters deep. Most islands, e.g. Raippaluoto, Mikkelinsaaret, Björköby and Bergö, are very young. Despite that fact that there are no steep cliffs in the Finnish coast, the topography is very diverse in small scale. Islands join in the mainland and small inlets transform into lakes, which may become swamps. Drumlins, flutings, De Geer moraines and several other landforms are born.

The Perämeri area was the centre of the continental ice sheet. The ice was even 3 km deep, and it depressed the crust even by 0.8 km. The Baltic Sea was even 300 m deep when the ice began melting, 240 m more than presently. In the beginning the uplift rate was several meters per year. The northern part of Perämeri lies on Archean bedrock, with an age of 3.1-2.5 billion years, but other parts are post- or mid-Proterozoic. Sandstones, conglomerates and clay stones are results of erosion, and they have accumulated in the upper parts of the basin due to gravity. Deeper layers of bedrock are dominated by igneous and metamorphic rocks with a higher density. Because Kvarken is geologically unique, it was accepted to the UNESCO World Heritage List in 2006. It will have a dry future: after 2000-2500 years, Finland will be connected to Sweden, and Perämeri will become the largest lake in Europe [2].

Tide gauge readings are a reliable way to determine land uplift on the coastline. All Finnish tide gauges (Kemi, Oulu, Raahe, Pietarsaari, Vaasa, Kaskinen, Mäntyluoto, Rauma, Turku, Föglö, Helsinki, Hamina) have time series longer than 75 years. In each location, the mean change of the water level has been positive, with highest values in Pietarsaari (8.2 mm/year), Vaasa (8.0 mm/year) and Raahe (7.8 mm/year). In the past, measurements were registered on paper rolls and collected manually, but nowadays they are saved digitally and they can be even delivered in no time. It will be interesting to observe whether or the climatic change will partly compensate the effect of land uplift, or not. The effect of rising

sea level will be visible globally, even in the Baltic Sea, where tides and concomitant erosion are almost non-existent. With the shoreline withdrawing, plant population dynamics will be affected, most strongly near the edge of the water.

Even though the land rises very rapidly on the coast of Ostrobothnia, mean sea level has gone up in south-western Finland. Records of Hanko tide gauge show that the sea level didn't descend any more between years 1990 and 2006. The average temperature of the seawater had risen, and its volume was increased, too. This is why nautical charts need to be updated regularly. In general, effects of land uplift and rise of seawater aren't easily separated in results of tide gauges. Because only vertical values are concerned, these coastal measuring devices cannot provide comprehensive information about the isostatic adjustment, but continuous GPS time series are for that purpose. Actually there is noticeable horizontal motion, too, even 3 mm/year in Finnish territory as seen in the crustal velocity map generated from NKG_RF03VEL model, seen in Figure 9 [18].

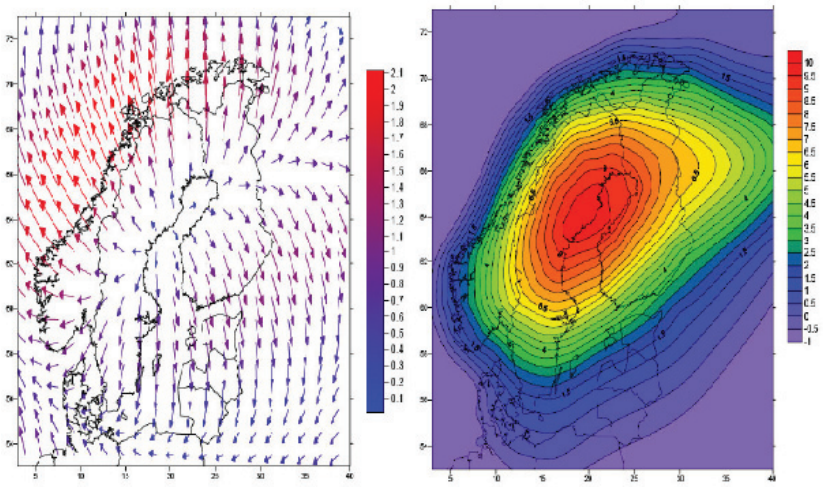

Figure 9. Horizontal deformation of the lithosphere in Northern Europe (left), and corresponding land uplift rates per year (right). In Finland, Ostrobothnia is the area with highest vertical change. Due to the post-glacial adjustment, southern and central Finland are moving to the south-east and large parts of Lapland to the north. The vertical shift is many times stronger [18].

Modelling of the Fennoscandian isostatic rebound has been made to enable the regional implementation of European Terrestrial Reference System (ETRS89) and its realizations. When coordinates are transformed between different ETRS datums, GIA cannot be neglected. The uplift phenomenon is connected to the tectonic deformation of the crust. [15]

published a 3D velocity model based on 13-year time series from 80 permanent GPS stations of BIFROST network. For the velocity solution, data from stations in other parts of Europe, even other continents, was used. However, seasonal variations were strong, and their effect was modelled with annual and semiannual sine and cosine functions. The absolute land uplift (with respect to the centre of the planet) v_{abs} was calculated as $v_{abs} = 1.06(v_{app} + 1.32mm/year)$, where v_{app} is the apparent land uplift from the model. The factor 1.06 accounts for the geoid rise and 1.32 is for the sea level rise. Calculations were in good agreement with velocities of individual stations, the accuracy being 0.5 mm/year. This study was a strong proof for the previous results that the Umeå region in Sweden peaks in uplift rates, but Finnish Ostrobothnia isn't far behind.

6 Conclusions

Theories of glacial isostatic adjustment cannot work with a proper height system, and it is a good question, what kind of a height system we Finns will have in 2050. A new precise levelling would be a project lasting for decades, and presently there are no plans to do that. As our coordinate system, EUREF-FIN can be used for a long time, because it has a sufficient accuracy and it works well with both GPS and Galileo satellite data. However, height systems become obsolete, and land uplift is the primary, though not the only thing to blame. Global warming will also affect sea level, and it is even possible that large masses of water are transported from one side of our planet to another. Even Baltic Sea will not be unaffected when parts of continental ice melt. In near future, geodesists will have a lot of work with generating new geoid models, as the rising seawater may partly compensate the uplift. Rivers and entire drainage systems have changed their flowing directions in a geologically short time, and the floods typical of Ostrobothnia can appear in other parts of Finland. Nobody knows, only future will tell the truth.

Bibliography

[1] ***. Finnish Geodetic Institute, Annual Report 2006. http://www.fgi.fi/vuosikertomus/vk2006.pdf. Accessed March 22, 2011.

[2] ***. Kvarken World Heritage Site. http://www.kvarken.fi. Accessed March 22, 2011.

[3] ***. Space Art - Planetary maps. http://www.johnstonsarchive.net/spaceart/cylmaps.html. Accessed March 22, 2011.

[4] ***. The Generic Mapping Tools. http://www.soest.hawaii.edu/gmt/. Accessed March 22, 2011.

[5] Chen, J. L., Wilson, C. R., Blankenship, D. D., and Tapley, B. D. (2006). Antarctic mass rates from grace. *Geophysical Research Letters*, 33(11).

[6] Farrell, W. E. and Clark, J. A. (1976). On postglacial sea level. *Geophysical Journal of the Royal Astronomical Society*, 46(3):647–667.

[7] Ivins, E. R. and James, T. S. (2005). Antarctic glacial isostatic adjustment: a new assessment. *Antarctic Science*, 17:541–553.

[8] James, T. S., Clague, J. J., Wang, K., and Hutchinson, I. (2000). Postglacial rebound at the northern Cascadia subduction zone. *Quaternary Science Reviews*, 19(14–15):1527 – 1541.

[9] Johansson, M. M., Kahma, K. K., Boman, H., and Launiainen, J. (2004). Scenarios for sea level on the finnish coast. *Boreal Environment Research*, 9(2):153–166.

[10] Kääriänen, E. (1953). On the recent uplift of the Earth's crust in Finland. Technical Report 42, Finnish Geodetic Institute. 106 pages.

[11] Kakkuri, J. and Vermeer, M. (1985). The study of land uplift using the Third Precise Levelling of Finland. Technical Report 85:1, Finnish Geodetic Institute. 11 pages.

[12] King, M., Altamimi, Z., Boehm, J., Bos, M., Dach, R., Elosegui, P., Fund, F., Hernández-Pajares, M., Lavallee, D., Mendes Cerveira, P., Penna, N., Riva, R., Steigenberger, P., Dam, T., Vittuari, L., Williams, S., and Willis, P. (2010). Improved constraints on models of glacial isostatic adjustment: A review of the contribution of ground-based geodetic observations. *Surveys in Geophysics*, 31(5):465–507.

[13] Klemann, V., Martinec, Z., and Ivins, E. R. (2008). Glacial isostasy and plate motion. *Journal of Geodynamics*, 46(3–5):95 – 103.

[14] Koivula, H. (2003). Maankohoamisen tutkimusta satelliittipaikannuksen avulla. In *XXII Geophysics Days*, Oulu, Finland.

[15] Lidberg, M. (2008). Geodetic Reference Frames in Presence of Crustal Deformations. In *FIG Working Week 2008*, Stockholm, Sweden.

[16] Manga, M. and O'Connell, R. J. (1995). The tectosphere and postglacial rebound. *Geophysical Research Letters*, 22(15):1949–1952.

[17] Milne, G. A., Mitrovica, J. X., and Davis, J. L. (1999). Near-field hydroisostasy: the implementation of a revised sea-level equation. *Geophysical Journal International*, 139(2):464–482.

[18] Nørbech, T., Ensager, K., Jivall, J., Knudsen, P., Koivula, H., Lidberg, M., Ollikainen, M., and Weber, M. (2006). Transformation from a Common Nordic Reference Frame to ETRF89 in Denmark, Finland, Norway, and Sweden. In *Proceedings of the NKG General assembly*, Copenhagen, Denmark.

[19] Peltier, W. (2004). Global Glacial Isostasy and the Surface of the Ice-Age Earth: The ICE-5G (VM2) Model and GRACE. *Annual Review of Earth and Planetary Science*, 32:111 – 149.

[20] Poutanen, M. (2006). Suomen uusi korkeusjärjestelmä N2000. *Maankäyttö*, 4:9–12.

[21] Saaranen, V. (2005). Tarkkavaaituksilla määritetty vuosittainen maannousu Suomen alueella. In *XXII Geophysics Days*, Helsinki, Finland.

[22] Saaranen, V. and Mäkinen, J. (2002). Determination of land uplift from the three precise levellings in Finland, status in 2002. In *Proceedings of the XIV General Meeting of the Nordic Geodetic Commission*, Espoo, Finland.

[23] Sasgen, I., Martinec, Z., and Fleming, K. (2007). Regional ice-mass changes and glacial-isostatic adjustment in antarctica from {GRACE}. *Earth and Planetary Science Letters*, 264(3–4):391 – 401.

[24] Scherneck, H.-G., Johansson, J. M., Vermeer, M., Davis, J. L., Milne, G. A., and Mitrovica, J. X. (2001). Bifrost project : 3-d crustal deformation rates derived from gps confirm postglacial rebound in fennoscandia. *Earth, Planets and Space*, 53(7):703–708.

[25] Suutarinen, O. (1983). Recomputation of land uplift values in Finland. Technical Report 83:1, Finnish Geodetic Institute. 16 pages.

[26] Tushingham, A. M. and Peltier, W. R. (1991). Ice-3G: A new global model of Late Pleistocene deglaciation based upon geophysical predictions of post-glacial relative sea level change. *Journal of Geophysical Research: Solid Earth*, 96(B3):4497–4523.

[27] Wang, H., Wu, P., and van der Wal, W. (2008). Using postglacial sea level, crustal velocities and gravity-rate-of-change to constrain the influence of thermal effects on mantle lateral heterogeneities. *Journal of Geodynamics*, 46(3–5):104 – 117.

[28] Wu, P. and Wang, H. (2008). Postglacial isostatic adjustment in a self-gravitating spherical earth with power-law rheology. *Journal of Geodynamics*, 46(3–5):118 – 130.

The Current State of GPS Meteorology and Climatology

Esa-Pekka Sundell

Department of Surveying
Otakaari 1, FIN-02150 Espoo Finland
esa-pekka.sundell@aalto.fi

Abstract

GPS meteorology and climatology utilise the observation power of the GPS technology and its solid satellite constellation to acquire accurate data of the Earth's atmosphere for the purposes of weather prediction and study of climatic processes. Currently, there are two main technique branches in GPS meteorology and climatology applications, dealing with ground-based GPS measurements and radio occultation with GPS.

Ground-based GPS measurements provide a means of estimating the total integrated water vapour in the vertical column above a receiver on the Earth's surface. From the continuous measurements of GPS arrays, the state of the atmosphere can be observed. Radio occultation is a satellite-to-satellite sounding technique based on measuring how the ray paths of GPS radio signals are bent by atmospheric refractive index gradients. The variation of bending angle with height can be inverted to yield a refractive index profile and subsequently a temperature, pressure or water vapour profile.

These techniques been actively developed for the past two decades, and they have grown more sophisticated as GPS technology has become more accurate and wide-spread. Using GPS measurement data in operational weather prediction and implementing it into meteorological and climatological models have produced very promising results.

1 Introduction

Water vapour plays a major role in atmospheric processes from global climate to micrometeorology, and the distribution of water vapour is closely coupled with the distribution of clouds and rainfall. Because of the unusually large heat amount associated to it's change of phase, water vapour plays a critical role in the vertical stability of the atmosphere and the structure and evolution of atmospheric storm systems. Also, the horizontal movement of water vapour and its latent heat has a significant effect on the Earth's energy balance. Water vapour also constitutes to the greenhouse effect more than any other gas in the atmosphere. Still, the specific role of water vapour in precipitation, energy transfer, or radiation budget remains poorly described. This is mostly because the distribution of water vapour in the atmosphere is very difficult to quantify due to its high variability in time and space. Atmospheric scientists have thus developed many different means to measure the distribution of water vapour.

The cornerstone of atmospheric studies and operational weather analysis and prediction has been the radiosonde, a balloon-borne instrument package that sends information of temperature, humidity, and pressure to ground stations by radio signal. A radiosonde provide continuous *in situ* measurements during its ascend with good vertical resolution. But the serious disadvantage in radiosonde measurements is that radiosondes are expendable, and the cost of these instruments restricts the number of launches typically to one to four launches daily at a limited number of stations. Because of the restricted horizontal and temporal resolution, radiosonde measurements are not able to properly resolve the spatial and temporal variability of temperature or winds and water vapour in the atmosphere. In fact, the uncertainty in the analysis of water vapour is the major source of error in short-term (0-24 hours) precipitation forecasts.

Ground-based, upward looking water vapour radiometers (WVRs) are instruments that measure the background microwave radiation produced by atmospheric water vapour. They measure the sky brightness temperature at specific frequencies from which they can estimate the integrated water vapour (IWV) content and integrated liquid water (ILW) along its line of sight. The WVRs must always be calibrated to local conditions using independent meteorological data (usually radiosonde data). While upward-looking WVRs measure water vapour emission lines against the cold background of space, space-based downward-looking WVRs measure

the corresponding absorption lines in the radiation from the hot background of the Earth. The recovery of IWV by space-based WVRs is greatly complicated over land because the background temperature is quite variable and difficult to determine. Difficulties also emerge in the presence of clouds, because the background temperature can quickly drop from 290 K (Earth's surface) to 220 K (cloud top). These changes are large and important but difficult to determine. Thus, satellite-based WVRs tend to be more useful over ocean than over land, and their utility is degraded in the presence of clouds. Ground-based WVRs are not affected by light or moderate cloud cover, but they generally do not work very well in the presence of heavy cloud. Also, few WVR instruments are able to provide useful data when it is raining. Ground and space-based WVRs are complementary systems, ground-based instruments provide good temporal but poor spatial coverage, whereas space-based instruments have the opposite characteristics. [3]

GPS has provided a new means of measuring water vapour in the atmosphere. GPS is a global satellite system conventionally used for navigation, time transfer and relative positioning. The potential GPS measurements have in meteorological and climatological applications is based on the fact that the propagation of the GPS L-band (1.2 and 1.6 GHz) microwave signals is greatly influenced by the constituents of the atmosphere. GPS geodesists and atmospheric scientists have devised many procedures for estimating how much atmosphere in general, and water vapour in particular, are slowing the propagation speed of GPS signals. From the total delay induced to the GPS measurements it is possible to determine the "zenith wet delay" caused only by water vapour in the atmosphere overlying the receiver, in contrast to "zenith hydrostatic delay" or "zenith dry delay" caused by the entire gas content in the overlying atmosphere. The wet delay is nearly proportional to the amount of precipitable water above the GPS receiver, and from continuous measurements on multiple locations the spatial and temporal variations can be observed. (The quantity of atmospheric water vapour overlying a given point is usually stated as the vertically integrated mass of water vapour per unit area (e.g. in kilograms per square meter) or as the height of equivalent column of liquid water (precipitable water).)

GPS measurements have been applied in meteorology and climatology applications for more than a decade, and they have proved their capability to measure the zenith integrated water vapour (IWV) with the same ac-

curacy as other methods, like radiosondes and WVRs. The GPS has been of great interest in meteorology and in climatology because of the high spatial density of observing GPS stations and its continuous observations of the state of the water vapour in the atmosphere. Compared to WVRs, GPS operates in all weather conditions without need of complicated calibration. With tomographic analysis techniques it is possible to process multiple GPS integrated water vapour measurements into three dimensional (plus the time-varying fourth dimension) water distribution models of the atmosphere. The assimilation of GPS measurements in numerical weather prediction models has been a much investigated topic and the GPS measurements have proven to improve the analysis of water vapour in the atmosphere and the precipitation forecasts. [5]

In this work, I present the most prominent techniques presently used in GPS meteorology and climatology. Tropospheric water vapour and its variations can be derived from GPS ground measurements effectively by utilising the continuous measurements of the dense GPS station networks around the world (section 2). In GPS radio occultation technique the properties of the the atmosphere are calculated from satellite-to-satellite measurements between the GPS constellation and special low Earth orbiter (LEO) satellites (Section 3). In the following sections I will describe the main points of these techniques. Particular attention is paid on how the techniques have evolved to their current state and the future prospects of GPS meteorology and climatology.

2 Tropospheric water vapour from GPS ground station measurements

2.1 Atmospheric propagation delays as meteorological signals

In GPS geodesy, distances between the satellites and the receivers are determined by measuring the time of flight of the time-tagged radio signals that propagate from satellites to receivers (pseudo-ranging) or by finding the associated path lengths with interferometric techniques (phase measurement). Both of these techniques are complicated by the Earth's atmosphere, since the atmosphere increases the optical path length between the satellite and receiver and induces delays to the time of flight of the GPS signal. On of the main tasks of geodetic GPS signal processing is to

get rid of these delays, reducing all optical path lengths to straight-line path lengths.

Both the ionosphere and the troposphere induce propagation delays to the signal. Propagation delays induced by the ionosphere depend on the frequency of the signal, and these delays can be determined and removed from the signal by detecting both GPS frequencies (L1 and L2). Propagation delays induced to the signal by the troposphere cannot be determined this way because troposphere is neutral and effectively non-dispersive. Troposphere is a mixture of dry gases and water vapour. Water vapour is a unique constituent in this mix in that it possesses a dipole moment contribution to its refractivity and, in fact, most of the refractivity water vapour causes is because of its dipole behaviour. This is why we treat the dipole component of the water vapour refractivity separately from the non-dipole components of water vapour and the other gases in the troposphere. The dipole component is called “wet delay” and the non-dipole component is called “hydrostatic delay” (sometimes erroneously referred to as “dry delay”). Hydrostatic delay is caused by hydrostatic refractivity effects of all the gases in the troposphere together. Both the tropospheric delays are smallest in the zenith, and larger with smaller elevation angles, getting to roughly 4 times the zenith delay at 15°elevation angle. The delays are usually mapped to the zenith with special mapping functions. [3, 1]

The zenith hydrostatic delay (ZHD) has a magnitude (equivalent GPS phase delay length) of about 2300 mm at sea level. It is possible to predict the ZHD to better than 1 mm given surface pressure measurements accurate to 0.3 hPa (millibar) or better. The zenith wet delay (ZWD) is smaller, but much more variable in space and time. It can vary from a few millimetres in desert conditions to more than 350 mm in very humid conditions. Once the ZHD parameters have been estimated from the measured GPS neutral delay, it is possible to estimate ZWD by subtracting ZHD from the ZND, where the ZHD is derived from the surface pressure readings. ZWD can then be transformed into an estimate of precipitable water vapour (PWV) by using either a numerical weather model or a statistical/analytical model of the vertical temperature distribution at the receiver site. [9]

In meteorological and climatological applications it is these delays we are concerned about. The wet delay and the PWV quantities are particularly important, because they contains information about the water

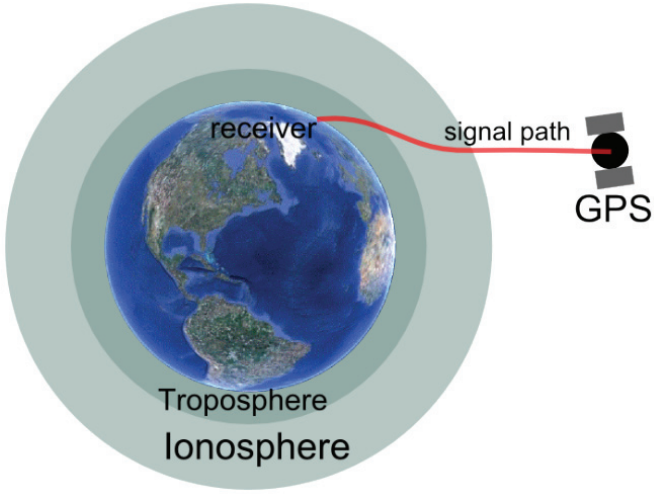

Figure 1. GPS signal propagation through the atmosphere. Refraction in the atmosphere results in bending and delays in the signal.

vapour in the overlying atmosphere. When we determine the delays from a GPS station network with each station tracking multiple GPS satellites, we can reconstruct a 3D water vapour distribution in the atmosphere. This is done by integrating these values with tomographic techniques.

2.2 About GPS water vapour tomography

GPS water vapour tomography is quite a new technique in which water vapour distributions in the atmosphere are derived from continuous GPS ground measurements. Numerical weather prediction models require precise 3D information of the water vapour distribution with a high temporal resolution to provide reliable predictions. In regions with a high density GPS network GPS tomography be an effective source for collecting data for them. The technique consists of the retrieval of a 3D scalar field of the water vapour from integrated measurements.

Tomographic techniques have been intensively used in recent decades in medicine to investigate the human body of in seismology to describe the seismic velocity anomaly of the Earth's interior. In these fields tomographic inversion is well constrained by a sufficient amount of data which can be accumulated because the structures do not change in time. The tomography of tospospheric water vapour, however, is not as well constrained because the limited number of simultaneously visible GPS satellites and because of the great temporal variability of the water vapour. The first tropospheric tomography studies have been performed by [7].

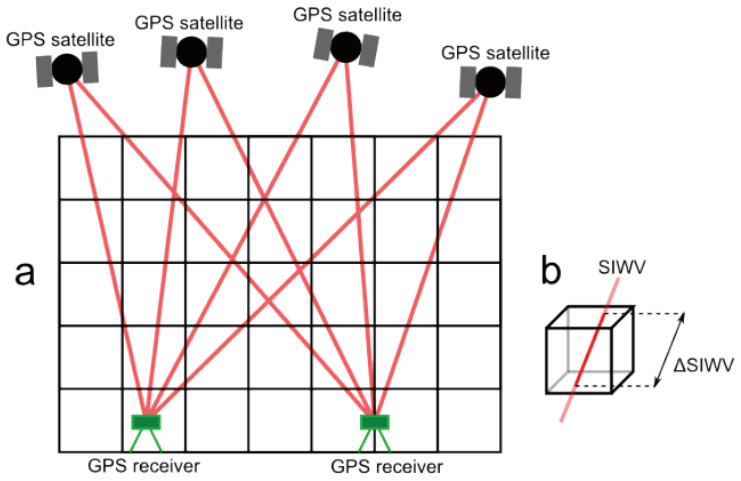

Figure 2. (a) A 2D view of the voxel discretization of the space (atmosphere) and the assumed rays between GPS satellites and ground receivers. (b) ΔSIWV is the path-length of one ray in one voxel.

Further validation of the technique with a dense GPS network has been conducted during the ESCOMPTE field experiment in Marseille in June and July 2001 [5]. GPS tomography has also been proved to work well with data from other densely arranged GPS networks, such as data from many national GPS ground station networks [10, 1]. From these kind of GPS ground measurements, long-term time-series of the total amount of water vapour with high spatial and temporal resolution can be provided at relatively low cost. Moreover, the high vertical resolution of water vapour distribution allows for numerous additional insights into global and regional airflow and chemical processes in the atmosphere.

2.3 From observed GPS delays to water vapour distribution

In GPS tomographic processing, the zenith delays between all the visible GPS satellites and all the ground receivers are observed continuously for certain time intervals. The zenith delays are mapped to the zenith to form the slant delays observed between the GPS satellites and receivers. The gradients in the hydrostatic component can be determined and removed from surface measurements, and the remaining ZWD is then used to construct the slant integrated water vapour (SIWV) values, which are the initial observation values in the tomographic processing. [5]

To effectively determine the distribution of the water vapour and its variation in the atmosphere, the space occupied by the observed atmo-

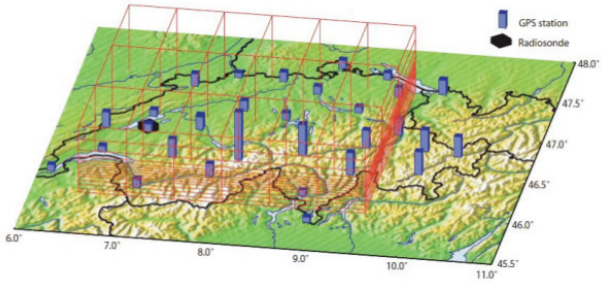

Figure 3. 3-D view of the tomographic voxel model above the Swiss territory. The figure shows the core voxel model of 6×3 voxels per layer, and layers up to 5000 m altitude. The GPS stations of the AGNES network are shown as pillars (length of pillar according to their station altitude). [10]

sphere is divided into voxels of appropriate size, each voxel having constant refractivity. See Figure 2a for an illustration of the setting. See Figure 3 for voxel model used in [10]. The number of traversing rays per voxel depends on the geometry defined by the distribution of the ground GPS stations as well as the satellite constellation and on the resolution of the voxel model. Usually, only a part of the voxel refractivities are sufficiently determined.

The reconstruction of a complete 3D water vapour distribution requires the solution of an inverse ill-posed problem with incomplete data. The input data is usually incomplete because only a very limited number of SIWVs can be obtained with a given constellation of GPS satellites and receivers. A reliable tomographic reconstruction would require a large number of SIWVs per voxel. The reconstruction of the atmospheric water vapour from GPS data alone would therefore be limited to cases of very dense local networks with receiver distances less than 1 km. In more sparse regional or national networks a priori knowledge, constraints and meteorological observations become more important [1]. The lack of GPS-data can to a certain extent be compensated by using for example a good initial distribution, by introducing inter-voxel constraints and by using additional non-GPS observations. [3]

Regardless of the difficulties in the technique, different tomographic reconstruction techniques have been successfully used to obtain good quality water vapour distributions in the troposphere [7, 10]. Most of the reconstruction techniques need a set of internal parameters which have to be optimised for atmospheric reconstructions. Furthermore, all these inverse methods depend strongly on the chosen initial conditions, like the initial water vapour field, and require additional information which can

be used during the reconstruction process. The reconstructed moisture distribution will finally be a representation of not only the the quality of the GPS input data but also the skills of the reconstruction algorithm, the chosen parameters and the initial conditions. There are many kinds of tomography software packages available for processing, such as AWATOS (Atmospheric WAter vapour TOmography Software) used in [10]. The software packages are under constant development and evolving quite rapidly.

2.4 Enhancing GPS tomography with other GNSS systems

The slant paths of one single GNSS system are always rather in-homogeneously distributed and different parts of the atmosphere are covered at different times. Usually, between 6 GPS and 12 GPS satellites can be tracked by one receiver. It is difficult to represent the atmospheric state with such a small number of slant paths. The satellite positions also change very fast and the signals detected propagate through different parts of the atmosphere. The information provided by a network of a single GNSS system receivers is therefore highly variable in space and time. Currently only GPS is used for operative water vapour tomography, but utilization of the extra observation capacity of other GNSS systems GLONASS and Galileo is also investigated. The situation can be considerably improved by combining the observations of the other GNSS. The distribution of slant paths becomes much more homogeneous if more satellites can be tracked (see Figures 4 and 5). With these additional observations, the temporal variations in the water vapour distribution are no longer dominated by the satellite constellation but represent the true atmospheric variations to much greater extent. Tracking two or three satellite systems simultaneously provides therefore considerably more information about the atmospheric state than the observations of a single system.

The spatial distribution then becomes much more homogeneous and the temporal variations are much smoother. It could therefore be expected that the quality of consecutive tomographic reconstructions will become more uniform. Another aspect is that the total coverage of the atmosphere would also be significantly improved. However, the highly increased amount of data to process places challenges for the tomographic analysis techniques used. [2]

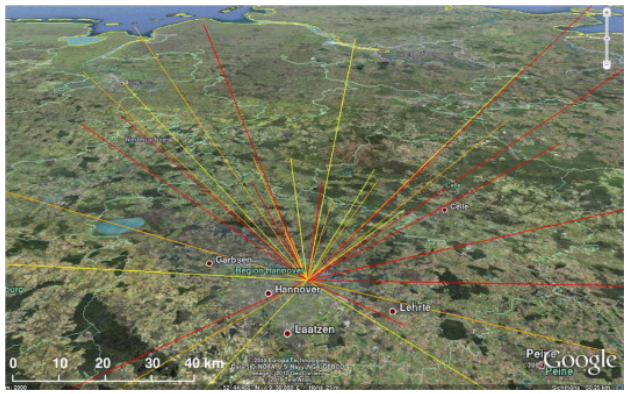

Figure 4. GPS paths observed by a single station, plotted up to a hight of 12 km. Paths to GPS satellites are given in red, to GLONASS satellites in yellow, and to Galileo satellites in orange. [2]

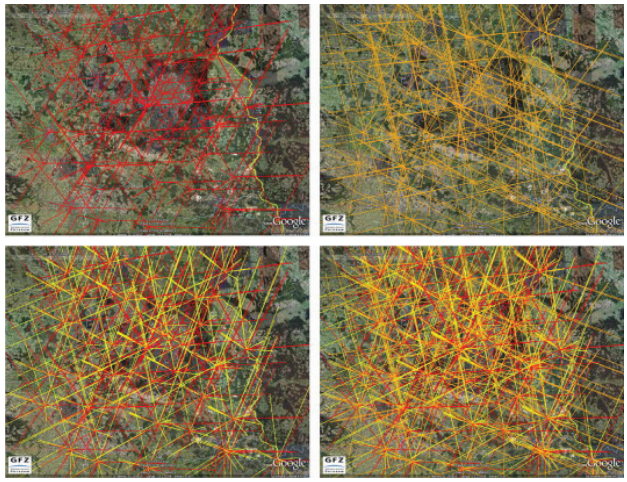

Figure 5. Spatial coverage of the atmosphere by slant paths of GPS observations (red, top left) and Galileo observations (orange, top right). Combining GPS and GLONASS (yellow, bottom left) or all three systems (bottom right) will result in considerably better spatial coverage of the troposphere. [2]

2.5 Other possible improvements in GPS Tomography

The ray paths of the fast moving GPS satellites traverse constantly changing regions of the atmosphere. Therefore, collecting data over a limited period of time would provide only little less information about the temporal change in the atmosphere but would substantially increase the spatial information. The resolution of the tomographic reconstruction can be improved by using data collected up to several hours. The reduced temporal resolution would be no consequence for several applications which require the data in certain intervals, such as data assimilation in numerical weather models.

One of the most critical parameters to the amount and quality of data provided by GPS networks depends on the elevation cut-off angle used by the GPS receivers and the processing algorithms. Reducing the minimum elevation angle would considerably increase not only the total amount of data but would also provide valuable information about the the lower regions of the troposphere.

Increasing the number of GPS ground stations would improve the data quality in several ways: The poor results at the outer boundary of the grids can be reduced by covering an ex- tended area. A higher density of stations will provide fields with an enhanced resolution, especially in the vertical direction. The vertical resolution can be further improved by making use of the topographic conditions, e.g. at mountain sides. Further improvements can be expected from low earth orbiters (LEOs) which provide horizontal views through the atmosphere, adding to the observation data in the tomographic process. Several LEOs providing radio occultation data are currently in orbit, and other missions are planned. See the next section for more about GPS radio occultations. [1]

3 GPS radio occultation

Global climate models need continuous atmospheric information from all around the Earth. Atmospheric information obtained with GPS ground measurements alone cannot cover the Earth completely, since they only have receivers set up on land. Other techniques are necessary to obtain global coverage. Radio occultation (RO) is an atmospheric remote sensing technique that is based on detection of the change in a radio signal as it passes through a planet's atmosphere, or in other words, as it is occulted by the atmosphere. When a radio signal passes through the atmosphere its phase is delayed and bent according to the atmospheric refractivity along the signal path. Measurements of the phase perturbations in the signal reveal the refractivity along the signal path, from which quantities as atmospheric temperature, pressure and water vapour content can be derived.

RO technique has been used actively from as far back as the 1960's on studying atmospheres of other planets and other celestial objects in the solar system. In these missions the radio signals between the Earth ground stations and the probe or spacecraft were observed during their occultation of the planet's atmosphere. These measurements were then

used to analyse the atmospheric content of the planet in question. This kind of radio sounding techniques have been applied successfully for decades everywhere else in the solar system, but have only recently become useful for the study of the Earth's atmosphere. The reason for this is that a proper occultation measurement requires both a transmitter and a receiver off the the planet of interest, and we have seldom had that possibility with the Earth in the past. To wield useful information about the whole atmosphere, the measurements must also be comprehensive, continuous and synoptic, so many transmitters and receivers are needed to be working at the same time.

The implementation of GPS network of satellites and the development of small, high- performance GPS receivers have since made the active remote sounding of the Earth's atmosphere with RO measurements possible at comparatively low cost. GPS RO technique possesses a unique combination of global coverage, high precision, high vertical resolution, insensitivity to atmospheric particulates, and long-term stability. These properties are well suited for several applications including numerical weather prediction and long-term monitoring of the Earth's climate. [13]

The first RO missions utilising GPS were launched in the early 1990s, with a low-cost demonstration experiment GPS/MET by University Corporation for Atmospheric Research (UCAR). GPS/MET satellites acquire RO observations with a low cost geodetic ground receiver on board. The mission produced good results, and afterwards many new spacecraft have been launched into low Earth orbit to provide RO observations: CHAMP (Germany), SAC-C (Argentina), GRACE (2 spacecraft, US/Germany) and IOX (US) for example. In 2006 a whole constellation of RO observing satellites called COSMIC (see section 3.2) was launched. The GPS receivers aboard shuttles and the International Space Station (ISS) have also been used for RO measurements.

New GPS occultation sensors can be used quite effortlessly to extend existing satellite systems. The data can be analysed using the existing ground infrastructure and processing systems. There is also no need for an additional calibration effort. This makes it relatively easy and affordable to build powerful multi-satellite RO observation systems.

3.1 From GPS signal occultations to atmospheric quantities

GPS radio occultation (RO) technique is used on Earth by observing how radio signals propagating between GPS satellites and receivers placed on

a low Earth orbit (LEO) satellites are bent or refracted by the atmosphere (see Figure 6). The bending is caused by gradients in the refractive index of the atmosphere. During an occultation event the movement of the satellites enables the observation of the variation in the bending of the signal path as a function of the signal path height above the surface. These bending angle profiles can then be inverted to provide vertical profiles of refractivity, and subsequently vertical profiles of atmospheric temperature, pressure, or water vapour with high accuracy (less than 1 Kelvin in temperature), and with a vertical resolution of a few hundred meters.

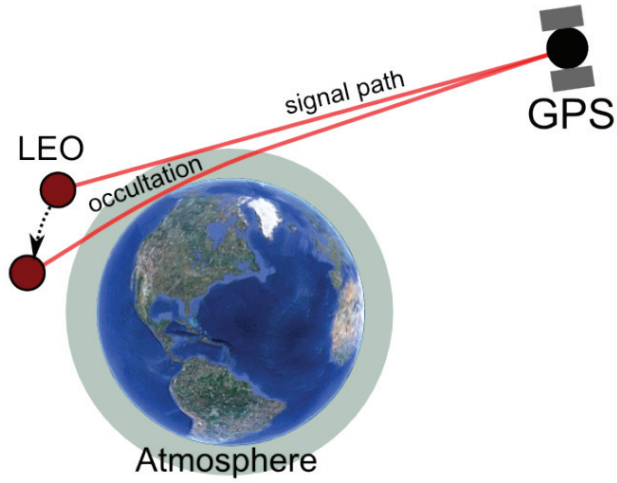

Figure 6. GPS occultation with a low Earth orbiter (LEO) satellite.

The refractive profiles cannot be separated to atmospheric quantities by themselves, however, and some a priori information is necessary when constructing different profiles. If temperature profile is desired, for instance, information about the atmospheric pressure is required for processing, and if pressure profile is desired, temperature information must be available. In the lower part of the troposphere, the uncertainty in water vapour content leads to a large error in the recovered temperature. In that region, since it is water vapour that is of greater consequence in weather modelling, it is easier and more beneficial to recover water vapour profiles instead.

A single LEO satellite can recover more than 500 atmospheric profiles each day, distributed almost uniformly around the globe. A constellation of multiple LEO satellites can produce thou- sands of atmospheric profiles daily. With their even distribution and good temporal resolution, RO observations greatly complement for example radiosonde measurements,

which are only conducted in very specific locations and only a few times a day (see Figure 8).

The potential of GPS occultation technique for both climate monitoring and climate model evaluation has been widely studied. RO observations are expected to provide useful information relating to near-tropopause temperature changes, humidity changes in the lower and middle troposphere, and the expansion of the troposphere due to global warming. They have also been found useful to study the water vapour transport to the upper troposphere and lower stratosphere by deep convective storms [4]. RO data can also be utilised in a global numerical weather prediction (NWP) system. An important feature of RO measurements is that they can be assimilated to a climate model without the need for bias correction. This enhances their ability to correct model biases which are otherwise difficult to rectify because other satellite data tend to be bias corrected to the assimilating model [8].

3.2 Constellation Observing System for Meteorology, Ionosphere and Climate (COSMIC)

After promising results with GPS radio occultation measurements from receivers on GPS/MET satellites, CHAMP and GRACE satellites and others, a demand for a larger GPS radio occultation observation system was raised. Constellation Observing System for Meteorology, Ionosphere, and Climate (COSMIC) is a satellite program designed to provide GPS radio occultation measurements and products to support meteorology, ionospheric research, climatology, and space weather research [6]. The COSMIC satellite constellation (also known as FORMOSAT-3) consists of 6 microsatellites (see Figure 7) equipped with GPS receivers that continuously provide GPS RO observations from their LEO orbits.

The constellation is a joint U.S.-Taiwanese project with major participants including the University Corporation for Atmospheric Research (UCAR), the National Science Foundation, the Naval Research Laboratory (NRL), the Air Force Research Laboratory (AFRL) on the U.S. side and the National Space Organization (NSPO) on the Taiwanese side. The COSMIC satellite constellation was launched from Vandenberg AFB on April 15, 2006. The satellites have since been raised to their final orbit to an altitude of 800 km and they have formed an operational constellation of six orbital planes separated by 30 degrees at the inclination of 72 degrees.

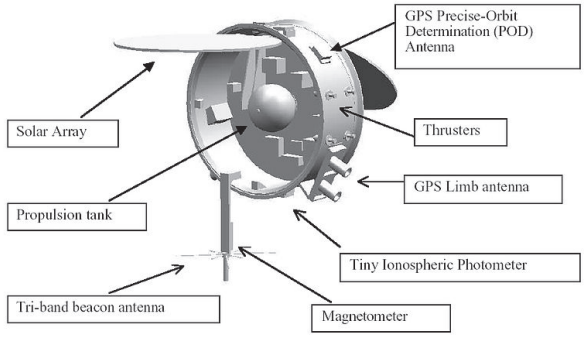

Figure 7. Components of a FORMOSAT-3 / COSMIC satellite. [12]

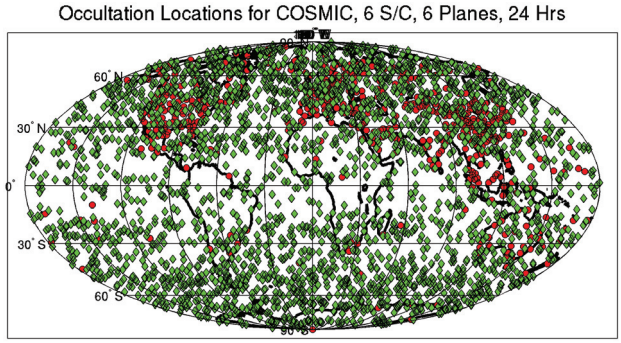

Figure 8. A map showing the typical occultation locations of 24 Hrs worth of COSMIC soundings (green diamonds) compared to existing radiosonde launch sites (red circles). (Illustration by Bill Schreiner [11])

COSMIC not only refers to the satellite constellation, but also to the organization now maintaining the constellation and processing the occultation measurements to various products. The COSMIC Data Analysis and Archive Center (CDAAC) processes data from COSMIC constellation together with data from other RO missions, including GPS/MET, CHAMP, SAC-C, and GRACE. CDAAC processes raw RO data into atmospheric profiles in near real time. Ninety percent of RO profiles are delivered to operational weather centres within 3 hours of observation. CDAAC reprocesses the data in a more accurate post-processed mode within 6 weeks of observation. CDAAC also periodically re-processes all RO missions every 1-2 years with consistent software and algorithms to provide the most accurate and stable products for use in climate studies. The products are constantly re-processed with the newest algorithms to ensure data consistency.

COSMIC is currently providing between 1000-2500 daily RO profiles in the neutral atmosphere, 1000-2500 daily electron density profiles and to-

tal electron content arcs, and TIP radiance products (see Figure 8). The data have demonstrated their value in operational weather forecasting, hurricane forecasting, and investigations of the atmospheric boundary layer. The data have been used extensively to test ionospheric models and their use in operational space weather models is under development. COSMIC GPS RO data also have the potential to be of great benefit in other climate studies due to their high precision and global coverage.

4 Conclusions

Water vapour is one of the most important constituents of the troposphere and its variations are very significant in weather formation. Temporally and spatially resolved humidity information are essential in many fields of meteorological research and applications, such as weather forecast, especially precipitation forecast and nowcasting, hazard mitigation and water management. These applications greatly benefit from the additional atmospheric observation power of the GPS meteorology and climatology techniques. The GPS measurement infrastructure is already there so the GPS meteorological and climatological techniques can be utilised with very small efforts and much less investment than other techniques.

GPS tehchniques are also able to observe continuously regardless of the weather. Some GPS ground station networks already provide moisture data operatively and plans to set-up GPS based water vapour retrieval systems exist in most European countries. Nowadays there are many GPS radio occultation capable low Earth orbiting satellites, which produce an in- creasing number of globally distributed atmospheric profiles of high quality. This allows for improved global weather forecasts and to detect relevant climate change variations of the Earth's atmosphere.

Much research has been done on GPS meteorology and climatology but it is still a relatively new field of study. The techniques are constantly being developed and they have not yet been utilised to their full potential. GPS techniques have, however, revolutionized the field of meteorology and climatology and more great results are expected from them.

Bibliography

[1] Bender, M. and Raabe, A. (2007). Preconditions to ground based GPS water vapour tomography. *Annales Geophysicae*, 25(8):1727–1734.

[2] Bender, M., Stosius, R., Zus, F., Dick, G., Wickert, J., and Raabe, A. (2011). GNSS water vapour tomography – Expected improvements by combining GPS, GLONASS and Galileo observations. *Advances in Space Research*, 47(5):886 – 897.

[3] Bevis, M., Businger, S., Herring, T. A., Rocken, C., Anthes, R. A., and Ware, R. H. (1992). GPS meteorology: Remote sensing of atmospheric water vapuor using the global positioning system. *Journal of Geophysical Research: Atmospheres*, 97(D14):15787–15801.

[4] Biondi, R., Neubert, T., Syndergaard, S., and Nielsen, J. (2011). Measurements of the upper troposphere and lower stratosphere during tropical cyclones using the GPS radio occultation technique. *Advances in Space Research*, 47(2):348 – 355.

[5] Champollion, C., Masson, F., Bouin, M.-N., Walpersdorf, A., Doerflinger, E., Bock, O., and Baelen, J. V. (2005). GPS water vapour tomography: preliminary results from the ESCOMPT field experiment. *Atmospheric Research*, 74(1–4):253 – 274.

[6] COSMIC (2011). Programme Office: Constellation Observing System for Meteorology, Ionosphere, and Climate. `http://www.cosmic.ucar.edu/`. [Online; accessed March-2011].

[7] Flores, A., Ruffini, G., and Rius, A. (2000). 4D tropospheric tomography using GPS slant wet delays. *Annales Geophysicae*, 18(2):223–234.

[8] Healy, S. B. and Thépaut, J.-N. (2006). Assimilation experiments with CHAMP GPS radio occultation measurements. *Quarterly Journal of the Royal Meteorological Society*, 132(615):605–623.

[9] Paroscientific, Inc (2007). GPS Meteorology. `http://www.paroscientific.com/gpsmet.htm`. [Online; accessed March-2011].

[10] Troller, M., Geiger, A., Brockmann, E., and Kahle, H.-G. (2006). Determination of the spatial and temporal variation of tropospheric water vapour using CGPS networks. *Geophysical Journal International*, 167(2):509–520.

[11] UCAR (2011). University Corporation for Atmospheric Research - COSMIC Visuals and Multimedia Gallery. `https://www2.ucar.edu/news/cosmic-visuals-multimedia-gallery`. [Online; accessed March-2011].

[12] Wikipedia (2011). Formosat-3. `http://de.wikipedia.org/wiki/FORMOSAT-3`. [Online; accessed March-2011].

[13] Yunck, T. P. (2002). An Overview of Atmospheric Radio Occultation. *Journal of Global Positioning Systems*, 1(1):58–60.

Matlab Application in VLBI Data Analysis

Niko Kareinen

Department of Real Estate, Planning and Geoinformatics
Otakaari 1, FIN-02150 Espoo Finland
niko.kareinen@aalto.fi

Abstract

Geodetic VLBI is an irreplaceable technique in the determination and combination of terrestrial and celestial reference frames. In this paper the basic principle of VLBI observations and data acquisition process are briefly discussed. Furthermore, the connection between observed delays and estimates for geodetic parameters is discussed. A Matlab based VLBI analysis software VieVS is introduced. The structure and functionality of VieVS is discussed to some detail and a demonstration of geodetic parameter estimation using VieVS is processed. The results for dUT1 and station coordinates for Wettzell VLBI station are investigated in more detail by using a Matlab script to read and generate corresponding time series vectors for the estimates. The obtained offsets varied within a reasonable range for both dUT1 and station coordinates.

1 Introduction

There exists a wide variety of space geodetic techniques for studying phenomena related to geodynamics and geodynamic models, which are connected to plate tectonic movement and Earth orientation. These techniques consist of five main components: Global Navigation Satellite Systems (GNSS), which includes mainly GPS and GLONASS, Satellite and Lunar Laser Ranging (SLR and LLR), Doppler Orbitography and Radiopositioning Integrated by Satellite (DORIS), and Very Long Baseline Interferometry (VLBI). Each of the techniques have their own advantages and drawbacks and to utilize these available techniques to their full potential, they are combined in order to produce as accurate data products as possible.

One of the main strengths of GNSS, in the context of global reference frames, is scalability. The relatively low cost of GNSS-stations has enabled the construction of a very dense observation network, which is continuously improved by building new observation sites. However, observations independent of GNSS are required to establish and maintain global reference frames as well as augment the positioning of satellites. SLR and DORIS are used for GNSS-independent satellite tracking, but they also contribute to other fields of research. Measurements from DORIS are used in the determination of station positions, geodynamics, tropospheric and ionospheric models, and gravitational models. SLR is used to obtain a highly accurate position for the origin of global reference frames, i.e. the center of mass of the Earth. LLR contributes to the observation of secular changes in nutation and precession as well as the obliquity of the ecliptic. These parameters are used in establishing the connection of celestial and terrestrial reference frames (CRF and TRF).

Compared to the other observation methods, VLBI has several advantages. It is the only space geodetic technique which allows for simultaneous high precision measurement of all the Earth Orientation Parameters (EOP), making it an essential component in measuring the variations in Earth rotation, Fand combining TRF and CRF. The development of VLBI started in the 1960s and was at the time motivated by astronomical observations of the recently found extragalactic radio sources of very small angular size, quasars, which required ever increasing baselines between conventional radio interferometers. This led to the situation where the radiotelescopes could not be physically connected, but measurements had

to be recorded in individual stations and combined afterwards. This characteristic design constitutes the VLBI technology.

Due to the great distance of hundreds of light years, quasars appear as fixed points relative to other astronomical objects, creating a network of reference points. When the source coordinates were established, VLBI could be utilized as a geodetic technique to observe baselines between radiotelescopes and earth orientation. The development of geodetic VLBI started in 1970s at the NASA Goddard Space Flight Centre with the Mark I VLBI system [7]. At that time, baselines spanned the United States and were typically in the region of 4000 km. Formal errors for these baselines were 70 mm and as the technology improved the errors approached subcentimetre category. Nowadays, the international VLBI campaign aims for a positional accuracy of 1 mm.

The international VLBI observation program is an extensive combination of technical and scientific research including observations, schedule management, data acquisition, correlation, post-processing, and analysis. To analyze VLBI data, a wide variety of VLBI analysis software of varying features is available, which are used to generate databases, process and simulate VLBI data to derive estimates for geodetic parameters and to test alternative models used in the analysis. This paper demonstrates an example of one such program, Vienna VLBI Software (VieVS). Written in Matlab, VieVS is one of the most recent VLBI analysis software. Both the capabilities and limitations of VieVS are discussed through the basic demonstration of the software and an example analysis using real VLBI data. Prior to analysis demonstration, the basic principle of VLBI and related observation and data acquisition techniques are discussed.

2 VLBI

VLBI is an astronomical interferometry technique that uses two or more telescopes to improve the resolution of the antenna system by recording the observed signals with highly accurate timestamps. Because the observed sources emit radio waves, the wavelengths range from millimeters to meters. The approximate relationship between the resolving power of the telescope, observed wavelength and aperture is presented in (1)

$$\theta \gtrsim \frac{\lambda}{D}, \tag{1}$$

where θ is the resolving power, λ the observed wavelength, and D the

aperture. The resolving power for the operating frequency range for the largest existing steerable radiotelescope, the 100 m Green Bank Radiotelescope [4], is 0.1-116 GHz, which translates to observable wavelengths from 2.6 mm to 3m. Using (1) this translates approximately to a resolving power of 5.3 to 6183.7 arcseconds. However, quasars have fine structure variations in the scale of milliarcseconds, thus making the only adjustable parameter, aperture, insufficiently small. To reach milliarcseconds resolving power for radiowaves requires an aperture size of hundreds of kilometers. This fundamental problem creates the need to increase baseline between stations and have the capability to combine the observations to create a radiotelescope array with the resolving power proportional to the baselines between observing stations.

VLBI can be divided into two components: astrometric and geodetic VLBI. With astrometric VLBI, sources are observed in order to produce a detailed image of the structure of the source. This usually means that the antenna network observes a single source for a period of time. In addition to source structure research, the achievable high resolution enables accurate measurements of positions and proper motions of extragalactic radio sources. The source positions are used in the realization of the barycentric International Celestial Reference System (ICRS). The realization of ICRS is the International Celestial Reference Frame (ICRF), which uses the measured positions as datum points. Figure 1 illustrates the distribution of 212 sources constituting the ICRF2. Geodetic VLBI can be seen as a reverse process to astrometric VLBI. In geodetic VLBI, the source coordinates of quasars can be regarded as time-invariant points of reference. The source coordinates are used to compute the lengths of baseline vectors between the stations in the observation network. Due to the high resolving power and thus accurate angular resolution, geodetic VLBI is also used to monitor Earth orientation by measuring EOPs. As opposed to astrometric VLBI, geodetic VLBI observation campaigns measure multiple sources, which are distributed in the sky in a way that aims to ensure an optimal observation geometry.

2.1 The basic principle of VLBI

Because of the sources properties discussed earlier, VLBI technique utilizes a network of telescopes. The recorded signals from all the stations have to be combined to produce observations with sufficient precision, exceeding the resolution of the individual antennas. In order to achieve

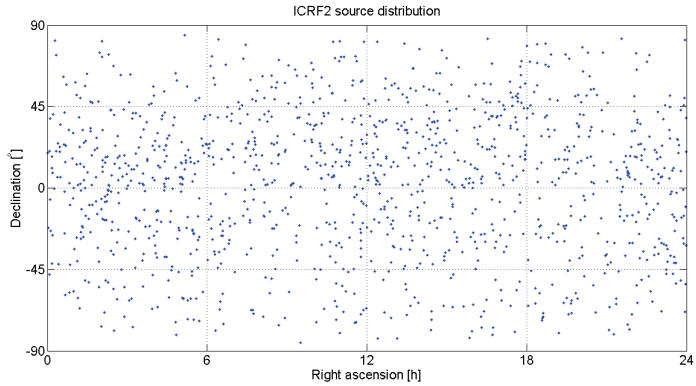

Figure 1. ICRF2 sources derived from VieVS ICRF2-file in right ascension - declination system.

this, the station network makes simultaneous observations of a selected source by measuring the incoming flux. Due to the fact that the stations are physically separated by hundreds to thousands of kilometers, a direct connection between the stations has been historically impossible between the sites and correlators. However, the VLBI data transfer using fibre optic cables is actively developed and implemented in an increasing number of stations. The data recording rates of modern VLBI systems in terms of current technology is very high, e.g. a Mark5 VLBI data system has a data rate up to 4096 Mbps, which leads to high data storage requirements. The data recording process will be discussed in more detail in section 2.2.

The signal from an extragalactic radio source, as is the case with geodetic VLBI, can be modelled as a plane wave approaching the stations. Due to the station positions and the rotation of the Earth, a time difference up to roughly 0.02 s is observed between stations receiving the same signal. Thus the data must be supplemented with an extremely accurate time signal in order to combine the individual observation data from VLBI stations. To realize the time signal, each station is equipped with an independent clock. To achieve the highest possible precision, the clocks used in modern VLBI stations are hydrogen masers. These clocks have very high degree of stability in order of 10^{-15} s, which translates approximately to a drift of 1 s per million years [3].

2.2 Correlation and VLBI data systems

The high data rates during the observations translate to large quantities of data. The data at VLBI stations could be stored either on magnetic disc

or tapes. However the development of magnetic disc technology has led it to be a far more cost-effective option compared to tapes [3]. A widely used VLBI data system is the Mark-series, developed in MIT Haystack Observatory. Currently, the most used Mark-system is the Mark5, but at the moment the new Mark6 system is planned for general use in the mid-2012. With the Mark6 system the development has shifted from the dedicated hardware of Mark5 to inexpensive and more flexible off the shelf hardware. With the Mark5 system data record rates up to 4096 Mbps can be achieved. This rate results in up to 40 TB of data for each station per day and during longer observation campaigns, the cumulative amount of data can reach 4 PB. The huge amount of data relative to practically available disk space poses a limit to the duration of observation campaigns. Furthermore, due to the fact that the most cost-effective way to increase the sensitivity of VLBI is to increase the observation bandwidth i.e. the data rate, an ever increasing storage space is required. Currently, the aim is to achieve data rates up to 32 Gbps and with the latest addition to Mark-series, the Mark6, a sustained data rate of 16Gbps has been achieved [1]. The drawback of storing the data locally on disks is the slow turnaroud of data, because the hard drives have to be physically sent to the correlators. This is a particular problem with rapid-determination of universal time (UT1). Although earlier the only way to transfer the observation data was to physically deliver the hard drive or magnetic tapes from VLBI stations to correlators, the development of high speed data transfer via fibre optic cables has made it possible to utilize e-VLBI, i.e. to transfer VLBI observation data electronically directly to correlators in real or near real time. Although e-VLBI is of 2012 widely used in Europe, a global use is still limited and there exists several challenges, such as hardware limitations, remote locations of the telescopes causing connectivity issues and network bottlenecks [1].

From the high precision timing of the signal time delay between telescopes, the distance between stations can be calculated. The observed time delay, τ_{obs}, between two radio telescopes is the basic geodetic VLBI observable. To compute the time delay between stations the VLBI data recorded at the individual stations is delivered to a correlation facility. The correlator is essentially a dedicated computer. The computer is designed to reproduce and combine the recorded signals pairwise between observed baselines to acquire the visibility function of the observed source. However, it is to be noted that in recent years software correlation has

also become computationally feasible. To combine the observations, the two signals are shifted in relation to each other and for each shift-value a correlation value is calculated. A fringe is observed at the maximum correlation point when the time shift equals the time delay between the two stations. There are a total of 7 correlators operating under International VLBI Service (IVS) in USA, Germany, Japan, Russia and China. The correlation centers in United States, in Haystack and Washington, operate a Mark IV, which is a dedicated hardware correlator developed in the 1990s. It has been upgraded to accommodate new Mark5 magnetic disk arrays and e-VLBI [2]. In addition to the USA, correlation centers in St. Petersburg, Russia, and Shangai, China use specially developed hardware correlation systems. Mark IV correlator was used in Bonn, Germany up to the year 2010, when after hardware failure the facility moved exclusively to a DiFX software correlator system. In Japan, centres at Tsukuba and Kashima use K5/VSSP and K5/VSI software correlator systems, respectively.

2.3 VLBI observables and geodetic parameters

The observed time delay, τ_{obs}, between two radio telescopes is the basic geodetic VLBI observable. The signal is converted to digital form at the VLBI station before correlation, from which the correlation peak corresponds to τ_{obs}. The correlated radio signals are governed by noise, thus making the recorded data effectively two high-precision timed sets of Gaussian noise. The delay is affected by a wide variety of distorting factors and technical limitations, which have to be accounted for in order to find an accurate epoch correlation fringe. The bandwidth, i.e. the sampling data rate, discussed in section 2.2 used in the observation affects the overall precision of the time delay. The relationship of delay precision to effective bandwidth and noise is given by (2) [6]

$$\delta\tau_{obs} = \frac{1}{\mathrm{SNR} \times B_{eff}}, \tag{2}$$

where $\delta\tau_{obs}$ is the delay precision, SNR is signal-to-noise ratio, and B_{eff} is the effective bandwidth of the observed signal. From this relationship it is evident that the way to improve delay precision is to increase the SNR and bandwidth. However, increasing the SNR would require more sensitive receivers and at the moment receivers are approaching quantum noise limits and the signal is heavily distorted by atmospheric noise [1].

The main component contributing to the total observed time delay is the geometric delay, τ_g, in the propagation time of the signal between station 1 and 2. The fundamental relationship between time delay and baseline is given by (3)

$$\tau c = -\vec{b} \cdot \vec{k}, \tag{3}$$

where τ is the time delay, c is the speed of light, $\vec{b}$ is the baseline vector, and $\vec{k}$ denotes a unit vector of the observed source perpendicular to the arriving plane wave. In addition to τ_g the observed delay contains numerous distorting factors, which have to added to the observation equation. The observation geometry is not static between telescopes, but during the observations the rotation of the Earth causes one of the telescopes in a baseline to move slightly before the radio signal recorded by receiver 1 at an epoch t_1 reaches receiver 2. Additionally, the signal propagates through the atmosphere before it reaches the antennas, which causes tropospheric and ionospheric delays, and thus the τ_g is adjusted accordingly. Furthermore, the signal is distorted by gravitation from bodies of mass in the solar system and special as well as general relativistic correction to the τ_g are required. At the stations, mis-synchronization between station clocks and the propagation of signal in the cables and instruments cause variable time delays for each station [9]. When taken into account all these factors, the observation equation is corrected with the sum of these terms according to (4)

$$-c\tau = \vec{b} \cdot \vec{k} + \Delta\tau_b + \Delta\tau_{clock} + \Delta\tau_{trop} + \Delta\tau_{ion} + \Delta\tau_{cal} + \Delta\tau_{rel} + ... \tag{4}$$

where the Δ denotes a change in propagation distance for the subindices accordingly. The subindices account for adjusted geometric baseline, clock error, troposphere, ionosphere, cable calibration, and relativistic effects respectively [5].

Using the correlated, corrected and post-processed time delay observations, geodetic parameters can be estimated from the data with VLBI analysis software. The estimated parameters depend on the applied software. The VLBI analysis software VieVS used in this paper can produce estimates of the following geodetic parameters: clock parameters, zenith wet delay (ZWD), troposphere total gradients (East and West), TRF station coordinates, CRF sources coordinates, and all five EOPs. The five Earth orientation parameters include polar motion (x_{pol}, y_{pol}), celestial

motion of the pole (dX_{nut},dY_{nut}) and universal time expressed as the difference UT1-UTC (dUT1). VLBI is essential in establishing the relationship between ITRF and ICRF, because it is the only space geodetic technique capable of measuring all of the EOPs simultaneously while observing the sources in CRF and station coordinates in TRF.

3 VLBI analysis software

The purpose of VLBI analysis software is to process and analyze the time delay data from VLBI observations to yield estimates for geodetic parameters. There are a wide variety of options available for analysis and the oldest VLBI analysis software dates back to the 1970s. Due to the long legacy of development, there still exist dependencies between the analysis software. This dependency is because some of the software have an important role in VLBI data flow process. Calc/Solve is the oldest and widely used analysis software among the VLBI community and it is used in the process to generate the National Geodetic Survey (NGS) database, which contains e.g. the delay observations for each observed and correlated session. The NGS database is used by other analysis software, such as VieVS, but the development is ongoing to make the analysis software compatible with raw correlator output.

3.1 VieVS

The development of VieVS started in 2008 at the Institute of Geodesy and Geophysics (IGG), Vienna University of Technology (TUWien). Prior to VieVS the research team at IGG had used an alternative VLBI analysis software OCCAM. As with many old VLBI analysis software, OCCAM had gathered a significant amount of obsolete code due to the long history of development with FORTRAN. This poses a difficulties with maintaining the source code up to date and the interpretation of functionality of the code can require a high level of expertise. Because of this difficulty, when a major update for OCCAM was required, it was decided that a new VLBI software would be the optimal approach. The new approach offered the possibility to modernize the existing and proven source code in a language, that would make maintenance of the program more flexible. Although in general open source approach is valued in the scientific community, VieVS was written in Matlab. The decision to use Matlab was

motivated by the fact, that the students at TUWien were familiar with the software, which would make the development and later source code modification for e.g. testing new algorithms significantly easier, when most of the time would not be spent on deciphering FORTRAN source code. However, due to the long history with OCCAM at IGG, VieVS was built based on existing OCCAM modules, which were ported to Matlab and obsolete modules removed [8]. Furthermore, VieVS was designed to be compatible with latest IERS conventions (2003 at the time) from the start and subsequent updates would be more efficient to introduce with the more streamlined source code.

VieVS is composed of separate modules, which have their own purpose and can be run individually if required, although for e.g. geodetic parameter estimation and simulated observations multiple modules are needed. The components of VieVS are *vie_setup*, *vie_init*, *vie_mod*, *vie_lsm*, *vie_sim*, *vie_glob* and *vie_sched*, which perform GUI initialization and auxiliary functions, data initialization, computations of theoretical delays, least squares adjustment (LSQ), data simulation, global solution and scheduling, respectively. The data initialization, theoretical delay and LSQ adjustment modules are the three main components of VieVS, which perform the estimation of geodetic parameters. The simulation module is used for simulating observations with desired criteria and it can be used for example to test alternative modeling algorithms. The global solution module creates combined solutions to determine TRF and CRF. The latest addition to module selection is the scheduling module, which is used to create observing schedules for VLBI stations. In addition to the modules, VieVS has a selection auxiliary scripts for e.g. process list generation.

VieVS can be operated both in batch and Graphical User Interface (GUI) modes. The batch mode is suitable for automatization of data processing, since it can be with little effort scripted to run as a background process using predefined modelling parameters. The GUI mode offers an efficient and practical interface for more thorough data analysis and interpretation of results. For this paper, the GUI mode was used, and all the following references to VieVS modules refer to the GUI-modules.

Setup and main modules

Prior to actual analysis options, *vie_setup* is executed. The sessions to be processed are selected either from VieVS session database or by using predefined session list. The session files are stored locally on the hard

drive and must be kept up to date to obtain results consistent with the latest a priori data. The files are maintained and updated on TUWien server.

The initialization module is used to read observation data from NGS files, station coordinates and velocities for the stations participating in the session from TRF catalogue, source coordinates from CRF catalogue, a modelling parameter file, outliers, station info, and an option file for the session. VieVS uses NGS files to read observed delays, meteorological data, cable calibration, and other data for each session. If the station is not included in the catalogue or the coordinates are not defined for the analysis period, the a priori station coordinates are read from the NGS file header. The delays in the NGS file have been corrected for ambiguity resolution and ionospheric correction using the Calc/Solve analysis software. For this reason, VieVS is dependent on external preprocessed observation files. That is why there is an ongoing effort to make VieVS able to solve ambiguity resolution and execute ionospheric corrections generated in order to span the scope of VieVS further into the VLBI data production flow. The option file (OPT-file) is created by the analyst during the initial processing of the sessions. While it is not mandatory to create OPT-files for sessions in practice, particularly if analyzing multiple sessions, it is highly probable that the sessions contain problems, which have to be taken into account in the option file. OPT-file input includes info about reference clock, clock breaks as well as excluded stations, sources, cable calibration, and baselines.

With vie_mod the theoretical delays for each session are computed. The computed delays are calculated using modelling parameters, which include EOPs and EOP interpolation, nutation model, solid Earth tides, ocean loading, ephemerides for celestial bodies, troposphere delay, thermal deformation and axis offset of the antenna, and atmosphere loading. The purpose of the computation is to generate theoretical delay values and their partial derivatives for the corresponding observation epochs, which are compared to the delay values read from NGS files. The difference of observed and computed delays is later included in the LSQ adjustment.

After the theoretical delays are computed, a LSQ adjustment is calculated with vie_lsm. The parameters selected by the user for estimation are modelled either as one offset per session or as continuous piecewise liner offsets (CPWLO). Estimation options include CPWLOs for clock parameters and quadratic polynomial coefficients (offset, rate, quadratic term),

ZWD, North and East troposphere gradients (NGR and EGR), EOPs and source coordinates. The station coordinates can be estimated either as CPWLOs or one offset per session. The LSQ adjustment module has the option for executing only the first solution without the main adjustment. This solution is used for initial processing of the data to detect problems within the session, e.g. clock breaks and bad stations. In addition to CPWLO estimates, the LSQ adjustment can set restrictions on the estimated parameters. These parameters are used to restrict the variations in the estimates according to desired analysis conditions and to tie together sessions with large gaps between scans. In general the constraint options can be separated in to three classes: tight, quasi-tight and loose. For different parameters a selection of absolute or relative constraints can be applied. While relative constraints limit the offset difference of adjacent scans to a certain standard deviation, absolute constraints limit offset values for all epochs to the selected standard deviance.

The offsets of estimated parameters are written into a results file. The file contains offsets, formal errors, and estimation epochs for all the stations included in the analysis. A priori values for appropriate parameters can be read from session parameter files. Because VieVS does not currently include any built-in visualization or evaluation utilities for the results, further examination of the results require some additional Matlab scripting.

Additional modules

In addition to the main modules, additional modules for data simulation and global solutions are included in VieVS. The latest module in development is the scheduling model, but it is yet to be implemented in the latest version of VieVS. The purpose of the model is to add the possibility to schedule observation sessions in VieVS. In this section a more detailed description is discussed for the simulation and global solution module, since both have already been implemented in the latest VieVS version.

The objective of the simulation module is to generate artificial zero input NGS files, which can be used for various testing purposes. With artificial NGS files, it is possible to control the input in order to study the effect of different modelling options and algorithms. Furthermore, because the contents of the simulated NGS files can be controlled, it is possible to test alternative scheduling options and observation network configurations. To generate artificial NGS files the simulated sessions are se-

lected in the initialization and theoretical time delays are computed with *vie_mod*. The computed delays are processed with *vie_sim* to simulate the observed-computed difference by simulating each station pair. The simulation includes ZWD, simulated using turbulence simulator, mapping function, clock parameter, simulated as random walk process and white noise per baseline. When the difference vector is computed, the artificial NGS files are created by summing the estimated observed-computed and computed vectors and writing the result into the generated NGS file. As opposed to the actual NGS files the artificial files are not corrected for ionosphere and cable calibration. These corrections have to be taken into account when analyzing the results. After the simulated NGS files are generated, they can be analyzed with the LSQ adjustment module similar to ordinary sessions.

The global solution module is used to combine results from the LSQ module to estimate source CRF coordinates, station TRF coordinates and velocities. Clock parameters, ZWD, troposphere gradients are estimated as reduced values. Global solution takes the datum free normal matrices (N) and right-hand side vectors (b) generated by *vie_lsm* as input and derives the reduced normal equations systems, which are then stacked to create a combined global solution. The module creates automatically TRF and CRF catalogues as results, which can be used as a priori input catalogues in VieVS.

4 VLBI analysis example with VieVS

In this section, a demonstration of VLBI analysis using VieVS is presented. The example describes the analysis process from session selection to final results and covers the issues arising with initial processing, which is the most labour-intensive segment of the analysis from the standpoint of the user.

For the analysis all the IVS-R1 and IVS-R4 24-hour sessions from 2008 were selected. The choice to use 24-hour sessions instead of for example intensive sessions was motivated by the fact that 24-hour sessions are adequate for both station coordinates and EOP estimation, whereas intensive sessions are designed for rapid estimation of UT1 and usually have an observation network of 2-3 stations, insufficient for estimating station coordinates. Both 24-hour sessions are scheduled to have an observation network of 8 station. Furthermore, the IVS-R1/R4 sessions are scheduled

to be carried out weekly, generating two observation sessions per week. This guarantees that the amount of available data for the analyzed time period is adequate and more comprehensive time series can be generated.

At first, a process list for the setup is created using an auxiliary script, *mk_list*, in VieVS. To select all the 24-hour sessions from 2008, *mk_list* is executed as follows

```
[process_list,sessions] = mk_list('R1',R4','YEARS','2008')
```

This process list containing all IVS-R1/R4 sessions from 2008 can be loaded in *vie_setup*. The selected sessions are analyzed individually as a single session analysis. Before the main analysis, each session must be processed individually to remove problems, discussed in section 3.1, in the sessions. To remove sources of error in the observations, the LSQ adjustment is run in first solution mode without a main solution. In this mode VieVS computes residual graphs for every station in the session. Prior to executing the first solution, modelling options for the analysis are selected. For consistency, the modelling options used in this example were chosen to be identical for each session in first and main solution. The modelling options are presented in Table 1

Table 1. Modelling options for 24-hour sessions

Modelling options for 24-hour sessions	
Ephemerides	JPL 421
A priori EOP	IERS C04 08
Precession/Nutation	IAU2006/2000
TRF	VTRF2008
CRF	ICRF2
Tidal ocean loading	FES2004
Pole tide	Cubic (IERS2010)
Mapping function	VM1

By visually inspecting the station-wise residuals, it is possible to detect problems with individual sessions. To detect problems with the session, it is sometimes necessary to also execute the main solution in order to inspect the a posteriori standard deviation of the main solution. This execution is also useful in assessing whether the corrections made resulted in any improvement in the solution. For clock breaks, the first solution mode

is usually very effective. Clock breaks can detected as large residuals associated with certain station in the residual plots and as an abrupt change in the sign of the offsets at some point during the observation period. The residual plot of the station with the clock break displays a sudden and disproportionately large change in the residual values. Figures 2 and 3 show the residual plots for two stations, in which the station in 2 has the clock break and the station in 3 shows the residuals to the station from a station with no problems. Figure 4 shows the residual for the station with the clock break after correction.

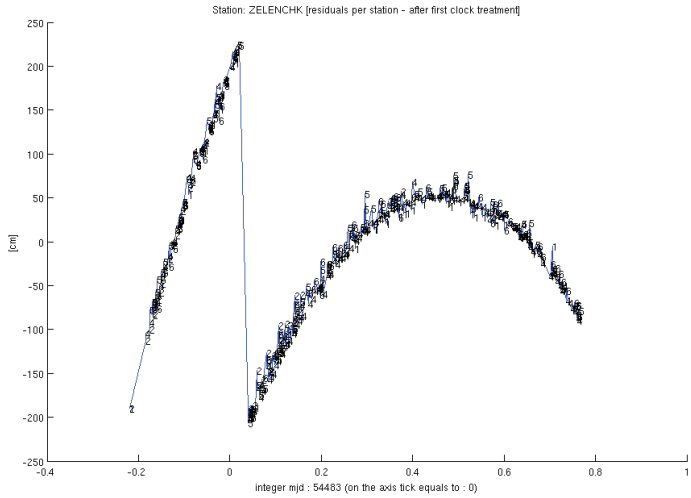

Figure 2. Clock break at ZELENCHK before correction.

Sometimes the data recorded at the station is noisy and causes large residuals with all of the stations reducing the accuracy of the main solution. A noisy station can usually be detected as a station having large residual throughout the observation period for no obvious reason, such as clock break. By examining the correlation reports associated with the observations session from the IVS observation schedule, it is possible to detect the cause, such as technical problems in the station, but usually the best approach is to remove the station from the analysis and check if the exclusion improved the a posterior standard deviation of the main solution. Figure 5 shows an example of a residual plot of a station, subsequently excluded from the analysis, with noisy data.

If all the stations in the network are otherwise performing without problems, but a single baseline between two stations has bad data, it is possible to exclude the baselines from the observations in order to keep the

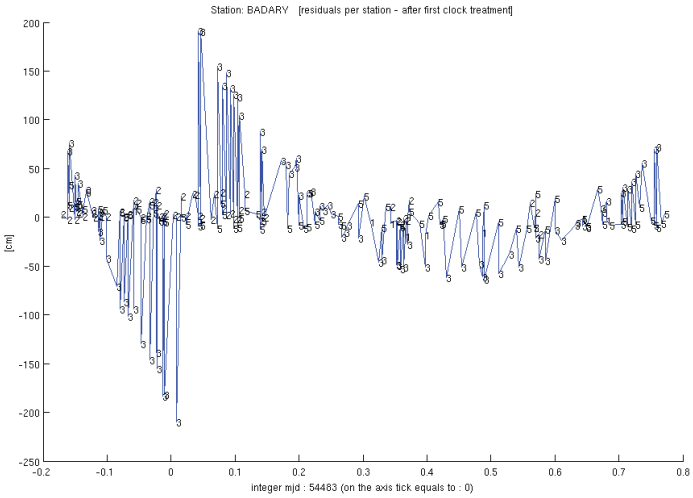

Figure 3. BADARY residuals with clock break at ZELENCHK.

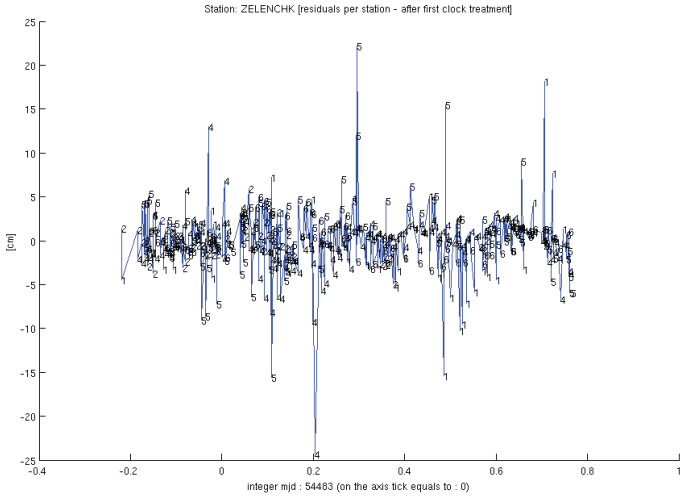

Figure 4. ZELENCHK residuals after clock break correction

stations in the analysis without discarding usable observations. Bad baselines are detected as large residuals between two particular stations in the residual plots. An example of a bad baseline is depicted in Figure **??**

All the options are written in individual OPT-files for each session requiring adjustment. In addition to clock breaks, excluded stations, and baselines the reference clock for the session can be specified in the OPT-file. The reference clock should be chosen from a station, which is known

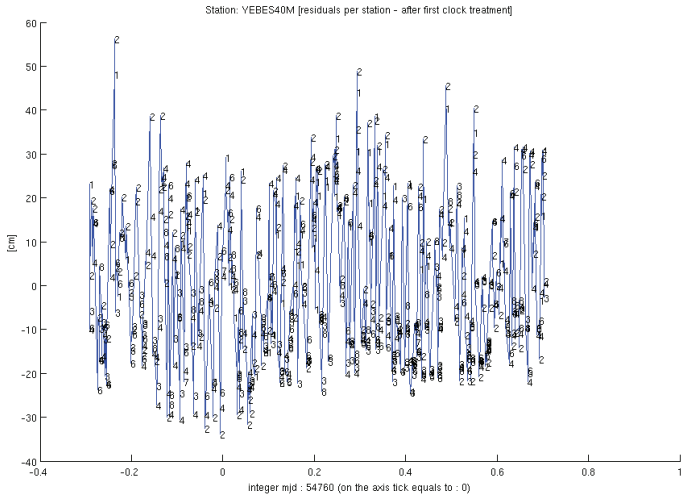

Figure 5. Noisy data at YEBES40M.

to have a stable clock. In this analysis Wettzell was chosen as the reference clock for the majority of the sessions.

In addition to the error sources discussed, the solution quality can be affected due to bad sources, too few observations at a station, cable calibration, bad individual observations, singularity problems in the normal equations arising from the number of estimated parameters, and large variability of clock parameter. Compared to clock breaks, bad stations and baselines, these error sources can be more difficult to detect and require closer inspection of the affected session. In this analysis no such errors were clearly evident. However, the amount of bad stations in sessions 08JAN10XE_N004 and 08MAY19XA_N004 was so large that after excluding the noisy stations only three were left in the analysis. Thus, the sessions were removed from the analysis.

After the initial processing is completed and all the problems with the sessions have been corrected with OPT-files, the LSQ adjustment is executed. For this analysis, all the geodetic parameters were estimated, using generally loose constraints. Station coordinates were estimated as one offset per session with No Net Translation and No Net Rotation (NNT/NNR) conditions applied to every station found in the TRF catalogue. When examining the main solution in the initial processing, identical parameter selection was used. To obtain the final results, the main solution have to be executed twice. During the first iteration, the LSQ module detects outliers according to preselected criteria and writes an

outlier file for every session. After outlier detection, the main solution is run again, with the option to exclude the detected outliers. The outlier criteria used in the analysis excluded all the observations which exceeded the a posteriori standard deviation of unit weight by a factor of 5. The estimated parameters are listed in Table 2.

Table 2. Estimated parameters, estimation intervals and constraints with 24-hour sessions

Parameters	Interval	Constraint
Clock parameter	60 min	Relative 0.5 $\frac{ps^2}{s}$
ZWD	20 min	Relative 0.7 $\frac{ps^2}{s}$
NGR/EGR	360 min	Relative 2 $\frac{mm}{day}$
Station coordinates (X,Y,Z)	One offset per session	NNT/NNR
EOP		
Polar motion (x,y)	24 hours	Relative 10^{-4} $\frac{mas}{day}$
Nutation offset (dX,dY)	24 hours	Relative 10^{-4} $\frac{mas}{day}$
dUT1	24 hours	Relative 10^{-4} $\frac{ms}{day}$

To inspect the results of the LSQ adjustment, a Matlab script was written to read in the estimates from the VieVS results files. A more comprehensive program could be written, but for this example it was adequate to read the solution vectors to the Matlab workspace and perform the subsequent plotting and analysis manually. For each session one dUT1 was read and aligned with the mean estimation epoch. Each results file contains the adjustment for all stations. For this demonstration, the Wettzell was chosen for closer investigation. The code for the script is included appendix 5.

Figures 6, 7 and 8 display the adjustment to (X,Y,Z) a priori station coordinates for Wettzell VLBI station in 2008.

The root mean square (RMS) values and mean formal errors for the estimates are listed in Table 3.

Table 3. Station position RMS values and mean formal errors for WETTZELL in 2008

RMS_X(cm)	RMS_Y (cm)	RMS_Z cm	$\overline{\sigma_X}$ cm	$\overline{\sigma_Y}$ cm	$\overline{\sigma_Z}$ cm
0.59	0.52	0.79	0.29	0.24	0.41

The adjustment to a priori UT1 in relation to a priori values derived

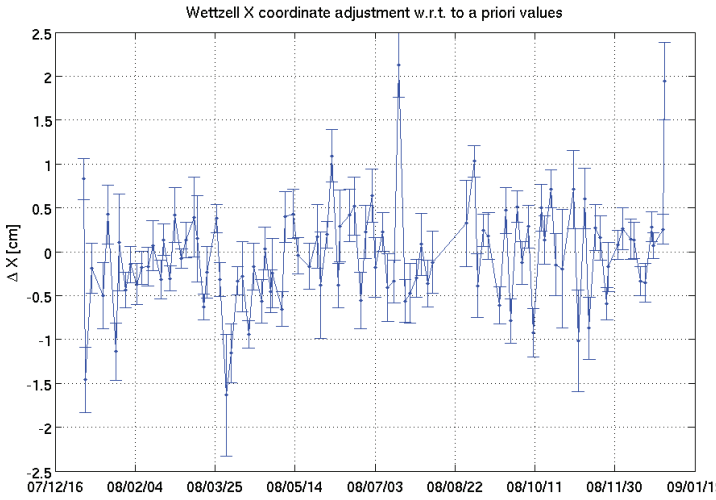

Figure 6. Adjustment in WETTZELL X coordinate w.r.t. a priori values in 2008

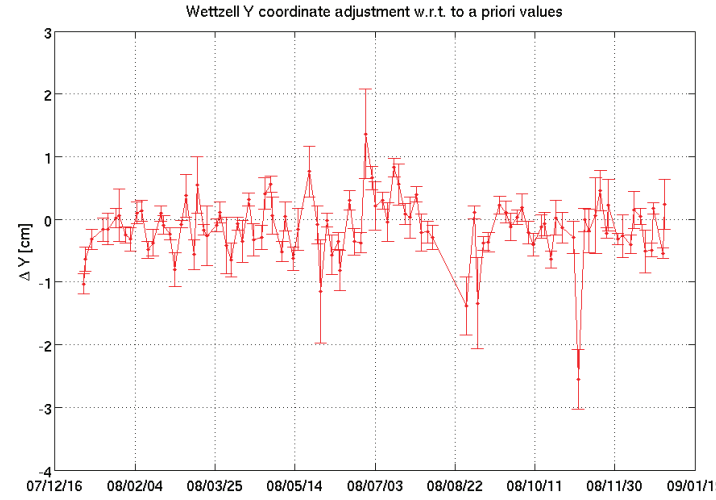

Figure 7. Adjustment in WETTZELL Y coordinate w.r.t. a priori values in 2008

from IVS-R1/R4 24-hour sessions in 2008 is displayed Figure 9.

The RMS values and mean formal errors for dUT1 estimates are listed in Table 4.

The estimated offsets to a priori values for Wettzell station coordinates and dUT1 are within reasonable range. After initial processing, no significant outlier values were detected. However, two observation sessions had to be excluded from the analysis altogether. The offset values for these

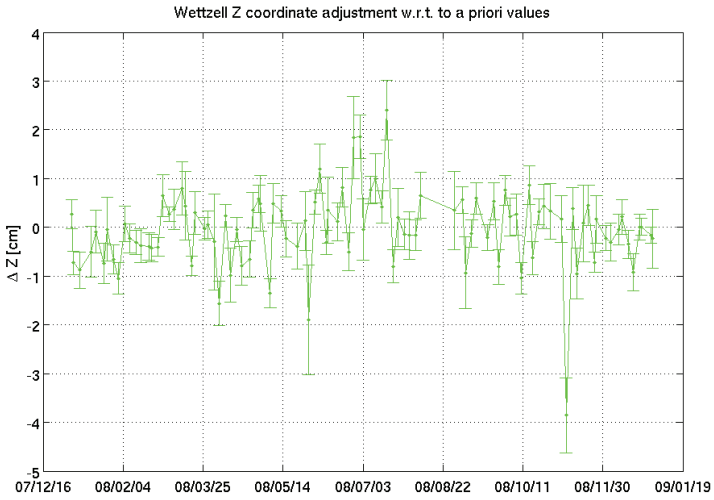

Figure 8. Adjustment in WETTZELL Z coordinate w.r.t. a priori values in 2008

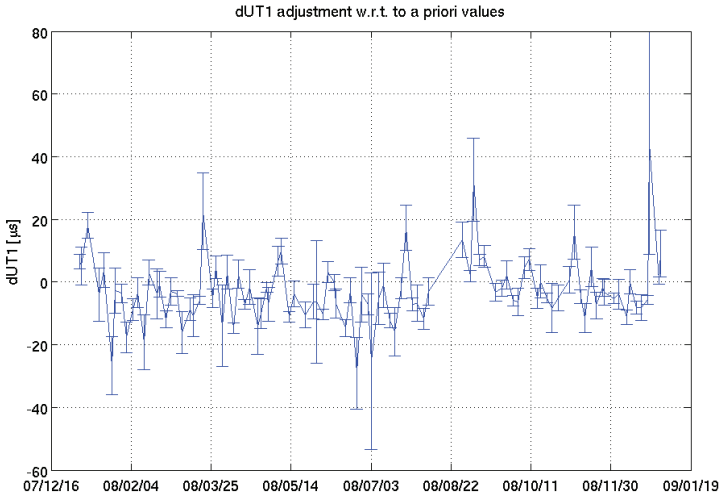

Figure 9. Adjustment to UT1 w.r.t. a priori values derived from IVS-R1/R4 sessions in 2008

Table 4. Adjustment to UT1 w.r.t. to a priori values derived from IVS-R1/R4 sessions in 2008

$RMS_{dUT1}(\mu s)$	$\overline{\sigma_{dUT1}}(\mu s)$
11.07	5.31

sessions deviated from the RMS values for both station position and dUT1 by an order of magnitude. Further analysis is required if these sessions are to be included in the analysis. If the reason for large station-wise residuals could be pinpointed to an appropriate source, it would be possible to correct for the error. Thus it would not be necessary to exclude the station from the observation session, increasing the number of stations in the network to approvable level and the session could be included in the analysis.

5 Conclusions

The VLBI observation process has several steps from observations to geodetic parameters. Challenges arise in observation and data acquisition as well as in data analysis. Due to the sensitive nature of the technique, some technological barriers, such as receiver quietness, are approaching levels in which it is extremely difficult to develop any improvement to the existing observation infrastructure. It is necessary to realize these limitations in order to lead the development in the most efficient direction. Modern precision and data turnaround requirements pose a challenge both technologically and economically. At the VLBI stations, ever increasing data recording rates are required in order to increase the effective observation bandwidth. VLBI2010 is the current criteria benchmark to which the VLBI observation network aims to accomplish. The main requirements postulated in VLBI2010 are 1 mm measurements accuracy on global baselines, continuous measurements for EOPs and station coordinates, and a turnaround time of less than 24h for initial geodetic results [2]. To reach these requirements, an updated VLBI observation network is being built. The approach is to increase the number of observing antennas by building fast moving unattended smaller antennas with continuous frequency broadband receivers. In addition to updates in observation equipment, the data handling is developed by creating more efficient and modern programs for correlation and VLBI data analysis. The VLBI analysis software VieVS used in this paper is an example of this modernization process. The development of the software becomes much more efficient, when it is decipherable without years of research in the field. It was demonstrated that using VieVS with a relatively straightforward analysis process geodetic parameters could be estimated to a reasonable degree of precision.

Bibliography

[1] Alan R. Whitney (2012). VLBI Data System & e-VLBI. URL: http://www.fs.wettzell.de/veranstaltungen/vlbi/tecspec2012/Session3/03-04_Whitney-VLBI data systems.pdf.

[2] Anon. (2012a). MIT Haystack Observatory geodesy information site. URL: http://www.haystack.mit.edu/geo/index.html.

[3] Anon. (2012b). MIT Haystack Observatory VLBI information site. URL: http://www.haystack.mit.edu/tech/vlbi/index.html.

[4] Anon. (2012c). NRAO information site for Green Bank Telescope. URL: https://science.nrao.edu/facilities/gbt/.

[5] Kamil Teke (2011). *Sub-daily parameter estimation in VLBI data analysis*. PhD thesis, Vienna University of Technology, TUWien.

[6] Karttunen, H. (2003). *Fundamental Astronomy*. Physics and Astronomy Online Library. Springer.

[7] Ryan, J. W. and Ma, C. (1998). Nasa-gsfc's geodetic vlbi program: a twenty-year retrospective. *Physics and Chemistry of the Earth*, 23(9-10):1041–1052.

[8] T. Nilsson, J. Böhm et al (2011). Status and future plans for the Vienna VLBI Software VieVS. In W. Alef, S. Bernhart and A. Nothnage, editor, *Proceedings of the 20th European VLBI for Geodesy and Astrometry Working Meeting*.

[9] Wayne Cannon (1999). Overview of VLBI. In International VLBI Service for Geodesy and Astrometry 1999 Annual Report, edited by N. R. Vandenberg.

Matlab code for reading VieVS result files

```
format long g

home = getenv('HOME');
vievsdir = '/vlbi/VieVS/VieVS_1d/VieVS';
subdir = 'data_final_out';
antenna = 'WETTZELL';

list = load([home vievsdir '/WORK/list_R1R4.mat']);

iter = length(list.process_list);

ind = 0;

for i=1:iter

        session = list.process_list(i,6:end);
```

```
remove = {'08JAN10XE_N004','08MAY19XA_N004'};

if(~max(strcmp(remove,session)))
        val = load([home vievsdir '/DATA/LEVEL3/' subdir, ...
                    '/x_' num2str(session)]);
else
        ind = ind + 1;
        del(ind) = i;
end

max_ind = length(val.x_.antenna);

for k=1:max_ind

        ant = val.x_.antenna(k);

        if(strcmp(antenna,ant.name))

                dut1_mjd = val.x_.dut1.mjd;
                dut1_val = val.x_.dut1.val;
                dut1_e = val.x_.dut1.mx;

                pos_mjd = val.x_.coorx(k).mjd;
                pos_x = val.x_.coorx(k).val;
                pos_xe = val.x_.coorx(k).mx;

                pos_y = val.x_.coory(k).val;
                pos_ye = val.x_.coory(k).mx;

                pos_z = val.x_.coorz(k).val;
                pos_ze = val.x_.coorz(k).mx;

                pos(i,1) = pos_mjd(1);
                pos(i,2) = pos_x(1);
                pos(i,3) = pos_xe(1);
                pos(i,4) = pos_y(1);
                pos(i,5) = pos_ye(1);
                pos(i,6) = pos_z(1);
                pos(i,7) = pos_ze(1);

        end

end

dut1(i,1) = mean(dut1_mjd);
dut1(i,2) = dut1_val(1);
dut1(i,3) = dut1_e(1);
```

```
end

pos(pos(:,1) == 0,:) = [];
pos(del,:) = [];
```

Science Network GNSS-verkon tasoitus ja antennikorkeuden ja -tyypin vaikutus koordinaatteihin

Ville Jussila

Aalto University School of Engineering
Department of Surveying and Planning
ville.jussila@aalto.fi

Abstract

Relative Positioning is the most accurate way to determine the coordinates with Global Navigation Satellite System. The methods and equipments varies a lot from basic GNSS positioning where distance between user and satellite is determined by code sent from satellites. Using more than one receiver which tracks GNSS signals carrier phase makes Relative Positioning possible. This seminar paper gives a short introduction to GNSS and explains the idea behind the Relative Positioning. Also theories of Adjustment Calculation and networks accuracy elements are explained in this paper. At spring 2011 Science Network GNSS campaign was carried out at Southern Finland. GNSS observations were done on eight scientifically interested places, including two Baltic Sea Mareographs. The goal of this paper is to determine the coordinates for those eight locations using Post Processing software and introduced Adjustment Theories. The accuracy of those eight points was in few millimetres in horizontal and vertical planes and network accuracy numbers gave an idea of reliable observations and well adjusted network. Also the importance of entering the correct antenna type and height to Post Processing software is introduced in this paper.

1. Johdanto

Keväällä 2011 suoritettiin Aalto yliopiston Maanmittaustieteiden laitoksen Geodesian maastoharjoitukset -kurssilla Science Network -mittauskampanja. Kurssin tarkoituksena oli tutustuttaa maanmittaustieteiden opiskelijat geodesian alan maastotöihin, kuten satelliitti- ja takymetrimittaukseen ja tarkkavaaitukseen. Mittauskampanjassa suoritettiin GNSS-mittaus seitsemällä tieteellisesti tärkeällä havaintokohteella Etelä-Suomessa.

Tämän tutkielma tarkoituksena on laskea havaintopaikkojen väliset havaintovektorit ja suorittaa havaintoverkon tasoitus. Kahden mareografin tasoitetut koordinaatit ovat erityisen mielenkiinnon kohteina. Tutkielmassa myös selvitetään väärän antenninkorkeuden ja antenniparametrien vaikutusta havaintopaikkojen koordinaatteihin. Työ toimii myös tutustumisena GNSS-havaintoverkkojen tasoitusprosessiin, joka on osa tulevaa diplomityötäni.

Työ on jaettu kuuteen osaan. Ensimmäisessä osassa esitellään Science Network ja itse mittauskampanja. Toisessa osassa tarkastellaan kirjallisuuslähteiden perusteella relatiivista mittausta, tasoituslaskentaa ja tasoituksen analysointia. Kirjallisuustutkielma perustuu kahteen satelliittipaikannusta käsittelevään kirjaan, yhteen tasoituslaskentaa käsittelevään ja yhteen tasoituksen tulosta käsittelevään julkaisuun. Kolmannessa osassa tarkastellaan Science Network -havaintojen käsittelyä ja neljännessä osassa tasoituksen tulokset ja tarkkuusluvut. Viides osa käsittelee kahta empiiristä koetta antennikorkeuden ja antennin kalibrointiarvojen vaikutuksesta havaitun pisteen tarkkuuteen. Lopuksi kuudennessa osassa esitellään johtopäätökset mittauskampanjasta, tuloksista ja empiirisistä kokeista.

2. Science Network

Science Network sisältää seitsemän havaintopaikkaa kattaen Länsi-Uudenmaan ja pääkaupunkiseudun. Havaintopaikkoja ovat Helsingin ja Hangon mareografit, Aalto yliopiston observatorio Espoon Otaniemessä, Ilmatieteenlaitoksen Kumpulan toimipiste Helsingissä, Tvärminnen biologinen tutkimusasema Hangossa ja Rokokallion ja Bredbergin EUREF-FIN-pisteet Vihdissä ja Inkoossa. Lisäksi havaintoaineistoa on saatu Geodeettisen laitoksen Sjökullan pysyvältä EUREF-pisteeltä

Kirkkonummelta ja Geotrim Oy:n VRS-verkon Hangon, Helsingin, Hyvinkään ja Lohjan tukiasemilta. Geotrim Oy:n ja Geodeettisen laitoksen pisteet toimivat havaintoverkossa kiinteinä pisteinä. Havaintopaikat ovat esitetty seuraavassa kuvassa: Kuva 1.

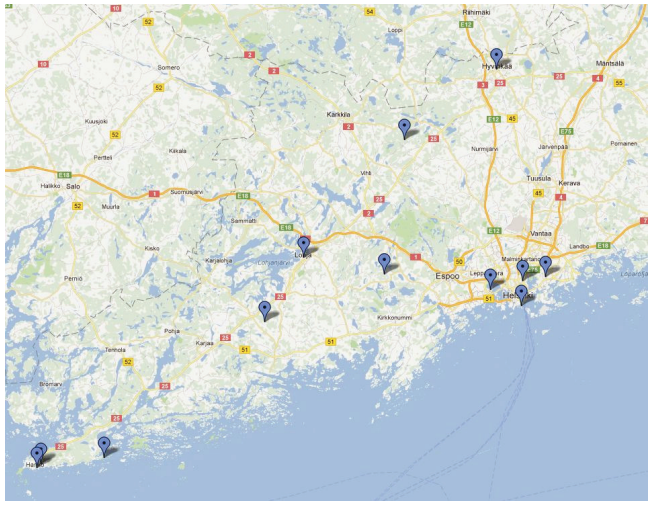

Kuva 1. Science Network -havaintopaikat keväällä 2011.

Taulukko 1. Mittausjaksot ja havaintoajat eri havaintopaikoilla.

Hav. paikka	Pist. tunnus	Havaintoaika (UTC)		Hav. väli (s)	Antenna tunnus	Antenna korkeus (m)
		24.5.2011	25.5.2011			
Bredberg	Bred	07:58:00–15:01:00	-	30	ASH700936A_M	1,4644
Rokokallio	Roko	-	06:39:00–12:00:15	15	ASH700936A_M	1,2551
Helsinki mareografi	Helsinki_mareo	06:25:00–15:00:30	05:57:00–11:59:30	30	ASH700936A_M	0,0350
Hanko mareografi	Hanko_mareo	09:15:20–15:01:30	06:17:00–11:05:15	15	ASH700936A_M	0,0350
Otaniemi	Otan	06:05:00–23:59:30	00:00:00–13:09:00	30	ASH700936A_M	0,3999
Kumpula	Kump	06:49:30–23:59:30	00:00:00–12:06:00	30	ASH700936A_M	0,0350
Tvärminne	Tvar	09:02:15–23:59:45	00:00:00–11:20:30	15	ASH700936A_M	1,2744
Metsähovi	METS	00:00:30–23:59:30	00:00:30–23:59:30	30	AOAD/M_T	0,0000
Hanko VRS	Hanko	06:00:00–23:59:45	00:00:00–14:59:45	15	TRM55971.00	0,0000
Helsinki VRS	Helsinki	06:00:00–23:59:45	00:00:00–14:59:45	15	TRM55971.00	0,0000
Hyvinkää VRS	Hyvinkaa	06:00:00–23:59:45	00:00:00–14:59:45	15	TRM55971.00	0,0000
Lohja VRS	Lohja	06:00:00–23:59:45	00:00:00–14:59:45	15	TRM55971.00	0,0000

GNSS-mittaus on suoritettu staattisena relatiivisena mittauksena 24.5.–25.5.2011 kuudella Ashtech Z-12 vastaanottimella ja Ashtech:n Choke Ring

-antennilla, joilla voidaan minimoida havaintosignaalin monitieheijastus. Otaniemen, Kumpulan ja Tvärminnen pisteillä havaintoaika on yli 24 tuntia, mareografeilla havainnot on suoritettu molempina päivinä kahtena 6-9 tuntia pitkänä sessiona, Rokokallion ja Bredbergin havaintoaika on 6–7 tuntia. Havaintoväli pisteillä on 5–30 sekuntia. Tarkat mittausjaksot ja havaintoväli havaintopaikoittain on esitetty seuraavassa taulukossa. Ks. Taulukko 1.

3. Menetelmät

Tässä osassa selvitetään havaintojen keräämiseen käytettyä staattisen relatiivisen satelliittipaikannuksen teoriaa. Aluksi tutustutaan lyhyesti GNSS-järjestelmään ja sen erilaisiin virhelähteisiin, jonka jälkeen tutustutaan relatiiviseen mittaukseen. Havaintojen käsittely, havaintoverkon tasoitus ja tulosten analysointi on tehty jälkilaskentaohjelmalla tilastollisia menetelmiä apuna käyttäen, jotka myös esitellään tässä osiossa.

3.1 Global Navigation Satellite System, GNSS

Satelliittipaikannusjärjestelmien kehittäminen on ollut pääasiassa suurvaltojen ja kansallisten yhteisöjen käsissä. Yhdysvaltojen GPS ja Venäjän GLONASS ovat tällä hetkellä ainoat täysin toimintakuntoiset paikannusjärjestelmät. Molempien järjestelmien luonteeseen kuuluu, että ne on kehitetty pääasiassa maiden asevoimien tarpeisiin. Euroopan Unioni, Japani ja Kiina ovat myös kehitelleet omia satelliittipaikannusjärjestelmiä.

Satelliittipaikannus perustuu trilateraatioon, jossa havaitsijan sijainti saadaan kolmen ympyrän leikkauskohdasta. Satelliitin ja havaitsijan välinen etäisyys ns. pseudoetäisyys saadaan signaali kulkuajan mittauksesta. Lähetysaika välitetään vastaanottimeen koodissa jota verrataan vastaanottimessa muodostettuun (koodihavainto). Pseudoetäisyydet ovat järjestelmällisesti liian lyhyitä tai pitkiä atomikellojen käynnistä johtuen, tästä syystä tarvitaan vielä yksi satelliitti vastaanottimen kellovirheen σ selvittämiseksi. Pseudoetäisyys ρ satelliitin xyz ja havaintopaikan XYZ välillä saadaan seuraavalla kaavalla:

$$\rho^k = \sqrt{(x^k - X)^2 + (y^k - Y)^2 + (z^k - Z)^2} - c\sigma\,. \qquad (1)$$

Yläindeksi kuvaa k-satelliittia ja c valonnopeutta tyhjiössä.

Järjestelmissä signaali kulkee vain yhteen suuntaan, satelliitista vastaanottimeen, mahdollistaen näin loputtoman käyttäjämäärän. Signaalia lähetetään suurilla kaistanleveyksillä, mikä mahdollistaa useiden signaalien vastaanottamisen samanaikaisesti. Satelliiteissa ja vastaanottimissa olevien atomikellojen avulla voidaan määrittää tarkasti signaalin lähetys- ja vastaanottoaika ja luoda kantoaaltojen taajuudet ja paikannussignaalit.

Atomikellojen laatu vaikuttaa suoraan paikannustarkkuuteen. Tästä syystä satelliiteissa käytetään tarkkoja Cesium- tai Rubium-atomikelloja tai uusimmissa satelliiteissa Vetymaser-atomikelloja. Vastaanottimissa kelloina toimivat heikompilaatuiset kvartsi-oskillaattorit. Atomikellot antavat paikannusjärjestelmälle sen mittakaavan.

GNSS-järjestelmät koostuvat kolmesta lohkosta: avaruus-, kontrolli- ja käyttäjälohko. Avaruuslohko käsittää satelliitit ja niiden konstellaation. Kontrollilohko käsittää hallinta-asemat, joista käsin järjestelmiä hallitaan ja ylläpidetään mm. ratojen hallinta ja ennustaminen, satelliittiajan ja kellokorjausten laskeminen ja tarvittavan referenssijärjestelmän ylläpito. Käyttäjälohko koostuu vastaanottimien siviilikäyttäjistä (Standard Positioning Service SPS) ja mahdollisesti vain järjestelmän haltijan valtuuttamista käyttäjistä (Presice Positioning Service PPS). (MISRA *et al,* 2001).

3.1.1 Satelliittipaikannuksen virhelähteet

Satelliittipaikannuksessa virhelähteitä on useita ja ne voidaan jakaa kontrollilohkon, signaalin kulkuun vaikuttaviin ja signaalin havaitsemiseen vaikuttaviin virheisiin. Virheiden suuruudet ovat esitetty seuraavassa taulukossa. Ks. Taulukko 2.

Kontrollilohkon virheitä ovat satelliitin kellovirheet ja satelliittien todelliset rataparametrit. Kontrolliasemat laskevat satelliiteille tarkat ratatiedot ns. ephemeriidit, jotka sisältävät satelliittien sijainnit ja nopeusvektorit radoilla. Kellokorjaukset ja ephemeriidit välitetään käyttäjille satelliittien navigointiviestien välityksellä.

Ilmakehä aiheuttaa radiosignaaliin refraktiota eli muutosta nopeuteen ja suuntaan. Ilmakehän alimmassa osassa Troposfäärissä signaalin kulkuun vaikuttaa siinä oleva vesihöyry. Suurin refraktion aiheuttaja on Ionosfääri, jossa sijaitseviin vapaisiin elektroneihin Auringon säteily vaikuttaa.

Signaalin havaitsemiseen liittyvät virheet ovat vastaanottimen elektroniikan ja antennin aiheuttama kohina ja signaalin monitieheijastus. Monitieheijastus tapahtuu, kun signaali ei saavu suoraan antenniin vaan heijastuu antennia lähellä olevasta kohteesta esimerkiksi rakennuksista, maasta ja vesipinnoista.

Taulukko 2. Paikannussignaalin virhelähteet ja niiden suuruudet.

Virhelaji	Suuruus (m)
Kontrollilohkon virhe	~3.0
Ionosfääri	1.0–10.0
Troposfääri	0.05–0.10
Monitieheijastus	1.0–5.0 (koodihavainnot) 0.01–0.05 (vaihehavainnot)
Vastaanottimen kohina	0.001–0.002

Käytettäessä koodihavaintoa SPS-käyttäjät pääsevät noin 15 m paikannustarkkuuteen edellä esitetyistä virhelähteistä johtuen.

Virheiden eliminoimiseksi ja tarkemman paikkaratkaisun saamiseksi tarvitaan kantoaaltohavaintoja. Kantoaaltohavainnoilla ja käytettäessä kaksitaajuus vastaanottimia kontrollilohkon virheet eliminoituvat ja ionosfäärin vaikutus saadaan lähes kokonaan poistettua. Troposfäärin aiheuttama refraktio voidaan korjata säähavainnoilla ja troposfäärimalleilla. Monitieheijastukset taas voidaan lähes kokonaan poistaa hyvällä antennisijoittelulla. Ainoaksi virhelähteeksi jää ideaaliolosuhteissa vastaanottimen kohina. (MISRA *et al,* 2001).

3.1.2 Kantoaaltohavainnot

Kantoaallon vaihe saadaan vertaamalla satelliitista vastaanotetun sinimuotoisen kantoaallon ja vastaanottimen luoman keinotekoisen kantoaallon eroa. Vastaanottimen pitää lisäksi selvittää täysien aallonpituuksien lukumäärä, jotta saadaan satelliitin ja vastaanottimen välinen etäisyys. Kantoaaltomittaus syklimuodossa satelliitin k ja havaitsijan u välillä on esitetty seuraavassa kaavassa:

$$\varphi_u^k = \frac{1}{\lambda} * [r_u^k - I_u^k + T_u^k] + f * (\sigma t_u - \sigma t^k) + N_u^k + \varepsilon_{\varphi,u}^k , \qquad (2)$$

missä λ on kantoaallon aallonpituus, r satelliitin ja havaitsijan välinen vektori, I ionosfääri-viive, T troposfääri-korjaus, f kantoaallon taajuus, σt_u vastaanottimen kellokorjaus, σt^k satelliitin kellokorjaus, N alkulukutuntematon ja ε mittausvirhe. Yhtälön välimerkit on asetettu plusmerkkisiksi, koska usein vaihe ja vektori ovat erimerkkiset.

Kantoaaltoon perustuva mittaus on jatkuvaa ja vastaanottimen kohinasta ja aiheutuneesta monitieheijastuksesta johtuen kantoaallon vaihe voidaan määrittää sadasosien tarkkuudella. Tämä mahdollistaa ideaaliolosuhteissa vaihe-etäisyyden havaitsemisen 2-10 mm tarkkuudella. Tarkkuutensa puolesta menetelmä on paljon käytetty geodeettisissa töissä. (MISRA *et al,* 2001).

3.2 Relatiivinen mittaus

Relatiivinen mittaus, suhteellinen mittaus, eroaa absoluuttipaikannuksesta siten, että siinä käytetään kahta vastaanotinta samanaikaisesti yhden sijasta. Havainnoista saadaan näiden kahden antennin välinen havaintovektori. Havaintovektorin ratkaisemiseksi taajuuksien kantoaaltohavainnoista muodostetaan erotushavaintoja. Relatiivisessa mittauksessa tärkeimpiä ovat kaksinkertaiset erotushavainnot, jotka saadaan yksinkertaisista erotushavainnoista. Paikannuksen virhelähteet, Ks. Taulukko 2, poistuvat havainnoista kaksinkertaisilla erotushavainnoilla jolloin paikannustarkkuus paranee. Relatiivisen mittauksen tarkkuus, eli havaintopaikkojen välisen vektorin suhteellinen tarkkuus on ≤ 5 mm + 1 ppm. (POUTANEN, 1998).

3.2.1 Yksinkertaiset erotushavainnot

Yksinkertainen erotushavainto muodostetaan kahden vastaanottimen u,r ja yhden satelliitin k välille:

$$\varphi_{ur}^{k} = \varphi_{u}^{k} - \varphi_{r}^{k} . \quad (3)$$

Erotushavainnossa satelliittien rata- ja kellovirheet eliminoituvat, samoin ionosfäärin ja troposfäärin vaikutukset kantoaaltoon, kun havaintopaikkojen välinen etäisyys on pieni ja signaalin voidaan olettaa kulkevan samanmuotoisen ilmakehän läpi. Yhtälöksi saadaan havaintopaikkojen välinen vaihe-ero, kun oletetaan, että ne havaitsevat samaa ajanhetkeä:

$$\varphi_{ur}^{k} = \frac{1}{\lambda} * r_{ur}^{k} + f * \sigma t_{ur} + N_{ur}^{k} + \varepsilon_{\varphi,ur}^{k} \quad (4)$$

(POUTANEN, 1998).

3.2.2 Kaksoiserotushavainnot

Tärkein kaksoiserotushavainto on kahden vastaanottimen ja kahden satelliitin välinen kaksoiserotus, joka on yksinkertaisten φ_{ur}^{k}, φ_{ur}^{l} erotushavaintojen erotus:

$$\varphi_{ur}^{kl} = \varphi_{ur}^{k} - \varphi_{ur}^{l} . \quad (5)$$

Kaksoiserotushavainnoilla päästää eroon vastaanottimen kellovirheestä, kun havaintoepookki on molemmilla vastaanottimilla sama:

$$\varphi_{ur}^{kl} = \frac{1}{\lambda} * r_{ur}^{kl} + N_{ur}^{kl} + \varepsilon_{\varphi,ur}^{kl} \quad (6)$$

Kantoaaltomittauksen havaintoyhtälöstä (2) jää kaksoiserotusten jälkeen vain paikkavektori r_{ur}^{kl}, alkulukutuntematon N_{ur}^{kl} ja mittausvirhe $\varepsilon_{\varphi,ur}^{kl}$. Signaalin kulkuun vaikuttavat ja kontrollilohkon virheet ovat poistuneet yhtälöstä. (POUTANEN, 1998).

3.2.3 Alkulukutuntematon

Alkulukutuntemattoman N oikea ratkaiseminen on oleellinen tekijä kantoaaltoon perustuvassa mittauksessa. Ratkaistaessa alkulukutuntematon väärin, on antennin ja satelliitin välinen etäisyys parhaimmassa tapauksessa virheellinen vain kantoaallon aallonpituuden verran.

Aloitettaessa mittaus vastaanotin havaitsee satelliitin lähettämän ja vastaanottimessa muodostetun kantoaallon vaihe-eron. Samalla alkaa se havaita muuttuneiden kokonaisten aallonpituuksien lukumäärää. Alkuhetken kokonaisten aallonpituuksien lukumäärä, alkulukutuntematon N, pysyy vakiona koko havaintojakson ajan. Signaalin tielle tulleet esteet (puut, rakennukset, havaitsijat), ionosfäärin äkillinen muutos, voimakas monitieheijastus tai vastaanottimen epäkunto aiheuttavat vaihekatkoja, jolloin saadaan uusi alkulukutuntematon N'. (POUTANEN, 1998).

3.3 Jälkilaskenta

Jälkilaskenta tapahtuu havaintotyön jälkeen ja sen hallinta ja oikeaoppisuus ovat tulosten kannalta tärkeitä. Jälkilaskentaohjelman tärkeimpiä ominaisuuksia on alkulukutuntemattomien ja vaihekatkojen havaitseminen ja korjaaminen. Jälkilaskentaohjelmaa tarvitaan myös paikannusjärjestelmien vertausjärjestelmien redukoimiseksi samaksi. Nykypäivänä käytössä olevat GPS- ja GLONASS-järjestelmät käyttävät molemmat eri referenssi- ja aikajärjestelmää, GPS-järjestelmällä referenssijärjestelmä on WGS84 ja aikastandardi GPSTime, kun GLONASS-järjestelmässä ne ovat vastaavasti PZ-90 ja GLONASSTime.

3.3.1 Alkulukutuntemattoman ratkaiseminen

Jälkilaskentaohjelmat ratkaisevat alkulukutuntemattoman kaksivaiheisesti. Aluksi saadaan alkulukutuntematon ratkaistua reaalilukuna ns. Float-ratkaisuna, jonka jälkeen käytetään lineaarikombinaatioita kokonaislukuratkaisun ns. Fixed-ratkaisun saamiseksi.

Alkulukutuntemattoman jäädessä reaaliluvuksi, heikentää se havaintovektorien ratkaisua.

Lineaarikombinaatiot muodostetaan kantoaallon taajuuksista summaamalla ja erottamalla niitä. Mahdollisia lineaarikombinaatioita ovat leveäkaista, kapeakaista ja ionosfäärivapaa kombinaatiot. (MISRA *et al,* 2001).

3.3.2 Havaintovektoreiden laskenta

Alkulukutuntemattoman ratkettua saadaan satelliitin ja antennin välinen etäisyys pituusyksiköissä:

$$L = \lambda \varphi_{ur}^{kl} , \tag{7}$$

missä λ on kantoaallon aallonpituus ja vaihehavainto sykleissä.

Paikkavektori r_{ur}^{kl} sisältää havaintopaikkojen koordinaattien kaksoiserotuksen:

$$r_{ur}^{kl} = (r_u^k - r_u^l) - (r_r^k - r_r^l). \tag{8}$$

Kukin näistä tekijöistä sisältää koordinaattituntemattomat satelliittiin ja antenniin Maan massakeskipisteen suhteen:

$$r_R^S = \sqrt{\left(X^s - X_r\right)^2 + \left(Y^s - Y_r\right)^2 + \left(Z^s - Z_r\right)^2}. \tag{9}$$

Satelliittien koordinaatit X^s, Y^s ja Z^s saadaan havaintoepookille navigointiviesteistä, jolloin niitä voidaan pitää laskennassa vakiona.

Vastaanottimen sijaintia voidaan nyt estimoida satelliitin sijainnin ja vaihe-etäisyyden avulla antamalla vastaanottimen sijainnille karkea arvio ja iteroimalla tulosta kunnes haluttu tarkkuus on saavutettu. Havaintopaikkojen välisen vektorin laskemiseksi toisen pisteen on oltava tunnettu. Jos kummatkaan pisteet eivät ole tunnettuja, voidaan toiselle laskea likiarvokoordinaatit muuntamalla toisesta järjestelmästä tai määrittää koodihavainnosta. Mitattaessa usean pisteen verkko relatiivisella mittauksella havaintovektorien laskeminen aloitetaan tunnetulta pisteeltä ja tuloksena saadaan vektorin toisen pisteen likiarvokoordinaatit, joita käytetään seuraavan pistevälin havaintovektorin laskennassa.

Vektorien laskeminen pitää suorittaa ennen varsinaista GNSS-verkon tasoitusta. Havaintovektoreiden avulla voidaan tarkastella mittauksen onnistumista, kun tutkitaan muodostuneiden kolmioiden ja monikulmioiden sulkuvirheitä. (KALLIO, 1998).

3.4 Tasoituslaskenta

GNSS-mittauksella havaintoja kerätään helposti huomattavasti enemmän kuin tuntemattomia on olemassa. Tämä mahdollistaa ns. pienimmän neliösumman estimaatin käytön tuntemattomien ratkaisemiseksi. Menetelmä on matemaattisesti suhteellisen yksinkertainen ja helppo käyttää, ja lisäksi sen avulla voidaan tilastollisesti testata havaintojen ja tulosten laatua. Jälkilaskettujen koordinaattien tarkkuus paranee tasoituksen jälkeen. Ks. Taulukko 3.

Taulukko 3. Jälkilaskettujen ja tasoitettujen koordinaattien tarkkuuksissa on eroja. Ylemmät koordinaatit ovat jälkilasketut ja alemmat tasoitetut koordinaatit, huomaa keskivirheen suuruus ylemmissä koordinaateissa.

Name	Latitude	Longitude	Ell.Height (m)	Std Dev n (m)	Std Dev e (m)	Std Dev u (m)
Bred	60°07'15,36817"N	23°54'27,04852"E	104,8429	0,0147	0,0112	0,0316
Kump	60°12'13,65719"N	24°57'39,77967"E	69,2324			
METS	60°13'02,90171"N	24°23'43,18182"E	93,9728	0,0166	0,0127	0,0358
Name	**Latitude**	**Longitude**	**Ell.Height (m)**	**Std Dev n (m)**	**Std Dev e (m)**	**Std Dev u (m)**
Bred	60°07'15,36817"N	23°54'27,04852"E	104,8429	0,0049	0,0039	0,0106
Kump	60°12'13,65724"N	24°57'39,77958"E	69,2287	0,0055	0,0042	0,0118
METS	60°13'02,90177"N	24°23'43,18170"E	93,9682	0,0033	0,0026	0,0071

3.4.1 Pienimmän neliösumman menetelmä

Pienimmän neliösumman estimaatissa etsitään havaitun ja tasoitetun arvon eroa, parannusta eli pienintä mahdollista arvoa. Muodostetaan ratkaistavista toisistaan riippumattomista n kappaletta olevista parametreista $x_i, i = 1 \ldots n$ $\boldsymbol{x}$-vektori ja m kappaletta olevista havaintosuureista $l_i, i = 1 \ldots m$ $\boldsymbol{l}$-vektori. Nämä vektorit liittyvät toisiinsa matemaattisen mallin avulla:

$$l = f(x) \tag{10}$$

Funktionaalinen malli koostuu yhtälöryhmästä, joilla esitetään havaintosuureiden ja tuntemattomien välinen suhde. (POUTANEN, 1998).

Tarvittavien yhtälöiden lukumäärä on $c = n - n_0 + u$, jossa n on havaintojen lukumäärä, n_0 havaintojen minimimäärä, jolla malli voidaan ratkaista ja u tuntemattomien parametrien lukumäärä. Redundanssi

$r = n - n_0$ eli ylimääritys on tasoituksen ns. vapausasteiden lukumäärä. (KALLIO, 1998).

Jos havainnot voidaan kirjoittaa parametrien lineaarisena funktiona, voidaan matemaattinen malli (10) kirjoittaa eksplisiittisessä muodossa:

$$l = A * x - v \tag{11}$$

missä A on havaintomatriisi, joka muuttaa parametriavaruuden x havaintoavaruudeksi l. Koska havaintoja on enemmän kuin tuntemattomia, tarvitaan lisäksi virhevektori v, jotta edellä annettu ehto toteutuisi. v:tä, residuaalia minimoidaan pienimmän neliösumman avulla kun $v_i = l_i - l_i$. Residuaali on siis tasoitetun havainnon l_i ja alkuperäisen havainnon erotus l_i.

Parannusten ääriarvo eli pienin neliösumma saadaan kun muodostetaan minimoitava funktio:

$$\sum_{i=1}^{n} v_i^2 = \sum_{i=1}^{n} (l_i - l_i)^2 = n * l_i^2 + \sum_{i=1}^{n} l_i^2 - 2 * l_i \sum_{i=1}^{n} l_i = minimi \tag{12}$$

ja lasketaan sen derivaatan nollakohdat. Saadaan yhtälöryhmä ns. normaaliyhtälö matriisimuodossa:

$$A^T P A x = A^T P l \tag{13}$$

Normaaliyhtälöstä saadaan tuntemattomien x ratkaisuksi:

$$x = A^T P l * (A^T P A)^{-1} \tag{14}$$

Normaaliyhtälössä P on painomatriisi, joka kuvaa havaintojen stokastista luonnetta. Havaintojen painot ovat kääntäen verrannollisia havaintojen variansseihin σ^2, kun havainnot eivät korreloi keskenään. Painomatriisia voidaan käyttää korostamaan tai heikentämään jotain havaintoa. Tunnettaessa havaintojen varianssit voidaan painot laskea. (POUTANEN, 1998).

3.4.2 Virheyhtälötasoitus

Usein käytetty tasoitusmalli on ns. virheyhtälötasoitus jossa jokaista havaintoa vastaa yksi yhtälö. Virheyhtälötasoituksessa l-vektori korvataan y-vektorilla sisältäen havainnot samalla tavalla. Tuntemattomat parametrit saadaan ratkaisemalla x, jonka jälkeen siirrytään tasoituksen analysointiin.

Jälkilaskennassa muodostetaan havaintopaikkojen välinen havaintovektori $(\Delta X, \Delta Y, \Delta Z)^T$, jota käytetään tasoituksessa havaintoina. Toisen pisteen koordinaatit asetetaan tunnetuksi ja lasketaan toiselle

pisteelle koordinaatit virheyhtälötasoituksena, jonka funktionaalinen malli on:

$$[X_B\ Y_B\ z_B]^T - [X_A\ Y_A\ Z_A]^T\ -\ [\Delta X_{AB}\ \Delta Y_{AB}\ \Delta Z_{AB}]^T = 0 \qquad (15)$$

Havaintopaikoista muodostetaan rakennematriisi A ja havainnoista, vektorikomponenteista havaintovektori y. Tuntemattomien eli havaintopaikan koordinaatit saadaan normaaliyhtälöiden ratkaisusta (14). (POUTANEN, 1998).

3.4.3 Virheyhtälötasoituksen analysointi

Tasoituksen analysoinnissa tarkastellaan residuaaleja v, painoyksikön keskivirhettä m_0^2, tuntemattomien parametrien kovarianssimatriisia C_x, tasoitettujen havaintojen kovarianssimatriisia $C_{l_{\hat{i}}}$ ja havaintojen redundanssilukuja. Kovarianssimatriisien lävistäjäalkioiden, varianssien σ^2 neliöjuurista saadaan keskivirheet σ kullekin havainnolle tai koordinaatille. Havaintojen ja tuntemattomien tarkkuutta kuvataan usein virhe-ellipseillä, joiden iso- ja pikkuakselien pituudet ovat akselien suunnassa olevat keskivirheet. (KALLIO, 1998).

3.5 Havaintoverkon tasoituksen vaiheet

Havaintoverkon tarkkuus siirtyy normaaliyhtälöiden myötä tuntemattomien parametrien kovarianssimatriisiin. Verkon tarkkuus on täysin riippuvainen verkon geometriasta, havaintojen tarkkuudesta ja siitä mikä verkossa on tunnettua eli nollavarianssikannasta. (KALLIO, 1998).

GNSS-havaintoverkon tasoitus tehdään kahdessa vaiheessa, ensiksi vapaana verkkona ja sitten kytkettynä verkkona. Vapaan verkon tasoituksella voidaan tutkia havaintoverkon sisäistä tarkkuutta, eli mittausmenetelmän tarkkuutta. Havaintoverkon ulkoista tarkkuutta, eli määritettävien pisteiden ja saadun vektoriverkon suhtautumista lähtöpisteisiin nähden, tutkitaan kytketyllä verkolla. (MARTIKAINEN *et al,* 2000; MAANMITTAUSLAITOS, 2003).

3.5.1 Sisäisen tarkkuuden tutkiminen

Mittauksen sisäistä tarkkuutta tutkitaan sulkeutuvien kuvioiden avulla. Kuvion havaintovektorit tulee olla mitattu vähintään kahdessa eri havaintojaksossa, jotta ne eivät korreloisi keskenään. Sulkeutuvista

kuvioista lasketaan suhteellinen sulkuvirhe, eli sulkuvirhevektorin ja silmukan pituuden D suhdeluku (ppm):

$$ppm = \frac{\sqrt{wX^2+wY^2+wZ^2}}{D} \quad (16)$$

Sisäistä tarkkuutta ja sessioiden välistä tarkkuutta voidaan tutkia kahteen kertaan mitattujen vektorien avulla. Suhdeluku (ppm) saadaan sessioiden välisen suurimman koordinaattieron ja vektorin pituuden S avulla:

$$ppm = \frac{\max(\Delta X,\Delta Y,\Delta Z)}{S} \quad (17)$$

(MARTIKAINEN *et al,* 2000).

3.5.2 Ulkoisen tarkkuuden tutkiminen

Mittauksen ulkoista tarkkuutta tutkitaan suhteellisella tasotarkkuudella. Tuntemattomien parametrien keskivirheiden neliösumman neliöjuuresta saadaan suhteellinen pistevirhe:

$$\Delta\sigma = \sqrt{\sigma_X^2 + \sigma_Y^2 + \sigma_z^2} \quad (18)$$

Suhteellisen pistevirheen $\Delta\sigma$ ja verkon lyhimmän vektorin etäisyyden S_{min} suhteesta saadaan ppm-luku, joka kertoo verkon tarkkuudesta:

$$ppm = \frac{\Delta\sigma}{s_{min}} \quad (19)$$

Mitä pienempi luku on sitä korkeammalla pistehierarkiassa havaintoverkko sijaitsee. (MARTIKAINEN *et al,* 2000).

3.5.3 Tulosteet

Havaintovektorien laskennan tuloksina tulee esittää

- pistevälien koordinaattierot
- alkulukutuntemattomien ratkaisut ja niiden tarkkuus
- koordinaattierojen kovarianssimatriisi
- pistevälin pituus ja
- painoyksikön keskivirhe

Verkkotasoituksen tuloksina tulee esittää

- vektorien jäännösvirheet, residuaalit
- pisteiden tasoitetut koordinaatit
- koordinaattien keskivirheet

– tasoituksen tunnusluvut ennen ja jälkeen tasoituksen
– painoyksikön keskivirhe ja
– painoyksikön keskivirhe / verkon lyhin sivunpituus.

(MARTIKAINEN *et al,* 2000)

4. Science Network -aineiston käsittely

Havaintoaineistojen binääritiedostot purettiin päivittäin ja varmuuskopioitiin tietokoneelle. Binääritiedostot muutettiin RINEX-formaattiin Teqc-ohjelmalla, jotta ne voitiin ladata jälkilaskentaohjelmaan, joka ei automaattisesti lukenut Ashtech:n tiedostoformaattia. Useamman päivän kestäneet havaintotiedostot jaettiin havaintopäiville erikseen helpottamaan tiedostojen käsittelyä. Jälkilaskenta suoritettiin Topcon Tools -ohjelmalla, jota voitiin käyttää sekä Demo-versiona viidellä havaintopisteellä että Yliopiston lisenssillä täydellisenä versiona. Jokaiselle havaintopaikalle määritettiin oikea käytetty antennityyppi, Ks. Taulukko 1, jotta antennityypin kalibrointitietojen perusteella voitiin määrittää antennin todellinen vaihekeskikohta, jossa signaali vastaanotetaan. Havaintopaikkojen koordinaatteja laskettiin myös ilman kalibrointitietoja.

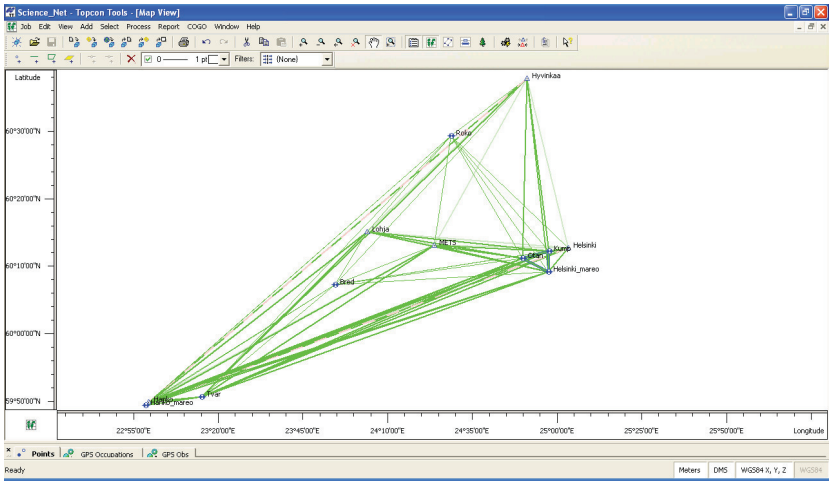

Kuva 2. Laskentaan hyväksytyt vektorit, kun alkulukutuntemattomien ratkaisun tarkkuudeksi asetettiin tasossa 0.03 ja korkeudessa 0.05 m.

Havaintovektorien ratkaiseminen oli jälkilaskennan ensimmäinen tehtävä. Tunnettujen pisteiden väliset havaintovektorit kytkettiin pois päältä niiden ollessa triviaalivektoreita. Havaintojen katkaisukulmaksi

asetettiin 15° horisontin yläpuolelle. Alkulukutuntemattomille saatiin Fixed-ratkaisut leveäkaista ja ionosfäärivapaalla kombinaatiolla.

Vektorien horisontaali- ja vertikaalitarkkuuksiksi asetettiin 0,03 m ja 0,05 m heikkojen kokonaislukuratkaisujen löytämiseksi ja vektorien sulkemiseksi pois laskennasta. Lyhimmillä vektoreilla tavoitetarkkuuksiin päästiin helposti. Pidemmillä vektoreilla Hangon ja pääkaupunkiseudun välillä etäisyyttä oli noin 135 km ja muutamassa tapauksessa horisontaalitarkkuus ylitti annetun arvon ja ko. vektorit suljettiin pois laskennasta: Kuva 2. Havaintovektorit, alkulukutuntemattomien ratkaisumenetelmät ja niiden tarkkuus, vektorien kovarianssimatriisi ja vektorin pituus vektoreittain on esitetty liitteissä: Liite 1.

5. Havaintoverkon tasoitus ja tulokset

5.1 Vapaan verkon ratkaisu

Vapaan verkon tasoituksen jälkeen tutkittiin mittauksen tarkkuutta kahdessa sessiossa havaittujen sulkeutuvien kuvioiden, silmukoiden avulla. Havaintoverkosta muodostettiin neljä silmukkaa, joissa kussakin oli kolme vektoria. Silmukat olivat Bred-Hanko-Tvar, Hanko-Tvar-Hanko_mareo, Helsinki_mareo-Otan-Kump ja METS-Roko-Kump. Tulokseksi saatiin jokaiselle silmukalla suhteellinen sulkuvirhe. Tulokset on esitetty seuraavassa taulukossa. Ks. Taulukko 4.

Taulukko 4. Mittauksen sisäisen tarkkuuden tutkiminen silmukoiden suhteellisten sulkuvirheiden avulla.

Loop	dHz (m)	dU (m)	Length (m)	dHz (ppm)	dU (ppm)
Bred-Hanko(24.5.2011 10:58:00) Bred-Tvar(24.5.2011 12:02:15) Hanko-Tvar(25.5.2011 3:00:00)	0,0029	0,0053	123065,9563	0,02	0,04
Hanko-Tvar(25.5.2011 3:00:00) Hanko-Hanko_mareo(24.5.2011 12:15:20) Hanko_mareo-Tvar(25.5.2011 9:17:00)	0,0061	0,0095	31320,4487	0,19	0,3
Helsinki_mareo-Otan(25.5.2011 8:57:00) Helsinki_mareo-Kump(25.5.2011 8:57:00) Kump-Otan(24.5.2011 9:49:30)	0,0017	0,0051	21188,2562	0,08	0,24
METS-Roko(25.5.2011 9:39:00) Kump-METS(24.5.2011 9:49:30) Kump-Roko(25.5.2011 9:39:00)	0,002	0,0111	103649,0125	0,02	0,11

Suhteellisten sulkuvirheiden perusteella voitiin todeta, että GNSS-mittaus onnistui erittäin hyvin, mihin vaikuttivat pitkät havaintoajat ja käytetyt Choke Ring -antennit signaalin monitieheijastusten minimoimiseksi.

Painoyksikön keskivirheellä tutkittiin havaintojen residuaalien ja havaintojen lukumäärän suhdetta. Á priori arvoksi asetettiin 1 ja vapaan verkon tasoituksen painoyksikön keskivirheeksi á posteriori saatiin 0,414. Tulos oli varsin odotettava, kun havainnoilla oli suuri ylimääritys ja havaintoajat olivat pitkiä. Vapaan verkon tasoituksen tunnusluvut on esitetty Liite 1:ssä.

5.2 Kytketyn verkon ratkaisu

Vapaan verkon tasoituksen jälkeen suoritettiin kytketyn verkon tasoitus. Hangon, Helsingin, Hyvinkään ja Lohjan VRS-tukiasemat ja Metsähovin EUREF-piste asetettiin verkon tunnetuiksi pisteiksi. Jälkilaskentaohjelmaan syötettiin pisteille niiden kolmiulotteiset WGS84-koordinaatit, jotka kerättiin pisteiden RINEX-tiedostoista. Ks. Taulukko 5.

Taulukko 5. Tunnettujen pisteiden kolmiulotteiset WGS84-koordinaatit.

Pnro	X(m)	Y(m)	Z(m)
Hanko	2958118,1720	1255094,4140	5491102,7140
Helsinki	2877741,4130	1345210,0990	5512290,0290
Hyvinkaa	2845663,2050	1318103,4840	5535418,6940
Lohja	2897031,7300	1293766,4410	5514557,6000
METS	2892571,1204	1311843,2621	5512633,9521

Kytketyn verkon tasoituksessa havaintovektoreille saatiin jäännösvirheet ja määritettäville pisteille keskivirheet. Kytketyn verkon tarkkuutta arvioitiin Roko-pisteellä ja Hanko-Hanko_mareo-vektorilla. Pisteen suhteellinen pistevirhe (18) oli kaikkein suurin, 0,0087 metriä, Ks. Taulukko 6 ja vektorin pituus lyhyin, 1275 m, Ks. Liite 1. Suhteellisen pistevirheen ja lyhimmän vektorin suhteeksi (19) saatiin 6,82 ppm.

Suhdeluvusta voitiin todeta, että vapaa verkko istuu hyvin lähtöpisteisiin nähden. Kytketyn verkon painoyksikön keskivirheeksi saatiin á posteriori 0,523 kun á priori arvo oli 1. Havaintovektorien residuaalit ja tasoituksen muut tunnusluvut on esitetty liitteissä. Ks. Liite 2. Määritettävien pisteiden maantieteelliset koordinaatit ETRS89-datumissa (GRS80 ellipsoidi) keskivirheineen on esitelty seuraavassa taulukossa. Ks. Taulukko 6.

Taulukko 6. Määritettävien pisteiden ETRS89 koordinaatit ja koordinaattien keskivirheet.

Name	Latitude	Longitude	Ell. Height (m)	Std Dev n (m)	Std Dev e (m)	Std Dev u (m)
Bred	60°07'15,35681"N	23°54'27,00063"E	105,4192	0,0032	0,0025	0,0069
Hanko_mareo	59°49'21,63864"N	22°58'35,43535"E	24,8138	0,0008	0,0007	0,0016
Helsinki_mareo	60°09'13,23541"N	24°57'24,23583"E	24,1269	0,0011	0,0009	0,0023
Kump	60°12'13,64608"N	24°57'39,73077"E	69,7839	0,0010	0,0008	0,0021
Otan	60°11'12,05953"N	24°49'42,88090"E	43,7080	0,0013	0,0010	0,0026
Roko	60°29'23,23201"N	24°28'39,79148"E	174,3559	0,0037	0,0028	0,0074
Tvar	59°50'36,30051"N	23°14'58,30964"E	21,7867	0,0021	0,0016	0,0042

6. Antenniparametrien vaikutus koordinaatteihin

Jälkilaskentaohjelmalla suoritettiin lisäksi tutkimus väärän antennikorkeuden vaikutuksesta määritettävän pisteen koordinaatteihin. Lisäksi testattiin, kuinka suuri merkitys on antennin kalibrointiarvojen käyttämisellä koordinaattien tarkkuuksiin.

Antennikorkeuden vaikutusta testattiin esittelemällä antennikorkeus kahdessa tapauksessa väärin. Referenssinä käytettiin Bred-METS-vektoria, jossa METS-havaintopaikka asetettiin tunnetuksi pisteeksi. Referenssiantennikorkeus Bred-pisteellä oli 1,4644 m. Ks. Taulukko 1. Ensimmäisessä tapauksessa antennikorkeudeksi asetettiin 14,644 m ja suoritettiin jälkilaskenta ja tulosten raportointi. Toisessa tapauksessa antennikorkeudeksi asetettiin 146,44 m ja suoritettiin jälkilaskenta ja raportointi. Tulokset antennikorkeuden muuttamiselle löytyvät liitteistä. Ks. Liite 3.

Antennikorkeuden muuttaminen aiheutti muutosta havaintovektorin pituuteen, kuten oli odotettavissa. Pitemmän/lyhyemmän havaintovektorin oletettiin muuttavan havaintopaikan maantieteellisiä koordinaatteja ja ellipsoidikorkeutta ja vaikuttavan sitä kautta keskivirheisiin ja havaintovektorien residuaaleihin. Antennikorkeuden muuttamiselle ei kuitenkaan ollut vaikutusta kuin ellipsoidikorkeuteen, samansuuruisena kuin esitelty antennin korkeusero. Pisteen ja havaintovektorien keskivirheet pysyivät samoina kuin referenssitapauksessa.

Antennin vaihekeskikohdan kalibrointiarvojen käyttöä tutkittiin tekemällä Bred-METS-vektorin jälkilaskenta kahdessa tapauksessa. Ensimmäisessä tapauksessa esiteltiin oikeat antennityypit havaintopaikoille ja laskettiin vektori. Toisessa tapauksessa jätettiin Bred-pisteen

antennityyppi esittelemättä. Tuloksista laskettiin kolmiulotteisten koordinaattien ero ja vektorin pituudeksi saatiin 0,0493 m. Ks. Liite 4.

7. Johtopäätökset

Yleisenä johtopäätöksenä voidaan sanoa, että kevään 2011 mittauskampanja onnistui hyvin. Mittauksen sisäinen tarkkuus, Ks. Taulukko 4 ja vähäinen käytöstä poistettujen vektorien määrä osoittavat tämän. Tasoituksen onnistumisesta kertovat sen tunnusluvut, havaintovektorien residuaalit pysyivät pieninä ja painoyksikön keskivirheeksi saatiin vapaan ja kytketyn verkon tasoituksessa alle annettu á priori arvo. Ulkoisen tarkkuuden tunnusluku 6,82 ppm osoittaa verkon yhtyvän hyvin lähtöpisteisiinsä. Tasoituksena tuloksena määritettäville pisteille saatiin maantieteelliset koordinaatit keskivirheineen ETRS89-datumissa. Ks. Taulukko 6. Vektoriverkon ja määritettävien pisteiden tarkkuuteen vaikuttivat suuresti pitkät havaintoajat ja käytetyt kaksitaajuusvastaanottimet.

Väärän antennikorkeuden esitteleminen ei antanut odotettuja tuloksia. Tuloksista voidaan kuitenkin päätellä, että antennikorkeuden syöttämisessä jälkilaskennassa tulee olla huolellinen, koska sen syöttäminen väärin ei näy havaintovektorien residuaaleissa tai pisteiden keskivirheissä. Tämä mahdollistaa huomattavan karkean virheen mahdollisuuden, mitä ei kyetä havaitsemaan residuaaleista tai keskivirheistä.

Antennin kalibrointitietojen syöttämisellä on myös suuri merkitys määritettävän pisteen tarkkuuteen. Tuloksista nähtiin, että esittelemättömillä antenniparametreilla on noin 5 cm vaikutus pisteen sijaintiin. Oikeiden antennikalibrointitietojen esittelyllä on siis suuri merkitys erityisesti runkopisteverkkojen laskennassa.

Tällä tutkimuksella oli myös suuri merkitys lopputyötäni ajatellen. Ennen tätä seminaarityötä en ollut käsitellyt GNSS-havaintoaineistoa, käyttänyt jälkilaskentaohjelmistoa verkkotasoitukseen tai analysoinut tasoituksen tuloksia. Tästä työstä saamani kokemus auttaa varmasti minua tulevassa projektissani.

Ongelmakohtien ymmärtäminen, jälkilaskentaohjelman käyttö ja tulosten oikea analysointi ovat nyt paremmin hallussa. Myös käsitys odotetuista tunnusluvuista on parempi. Työ oli mielenkiintoinen ja hyvä johdanto relatiivisten paikannushavaintojen käsittelyyn ja verkkotasoituksen maailmaan.

Viitteet

KALLIO, U. 1998. Tasoituslasku. Helsinki: Otatieto. 166 s. ISBN 951-672-267-9.

MAANMITTAUSLAITOS. 2003. Kaavoitusmittausohjeet. Helsinki. 57 s. MML/1/012/2003.

MARTIKANEN, M. & al. 2000. Numeerisen kartoituksen maastomittausohjeet. Otaniemi: Teknillinen korkeakoulu. 2. painos. 53 s. ISBN 951-22-5552-9.

MISRA, P. & ENGE, P. 2001. Global positioning system: signals, measurements, and performance. Lincoln (MA): Ganga-Jamuna Press. 390 s. ISBN 0-9709544-0-9.

POUTANEN, M. 1998. GPS-paikanmääritys. Helsinki, Suomi: Tähtitieteellinen yhdistys Ursa. 269 s. (URSAn julkaisuja, 0357-7937; [64]). ISBN 951-9269-89-4.

Liite 1: Raportti vapaan verkon tasoituksesta

Project name: Science_Net.ttp
Project folder: E:\Kurssit\Maa-6.3255 Seminar on Geodesy, Navigation and Positioning\Science_aineisto
Creation time: 8.3.2012 9:27:49
Created by: Ville
Comment:
Linear unit: Meters
Angular unit: DMS
Projection: FINLAND-TM35FIN
Datum: ETRS89
Geoid:
Time Zone: FLE Standard Time

GPS Observations

Name	dX (m)	dY (m)	dZ (m)	Distance (m)	Solution Type	Horz RMS (m)	Vert RMS (m)	SigmaX (m)	SigmaY (m)	SigmaZ (m)	CorrXY	CorrXZ	CorrYZ	Res X (m)	Res Y (m)	Res Z (m)
Bred–Hanko	45947,9703	-35857,8903	-16190,2546	60490,7316	Fixed,Wide Lane	0,0192	0,0316	0,0178	0,0146	0,0289	0,4460	0,5356	0,3895	-0,0013	-0,0020	-0,0034
Bred–Hanko_mareo	47040,9345	-36273,2666	-16698,6778	61704,4992	Fixed,Wide Lane	0,0208	0,0310	0,0171	0,0175	0,0282	0,5375	0,5762	0,2490	-0,0036	-0,0008	-0,0139
Bred–Helsinki	-34428,7908	54257,8001	4997,0815	64453,2492	Fixed,Wide Lane	0,0192	0,0330	0,0185	0,0143	0,0301	0,4789	0,5400	0,4220	0,0030	0,0059	0,0112
Bred–Helsinki_mareo	-27032,6678	51757,8464	1746,0391	58418,2201	Fixed,Wide Lane	0,0183	0,0314	0,0172	0,0138	0,0288	0,4756	0,5365	0,4130	0,0092	0,0052	0,0096
Bred–Hyvinkaa	-66507,0088	27151,1806	28125,7298	77145,4827	Fixed,Wide Lane	0,0210	0,0360	0,0204	0,0153	0,0330	0,4357	0,5381	0,3966	-0,0027	-0,0010	-0,0010
Bred–Kump	-31504,6487	49939,9203	4562,3150	59222,9115	Fixed,Wide Lane	0,0184	0,0316	0,0176	0,0137	0,0290	0,4672	0,5352	0,4168	0,0028	0,0063	0,0138
Bred–Lohja	-15138,4780	2814,1426	7264,6414	17025,5082	Fixed,Iono Free	0,0060	0,0101	0,0056	0,0042	0,0094	0,3896	0,5330	0,3302	-0,0017	-0,0007	-0,0027
Bred–METS	-19599,1030	20890,9531	5340,9660	29139,0233	Fixed,Iono Free	0,0100	0,0169	0,0090	0,0075	0,0158	0,4430	0,5174	0,3995	0,0008	-0,0013	0,0019
Bred–Otan	-26923,1442	43965,7645	3592,2893	51679,2868	Fixed,Wide Lane	0,0172	0,0295	0,0166	0,0126	0,0270	0,4673	0,5401	0,4041	0,0057	-0,0004	0,0081
Bred–Tvar	39191,8599	-22975,7427	-15540,1722	48014,4103	Fixed,Wide Lane	0,0151	0,0291	0,0158	0,0130	0,0256	0,6053	0,6310	0,6101	-0,0013	-0,0006	-0,0047
Hanko–Hanko_mareo	1092,9665	-415,3774	-508,4134	1274,9895	Fixed	0,0007	0,0012	0,0006	0,0005	0,0011	0,3646	0,4775	0,3218	0,0001	0,0003	-0,0006
Hanko–Hanko_mareo	1092,9666	-415,3778	-508,4120	1274,9892	Fixed	0,0007	0,0011	0,0007	0,0005	0,0011	0,4033	0,4566	0,2945	0,0001	-0,0001	0,0007
Hanko–Helsinki_mareo	-72980,6480	87615,7276	17936,2706	115431,3671	Fixed,Wide Lane	0,0280	0,0427	0,0254	0,0209	0,0392	0,3811	0,5160	0,2793	0,0005	-0,0017	-0,0101
Hanko–Helsinki_mareo	-72980,6424	87615,7342	17936,2862	115431,3710	Fixed,Wide Lane	0,0265	0,0437	0,0249	0,0172	0,0411	0,3723	0,4660	0,3625	0,0062	0,0048	0,0055
Hanko–Kump	-77452,6228	85797,8086	20752,5640	117434,4143	Fixed,Wide Lane	0,0264	0,0442	0,0241	0,0185	0,0416	0,4163	0,4914	0,3595	0,0004	0,0063	0,0116
Hanko–Kump	-77452,6304	85797,7978	20752,5379	117434,4067	Fixed,Wide Lane	0,0260	0,0444	0,0253	0,0200	0,0402	0,3777	0,6045	0,3327	-0,0074	-0,0043	-0,0146
Hanko–Otan	-72871,1160	79823,6556	19782,5406	109878,8626	Fixed,Wide Lane	0,0257	0,0427	0,0246	0,0171	0,0398	0,3771	0,5017	0,3282	0,0055	0,0024	0,0082
Hanko–Otan	-72871,1236	79823,6455	19782,5163	109878,8560	Fixed,Wide Lane	0,0253	0,0429	0,0232	0,0178	0,0403	0,3424	0,5593	0,2167	-0,0023	-0,0075	-0,0162
Hanko–Roko	-91400,6448	49997,9889	36608,9699	110426,8692	Fixed,Wide Lane	0,0272	0,0420	0,0302	0,0156	0,0367	0,2506	0,5629	0,1844	0,0037	-0,0042	0,0000
Hanko–Tvar	-6756,1102	12882,1458	650,0863	14560,8144	Fixed,Iono Free	0,0053	0,0088	0,0050	0,0042	0,0079	0,5104	0,5398	0,4524	0,0001	-0,0004	0,0027
Hanko–Tvar	-6756,1140	12882,1442	650,0789	14560,8144	Fixed,Iono Free	0,0055	0,0088	0,0052	0,0043	0,0078	0,5440	0,5511	0,4134	-0,0036	-0,0020	-0,0048
Hanko_mareo–Helsinki	-81469,7414	90531,0586	21695,7194	123708,9147	Fixed,Wide Lane	0,0275	0,0451	0,0265	0,0196	0,0412	0,4406	0,5036	0,4091	-0,0099	-0,0010	-0,0148
Hanko_mareo–Helsinki_mareo	-74073,5995	88031,1132	18444,7199	116518,5939	Fixed,Wide Lane	0,0288	0,0426	0,0228	0,0241	0,0393	0,5335	0,5561	0,2345	0,0155	0,0061	0,0264
Hanko_mareo–Helsinki_mareo	-74073,6213	88031,1055	18444,6757	116518,5950	Fixed,Wide Lane	0,0261	0,0441	0,0257	0,0172	0,0409	0,4105	0,5090	0,3521	-0,0066	-0,0012	-0,0176
Hanko_mareo–Hyvinkaa	-113547,9466	63424,4456	44824,3947	137568,2479	Fixed,Wide Lane	0,0292	0,0474	0,0281	0,0190	0,0442	0,3938	0,4798	0,3139	-0,0027	-0,0017	0,0001
Hanko_mareo–Kump	-78545,5824	86213,1873	21260,9902	118550,2083	Fixed,Wide Lane	0,0294	0,0428	0,0225	0,0247	0,0398	0,5187	0,5410	0,2286	0,0071	0,0075	0,0250
Hanko_mareo–Kump	-78545,6006	86213,1779	21260,9484	118550,2060	Fixed,Wide Lane	0,0266	0,0444	0,0256	0,0196	0,0405	0,4648	0,5200	0,4254	-0,0113	-0,0016	-0,0166
Hanko_mareo–Lohja	-62179,4129	39087,4100	23963,3039	77255,0642	Fixed,Wide Lane	0,0218	0,0357	0,0202	0,0144	0,0336	0,3775	0,4739	0,3338	0,0013	0,0009	-0,0040
Hanko_mareo–Lohja	-62179,4111	39087,4114	23963,3172	77255,0676	Fixed,Wide Lane	0,0245	0,0339	0,0179	0,0196	0,0324	0,4515	0,5101	0,0887	0,0030	0,0022	0,0093
Hanko_mareo–METS	-66640,0454	57164,2169	22039,6153	90522,8588	Fixed,Wide Lane	0,0217	0,0396	0,0208	0,0143	0,0375	0,3239	0,5477	0,3200	-0,0038	-0,0032	-0,0127
Hanko_mareo–METS	-66640,0371	57164,2202	22039,6453	90522,8622	Fixed,Wide Lane	0,0254	0,0373	0,0196	0,0213	0,0347	0,5210	0,5488	0,2265	0,0046	-0,0001	0,0173
Hanko_mareo–Otan	-73964,0947	80239,0255	20290,9288	110998,6951	Fixed,Wide Lane	0,0258	0,0429	0,0247	0,0166	0,0402	0,3941	0,4760	0,3530	-0,0071	-0,0049	-0,0163
Hanko_mareo–Otan	-73964,0760	80239,0319	20290,9709	110998,6950	Fixed,Wide Lane	0,0284	0,0414	0,0223	0,0240	0,0381	0,5274	0,5608	0,2244	0,0119	0,0012	0,0257
Hanko_mareo–Roko	-92493,6140	50413,3647	37117,3897	111688,3010	Fixed,Wide Lane	0,0296	0,0407	0,0301	0,0184	0,0359	0,1467	0,5461	0,0103	0,0008	-0,0060	0,0072
Hanko_mareo–Tvar	-7849,0714	13297,5255	1158,4974	15484,6447	Fixed,Iono Free	0,0063	0,0091	0,0065	0,0044	0,0078	0,5612	0,4782	0,4772	0,0054	0,0018	0,0009
Hanko_mareo–Tvar	-7849,0783	13297,5240	1158,4941	15484,6467	Fixed,Iono Free	0,0056	0,0096	0,0057	0,0046	0,0084	0,6394	0,5715	0,5681	-0,0015	0,0003	-0,0023
Helsinki–Helsinki_mareo	7396,1163	-2499,9527	-3251,0419	8457,0428	Fixed	0,0030	0,0050	0,0029	0,0020	0,0046	0,3609	0,4972	0,3439	-0,0006	0,0002	-0,0011
Helsinki–Helsinki_mareo	7396,1157	-2499,9507	-3251,0388	8457,0405	Fixed	0,0032	0,0050	0,0027	0,0024	0,0047	0,4375	0,5000	0,3406	-0,0011	0,0022	0,0020
Helsinki–Kump	2924,1429	-4317,8773	-434,7658	5232,9435	Fixed	0,0020	0,0033	0,0018	0,0015	0,0031	0,3426	0,5175	0,3034	0,0006	0,0029	0,0033
Helsinki–Kump	2924,1413	-4317,8807	-434,7718	5232,9459	Fixed	0,0021	0,0034	0,0018	0,0014	0,0033	0,3101	0,4537	0,3113	-0,0010	-0,0005	-0,0028
Helsinki–Otan	7505,6453	-10292,0355	-1404,7930	12815,3872	Fixed,Iono Free	0,0046	0,0075	0,0038	0,0031	0,0072	0,3070	0,4571	0,3062	0,0013	-0,0063	-0,0038
Helsinki–Otan	7505,6457	-10292,0342	-1404,7912	12815,3862	Fixed,Iono Free	0,0045	0,0075	0,0039	0,0033	0,0070	0,3636	0,5464	0,2630	0,0017	-0,0050	-0,0021
Helsinki–Roko	-11023,8725	-40117,6930	15421,6579	44370,9656	Fixed,Wide Lane	0,0159	0,0254	0,0188	0,0092	0,0214	0,2905	0,6234	0,2358	0,0106	-0,0037	0,0096
Helsinki–Tvar	73620,6646	-77233,5345	-20537,2194	108659,0930	Fixed,Wide Lane	0,0269	0,0416	0,0275	0,0212	0,0354	0,5445	0,5743	0,4379	0,0092	0,0020	0,0185
Helsinki–Tvar	73620,6506	-77233,5452	-20537,2530	108659,0974	Fixed,Wide Lane	0,0256	0,0425	0,0261	0,0214	0,0363	0,6072	0,5914	0,5426	-0,0046	-0,0090	-0,0152
Helsinki_mareo–Hyvinkaa	-39474,3382	-24606,6629	26379,6939	53475,2231	Fixed,Wide Lane	0,0180	0,0298	0,0174	0,0117	0,0277	0,3547	0,4969	0,3170	-0,0091	-0,0033	-0,0074
Helsinki_mareo–Hyvinkaa	-39474,3270	-24606,6602	26379,7106	53475,2218	Fixed,Wide Lane	0,0194	0,0288	0,0165	0,0145	0,0269	0,3894	0,4774	0,2649	0,0022	-0,0006	0,0092
Helsinki_mareo–Kump	-4471,9745	-1817,9274	2816,2718	5588,8105	Fixed	0,0021	0,0034	0,0020	0,0014	0,0032	0,3784	0,4868	0,3882	0,0001	-0,0001	0,0000
Helsinki_mareo–Kump	-4471,9747	-1817,9279	2816,2707	5588,8102	Fixed	0,0021	0,0034	0,0019	0,0017	0,0032	0,4818	0,5123	0,3959	-0,0001	-0,0006	-0,0011
Helsinki_mareo–Lohja	11894,1955	-48943,7006	5518,6081	50669,6433	Fixed,Wide Lane	0,0176	0,0290	0,0161	0,0112	0,0277	0,3153	0,4541	0,3241	-0,0052	-0,0026	-0,0064
Helsinki_mareo–Lohja	11894,2016	-48943,6957	5518,6221	50669,6415	Fixed,Wide Lane	0,0187	0,0283	0,0164	0,0133	0,0266	0,3442	0,4846	0,2146	0,0009	0,0023	0,0076
Helsinki_mareo–METS	7433,5673	-30866,8910	3594,9298	31952,2519	Fixed,Wide Lane	0,0111	0,0184	0,0108	0,0073	0,0171	0,3764	0,4926	0,3587	-0,0059	-0,0042	-0,0048
Helsinki_mareo–METS	7433,5753	-30866,8872	3594,9423	31952,2515	Fixed,Wide Lane	0,0104	0,0188	0,0107	0,0076	0,0170	0,4247	0,6144	0,3075	0,0021	-0,0003	0,0077
Helsinki_mareo–Otan	109,5247	-7792,0751	1846,2521	8008,5627	Fixed	0,0029	0,0048	0,0026	0,0019	0,0046	0,3195	0,4480	0,2798	-0,0024	0,0012	0,0004
Helsinki_mareo–Otan	109,5291	-7792,0736	1846,2539	8008,5618	Fixed	0,0030	0,0049	0,0027	0,0021	0,0046	0,4104	0,4819	0,3090	0,0019	0,0027	0,0022
Helsinki_mareo–Roko	-18420,0004	-37617,7357	18672,6923	45859,1309	Fixed,Wide Lane	0,0175	0,0256	0,0195	0,0096	0,0221	0,2156	0,5303	0,2295	-0,0005	0,0006	0,0031
Helsinki_mareo–Tvar	66224,5428	-74733,5791	-17286,1972	101339,0869	Fixed,Wide Lane	0,0232	0,0424	0,0262	0,0173	0,0367	0,5386	0,6067	0,5440	0,0045	0,0043	-0,0001
Helsinki_mareo–Tvar	66224,5370	-74733,5834	-17286,1825	101339,0837	Fixed,Wide Lane	0,0267	0,0400	0,0263	0,0202	0,0348	0,5742	0,5379	0,3474	-0,0015	0,0002	0,0145
Hyvinkaa–Kump	35002,3591	22788,7368	-23563,4183	47955,4621	Fixed,Wide Lane	0,0164	0,0278	0,0150	0,0114	0,0262	0,3937	0,4928	0,3537	0,0045	0,0045	0,0113
Hyvinkaa–Kump	35002,3484	22788,7326	-23563,4335	47955,4598	Fixed,Wide Lane	0,0169	0,0275	0,0145	0,0131	0,0257	0,3961	0,5258	0,3519	-0,0062	0,0003	-0,0039
Hyvinkaa–Otan	39583,8636	16814,5819	-24533,4399	49512,6458	Fixed,Wide Lane	0,0170	0,0286	0,0154	0,0117	0,0271	0,3702	0,4883	0,3251	0,0073	-0,0013	0,0098
Hyvinkaa–Otan	39583,8533	16814,5784	-24533,4561	49512,6444	Fixed,Wide Lane	0,0174	0,0283	0,0150	0,0123	0,0270	0,3673	0,4971	0,2412	-0,0030	-0,0049	-0,0065
Hyvinkaa–Roko	21054,3276	-13011,0771	-7707,0144	25922,4016	Fixed,Iono Free	0,0095	0,0151	0,0112	0,0055	0,0127	0,3171	0,6163	0,2423	-0,0017	-0,0004	-0,0021
Hyvinkaa–Tvar	105698,8578	-50126,9312	-43665,9104	124866,6069	Fixed,Wide Lane	0,0275	0,0454	0,0254	0,0217	0,0413	0,5268	0,5300	0,4309	-0,0095	-0,0075	-0,0122
Hyvinkaa–Tvar	105698,8649	-50126,9205	-43665,8917	124866,6020	Fixed,Wide Lane	0,0290	0,0445	0,0282	0,0238	0,0383	0,6121	0,5580	0,4451	-0,0026	0,0033	0,0065
Kump–Lohja	16366,1732	-47125,7740	2702,3345	49959,9120	Fixed,Wide Lane	0,0170	0,0291	0,0159	0,0113	0,0274	0,3331	0,5085	0,3189	-0,0021	-0,0033	-0,0082
Kump–Lohja	16366,1825	-47125,7682	2702,3498	49959,9104	Fixed,Wide Lane	0,0178	0,0286	0,0166	0,0132	0,0261	0,3318	0,5525	0,3005	0,0072	0,0026	0,0071
Kump–METS	11905,5480	-29048,9644	778,6541	31403,6735	Fixed,Wide Lane	0,0108	0,0183	0,0094	0,0076	0,0174	0,3916	0,4787	0,3725	0,0002	-0,0049	-0,0087
Kump–METS	11905,5520	-29048,9601	778,6634	31403,6713	Fixed,Wide Lane	0,0100	0,0187	0,0096	0,0079	0,0172	0,4469	0,6366	0,3700	0,0042	-0,0006	0,0006

Kump–Otan	4581,5002	-5974,1476	-970,0204	7590,8842	Fixed	0,0029	0,0048	0,0024	0,0020	0,0046	0,3212	0,4402	0,3225	-0,0016	0,0014	-0,0004
Kump–Otan	4581,5014	-5974,1467	-970,0190	7590,8841	Fixed	0,0028	0,0046	0,0024	0,0021	0,0044	0,3287	0,5062	0,2759	-0,0003	0,0023	0,0011
Kump–Roko	-13948,0194	-35799,8095	15856,4207	41564,4040	Fixed,Wide Lane	0,0159	0,0235	0,0180	0,0093	0,0198	0,3083	0,5595	0,3033	0,0060	-0,0005	0,0033
Kump–Tvar	70696,5095	-72915,6622	-20102,4801	103531,6374	Fixed,Wide Lane	0,0234	0,0425	0,0249	0,0191	0,0370	0,5969	0,6050	0,5548	-0,0034	-0,0061	-0,0113
Kump–Tvar	70696,5202	-72915,6533	-20102,4532	103531,6332	Fixed,Wide Lane	0,0255	0,0413	0,0258	0,0207	0,0355	0,5953	0,5870	0,4618	0,0071	0,0030	0,0156
Lohja–Otan	-11784,6710	41151,6191	-3672,3594	42963,0125	Fixed,Wide Lane	0,0150	0,0248	0,0138	0,0099	0,0235	0,3453	0,4821	0,3164	0,0026	-0,0026	0,0034
Lohja–Otan	-11784,6771	41151,6159	-3672,3731	42963,0123	Fixed,Wide Lane	0,0152	0,0246	0,0139	0,0106	0,0230	0,3392	0,5264	0,2131	-0,0035	-0,0057	-0,0103
Lohja–Roko	-30314,2114	11325,9617	13154,0651	34932,1950	Fixed,Wide Lane	0,0127	0,0201	0,0155	0,0067	0,0167	0,1418	0,6578	0,1444	-0,0107	0,0000	-0,0094
Lohja–Tvar	54330,3438	-25789,8821	-22804,8089	64319,2318	Fixed,Wide Lane	0,0194	0,0330	0,0206	0,0153	0,0283	0,6178	0,5914	0,5012	0,0062	0,0033	0,0027
Lohja–Tvar	54330,3447	-25789,8777	-22804,7973	64319,2268	Fixed,Wide Lane	0,0207	0,0322	0,0205	0,0169	0,0276	0,6384	0,5650	0,4509	0,0071	0,0078	0,0142
METS–Otan	-7324,0442	23074,8096	-1748,6801	24272,3370	Fixed,Iono Free	0,0088	0,0140	0,0071	0,0060	0,0137	0,3019	0,4325	0,2767	0,0019	-0,0009	0,0028
METS–Otan	-7324,0458	23074,8012	-1748,6857	24272,3299	Fixed,Iono Free	0,0088	0,0139	0,0074	0,0063	0,0132	0,2850	0,5120	0,1950	0,0002	-0,0093	-0,0028
METS–Roko	-25853,5706	-6750,8472	15077,7559	30680,9350	Fixed,Wide Lane	0,0102	0,0186	0,0133	0,0059	0,0155	0,3133	0,7275	0,2217	0,0025	0,0023	0,0014
METS–Tvar	58790,9527	-43866,7048	-20881,1497	76267,2035	Fixed,Wide Lane	0,0211	0,0359	0,0199	0,0172	0,0323	0,5703	0,5519	0,4938	-0,0123	-0,0082	-0,0181
METS–Tvar	58790,9636	-43866,6984	-20881,1222	76267,2006	Fixed,Wide Lane	0,0228	0,0349	0,0229	0,0189	0,0292	0,6905	0,5871	0,4408	-0,0016	-0,0017	0,0094
Otan–Roko	-18529,5242	-29825,6569	16826,4425	38936,3872	Fixed,Wide Lane	0,0146	0,0220	0,0165	0,0083	0,0189	0,2592	0,5561	0,2499	0,0029	0,0031	0,0051
Otan–Tvar	66115,0145	-66941,5013	-19132,4316	96012,5496	Fixed,Wide Lane	0,0246	0,0398	0,0244	0,0201	0,0344	0,6186	0,5813	0,4403	0,0032	0,0059	0,0171
Otan–Tvar	66115,0088	-66941,5079	-19132,4562	96012,5551	Fixed,Wide Lane	0,0229	0,0407	0,0247	0,0181	0,0353	0,5878	0,6013	0,5268	-0,0023	-0,0008	-0,0074
Roko–Tvar	84644,5559	-37115,8438	-35958,8673	99173,2164	Fixed,Wide Lane	0,0239	0,0413	0,0310	0,0151	0,0330	0,4498	0,7087	0,3930	0,0179	0,0032	0,0188

Adjustment type: Plane + Height, Inner constraint
Confidence level: 95 %
Number of adjusted points: 12
Number of plane control points: 0
Number of used GPS vectors: 88
A posteriori plane or 3D UWE: 0,4142163 , Bounds: (0,8883424 , 1,111492)
Number of height control points: 0
A posteriori height UWE: 0,4045537 , Bounds: (0,8422008 , 1,15748)

Point Summary

Name	Latitude	Longitude	Ell.Height (m)	Std Dev n (m)	Std Dev e (m)	Std Dev u (m)	Control
Bred	60°07'15,35697"N	23°54'27,00126"E	105,4214	0,0036	0,0028	0,0077	None
Hanko	59°49'53,47317"N	22°59'27,36945"E	40,1387	0,0021	0,0017	0,0042	None
Hanko_mareo	59°49'21,63859"N	22°58'35,43573"E	24,8181	0,0020	0,0017	0,0041	None
Helsinki	60°12'43,75084"N	25°03'14,03743"E	37,3475	0,0016	0,0012	0,0035	None
Helsinki_mareo	60°09'13,23563"N	24°57'24,23627"E	24,1311	0,0016	0,0011	0,0034	None
Hyvinkaa	60°37'51,19661"N	24°51'12,40022"E	150,7858	0,0043	0,0033	0,0090	None
Kump	60°12'13,64630"N	24°57'39,73121"E	69,7883	0,0015	0,0011	0,0033	None
Lohja	60°15'07,73864"N	24°03'53,09548"E	100,7881	0,0035	0,0027	0,0073	None
METS	60°13'02,89069"N	24°23'43,13404"E	94,5408	0,0028	0,0022	0,0061	None
Otan	60°11'12,05975"N	24°49'42,88135"E	43,7112	0,0016	0,0012	0,0035	None
Roko	60°29'23,23220"N	24°28'39,79204"E	174,3559	0,0039	0,0030	0,0079	None
Tvar	59°50'36,30050"N	23°14'58,31005"E	21,7909	0,0024	0,0019	0,0050	None

Liite 2: Raportti kytketyn verkon tasoituksesta

Project name: Science_Net.ttp
Project folder: E:\Kurssit\Maa-6.3255 Seminar on Geodesy, Navigation and Positioning\Science_aineisto
Creation time: 8.3.2012 9:27:49
Created by: Ville
Comment:
Linear unit: Meters
Angular unit: DMS
Projection: FINLAND-TM35FIN
Datum: ETRS89
Geoid:
Time Zone: FLE Standard Time

GPS Observations

Name	dX (m)	dY (m)	dZ (m)	Distance (m)	Solution Type	Horz RMS (m)	Vert RMS (m)	SigmaX (m)	SigmaY (m)	SigmaZ (m)	CorrXY	CorrXZ	CorrYZ	Res X (m)	Res Y (m)	Res Z (m)
Bred–Hanko	45947,9703	-35857,8903	-16190,2546	60490,7316	Fixed,Wide Lane	0,0192	0,0316	0,0178	0,0146	0,0289	0,4460	0,5356	0,3895	0,0070	-0,0027	-0,0046
Bred–Hanko_mareo	47040,9345	-36273,2666	-16698,6778	61704,4992	Fixed,Wide Lane	0,0208	0,0310	0,0171	0,0175	0,0282	0,5375	0,5762	0,2490	0,0044	-0,0014	-0,0150
Bred–Helsinki	-34428,7908	54257,8001	4997,0815	64453,2492	Fixed,Wide Lane	0,0192	0,0330	0,0185	0,0143	0,0301	0,4789	0,5400	0,4220	0,0050	0,0026	0,0165
Bred–Helsinki_mareo	-27032,6678	51757,8464	1746,0391	58418,2201	Fixed,Wide Lane	0,0183	0,0314	0,0172	0,0138	0,0288	0,4756	0,5365	0,4130	0,0098	0,0022	0,0122
Bred–Hyvinkaa	-66507,0088	27151,1806	28125,7298	77145,4827	Fixed,Wide Lane	0,0210	0,0360	0,0204	0,0153	0,0330	0,4357	0,5381	0,3966	-0,0051	-0,0017	-0,0002
Bred–Kump	-31504,6487	49939,9203	4562,3150	59222,9115	Fixed,Wide Lane	0,0184	0,0316	0,0176	0,0137	0,0290	0,4672	0,5352	0,4168	0,0036	0,0033	0,0167
Bred–Lohja	-15138,4780	2814,1426	7264,6414	17025,5082	Fixed,Iono Free	0,0060	0,0101	0,0056	0,0042	0,0094	0,3896	0,5330	0,3302	0,0007	0,0032	0,0053
Bred–METS	-19599,1030	20890,9531	5340,9660	29139,0233	Fixed,Iono Free	0,0100	0,0169	0,0090	0,0075	0,0158	0,4430	0,5174	0,3995	-0,0147	-0,0073	-0,0221
Bred–Otan	-26923,1442	43965,7645	3592,2893	51679,2868	Fixed,Wide Lane	0,0172	0,0295	0,0166	0,0126	0,0270	0,4673	0,5401	0,4041	0,0059	-0,0033	0,0099
Bred–Tvar	39191,8599	-22975,7427	-15540,1722	48014,4103	Fixed,Wide Lane	0,0151	0,0291	0,0158	0,0130	0,0256	0,6053	0,6310	0,6101	0,0048	-0,0014	-0,0057
Hanko–Hanko_mareo	1092,9665	-415,3774	-508,4134	1274,9895	Fixed	0,0007	0,0012	0,0006	0,0005	0,0011	0,3646	0,4775	0,3218	-0,0003	0,0003	-0,0005
Hanko–Hanko_mareo	1092,9666	-415,3778	-508,4120	1274,9892	Fixed	0,0007	0,0011	0,0007	0,0005	0,0011	0,4033	0,4566	0,2945	-0,0003	-0,0001	0,0008
Hanko–Helsinki_mareo	-72980,6480	87615,7276	17936,2706	115431,3671	Fixed,Wide Lane	0,0280	0,0427	0,0254	0,0209	0,0392	0,3811	0,5160	0,2793	-0,0071	-0,0042	-0,0062
Hanko–Helsinki_mareo	-72980,6424	87615,7342	17936,2862	115431,3710	Fixed,Wide Lane	0,0265	0,0437	0,0249	0,0172	0,0411	0,3723	0,4660	0,3625	-0,0015	0,0023	0,0094
Hanko–Kump	-77452,6228	85797,8086	20752,5640	117434,4143	Fixed,Wide Lane	0,0264	0,0442	0,0241	0,0185	0,0416	0,4163	0,4914	0,3595	-0,0071	0,0038	0,0159
Hanko–Kump	-77452,6304	85797,7978	20752,5379	117434,4067	Fixed,Wide Lane	0,0260	0,0444	0,0253	0,0200	0,0402	0,3777	0,6045	0,3327	-0,0149	-0,0068	-0,0103
Hanko–Otan	-72871,1160	79823,6556	19782,5406	109878,8626	Fixed,Wide Lane	0,0257	0,0427	0,0246	0,0171	0,0398	0,3771	0,5017	0,3282	-0,0026	-0,0001	0,0113
Hanko–Otan	-72871,1236	79823,6455	19782,5163	109878,8560	Fixed,Wide Lane	0,0253	0,0429	0,0232	0,0178	0,0403	0,3424	0,5593	0,2167	-0,0104	-0,0100	-0,0131
Hanko–Roko	-91400,6448	49997,9889	36608,9699	110426,8692	Fixed,Wide Lane	0,0272	0,0420	0,0302	0,0156	0,0367	0,2506	0,5629	0,1844	-0,0063	-0,0054	-0,0001
Hanko–Tvar	-6756,1102	12882,1458	650,0863	14560,8144	Fixed,Iono Free	0,0053	0,0088	0,0050	0,0042	0,0079	0,5104	0,5398	0,4524	-0,0021	-0,0005	0,0028
Hanko–Tvar	-6756,1140	12882,1442	650,0789	14560,8144	Fixed,Iono Free	0,0055	0,0088	0,0052	0,0043	0,0078	0,5440	0,5511	0,4134	-0,0059	-0,0021	-0,0046

Hanko_mareo–Helsinki	-81469,7414	90531,0586	21695,7194	123708,9147	Fixed,Wide Lane	0,0275	0,0451	0,0265	0,0196	0,0412	0,4406	0,5036	0,4091	-0,0159	-0,0039	-0,0084
Hanko_mareo–Helsinki_mareo	-74073,5995	88031,1132	18444,7199	116518,5939	Fixed,Wide Lane	0,0288	0,0426	0,0228	0,0241	0,0393	0,5335	0,5561	0,2345	0,0082	0,0036	0,0302
Hanko_mareo–Helsinki_mareo	-74073,6213	88031,1055	18444,6757	116518,5950	Fixed,Wide Lane	0,0261	0,0441	0,0257	0,0172	0,0409	0,4105	0,5090	0,3521	-0,0139	-0,0037	-0,0139
Hanko_mareo–Hyvinkaa	-113547,9466	63424,4456	44824,3947	137568,2479	Fixed,Wide Lane	0,0292	0,0474	0,0281	0,0190	0,0442	0,3938	0,4798	0,3139	-0,0131	-0,0020	0,0020
Hanko_mareo–Kump	-78545,5824	86213,1873	21260,9902	118550,2083	Fixed,Wide Lane	0,0294	0,0428	0,0225	0,0247	0,0398	0,5187	0,5410	0,2286	-0,0001	0,0049	0,0291
Hanko_mareo–Kump	-78545,6006	86213,1779	21260,9484	118550,2060	Fixed,Wide Lane	0,0266	0,0444	0,0256	0,0196	0,0405	0,4648	0,5200	0,4254	-0,0185	-0,0041	-0,0126
Hanko_mareo–Lohja	-62179,4129	39087,4100	23963,3039	77255,0642	Fixed,Wide Lane	0,0218	0,0357	0,0202	0,0144	0,0336	0,3775	0,4739	0,3338	-0,0042	0,0053	0,0052
Hanko_mareo–Lohja	-62179,4111	39087,4114	23963,3172	77255,0676	Fixed,Wide Lane	0,0245	0,0339	0,0179	0,0196	0,0324	0,4515	0,5101	0,0887	-0,0024	0,0066	0,0184
Hanko_mareo–METS	-66640,0454	57164,2169	22039,6153	90522,8588	Fixed,Wide Lane	0,0217	0,0396	0,0208	0,0143	0,0375	0,3239	0,5477	0,3200	-0,0273	-0,0087	-0,0355
Hanko_mareo–METS	-66640,0371	57164,2202	22039,6453	90522,8622	Fixed,Wide Lane	0,0254	0,0373	0,0196	0,0213	0,0347	0,5210	0,5488	0,2265	-0,0189	-0,0056	-0,0056
Hanko_mareo–Otan	-73964,0947	80239,0255	20290,9288	110998,6951	Fixed,Wide Lane	0,0258	0,0429	0,0247	0,0166	0,0402	0,3941	0,4760	0,3530	-0,0148	-0,0074	-0,0134
Hanko_mareo–Otan	-73964,0760	80239,0319	20290,9709	110998,6950	Fixed,Wide Lane	0,0284	0,0414	0,0223	0,0240	0,0381	0,5274	0,5608	0,2244	0,0041	-0,0013	0,0286
Hanko_mareo–Roko	-92493,6140	50413,3647	37117,3897	111688,3010	Fixed,Wide Lane	0,0296	0,0407	0,0301	0,0184	0,0359	0,1467	0,5461	0,0103	-0,0088	-0,0073	0,0069
Hanko_mareo–Tvar	-7849,0714	13297,5255	1158,4974	15484,6447	Fixed,Iono Free	0,0063	0,0091	0,0065	0,0044	0,0078	0,5612	0,4782	0,4772	0,0036	0,0016	0,0011
Hanko_mareo–Tvar	-7849,0783	13297,5240	1158,4941	15484,6467	Fixed,Iono Free	0,0056	0,0096	0,0057	0,0046	0,0084	0,6394	0,5715	0,5681	-0,0034	0,0001	-0,0022
Helsinki–Helsinki_mareo	7396,1163	-2499,9527	-3251,0419	8457,0428	Fixed	0,0030	0,0050	0,0029	0,0020	0,0046	0,3609	0,4972	0,3439	-0,0019	0,0005	-0,0037
Helsinki–Helsinki_mareo	7396,1157	-2499,9507	-3251,0388	457,0405	Fixed	0,0032	0,0050	0,0027	0,0024	0,0047	0,4375	0,5000	0,3406	-0,0024	0,0025	-0,0006
Helsinki–Kump	2924,1429	-4317,8773	-434,7658	5232,9435	Fixed	0,0020	0,0033	0,0018	0,0015	0,0031	0,3426	0,5175	0,3034	-0,0006	0,0032	0,0010
Helsinki–Kump	2924,1413	-4317,8807	-434,7718	5232,9459	Fixed	0,0021	0,0034	0,0018	0,0014	0,0033	0,3101	0,4537	0,3113	-0,0022	-0,0003	-0,0051
Helsinki–Otan	7505,6453	-10292,0355	-1404,7930	12815,3872	Fixed,Iono Free	0,0046	0,0075	0,0038	0,0031	0,0072	0,3070	0,4571	0,3062	-0,0005	-0,0060	-0,0073
Helsinki–Otan	7505,6457	-10292,0342	-1404,7912	12815,3862	Fixed,Iono Free	0,0045	0,0075	0,0039	0,0033	0,0070	0,3636	0,5464	0,2630	-0,0001	-0,0047	-0,0056
Helsinki–Roko	-11023,8725	-40117,6930	15421,6579	44370,9656	Fixed,Wide Lane	0,0159	0,0254	0,0188	0,0092	0,0214	0,2905	0,6234	0,2358	0,0070	-0,0023	0,0029
Helsinki–Tvar	73620,6646	-77233,5345	-20537,2194	108659,0930	Fixed,Wide Lane	0,0269	0,0416	0,0275	0,0212	0,0354	0,5445	0,5743	0,4379	0,0136	0,0043	0,0122
Helsinki–Tvar	73620,6506	-77233,5452	-20537,2530	108659,0974	Fixed,Wide Lane	0,0256	0,0425	0,0261	0,0214	0,0363	0,6072	0,5914	0,5426	-0,0002	-0,0067	-0,0215
Helsinki_mareo–Hyvinkaa	-39474,3382	-24606,6629	26379,6939	53475,2231	Fixed,Wide Lane	0,0180	0,0298	0,0174	0,0117	0,0277	0,3547	0,4969	0,3170	-0,0121	-0,0011	-0,0093
Helsinki_mareo–Hyvinkaa	-39474,3270	-24606,6602	26379,7106	53475,2218	Fixed,Wide Lane	0,0194	0,0288	0,0165	0,0145	0,0269	0,3894	0,4774	0,2649	-0,0008	0,0016	0,0074
Helsinki_mareo–Kump	-4471,9745	-1817,9274	2816,2718	5588,8105	Fixed	0,0021	0,0034	0,0020	0,0014	0,0032	0,3784	0,4868	0,3882	0,0002	-0,0001	0,0004
Helsinki_mareo–Kump	-4471,9747	-1817,9279	2816,2707	5588,8102	Fixed	0,0021	0,0034	0,0019	0,0017	0,0032	0,4818	0,5123	0,3959	0,0000	-0,0006	-0,0007
Helsinki_mareo–Lohja	11894,1955	-48943,7006	5518,6081	50669,6433	Fixed,Wide Lane	0,0176	0,0290	0,0161	0,0112	0,0277	0,3153	0,4541	0,3241	-0,0033	0,0043	-0,0011
Helsinki_mareo–Lohja	11894,2016	-48943,6957	5518,6221	50669,6415	Fixed,Wide Lane	0,0187	0,0283	0,0164	0,0133	0,0266	0,3442	0,4846	0,2146	0,0027	0,0093	0,0129
Helsinki_mareo–METS	7433,5673	-30866,8910	3594,9298	31952,2519	Fixed,Wide Lane	0,0111	0,0184	0,0108	0,0073	0,0171	0,3764	0,4926	0,3587	-0,0219	-0,0073	-0,0314
Helsinki_mareo–METS	7433,5753	-30866,8872	3594,9423	31952,2515	Fixed,Wide Lane	0,0104	0,0188	0,0107	0,0076	0,0170	0,4247	0,6144	0,3075	-0,0139	-0,0035	-0,0190
Helsinki_mareo–Otan	109,5247	-7792,0751	1846,2521	8008,5627	Fixed	0,0029	0,0048	0,0026	0,0019	0,0046	0,3195	0,4480	0,2798	-0,0029	0,0012	-0,0004
Helsinki_mareo–Otan	109,5291	-7792,0736	1846,2539	8008,5618	Fixed	0,0030	0,0049	0,0027	0,0021	0,0046	0,4104	0,4819	0,3090	0,0015	0,0027	0,0013
Helsinki_mareo–Roko	-18420,0004	-37617,7357	18672,6923	45859,1309	Fixed,Wide Lane	0,0175	0,0256	0,0195	0,0096	0,0221	0,2156	0,5303	0,2295	-0,0028	0,0019	-0,0009
Helsinki_mareo–Tvar	66224,5428	-74733,5791	-17286,1972	101339,0869	Fixed,Wide Lane	0,0232	0,0424	0,0262	0,0173	0,0367	0,5386	0,6067	0,5440	0,0101	0,0065	-0,0037
Helsinki_mareo–Tvar	66224,5370	-74733,5834	-17286,1825	101339,0837	Fixed,Wide Lane	0,0267	0,0400	0,0263	0,0202	0,0348	0,5742	0,5379	0,3474	0,0041	0,0024	0,0109
Hyvinkaa–Kump	35002,3591	22788,7368	-23563,4183	47955,4621	Fixed,Wide Lane	0,0164	0,0278	0,0150	0,0114	0,0262	0,3937	0,4928	0,3537	0,0076	0,0022	0,0135
Hyvinkaa–Kump	35002,3484	22788,7326	-23563,4335	47955,4598	Fixed,Wide Lane	0,0169	0,0275	0,0145	0,0131	0,0257	0,3961	0,5258	0,3519	-0,0031	-0,0019	-0,0018
Hyvinkaa–Otan	39583,8636	16814,5819	-24533,4399	49512,6458	Fixed,Wide Lane	0,0170	0,0286	0,0154	0,0117	0,0271	0,3702	0,4883	0,3251	0,0098	-0,0036	0,0108
Hyvinkaa–Otan	39583,8533	16814,5784	-24533,4561	49512,6444	Fixed,Wide Lane	0,0174	0,0283	0,0150	0,0123	0,0270	0,3673	0,4971	0,2412	-0,0004	-0,0071	-0,0055
Hyvinkaa–Roko	21054,3276	-13011,0771	-7707,0144	25922,4016	Fixed,Iono Free	0,0095	0,0151	0,0112	0,0055	0,0127	0,3171	0,6163	0,2423	-0,0009	-0,0014	-0,0043
Hyvinkaa–Tvar	105698,8578	-50126,9312	-43665,9104	124866,6069	Fixed,Wide Lane	0,0275	0,0454	0,0254	0,0217	0,0413	0,5268	0,5300	0,4309	-0,0010	-0,0076	-0,0139
Hyvinkaa–Tvar	105698,8649	-50126,9205	-43665,8917	124866,6020	Fixed,Wide Lane	0,0290	0,0445	0,0282	0,0238	0,0383	0,6121	0,5580	0,4451	0,0059	0,0033	0,0048
Kump–Lohja	16366,1732	-47125,7740	2702,3345	49959,9120	Fixed,Wide Lane	0,0170	0,0291	0,0159	0,0113	0,0274	0,3331	0,5085	0,3189	-0,0003	0,0037	-0,0032
Kump–Lohja	16366,1825	-47125,7682	2702,3498	49959,9104	Fixed,Wide Lane	0,0178	0,0286	0,0166	0,0132	0,0261	0,3318	0,5525	0,3005	0,0089	0,0095	0,0121
Kump–METS	11905,5480	-29048,9644	778,6541	31403,6735	Fixed,Wide Lane	0,0108	0,0183	0,0094	0,0076	0,0174	0,3916	0,4787	0,3725	-0,0159	-0,0080	-0,0357
Kump–METS	11905,5520	-29048,9601	778,6634	31403,6713	Fixed,Wide Lane	0,0100	0,0187	0,0096	0,0079	0,0172	0,4469	0,6366	0,3700	-0,0119	-0,0037	-0,0264
Kump–Otan	4581,5002	-5974,1476	-970,0204	7590,8842	Fixed	0,0029	0,0048	0,0024	0,0020	0,0046	0,3212	0,4402	0,3225	-0,0021	0,0015	-0,0015
Kump–Otan	4581,5014	-5974,1467	-970,0190	7590,8841	Fixed	0,0028	0,0046	0,0024	0,0021	0,0044	0,3287	0,5062	0,2759	-0,0009	0,0023	0,0000
Kump–Roko	-13948,0194	-35799,8095	15856,4207	41564,4040	Fixed,Wide Lane	0,0159	0,0235	0,0180	0,0093	0,0198	0,3083	0,5595	0,3033	0,0036	0,0008	-0,0011
Kump–Tvar	70696,5095	-72915,6622	-20102,4801	103531,6374	Fixed,Wide Lane	0,0234	0,0425	0,0249	0,0191	0,0370	0,5969	0,6050	0,5548	0,0019	-0,0039	-0,0152
Kump–Tvar	70696,5202	-72915,6533	-20102,4532	103531,6332	Fixed,Wide Lane	0,0255	0,0413	0,0258	0,0207	0,0355	0,5953	0,5870	0,4618	0,0125	0,0052	0,0117
Lohja–Otan	-11784,6710	41151,6191	-3672,3594	42963,0125	Fixed,Wide Lane	0,0150	0,0248	0,0138	0,0099	0,0235	0,3453	0,4821	0,3164	0,0003	-0,0094	-0,0028
Lohja–Otan	-11784,6771	41151,6159	-3672,3731	42963,0123	Fixed,Wide Lane	0,0152	0,0246	0,0139	0,0106	0,0230	0,3392	0,5264	0,2131	-0,0058	-0,0126	-0,0165
Lohja–Roko	-30314,2114	11325,9617	13154,0651	34932,1950	Fixed,Wide Lane	0,0127	0,0201	0,0155	0,0067	0,0167	0,1418	0,6578	0,1444	-0,0149	-0,0056	-0,0188
Lohja–Tvar	54330,3438	-25789,8821	-22804,8089	64319,2318	Fixed,Wide Lane	0,0194	0,0330	0,0206	0,0153	0,0283	0,6178	0,5914	0,5012	0,0099	-0,0014	-0,0064
Lohja–Tvar	54330,3447	-25789,8777	-22804,7973	64319,2268	Fixed,Wide Lane	0,0207	0,0322	0,0205	0,0169	0,0276	0,6384	0,5650	0,4509	0,0108	0,0030	0,0052
METS–Otan	-7324,0442	23074,8096	-1748,6801	24272,3370	Fixed,Iono Free	0,0088	0,0140	0,0071	0,0060	0,0137	0,3019	0,4325	0,2767	0,0175	0,0022	0,0287
METS–Otan	-7324,0458	23074,8012	-1748,6857	24272,3299	Fixed,Iono Free	0,0088	0,0139	0,0074	0,0063	0,0132	0,2850	0,5120	0,1950	0,0159	-0,0062	0,0230
METS–Roko	-25853,5706	-6750,8472	15077,7559	30680,9350	Fixed,Wide Lane	0,0102	0,0186	0,0133	0,0059	0,0155	0,3133	0,7275	0,2217	0,0164	0,0066	0,0240
METS–Tvar	58790,9527	-43866,7048	-20881,1497	76267,2035	Fixed,Wide Lane	0,0211	0,0359	0,0199	0,0172	0,0323	0,5703	0,5519	0,4938	0,0092	-0,0029	0,0050
METS–Tvar	58790,9636	-43866,6984	-20881,1222	76267,2006	Fixed,Wide Lane	0,0228	0,0349	0,0229	0,0189	0,0292	0,6905	0,5871	0,4408	0,0199	0,0036	0,0325
Otan–Roko	-18529,5242	-29825,6569	16826,4425	38936,3872	Fixed,Wide Lane	0,0146	0,0220	0,0165	0,0083	0,0189	0,2592	0,5561	0,2499	0,0011	0,0043	0,0018
Otan–Tvar	66115,0145	-66941,5013	-19132,4316	96012,5496	Fixed,Wide Lane	0,0246	0,0398	0,0244	0,0201	0,0344	0,6186	0,5813	0,4403	0,0092	0,0081	0,0143
Otan–Tvar	66115,0088	-66941,5079	-19132,4562	96012,5551	Fixed,Wide Lane	0,0229	0,0407	0,0247	0,0181	0,0353	0,5878	0,6013	0,5268	0,0036	0,0014	-0,0102
Roko–Tvar	84644,5559	-37115,8438	-35958,8673	99173,2164	Fixed,Wide Lane	0,0239	0,0413	0,0310	0,0151	0,0330	0,4498	0,7087	0,3930	0,0257	0,0041	0,0192

Control Tie Analysis: success
Adjustment type: Plane + Height, Constraint
Confidence level: 95 %
Number of adjusted points: 12
Number of plane control points: 5
Number of used GPS vectors: 88
A posteriori plane or 3D UWE: 0,5227703 , Bounds: (0,8911311 , 1,108711)
Number of height control points: 5
A posteriori height UWE: 0,7442316 , Bounds: (0,8461352 , 1,153561)

Point Summary

Name	Latitude	Longitude	Ell.Height (m)	Std Dev n (m)	Std Dev e (m)	Std Dev u (m)	Control
Bred	60°07'15,35681"N	23°54'27,00063"E	105,4192	0,0032	0,0025	0,0069	None
Hanko	59°49'53,47323"N	22°59'27,36908"E	40,1340	0,0000	0,0000	0,0000	Both
Hanko_mareo	59°49'21,63864"N	22°58'35,43535"E	24,8138	0,0008	0,0007	0,0016	None
Helsinki	60°12'43,75061"N	25°03'14,03705"E	37,3406	0,0000	0,0000	0,0000	Both
Helsinki_mareo	60°09'13,23541"N	24°57'24,23583"E	24,1269	0,0011	0,0009	0,0023	None

Hyvinkaa	60°37'51,19637"N	24°51'12,39956"E	150,7842	0,0000	0,0000	0,0000	Both
Kump	60°12'13,64608"N	24°57'39,73077"E	69,7839	0,0010	0,0008	0,0021	None
Lohja	60°15'07,73846"N	24°03'53,09469"E	100,7771	0,0000	0,0000	0,0000	Both
METS	60°13'02,89046"N	24°23'43,13336"E	94,5678	0,0000	0,0000	0,0000	Both
Otan	60°11'12,05953"N	24°49'42,88090"E	43,7080	0,0013	0,0010	0,0026	None
Roko	60°29'23,23201"N	24°28'39,79148"E	174,3559	0,0037	0,0028	0,0074	None
Tvar	59°50'36,30051"N	23°14'58,30964"E	21,7867	0,0021	0,0016	0,0042	None

Liite 3: Väärän antennikorkeuden vaikutus havaintopaikan koordinaatteihin.

Antennikorkeus 1,4644 m (referenssi)

Point Summary

Name	Latitude	Longitude	Ell.Height (m)	Std Dev n (m)	Std Dev e (m)	Std Dev u (m)	Control
Bred	60°07'15,35671"N	23°54'27,00068"E	105,4471	0,0079	0,0062	0,017	None
METS	60°13'02,89046"N	24°23'43,13336"E	94,5678	0	0	0	Both

GPS Observations

Name	dX (m)	dY (m)	dZ (m)	Distance (m)	Solution Type	Horz RMS (m)	Vert RMS (m)	SigmaX (m)	SigmaY (m)	SigmaZ (m)
Bred–METS	-19599,1031	20890,9532	5340,9656	29139,0233	Fixed,Iono Free	0,01	0,0169	0,009	0,0075	0,0158

Antennikorkeus 14,644 m

Point Summary

Name	Latitude	Longitude	Ell.Height (m)	Std Dev n (m)	Std Dev e (m)	Std Dev u (m)	Control
Bred	60°07'15,35671"N	23°54'27,00068"E	92,2675	0,0079	0,0062	0,017	None
METS	60°13'02,89046"N	24°23'43,13336"E	94,5678	0	0	0	Both

GPS Observations

Name	dX (m)	dY (m)	dZ (m)	Distance (m)	Solution Type	Horz RMS (m)	Vert RMS (m)	SigmaX (m)	SigmaY (m)	SigmaZ (m)
Bred–METS	-19593,1008	20893,614	5352,3934	29138,9914	Fixed,Iono Free	0,01	0,0169	0,009	0,0075	0,0158

Antennikorkeus 146,44 m

Point Summary

Name	Latitude	Longitude	Ell.Height (m)	Std Dev n (m)	Std Dev e (m)	Std Dev u (m)	Control
Bred	60°07'15,35671"N	23°54'27,00068"E	-39,5285	0,0079	0,0062	0,017	None
METS	60°13'02,89046"N	24°23'43,13336"E	94,5678	0	0	0	Both

GPS Observations

Name	dX (m)	dY (m)	dZ (m)	Distance (m)	Solution Type	Horz RMS (m)	Vert RMS (m)	SigmaX (m)	SigmaY (m)	SigmaZ (m)
Bred–METS	-19533,0771	20920,2222	5466,6709	29138,9995	Fixed,Iono Free	0,01	0,0169	0,009	0,0075	0,0158

Liite 4: Antennin kalibrointiparametrien vaikutus mittaustarkkuuteen.

Antennityyppi esitelty

Point Summary

Name	X (m)	Y (m)	Z (m)	Std Dev n (m)	Std Dev e (m)	Std Dev u (m)	Control
$Bred_0$	2912170,224	1290952,309	5507292,987	0,0078	0,0062	0,0169	None
METS	2892571,12	1311843,262	5512633,952	0	0	0	Both

GPS Observations

Name	dX (m)	dY (m)	dZ (m)	Distance (m)	Solution Type	Horz RMS (m)	Vert RMS (m)	SigmaX (m)	SigmaY (m)	SigmaZ (m)
Bred–METS	-19599,1031	20890,9532	5340,9656	29139,0233	Fixed,Iono Free	0,01	0,0169	0,009	0,0075	0,0158

Antennityyppiä ei esitelty

Point Summary

Name	X (m)	Y (m)	Z (m)	Std Dev n (m)	Std Dev e (m)	Std Dev u (m)	Control
Bred	2912170,247	1290952,314	5507293,03	0,0079	0,0062	0,0169	None
METS	2892571,12	1311843,262	5512633,952	0	0	0	Both

GPS Observations

Name	dX (m)	dY (m)	dZ (m)	Distance (m)	Solution Type	Horz RMS (m)	Vert RMS (m)	SigmaX (m)	SigmaY (m)	SigmaZ (m)
Bred–METS	-19599,1262	20890,9478	5340,9224	29139,027	Fixed,Iono Free	0,01	0,0169	0,009	0,0075	0,0158

Erotusten laskenta

Name	K X (m)	K Y (m)	K Z (m)	Vekt.pituus (m)
Bred-$Bred_0$	0,0231	0,0054	0,0432	0,0493

Koordinaattien laskenta Precise Point Positioning -menetelmällä

Ville Vuokko

Aalto University School of Engineering
Department of Surveying and Planning
ville.vuokko@aalto.fi

Abstract

Precise Point Positioning (PPP) is a relatively new method for determination of coordinates. It's a potential alternative to differential methods for precise positioning using Global Navigation Satellite Systems (GNSS). This seminar paper discusses the PPP method, its advantages and challenges and its usage in the post-process of GNSS data. In this paper the basic principles of PPP will be introduced and the coordinates of seven Science Network points will be determined by using two PPP online services. The goal of this paper is to give a good overview of PPP, PPP online services and to evaluate the accuracy of the determined coordinates. This seminar paper is based on various scientific articles and information about CSRS-PPP and MagicPPP the online services. Both online services were able to determine all the coordinates of the seven Science Network points. The accuracy of the coordinates were a few centimetres and there were no major differences between the services. After all PPP is a suitable alternative to the post-process of GNSS data and in the future it might also be a suitable method for real-time measurements.

1. Johdanto

Satelliittipaikanmäärityksessä on useita vaihtoehtoisia menetelmiä, joilla mittaukset voidaan tehdä ja mittausten havainnot käsitellä. Useimmat menetelmät perustuvat relatiiviseen paikannukseen, jossa mitataan kahdella tai useammalla pisteellä samanaikaisesti ja määritetään pisteiden väliset koordinaattierot. Relatiivisessa paikannuksessa tehdään kaksoiserotushavaintoja kahden pisteen ja kahden satelliitin välillä. Tällä tavalla useimmat virhelähteet kuten satelliitin ratavirhe ja ilmakehän vaikutus voidaan poistaa havainnoista tai ainakin merkittävästi pienentää niiden vaikutusta.

Relatiiviseen paikannukseen perustuvia menetelmiä ovat esimerkiksi differentiaalinen GPS (Differential Global Positioning System, DGPS) ja reaaliaikainen kinemaattinen paikannus (Real Time Kinematic, RTK). Koodihavaintoihin perustuvalla DGPS:llä voidaan saavuttaa muutaman desimetrin tarkkuus paikanmäärityksessä ja kantoaallon vaihe-eroon perustuvalla RTK:lla muutaman senttimetrin tarkkuus. Nämä menetelmät vaativat kuitenkin oman tukiaseman perustamista tai vaihtoehtoisesti kaupallisen tukiasemien verkoston hyödyntämistä. Tukiasemien verkoston perustaminen ei ole kaikkialle taloudellisesti kannattavaa eikä joillekin alueille edes mahdollista. Lisäksi relatiivisen paikannuksen tarkkuus riippuu mitattavan pisteen etäisyydestä tukiasemasta, joten mittaukset on tehtävä tukiaseman läheisyydessä.

1990-luvun lopulla kehitettiin vaihtoehtoinen menetelmä relatiiviselle paikanmääritykselle. Menetelmä on nimeltään Precise Point Positioning (PPP) ja se perustuu absoluuttiseen paikanmääritykseen. PPP:n toimintaperiaate perustuu tarkkoihin satelliittien ratoihin ja kellokorjauksiin. Menetelmä tuli mahdolliseksi, kun International GNSS Service (IGS) alkoi tuottamaan satelliittien tarkkoja ratoja ja kellokorjauksia 1990-luvulla. PPP-menetelmässä mitataan ainoastaan yhdellä vastaanottimella ilman tukiasemaa ja korvataan satelliittipaikannusjärjestelmästä (Global Navigation Satellite System, GNSS) saadut ennustetut satelliittien radat ja kellokorjaukset tarkoilla radoilla ja kellokorjauksilla. Tämän lisäksi ilmakehän vaikutus ja vastaanottimen kellovirhe estimoidaan ja poistetaan sitä kautta. Menetelmällä voidaan määrittää pisteen koordinaatit jopa muutaman senttimetrin tarkkuudella. (Andrei et al., 2010.)

Tämän työn tarkoituksena on perehtyä PPP-menetelmään ja esitellä sen käyttämistä koordinaattien laskennassa. Työn tavoitteena on luoda hyvä yleiskuva PPP-menetelmästä ja sen madollisuuksista. Työssä tarkastellaan

sekä staattista että kinemaattista PPP:tä. Työssä esitellään PPP:n toimintaperiaate, tutustutaan menetelmän etuihin ja haasteisiin sekä esitellään mahdollisia sovelluksia. Lisäksi perehdytään kahteen Internetissä olevaan PPP-sovellukseen ja lasketaan niiden avulla seitsemän Science Network -verkon pisteen koordinaatit. PPP-soveluksilla saatuja tuloksia, niiden tarkkuutta ja suhdetta toisiinsa tutkitaan. PPP menetelmää voidaan soveltaa myös reaaliajassa, mutta tässä työssä keskitytään pääasiassa sen käyttämiseen jälkilaskennassa.

Tämä työ koostuu kahdesta osasta. Työn alkupuolella tutkitaan kirjallisuustutkielmana PPP-menetelmää aiempia kirjoituksia pohtien ja yhdistellen. Työn loppupuoli koostuu käytännön osuudesta, jossa tutkitaan kahden PPP-sovelluksen toimintaa. Työssä on käytetty tietolähteinä tieteellisiä artikkeleita ja tutkittavien sovellusten verkkosivuja. Työ on jaettu viiteen päälukuun. Toisessa luvussa perehdytään PPP-menetelmän toimintaperiaatteeseen, tarkkoihin satelliittien ratoihin ja kellokorjauksiin, menetelmän etuihin ja haasteisiin sekä mahdollisiin sovelluksiin. Kolmannessa luvussa tarkastellaan työssä hyödynnettyjä PPP-sovelluksia ja esitellään käytetty "Science Network"-data. Neljännessä pääluvussa tutkitaan sovellusten avulla laskettuja tuloksia ja vertaillaan niitä keskenään. Työn viimeisessä luvussa vedetään yhteen aiemmat luvut ja tehdään havaintoja sekä johtopäätöksiä työstä.

2. Precise Point Positioning

Precise Point Positioning (PPP) on menetelmä, jolla voidaan käsitellä maailmanlaajuisen satelliittipaikannusjärjestelmän (Global Navigation Satellite System, GNSS) havaintoja ja laskea pisteiden tarkkoja koordinaatteja jopa muutaman senttimetrin tarkkuudella. PPP on vaihtoehtoinen menetelmä relatiiviselle paikannukselle, jossa pisteen koordinaatit lasketaan aina suhteessa toiseen pisteeseen tai pisteiden muodostamaan verkkoon. PPP-menetelmässä pisteen koordinaatit mitataan yhdellä GNSS -vastaanottimella ja havaintoja korjataan tarkkojen satelliittien ratojen sekä kellokorjausten avulla. Mittauksissa tehdään sekä koodihavaintoja, että kantoaallon vaihe-eron havaintoja. PPP-menetelmää voidaan käyttää myös yksitaajuusvastaanottimen kanssa, mutta tässä työssä keskitytään kaksitaajuusvastaanottimen hyödyntämiseen. Seuraavaksi tarkastellaan PPP-menetelmän toimintaperiaatetta ja sen mahdollistavia tarkkoja satelliittien ratatietoja sekä kellokorjauksia. Lisäksi perehdytään

menetelmän etuihin ja haasteisiin sekä mahdollisiin sovelluksiin. (BISNATH & GAO, 2008)

2.1 Toimintaperiaate

Kahdella taajuudella tehtyjä havaintoja hyödyntävä Precise Point Positioning -menetelmä perustuu koodi- ja vaihe-erohavaintojen ionosfäärivapaisiin havaintosuureisiin (KOUBA & HÉROUX, 2001). PPP-menetelmällä ei kuitenkaan pystytä ratkaisemaan alkutuntemattomia kokonaislukuna toisin kuin menetelmillä, jotka hyödyntävät kaksoiserotushavaintoja (ANDREI *et al.*, 2010). Tämä johtuu siitä, että vastaanottimen ja satelliitin nollasta eroavaa alkuperäistä vaihepoikkeamaa ei voida määrittää eikä alkutuntemattomia pystytä pyöristämään lähimpään kokonaislukuun (GE *et al.,* 2007; ANDREI *et al.,* 2010). Alkutuntemattomat pystytään siis estimoimaan vain reaalilukuna mikä heikentää ratkaisun tarkkuutta ja pidentää ratkaisun suppenemisaikaa (MERVART *et al.,* 2008).

Koodi- ja vaihe-erohavainnoista muodostetaan kaavojen (1) ja (2) mukaiset ionosfäärivapaat havaintoyhtälöt (ANDREI *et al.,* 2010). Ionosfäärivapailla havaintoyhtälöillä signaalista saadaan poistettua ionosfäärin aiheuttama taajuudesta riippuvainen virhe. Yhtälöistä on jätetty yksinkertaisuuden takia pois muun muassa kiinteän maan vuoksen ja valtamerten kuormituksen aiheuttamat virheet. Ionosfäärivapaiksi havaintoyhtälöiksi saadaan:

$$P_{IF} = \frac{f_1^2 P_1 - f_2^2 P_2}{f_1^2 - f_2^2} =$$

$$\rho + c(dt - dT) + d_{orb} + d_{rel} + d_{trop} + b_P + b^P + d_{pcv} + d_{mpP} + \varepsilon_P \,, \quad (1)$$

$$\Phi_{IF} = \frac{f_1^2 \Phi_1 - f_2^2 \Phi_2}{f_1^2 - f_2^2} =$$

$$\rho + c(dt - dT) + d_{orb} + d_{rel} + d_{trop} + \lambda_{IF}\left(N_{IF} + b_\Phi + b^\Phi\right) +$$

$$d_{pcv} + d_{mp\Phi} + \varepsilon_\Phi \,, \quad (2)$$

joissa P_i on koodihavaintoon perustuva pseudoetäisyys kantoaallolla L_i (m); Φ_i on vaihe-erohavaintoon perustuva vaihekulma kantoaallolla L_i (m); f_i on kantoaallon L_i taajuus (MHz); ρ on geometrinen etäisyys satelliitin ja vastaanottimen välillä (m); c on valonnopeus tyhjiössä (m/s); dt on vastaanottimen kellon poikkeama (s); dT on satelliitin kellon poikkeama

(s); d_{orb} on satelliitin ratavirhe (m); d_{rel} on relativistinen viive (m); d_{trop} on troposfäärin aiheuttama viive (m); b_P ja b^P ovat vastaanottimen ja satelliitin koodipoikkeamat (m); λ_{IF} on ionosfäärivapaan havaintosuureen aallonpituus (m); N_{IF} on ionosfäärivapaan havaintosuureen alkutuntematon (kierrosta); b_Φ ja b^Φ ovat vastaanottimen ja satelliitin alkuperäiset vaihepoikkeamat (kierrosta); d_{pcv} on vastaanottimen ja satelliitin antennin vaihekeskipisteestä aiheutuva virhe (m); $d_{mp(.)}$ on monitieheijastuksen aiheuttama virhe ja ε(.) on mittauksen kohina (m) (ANDREI *et al.,* 2010).

Useimmat havaintoyhtälöissä esiintyvät virheet saadaan eliminoitua ja jäljelle jäävät virheet pyritään estimoimaan. Satelliitin ratavirheestä d_{orb} ja satelliitin kellovirheestä dT päästään eroon, kun käytetään tarkkoja satelliitin ratoja ja kellokorjausta. Troposfäärin aiheuttama viive d_{trop} pystytään pienentämään senttimetrin tasolle mallintamalla. Tämä viive koostuu kahdesta osasta: hydrostaattisesta viiveestä (Zenith Hydrostatic Delay, ZHD) ja kosteasta viiveestä (Zenith Wet Delay, ZWD). Hydrostaattinen viive pystytään ratkaisemaan muutaman millimetrin tarkkuudella ilmanpainehavaintojen perusteella. Kostean viiveen ratkaiseminen ei sen sijaan ole yhtä yksinkertaista, joten se lisätään tuntemattomien vektoriin ja estimoidaan sitä kautta. Vastaanottimen ja satelliitin koodivirheet d_P ja d^P saadaan poistettua differential code bias -menetelmällä (DCB) muodostamalla kahdesta havaitusta koodista lineaarikombinaatio. Antennin vaihekeskipisteestä aiheutuva virhe d_{pcv} saadaan eliminoitua määrittämällä vaihekeskipisteen paikka antennin absoluuttisessa kalibroinnissa. Viimeisenä virhelähteenä ovat monitieheijastukset $d_{mp(.)}$, joiden vaikutusta pystytään vähentämään Choke Ring-tyyppisillä antenneilla ja korkeuskulman katkaisurajaa säätämällä. (ANDREI *et al.,* 2010.)

Edellä mainittujen virheiden käsittelyn jälkeen havaintoyhtälöt (1) ja (2) saadaan muotoon:

$$P_{IF} = \bar{\rho} + cdt + m_w ZWD + \varepsilon_P \,, \tag{3}$$

$$\Phi_{IF} = \bar{\rho} + cdt + m_w ZWD + \lambda_{IF}\bar{N}_{IF} + \varepsilon_\Phi \,, \tag{4}$$

joissa $\bar{\rho}$ on korjattu pseudoetäisyys satelliitin ja vastaanottimen antennien vaihekeskipisteiden välillä, m_w on troposfäärin kosteaa osaa kuvaava funktio, ZWD on troposfäärin kostea viive ja $\bar{N}_{IF}$ on reaaliarvoinen alkutuntemattomien määrä (ANDREI *et al.,* 2010). $\bar{N}_{IF}$ on yhtälön (5) mukaisesti muotoa:

$$\bar{N}_{IF} = N_{IF} + b_{\Phi +} b^\Phi . \tag{5}$$

Yhtälöiden (3) ja (4) tuntemattomista muodostetaan vektori, joka ratkaistaan Kalman-suodinta hyödyntäen. Tuntemattomien vektori koostuu vastaanottimen koordinaateista (dx, dy, dz), vastaanottimen kellovirheestä (dt), troposfäärin kosteasta viiveestä ZWD ja alkutuntemattomista $\bar{N}_{IF}$. Tämän vektorin ratkaisemiseksi tarvitaan havaintoja yhtä monesta satelliitista kuin mitä on tuntemattomia. Kalman-suotimen avulla tuntemattomien vektori (tilavektori) voidaan ratkaista epookki epookilta. Kalman-suodin koostuu joukosta lineaarisia yhtälöitä ja sen avulla saadaan pienimmän neliösumman menetelmän mukaiset estimaatit tuntemattomille. Tuntemattomien vektorin lisäksi Kalman-suodin koostuu mallinnettavien parametrien käyttäytymistä kuvaavasta dynaamisesta mallista ja havainnoista koostuvasta havaintomallista. Kalman-suodin on tehokas menetelmä tuntemattomien ratkaisuun, kun tuntemattomien käyttäytyminen on hyvin tiedossa. Vastaanottimen kellovirheen käyttäytymistä mallinnetaan yleensä Random Walk tai Gauss Markov prosesseina. Vastaanottimen koordinaatteja voidaan pitää vakioina staattisessa mittausmoodissa. Kinemaattisessa mittausmoodissa niiden käyttäytymistä mallinnetaan funktiolla, joka kuvaa vastaanottimen liikettä. Troposfäärin kostean osan viivettä mallinnetaan myös Random Walk prosessina. Alkutuntemattomia voidaan pitää vakiona edellyttäen, ettei vaihekatkoa pääse tapahtumaan. (ANDREI *et al.,* 2010; KOUBA & HÉROUX, 2001)

Tarkoissa mittauksissa tulisi huomioida muitakin virhelähteitä, kuin edellä on esitetyt. Tässä työssä ei kuitenkaan tarkemmin perehdytä näiden virhelähteiden käsittelyyn. Tällaisia virhelähteitä ovat satelliitin "phase wind-up"-ilmiö, kiinteän maan vuokset, valtamerten kuormitus ja maan rotaatioparametrit. (KOUBA & HÉROUX, 2001)

2.2 Satelliittien tarkat radat ja kellokorjaukset

International GNSS Service (IGS) on vapaaehtoisuuteen perustuva yli 200 organisaation yhteenliittymä, jossa on jäseniä yli 80 maasta. IGS on tuottanut vuodesta 1994 lähtien GPS-satelliittien tarkkoja kiertoratoja ja kellokorjauksia tieteellisten yhteisöjen vapaaseen käyttöön. IGS:n maailmanlaajuiseen pysyvien GNSS-asemien verkkoon kuuluu yli 300 asemaa, jotka suorittavat jatkuvasti tarkkoja GNSS-mittauksia. Näiden asemien havainnoista lasketaan satelliittien radat ja kellokorjaukset kahdeksassa IGS:n analysointikeskuksessa (IGS Analysis Centers, AC), jonka jälkeen ne on käyttäjien vapaasti ladatavissa IGS:n verkkosivuilta. Viimeisten 15 vuoden aikana IGS:n tuottamien tarkkojen ratojen ja kellokorjausten tarkkuus on parantunut merkittävästi, mikä mahdollistaa

tarkan PPP-mittauksen. Tarkimpien ratojen eli Final-efemeridiien tarkkuus on nykyään satelliitin ratojen kohdalla 2,5 senttimetriä ja satelliitin kellokorjaus pystytään määrittämään 0,1 nanosekunnin tarkkuudella. (KOUBA, 2009)

IGS tuottaa viiden tyyppisiä satelliittien ratoja ja kellokorjauksia, joiden tarkkuudet toisiinsa nähden vaihtelevat. Tuotteet ovat nimeltään Broadcast, Ultra-Rapid (ennustettu), Ultra-Rapid (havaittu), Rapid ja Final. Final-efemeriidit ovat tarkkuudeltaan parhaimmat, mutta ne on saatavilla vasta 12-18 päivän kuluttua havaintohetkestä. Sen sijaan Broadcast- ja Ultra-Rapid-efemeriidit ovat saatavilla reaaliajassa, mutta ne ovat tarkkuudeltaan selvästi Final-efemeriidit heikompia. IGS:n eri tuotteiden tarkemmat tiedot on esitetty taulukossa 1. Final-efemeriidit ovat ratoja, joita käytetään PPP-menetelmässä jälkilaskennassa. Näiden efemeriidien näytteenottoväli on ratojen kohdalla 15 minuuttia ja kellokorjauksen kohdalla 30 sekuntia. Satelliittien radat ovat suhteellisen säännöllisiä, joten 15 minuutin näytteenottoväli on täysin riittävä. Sen sijaan satelliitin kellon käynnissä on paljon epäsäännöllisyyksiä ja niitä on vaikea ennustaa, joten tarvitaan 30 sekunnin näytteenottoväli. Bernissä sijaitseva IGS:n analysointikeskus CODE (Centre for Orbit Determination in Europe) tuottaa lisäksi kellokorjauksia viiden sekunnin näytteenottovälillä. (ANDREI *et al.,* 2010, IGS, 2012)

Taulukko 1. IGS:n tuottamat satelliittien radat ja kellokorjaukset (IGS, 2012).

Tuote	**Tarkkuus (rata / kello)**	**Viive**	**Näytteenottoväli**
Broadcast	100 cm / 5 ns	Reaaliaikainen	Päivittäin
Ultra-Rapid (ennustettu)	5 cm / 3 ns	Reaaliaikainen	15 min
Ultra-Rapid (havaittu)	3 cm / 0,15 ns	3-9 h	15 min
Rapid	2,5 cm / 0,075 ns	17-41 h	Radat 15 min / Kello 5 min
Final	2,5 cm / 0,075 ns	12-18 vrk	Radat 15 min / Kello 30 s

2.3 Menetelmän edut ja haasteet

Precise Point Positioning -menetelmässä on monta huomattavaa etua verrattuna relatiiviseen paikannukseen perustuviin menetelmiin, joissa joudutaan mittaamaan kahdella tai useammalla pisteellä samanaikaisesti. Toisaalta PPP-menetelmässä on myös muutamia keskeisiä haasteita verrattuna relatiivisiin menetelmiin. PPP:n suurin etu on se, että siinä ei tarvita tunnettua referenssipistettä, jolla täytyisi mitata samanaikaisesti

(ANDREI *et al.,* 2010). Tukiasemaa tai tukiasemien verkkoa ei siis tarvita, mikä tekee mittausjärjestelyistä joustavampia ja logistisesti helpompia, tuo taloudellisia säästöjä sekä mahdollistaa tarkan mittaamisen myös syrjäisillä alueilla (ANDREI *et al.,* 2010). Mittaukset pystytään tekemään myös pienemmällä määrällä vastaanottimia ja työntekijöitä (GAO & CHEN, 2004). Kun tukiasemia ei tarvita, ei PPP:n tarkkuus myöskään riipu etäisyydestä tukiasemaan toisin kuin relatiivisissa menetelmissä. PPP:n tarkkuus on kinemaattisissa mittauksissa muutaman desimetrin luokkaa ja staattisissa mittauksissa muutaman senttimetrin luokkaa (BISNATH & GAO, 2008). Nämä tarkkuudet ovat hyvin kilpailukykyisiä DGPS:ään ja RTK:hon verrattuna. PPP:llä saadut koordinaatit tosin ovat samassa koordinaatistossa kuin satelliittien radat eli kyseisen epookin ITRF-koordinaatistossa (International Terrestrial Reference Frame). Tämän takia tarvitaan vielä koordinaattimuunnos paikalliseen koordinaatistoon. (BISNATH & GAO, 2008)

PPP:n merkittävin haaste on sen tarvitsema alustusaika mikä tarvitaan ennen kuin menetelmän tuottamat ratkaisut suppenevat kohti oikeita arvoja (BISNATH & GAO, 2008). Vasta tämän alustusajan jälkeen voidaan ryhtyä tekemään tarkkoja mittauksia. Alustusaika johtuu siitä, että alkutuntemattomat estimoidaan reaaliarvoisina ja estimointi vaatii tietyn suppenemisajan ennen kuin estimaatit lähestyvät oikeita arvoja (OVSTEDAL *et al.,* 2006). Alustusaika on normaaleissa olosuhteissa noin 30 minuuttia, kun tarkkuudeksi riittää desimetrin taso, mutta senttimetrin tason tarkkuus saavutetaan huomattavasti pidemmän ajan kuluttua (BISNATH & GAO, 2008). Ratkaisun suppenemisaika riippuu monista tekijöistä kuten käytettävissä olevien satelliittien lukumäärästä, mittausten geometriasta ja mittausvälistä (BISNATH & GAO, 2008). PPP vaatii myös avoimen ja esteettömän näkyvyyden taivaalle säilyttääkseen yhteyden riittävän moneen satelliittiin. Jos käytössä olevien satelliittien määrä putoaa alle kuuteen ja tapahtuu vaihekatko, tarvitsee menetelmä uuden alustusajan, jotta alkutuntemattomat voidaan jälleen ratkaista (BISNATH & GAO, 2008).

PPP-menetelmällä ei tällä hetkellä voi saavuttaa muutamaa senttimetriä parempaa tarkkuutta. Tarkkuutta rajoittaa tarkkojen satelliittien ratojen ja kellokorjausten epätarkkuudet ja mallintamattomat virhelähteet (BISNATH & GAO, 2008). Lisäksi tarkkuutta rajoittaa se, että alkutuntemattomia ei pystytä ratkaisemaan kokonaislukuna (BISNATH & GAO, 2008). Tulevaisuudessa PPP:n tarkkuutta sen tarvitsemaa alustusaikaa ja käytettävyyttä tulevat parantamaan useiden GNSS-järjestelmien yhteiskäyttö (BISNATH & GAO, 2008). Tällöin pystytään tekemään havaintoja useampiin satelliitteihin ja saavutetaan parempi mittausgeometria (BISNATH & GAO, 2008).

Jos tulevaisuudessa alkutuntemattomat pystyttäisiin ratkaisemaan kokonaislukuina se parantaisi merkittävästi PPP:n tarkkuutta ja lyhentäisi alustusaikaa (BISNATH & GAO, 2008). Eräs vaihtoehto tähän on PPP:n ja RTK:n integroiminen, jolloin kummastakin menetelmästä saataisiin parhaat puolet käyttöön (MERVART *et al.,* 2008). Tällöin alustusaika lyhenisi kymmeneen minuuttiin ja mittausten tarkkuus olisi senttimetrin luokkaa vielä satoja kilometrejä referenssiasemien ulkopuolella, mutta toisaalta se vaatisi huomattavaa infrastruktuuria tukiasemien muodossa (MERVART *et al.,* 2008).

2.4 Sovelluskohteet

PPP:tä voidaan käyttää periaatteessa samoissa sovelluksissa kuin DGPS:ää ja RTK:ta, mutta sen vaatima alustusaika voi olla joihinkin sovelluksiin liian pitkä. PPP voidaan hyödyntää sekä staattisissa että kinemaattisissa mittauksissa, joko reaaliajassa tai jälkilaskennassa (BISNATH & GAO, 2008). PPP:n ensimmäisiä sovelluskohteita olivat GNSS-asemien paikannus, deformaatiomittaukset ja LEO-kiertoradoilla (Low Earth Orbit) kiertävien satelliittien ratojen määritys (BISNATH & GAO, 2008). Myöhemmin sitä on sovellettu maataloudessa, merenkulussa, merenpohjan mittauksessa ja ilmakuvauksessa (BISNATH & GAO, 2008). Menetelmä on myös leviämässä maanmittauksen, rakentamisen, ilmakehän kaukokartoituksen ja tarkan ajan välityksen pariin (BISNATH & GAO, 2008). PPP soveltuu myös GNSS-meteorologian käyttöön (GAO & CHEN, 2004). Erityisen hyvin PPP soveltuu tarkkoihin mittauksiin syrjäisillä alueilla, jossa tukiasemien verkkoa ei ole käytettävissä ja sen luominen tulisi liian kalliiksi (BISNATH & GAO, 2008). Tällaisia kohteita ovat esimerkiksi luonnonvarojen kartoitus ja etsintä (BISNATH & GAO, 2008).

3. Science Network -data ja PPP-verkkosovellukset

Seuraavaksi tarkastellaan kahta Internetistä löytyvää PPP-menetelmää hyödyntävää sovellusta. Näillä sovelluksilla voidaan jälkilaskennassa laskea pisteiden tarkat koordinaatit. Lisäksi luvussa esitellään lyhyesti Science Network -data, jota käytetään tässä työssä.

3.1 Science Network -data

Science Network -data koostuu seitsemästä pisteestä, jotka mitattiin Geodesian maastoharjoitukset -kurssin yhteydessä 24.5.-25.5.2011. Pisteet olivat Helsingin mareografi, Hangon mareografi, kaksi EUREF-FIN-pistettä (Rokokallio ja Bredberg), Tvärminnen eläintieteellinen asema, Ilmatieteen laitos Kumpulassa ja Teknillisen korkeakoulun päärakennus Otaniemessä. Kaksi viimeistä pistettä sijaitsivat rakennusten katoilla. Mitatut pisteet on esitetty kuvassa 1. Osa pisteistä mitattiin yhdessä kuuden tunnin mittaussessiossa, osa kahdessa kuuden tunnin sessiossa ja osa yhdessä 24 tunnin sessiossa. Havaintoväli oli osassa pisteistä 15 sekuntia ja osassa 30 sekuntia. Mitatut pisteet ja sessiot on esitetty taulukossa 2.

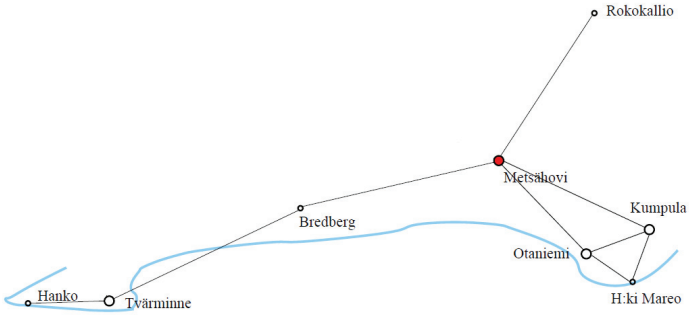

Kuva 1. Mitatun Science Network -verkon pisteet. Kuvassa myös Metsähovin piste, joka toimi mittausten aikana pysyvänä GPS-asemana (Geodesian maastoharjoitukset 2011).

Taulukko 2. Mitatut pisteet, mittaussessioiden kestot, havaintovälit ja satelliittien minimäärä mittauksien aikana.

	Mittaussessio 144			Mittaussessio 145		
Piste	**Kesto (h)**	**Havain-toväli (s)**	**Satelliitteja minimissään (kpl)**	**Kesto (h)**	**Havain-toväli (s)**	**Satelliitteja minimissään (kpl)**
Bredberg	7,5	30	6	-	-	-
Hanko	6	15	7	5	15	8
Helsinki	8,5	30	7	6,5	30	6
Kumpula	29	30	3			
Otaniemi	31	30	5			
Rokokallio	-	-	-	5	30	5
Tvärminne	26	15	4			

Mittaukset tehtiin Ashtechin Z-XII3 vastaanottimilla ja Dorne-Margolin choke ring -tyyppisillä antenneilla. Mittausten jälkeen havaintotiedostot muunnettiin RINEX-formaattiin (Receiver Independent Exchange Format) ja niihin lisättiin antennien pystysuorat korkeudet. Antennien korkeuksien puuttuminen aiheuttaisi saman suuruisen virheen tuloksiin. Lisäksi

tiedostoihin merkittiin vastaanottimien ja antennien oikeat tyypit. Oikeiden antennien merkitseminen tiedostoihin on tärkeää, koska käytetyt PPP-sovellukset korjaavat antennin vaihekeskipisteen paikan antennikohtaisen absoluuttisen kalibroinnin perusteella. Jos oikeaa antennia ei tiedostossa ole, ei kyseisen antennin kalibrointitietoja voida hyödyntää.

3.2 CSRS-PPP-sovellus

CSRS-PPP (Canadian Spatial Reference System-Precise Point Positioning) on Natural Resources Canadan tuottama PPP-verkkosovellus tarkkojen koordinaattien jälkilaskentaan. Sovellus vaatii rekisteröitymisen, mutta on sen jälkeen käyttäjän vapaassa käytössä. Ohjelma löytyy osoitteesta http://www.geod.nrcan.gc.ca/products-produits/ppp_e.php. Sovelluksessa on mahdollista käsitellä myös yksitaajuusvastaanottimen havaintotiedostoja, jolloin ionosfäärin vaikutus mallinnetaan. Tähän ominaisuuteen ei kuitenkaan perehdytä tarkemmin tässä työssä. Käyttäjä voi tehdä sovelluksessa muutamia valintoja, jotka vaikuttavat laskennan lopputulokseen. Käyttäjän valittavissa on tehdäänkö laskenta staattisessa vai kinemaattisessa moodissa. Lisäksi käyttäjä voi valita lasketaanko tulokset NAD83- (North American Datum of 1983) tai ITRF08-koordinaatistoon. NAD83-koordinaatistossa on valittavana muutama eri epookki, mutta ITRF-koordinaatiston mukaiset koordinaatit lasketaan havaintohetken epookissa. Käyttäjä voi myös ladata sovellukseen oman OTL-tiedoston (Ocean Tidal Loading), jonka avulla valtamerten vuoksen vaikutus poistetaan. (NRC, 2012)

Sovelluksen käyttö on varsin yksinkertaista. Käyttäjä tekee edellä mainitut asetukset verkkosivustolla, lataa sinne RINEX- sekä OTL-tiedostonsa ja saa tulokset antamaansa sähköpostiosoitteeseen. Käyttäjä saa sähköpostiinsa neljä eri tiedostoa: yhteenvedon laskennasta ja siinä käytetyistä parametreista (sum-tiedosto), kaikkien tuntemattomien estimaatin epookki epookilta (pos-tiedosto), satelliittien residuaalit ja alkutuntemattomien estimaatit (res-tiedosto) sekä tulosten tarkkuutta kuvaavia kuvaajia sisältävän pdf-tiedoston. Sum-tiedostossa on varsin tarkat tiedot laskennassa käytetyistä parametreista, mikä tuo läpinäkyvyyttä sovellukselle. Tiedostosta ilmenee laskennassa käsitelty data, käytetyt satelliittien radat ja kellokorjaukset, käytetty troposfäärimalli ja vaihekatkojen tunnistamiseen käytetyt raja-arvot. Lisäksi tiedostosta ilmenee vastaanottimen sekä satelliittien antennien vaihekeskipisteiden paikat ja OTL-parametrit. Tiedoston lopussa on vielä yhteenveto laskennan tuloksista ja virhearviot. Näistä tuloksista ilmenee pisteen ellipsoidiset sekä suorakulmaiset koordinaatit, koodi- ja vaihe-erohavaintojen residuaalit,

vastaanottimen kellon estimaatit ja listaus hylätyistä koodi- sekä vaihe-erohavainnoista. Tiedostossa on myös laskettuna koordinaattierot RINEX-tiedostossa olevien pisteen arvioitujen koordinaattien ja havaittujen koordinaattien välillä. Jos RINEX-tiedostoon syöttää pisteen tunnetut koordinaatit, voidaan näiden koordinaattierojen perusteella arvioida mittausten tarkkuutta. (NRC, 2012)

Varsinaiset mittaustulokset selviävät pos-tiedostosta, jossa ne on listattu epookki epookilta. Tiedostosta selviää ellipsoidisten koordinaattien lisäksi troposfäärin aiheuttama virhe, vastaanottimen kellon virhe, havaittujen satelliittien lukumäärä, koodi- ja vaihe-erohavaintojen keskihajonnat. Edellä mainittujen keskihajontojen lisäksi tiedostosta ilmenee koordinaattien, vastaanottimen kellovirheen ja troposfäärin virheen keskihajonnat. Pos-tiedostossa on myös laskettuna koordinaattierot RINEX-tiedostossa olevien pisteen arvioitujen koordinaattien ja havaittujen koordinaattien välillä. Res-tiedostosta löytyy epookki epookilta jokaisen havaitun satelliitin atsimuti- ja korkeuskulmat sekä koodi- ja vaihe-erohavaintojen residuaalit. Lisäksi tiedostossa on myös esitetty ratkaistujen alkutuntemattomien estimaatit. (NRC, 2012)

Pdf-tiedostosta ilmenee lyhyen yhteenvedon lisäksi mittauksen tulokset ja virhearviot kuvaajien muodossa. Kuvaajista ilmenee muun muassa laskettujen koordinaattien ja niiden tarkkuuden muutokset ajan suhteen sekä troposfäärin virheen ja vastaanottimen kellon virheen käyttäytyminen ajan suhteen. Lisäksi tiedostossa on esitetty x- ja y-koordinaattien hajonta tasossa. Tiedostossa on myös kuvattu havaintojen residuaalien käyttäytymistä ajan suhteen. Kokonaisuudessaan kuvaajista pystyy päättelemään paljon tulosten tarkkuudesta ja luotettavuudesta sekä havaitsemaan mahdollisen vaihekatkon. (NRC, 2012)

3.3 MagicPPP-sovellus

MagicPPP on GMV:n tuottama PPP-verkkosovellus tarkkojen koordinaattien jälkilaskentaan. Sovellusta voi käyttää joko sähköpostin kautta tai rekisteröitymällä verkkosivustolle. Rekisteröitymisen jälkeen palvelu on kuukauden ajan käyttäjän vapaassa koekäytössä. Palvelu löytyy osoitteesta http://magicgnss.gmv.com/ppp/. Ilman rekisteröitymistä käyttäjä ei voi vaikuttaa kaikkiin laskennan asetuksiin eikä käyttää yli 24 tunnin havaintotiedostoja. Sovelluksen avulla voi käsitellä sekä GPS:n, että GLONASSin havaintotiedostoja. Sovelluksessa voi myös käsitellä havaintotiedostoja lähes reaaliajassa (Near Real-Time PPP), jolloin sovellus käyttää GMV:n laskemia ratatuotteita. Tähän ominaisuuteen ei kuitenkaan perehdytä tarkemmin tässä työssä. Sovellus laskee pisteen koordinaatit

ITRF08- ja ETRS89-koordinaatistoissa havaintohetken epookissa. Käyttäjä voi valita, tehdäänkö laskenta staattisessa vai kinemaattisessa moodissa. Lisäksi käyttäjä voi valita näytteenottovälin ja korkeuskulman katkaisurajan. Käyttäjän valittavissa on myös, onko vastaanotin maan pinnalla vai lentokoneessa ja iteraatiokierrosten lukumäärä. (MagicGNSS, 2012)

Sovellus on varsin helppokäyttöinen. Rekisteröitymisen jälkeen käyttäjä lataa RINEX-tiedostonsa verkkosivustolle ja tekee haluamansa asetukset. Tulokset ovat ladattavissa samaiselta sivustolta. Tulokseksi käyttäjä saa seitsemän eri tiedostoa: vastaanottimen kellovirheiden estimaatit , troposfäärin aiheuttaman virheen estimaatit, pisteen ETRS89-koordinaatit ja tarkkuudet, pisteen ITRF08-koordinaatit ja tarkkuudet, vastaanottimen kulkeman reitin KML-tiedostona kummassakin koordinaatistossa ja tuloksia sekä niiden tarkkuuksia kuvaavia kuvaajia sisältävän pdf-tiedoston. Toisin kuin CSRS-PPP-sovelluksessa käyttäjä ei saa mitään tietoa alkutuntemattomista. Käyttäjä saa myös suhteellisen rajallisesti tietoa sovelluksen käyttämistä parametreista. (MagicGNSS, 2012)

Vastaanottimen kellovirheet ja troposfäärin aiheuttamat virheet on listattu tiedostoissa epookki epookilta. Samoin kuin lasketut suorakulmaiset ja ellipsoidiset koordinaatit virhearvioineen. Pdf-tiedostossa on kuvattu laskennassa käytettyjä parametreja kuten satelliittien ratoja ja kellokorjauksia, näytteenottoväliä, korkeuden katkaisukulmaa ja iteraatiokierrosten määrää. Tämän enempää tietoa ei käytetyistä parametreista ole saatavilla. Tiedostossa on myös esitetty hylättyjen ja hyväksyttyjen havaintojen määrät sekä havaintojen residuaalit satelliittikohtaisesti. Tiedostossa esitetään kuvaajien laskettujen koordinaattien ja tarkkuuksien käyttäytymistä ajansuhteen. Myös x- ja y-koordinaattien hajonta tasossa on esitetty. Kuvaajista ilmenee lisäksi troposfäärin virheen ja vastaanottimen kellon virheen käyttäytyminen ajan suhteen. Tuloksia kuvaavia kuvaajia ei ole yhtä kattavasti kuin CSRS-PPP-sovelluksessa, mutta niistä saa riittävän tiedon tulosten tarkkuudesta. (MagicGNSS, 2012)

4. Tulokset

Havainnot käsiteltiin edellä mainituilla PPP-verkkosovelluksilla. Sovellukset käyttivät IGS:n Final-efemeriidejä, 10 asteen korkeuden katkaisukulmaa ja 30 sekunnin havaintoväliä. Hangon ja Tvärminnen pisteiden kohdalla käytettiin kuitenkin 15 sekunnin havaintoväliä.

Jälkilaskenta tehtiin kinemaattisessa moodissa. Lisäksi laskennassa CSRS-PPP-sovelluksella käytettiin OTL-korjausta (Ocean Tidal Loading). Poikkeuksena on piste Hanko 144, jonka kohdalla ei käytetty OTL-korjausta laskennassa ilmenneiden ongelmien takia. Laskentaan tarvittava OTL-tiedosto luotiin osoitteessa http://froste.oso.chalmers.se/loading/ olevassa palvelussa käyttäen pisteiden arvioituja koordinaatteja. Seuraavaksi esitellään sovelluksilla saadut tulokset.

4.1 Tulokset CSRS-PPP-sovelluksella

Sovelluksella saatiin laskettua kaikkien pisteiden koordinaatit epookki epookilta. Taulukossa 3 on esitetty saadut pisteiden koordinaatit kaikkien epookkien keskiarvoina. Hangon ja Helsingin mareografit mitattiin kahtena eri päivänä. Hangon osalta näiden päivien koordinaattien keskiarvot eroavat toisistaan latitudin ja longitudin osalta noin 1,5 cm ja korkeuden osalta 2,5 cm. Helsingin osalta kaikkien koordinaattien väliset erot olivat alle sentin luokkaa. Saatujen tulosten tarkkuus oli muutamaa poikkeusta lukuun ottamatta hyvä. Latitudien keskihajonnat vaihtelivat välillä 1,7 - 7,2 cm ollen keskimäärin noin 2,5 cm ja longitudien keskihajonnat välillä 1,4 - 6,4 cm ollen keskimäärin noin 2,1 cm. Longitudi saatiin siis ratkaistua keskimäärin tarkemmin kuin latitudi. Ellipsoidisien korkeuksien keskihajonnat vaihtelivat välillä 3,3 - 13,6 cm ja oli keskimäärin noin 4,5 cm. Korkeuksissa oli siis eniten hajontaa, kuten voitiin olettaa. OTL-korjauksen puuttumisella havaintojen Hanko 144 käsittelyssä ei näyttäisi olevan suurta vaikutusta lopputulokseen tai se peittyy muiden virhelähteiden alle.

Taulukko 3. CSRS-PPP:llä laskettujen koordinaattien keskiarvot ITRF08-koordinaatistossa.

Piste	X (m)	Y (m)	Z (m)
Bredberg	2912169,7684	1290952,5619	5507293,2034
Hanko 144	2959210,7223	1254679,3174	5490594,5655
Hanko 145	2959210,7064	1254679,3025	5490594,5416
Helsinki 144	2885137,1043	1342710,4214	5509039,2500
Helsinki 145	2885137,1048	1342710,4166	5509039,2406
Kumpula	2880665,1165	1340892,4905	5511855,5112
Otaniemi	2885246,6333	1334918,3350	5510885,5037
Rokokallio	2866717,1075	1305092,6485	5527711,9210
Tvärminne	2951361,6358	1267976,8709	5491753,0565

Poikkeuksena edellä mainituista tarkkuuksista olivat Rokokallion ja Tvärminnen pisteet, joiden kohdalla ei päästy yhtä hyviin tarkkuuksiin. CSRS-PPP-sovellus hylkäsi tuntemattomasta syystä 77 % Rokokallion havainnoista, joten havaintosession pituudeksi jäi vain kaksi tuntia. Tvärminnen kohdalla on ilmeisesti tapahtunut vaihekatko, jonka takia keskellä havaintosessiota on noin 30 minuutin jakso, jolloin ei ole saatu luotettavia havaintoja. Jostakin syystä CSRS-PPP on ottanut ratkaisuun mukaan selvästi virheellisiä koordinaatteja, joiden keskihajonta on ollut varsin suuri. Esimerkiksi Tvärminnessä keskihajontojen maksimit olivat latitudin kohdalla 3,3 metriä, longitudissa 1,8 metriä ja korkeudessa 4,7 metriä. Pisteiden koordinaattien keskihajontojen minimit, maksimit ja keskiarvot on esitetty kuvassa 2. Tvärminnen osalta nämä kuvaajat esitetään tulosten vertailujen yhteydessä kohdassa 4.3.

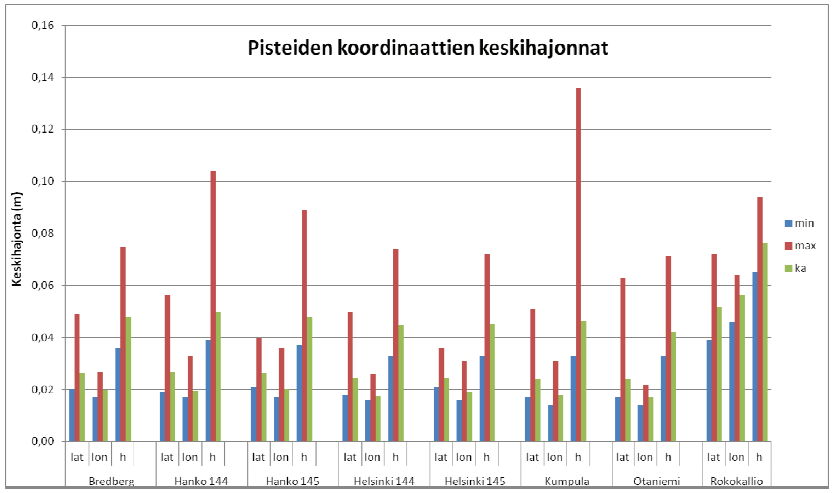

Kuva 2. Epookki epookilta ratkaistujen koordinaattien keskihajontojen minimit, maksimit ja keskiarvot.

CSRS-PPP:n sovelluksesta saatiin lukuarvojen lisäksi kuvaajia, joiden avulla pystytään tulkitsemaan tulosten tarkkuutta ja luotettavuutta. Kuvassa 3 on esitetty Tvärminnessä havaittujen satelliittien lukumäärä ja nollautuneiden alkutuntemattomien prosenttiosuus. Kuten kuvasta nähdään noin, kello 21 havaittujen satelliittien määrä on tippunut alle kuuteen ja alkutuntemattomat ovat nollautuneet. Tämän vaihekatkon vaikutus voidaan nähdä kuvasta 4, jossa on esitetty pisteen ratkaistut korkeudet ja niiden keskihajonnat. Heti vaihekatkon jälkeen ratkaisuja ei ole saatu ollenkaan ja noin kello 22 saatujen ratkaisujen keskihajonnat ovat useita metrejä. Samanlaisia kuvaajia on myös latitudin, longitudin, troposfäärikorjauksen ja vastaanottimen kellokorjauksen vaihteluista.

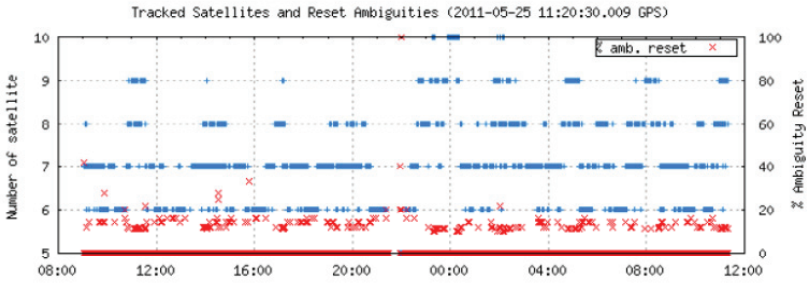

Kuva 3. Tvärminnessä havaittujen satelliittien lukumäärä ja nollautuneiden alkutuntemattomien prosenttiosuus (CSRS-PPP).

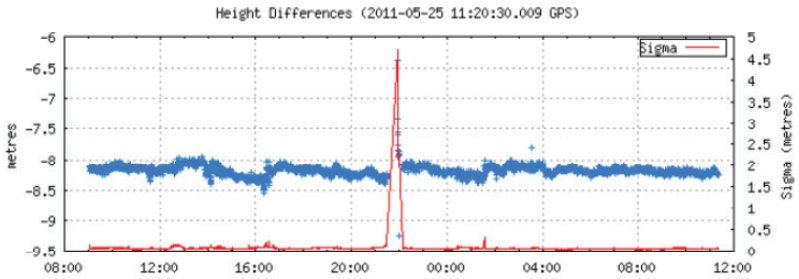

Kuva 4. Tvärminnen ratkaistut korkeudet ja niiden keskihajonnat (CSRS-PPP).

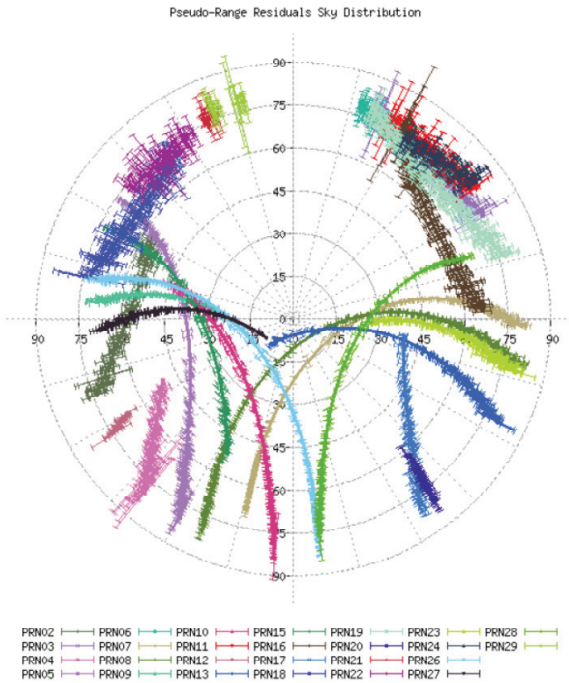

Kuva 5. Vaihe-erohavaintojen residuaalien riippuvuus satelliitin korkeuskulmasta. Kuva Bredbergin havainnoista (CSRS-PPP).

Kuvassa 5 on havainnollistettu satelliittien vaihe-erohavaintojen residuaalien riippuvuutta satelliitin korkeuskulmasta. Kuten kuvasta näkyy residuaalit kasvavat, kun korkeuskulma pienenee. Pisteiden vaihe-erohavaintojen residuaalit olivat välillä 4,3 - 7,6 mm ja koodihavaintojen residuaalit välillä 1,38 - 3,10 m. Suurimmat residuaalit olivat Rokokallion ja Tvärminnen pisteillä.

Lopuksi kuvassa 6 on esitetty Otaniemen latitudi- ja longitudiratkaisujen hajonta. Kuvasta voidaan nähdä, että suurin osa ratkaisuista sijoittuu 3 - 4 cm alueelle.

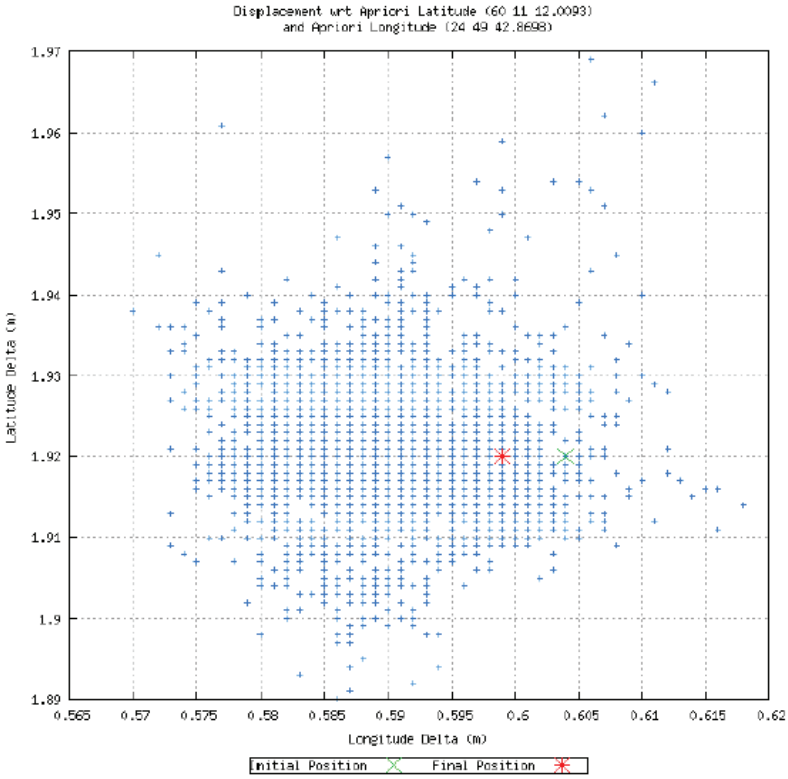

Kuva 6. Otaniemen latitudi- ja longitudiratkaisujen hajonta (CSRS-PPP).

4.2 Tulokset MagicPPP-sovelluksella

MagicPPP-sovelluksella saatiin ratkaistua kaikkien pisteiden koordinaatit epookki epookilta. Saatujen koordinaattien keskiarvot on esitetty taulukossa 4. Kahtena eri päivänä mitattujen Hangon ja Helsingin mareografien koordinaattien keskiarvot poikkesivat toisistaan Hangon osalta alle 2 senttimetriä sekä Helsingin osalta alle senttimetrin. Laskettujen koordinaattien keskihajonnoissa oli paljon vaihtelua. Latitudien keskihajonnat vaihtelivat välillä 1,1 - 12,1 cm ollen keskimäärin

noin 1,9 cm. Longitudin osalta keskihajonnat vaihtelivat välillä 1,1 - 14,4 cm ja oli keskimäärin noin 1,5 cm. Longitudi saatiin siis ratkaistua keskimäärin tarkemmin kuin latitudi. Ellipsoidisen korkeuden keskihajonnat vaihtelivat välillä 2,4 - 40,1 cm ollen keskimäärin noin 4 cm. Korkeuksissa oli siis selvästi enemmän hajontaa kuin muissa koordinaateissa. Poikkeuksena edellä mainituista keskihajontojen maksimeista oli Tvärminnen piste. Tvärminnessä keskihajontojen maksimi oli latitudissa 17,5 cm, longitudissa 24,6 cm ja korkeudessa 49,1 cm. Pisteiden koordinaattien keskihajontojen minimit, maksimit ja keskiarvot on esitetty kuvassa 7. Tvärminnen osalta nämä kuvaajat esitetään tulosten vertailujen yhteydessä kohdassa 4.3. Keskihajontojen perusteella koordinaatit saatiin ratkaistua hyvällä tarkkuudella. Poikkeuksena olivat Rokokallion ja Tvärmminnen pisteet, joita ei saatu määritettyä yhtä tarkasti kuin muita pisteitä.

Taulukko 4. MagicPPP:llä laskettujen koordinaattien keskiarvot ITRF08-koordinaatistossa.

Piste	X (m)	Y (m)	Z (m)
Bredberg	2912169,7640	1290952,5590	5507293,1992
Hanko 144	2959210,7128	1254679,3062	5490594,5572
Hanko 145	2959210,7024	1254679,3079	5490594,5391
Helsinki 144	2885137,0975	1342710,4120	5509039,2441
Helsinki 145	2885137,0979	1342710,4191	5509039,2363
Kumpula	2880665,1060	1340892,4938	5511855,5037
Otaniemi	2885246,6333	1334918,3350	5510885,5037
Rokokallio	2866717,0622	1305092,7160	5527711,8861
Tvärminne	2951361,6296	1267976,8608	5491753.0614

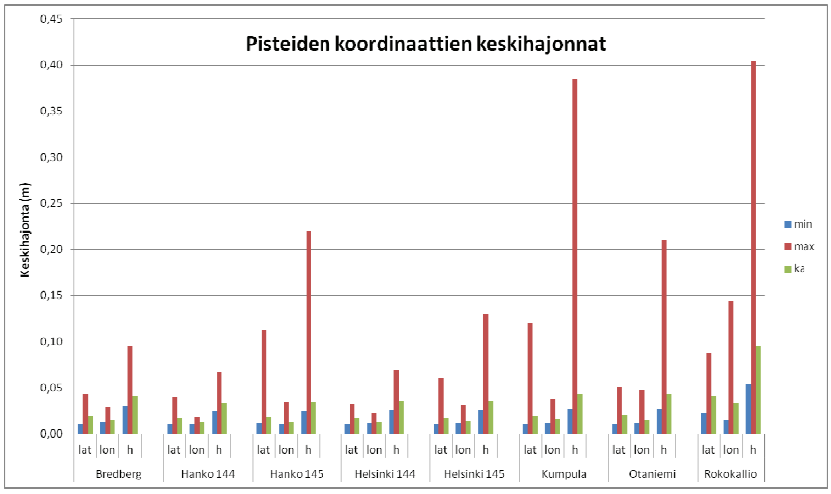

Kuva 7. Epookki epookilta ratkaistujen koordinaattien keskihajontojen minimit, maksimit ja keskiarvot.

MagicPPP tuotti koordinaattiratkaisujen lisäksi useita kuvaajia, joiden avulla ratkaisujen tarkkuutta pystytään arvioimaan. Kuvassa 8 on esitetty neljä kuvaajaa, jotka kuvaavat Tvärminnen koordinaattiratkaisuja. Kuvassa on esitetty latitudin, longitudin ja ellipsoidisen korkeuden ratkaisut sekä keskihajonnat ajan suhteen. Lisäksi yhdessä kuvaajassa latitudi- ja longitudiratkaisujen hajonta. Latitudia, longitudia ja korkeutta esittävistä kuvaajista voidaan nähdä, kuinka noin kello 21 on alkanut yli 30 minuutin jakso, jolloin ratkaisuja ei ole saatu ollenkaan. Tämän ajanjakson lopulla koordinaatit on saatu ratkaistua, mutta ne poikkeavat huomattavasti edeltävistä ratkaisuista, vaikka keskihajonnat näyttävätkin pysyvän hyvällä tasolla. Myös latitudin ja longitudin hajontaa esittävästä kuvaajasta voidaan nähdä selvästi virheellisten ratkaisujen joukko.

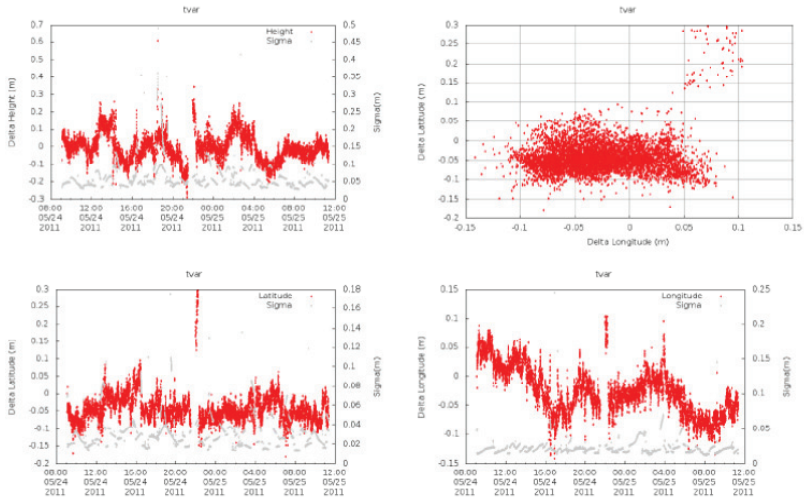

Kuva 8. Latitudin, longitudin ja ellipsoidisen korkeuden ratkaisut ja keskihajonnat ajan suhteen sekä latitudi- ja longitudiratkaisujen hajonta Tvärminnessä (MagicPPP).

Kuvassa 9 on vielä esitetty kaksi kuvaajaa, jotka kuvaavat havaittujen satelliittien koodi- ja vaihe-erohavaintojen residuaalien riippuvuutta satelliittien korkeuskulmasta. Kuten kuvaajista nähdään, kummatkin residuaalit kasvavat kun korkeuskulma lähestyy nollaa.

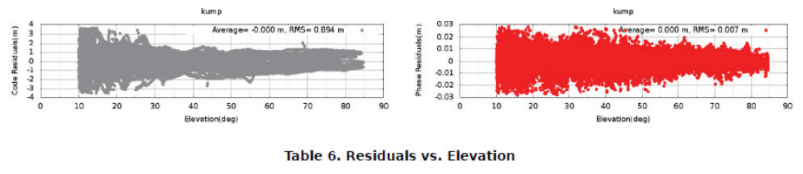

Kuva 9. Koodi- ja vaihe-erohavaintojen residuaalien riippuvuus satelliitin korkeuskulmasta Kumpulassa (MagicPPP).

4.3 Tulosten vertailu

Kummallakin sovelluksella saatiin hyvin saman tyyppisiä tuloksia, mutta tuloksista löytyi myös pieniä eroja. Taulukossa 5 on esitetty CSRS-PPP:llä ja MagicPPP:llä laskettujen suorakulmaisten koordinaattien keskiarvojen erotukset millimetreissä. Taulukosta huomataan, että lähes kaikkien pisteiden kohdalla koordinaattien erot ovat maksimissaan senttimetrin luokkaa. Poikkeuksena tästä on Rokokallio, jossa koordinaattien erot ovat useita senttimetrejä. Tosin Rokokallion kohdalla koordinaattien keskihajonnatkin olivat kummallakin sovelluksella muita pisteitä suurempia. Rokokalliossa mittausten geometria oli huono tai mittauksissa oli jotain muuta häiriötä.

Taulukko 5. CSRS-PPP:llä ja MagicPPP:llä laskettujen suorakulmaisten ITRF08-koordinaattien keskiarvojen erotukset ja pisteiden välinen etäisyys d.

Piste	**ΔX (mm)**	**ΔY (mm)**	**ΔZ (mm)**	**d (mm)**
Bredberg	4,4	2,9	4,2	6,8
Hanko 144	9,5	11,2	8,3	16,9
Hanko 145	4,0	-5,4	2,5	7,1
Helsinki 144	6,8	9,4	5,9	13,0
Helsinki 145	6,9	-2,5	4,3	8,5
Kumpula	10,5	-3,3	7,5	13,4
Otaniemi	11,2	4,8	11,2	16,6
Rokokallio	45,3	-67,5	34,9	88,5
Tvärminne	6,2	10,1	-4,9	12,8

MagicPPP:n laskemien koordinaattien keskihajontojen keskiarvot olivat jokaisen pisteen kohdalla hieman pienempiä kuin CSRS-PPP:n tuottamat arvot. Tämän perusteella MagicPPP:llä laskettujen koordinaattien tarkkuus vaikuttaisi olevan parempi kuin CSRS-PPP:llä laskettujen koordinaattien. Sovellusten tuottamaa absoluuttista tarkkuutta on kuitenkin mahdoton arvioita, koska vertailua pisteiden oikeisiin koordinaatteihin ei tehty. MagicPPP:llä lasketuissa ratkaisuissa maksimikeskihajonnat ovat useimpien pisteiden kohdalla selvästi CSRS-PPP:llä laskettuja suurempia. Kuitenkin selvänä poikkeuksena tästä on Tvärminnen piste, jonka kummallakin sovelluksella laskettujen koordinaattien keskihajontojen minimit, maksimit ja keskiarvot on esitetty kuvassa 10. CSRS-PPP on ottanut Tvärminnen ratkaisuihin mukaan selvästi virheellisiä ratkaisuja. Kokonaisuudessaan kummallakin sovelluksella laskettujen koordinaattien keskihajonnat vaihtelevat pisteiden välillä samanlaisen trendin mukaisesti. Tämän voi havaita vertailemalla kuvia 2 ja 7.

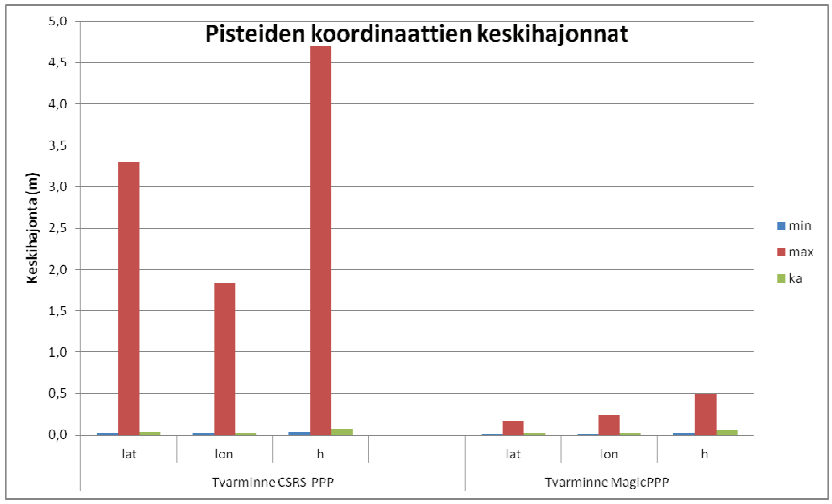

Kuva 10. Tvärminnen koordinaattien keskihajontojen minimit, maksimit ja keskiarvot kummallakin sovelluksella ratkaistuina.

CSRS-PPP tuotti MagicPPP:tä selkeämmät kuvaajat ja enemmän informaatiota ratkaisuista. CSRS-PPP:n kuvaajia on helpompi tulkita ja niiden avulla pystyy paremmin arvioimaan ratkaisujen laatua. CSRS-PPP antoi lisäksi kaikki kuvaajissa esitetyt tiedot numeerisessa muodossa, joten käyttäjä pystyy myös itse piirtämään vastaavat kuvaajat. MagicPPP:n ulosanti oli CSRS-PPP:hen verrattuna suppeaa ja siinä keskityttiin lähinnä vain koordinaattiratkaisuihin. CSRS-PPP antoi myös tarkemmat tiedot laskennassa käytetyistä parametreista. Loppujen lopuksi koordinaattiratkaisujen tarkkuuksissa ei ollut suuria eroja, vaan suuremmat erot löytyvät sovellusten ulosannista ja tavasta kuvata ratkaisuja.

5. Yhteenveto

Tässä työssä perehdyttiin Precise Point Positioning -menetelmään, sen mahdollistaviin IGS:n tarkkoihin satelliittien ratoihin ja kahteen PPP-verkkosovellukseen. Työssä esiteltiin myös PPP:n mahdollisia sovelluskohteita sekä menetelmän etuja ja haasteita. Työn tarkoituksena oli esitellä PPP-menetelmä, perehtyä kahteen PPP-verkkosovellukseen ja tarkastella miten pisteiden koordinaattien laskenta näillä sovelluksilla onnistuu. Tarkoituksena oli tutkia PPP-sovellusten koordinaattiratkaisujen tarkkuutta ja vertailla niitä keskenään. Aiheeseen perehdyttiin tutustumalla monipuolisesti tieteellisiin artikkeleihin, jotka keskittyivät PPP-

menetelmää ja sen teoreettista perustaa. Lisäksi työssä hyödynnettiin tutkittujen PPP-sovellusten ja IGS:n verkkosivuja.

PPP on vaihtoehto relatiiviseen paikannukseen perustuville DGPS:lle ja RTK:lle. PPP ei tarvitse tukiasemaa tai tukiasemien verkkoa toisin kuin edellä mainitut menetelmät. Tämän takia menetelmä tekee mittauksista logistisesti yksinkertaisempia ja tuo taloudellisia säästöjä. PPP:llä voidaan ratkaista pisteen koordinaatit muutaman senttimetrin tarkkuudella mikä vastaa RTK:n tarkkuutta. Menetelmä mahdollistaa myös tarkkojen koordinaattien mittaamisen syrjäisillä alueilla. Toisaalta PPP vaatii jopa 30 minuutin alustusajan ennen kuin tarkkoja mittauksia voidaan tehdä. Lisäksi menetelmä vaatii jatkuvia havaintoja vähintään kuuteen satelliittiin. Tämän takia PPP edellyttää esteetöntä näkyvyyttä taivaalle ja toimii parhaiten täysin avoimilla paikoilla. Tulevaisuudessa PPP on hyvin kilpailukykyinen vaihtoehto RTK:lle, jos sen tarvitsemaa alustusaikaa voidaan lyhentää ja nykyinen tarkkuus voidaan saavuttaa myös reaaliajassa.

Työssä perehdyttiin CSRS-PPP- ja MagicPPP-sovellukseen, joiden avulla laskettiin seitsemän pisteen koordinaatit. Käytetyt sovellukset sopivat hyvin koordinaattien jälkilaskentaa ja saadut tuloksen olivat pääasiassa hyviä. Kummallakin sovelluksella laskettujen koordinaattiratkaisujen tarkkuudet olivat muutamien senttimetrien luokkaa. Sovelluksien välillä ratkaisujen tarkkuudessa ei havaittu suurta eroa. Sen sijaan CSRS-PPP tuotti laajemmin tietoa ratkaisuista ja esitti tulokset selkeämmässä muodossa.

Työlle asetetut tavoitteet ja odotukset saatiin täytettyä. Työtä voisi jatkaa vertailemalla pisteiden laskettuja koordinaatteja pisteiden tunnettuihin koordinaatteihin. Tällä tavalla menetelmän tarkkuudesta saataisiin tarkempaa tietoa. Toisaalta pisteiden laskettuja koordinaatteja voisi myös verrata verkkotasoituksessa pisteille laskettuihin koordinaatteihin, vaikka lähtökohtaisesti PPP:llä ei pitäisi saavuttaa yhtä hyvää tarkkuutta.

6. Viitteet

ANDREI, C-O. & SALAZAR, D. & CHEN, R. (2010). Performance analysis of the Precise Point Positioning technique at BUCU IGS station. Journal of Geodesy and Cadastre. Vol. 10, sivut 9-20. ISSN 1583-2279. Saatavilla http://users.tkk.fi/~coandrei/pdf/Andrei_GeoCAD10_v0520.pdf.

BISNATH, S. & GAO, Y. (2008). Current State of Precise Point Positioning and Future Prospects and Limitations. International Association of Geodesy Symposia 133: "Observing our changing earth," Sideris, M. (toim.). Sivut 615-623. ISBN 9783540854265. Saatavilla http://gge.unb.ca/Research/GRL/GNSS/BisnathGaoIUGG2007.pdf.

GAO, Y. & CHEN, K. (2004). Performance Analysis of Precise Point Positioning Using Real-Time Orbit and Clock Products. Journal of Global Positioning Systems.Vol. 3, no. 1-2, sivut 95-100. ISSN 2150-8526. Saatavilla http://www.gnss.com.au/JoGPS/v3n12/v3n12p14.pdf.

GE, M. & GENDT, G. & ROTHACHER, M. & SHI, C. & LIU, J. (2008). Resolution of GPS carrier-phase ambiguities in Precise Point Positioning (PPP) with daily observations. Journal of Geodesy. Vol. 82, sivut 389-399. ISSN 09497714. Saatavilla http://ppp-wizard.net/Articles/JG2008.pdf.

IGS. (2012). International GNSS Servicen verkkosivut. [viitattu 24.2.2012]. Saatavilla http://igscb.jpl.nasa.gov/.

KOUBA, J. (2009). A guide to using International GNSS Service (IGS) products. Geodetic Survey Division Natural Resources Canada. 34 sivua.

KOUBA, J. & HEROUX, P. (2001). GPS Precise Point Positioning Using IGS Orbit Products. GPS Solution. Vol. 5, no 2, sivut 12–28. Saatavilla ftp://ftp.glonass-ianc.rsa.ru/REPORTS/OLD/NRCAN/final.pdf.

MAGICGNSS. (2012). MagicGNSS:n verkkosivut. [viitattu 28.2.2012]. Saatavilla http://magicgnss.gmv.com/.

MERVART, L. & LUKES, Z. & ROCKEN, C. & IWABUCHI, T. (2008). Precise Point Positioning With Ambiguity resolution In Real-Time. Proceedings of the 21st International Technical Meeting of the Satellite Division of The Institute of Navigation (ION GNSS 2008), September 16-19, 2008, Savannah International Convention Center, Savannah, GA. Vol. 11, sivut 397-405. Saatavilla http://www.ppp-wizard.net/Articles/PPP_RTK.pdf.

NRC. (2012). On-line Precise Point Positioning 'How To Use' Document. Natural Resources Canada, Centre for Remote Sensing, Geodetic Survey Division. 23 sivua. Saatavilla http://198.103.48.76/userguide/pdf/howtouse.pdf.

OVSTEDAL, O. & KJORSVIK, N. & GJEVESTAD, J. (2006). Surveying using GPS Precise Point Positioning. Proceedings of Shaping the Change, XXIII FIG Congress, Munich, Germany, October 8-13, 2006. 10 sivua. Saatavilla http://www.fig.net/pub/fig2006/papers/ts43/ts43_03_ovstedal_etal_0612.pdf.

GOCE User Toolboxin käyttö Itämeren meritopografian visualisoinnissa

Timo Saari

Aalto University School of Engineering
Department of Real Estate, Planning and Geoinformatics
timo.saari@aalto.fi

Abstract

NN

1 Johdanto

1.1 Tutkimuksen tavoite, rajaus sekä rakenne

Tämän seminaarityön tarkoituksena on tutkia, kuinka Itämeren meritopografia mallinnetaan GOCE User Toolboxin (GUT) avulla ja kuinka tarkkoja ratkaistut mallit ovat. Itämeren lisäksi mallinnetaan osia Pohjanmerestä sekä Norjanmerestä siten, että havaintoalueeksi rajataan -5–52 itäistä pituutta, sekä leveyspiireinä 51–73 pohjoista pituutta. Painovoimamalleina käytetään pelkästään GOCEn ratkaisuja, joihin ei ole lisätty maanpäällisiä havaintoja, jotta saataisiin selkeimmät eroavaisuudet avaruusgeodeettisille sekä geodeettisille ratkaisuille.

Tutkimus sisältää neljä lukua, jossa ensimmäisessä käsitellään lyhyesti meritopografian käsitettä sekä GOCE-missiota, jolla meritopografia pystytään ratkaisemaan. Toisessa luvussa tutustutaan erilaisiin meritopografiamalleihin, joita GUT-ohjelmalla saadaan luoduiksi ja pyritään löytämään parhaimmat mahdolliset asetukset kyseisille malleille. Kolmannessa luvussa tehdään kirjallisuustutkimusta maanpäällisesti suoritettuihin Itämeren meritopografiamalleihin, joiden tuloksia vertaillaan GOCElla saatujen tuloksien kanssa. Luvussa neljä esitetään tutkimuksen yhteenveto.

1.2 Meritopografia

Mitä on meritopografia ja mihin sitä tarvitaan? Meritopografia (mean dynamic topography, MDT), kuvastaa keskimerenpinnan pysyvää poikkeamaa ekvipotentiaalipinnasta, eli geoidista. Mikäli merivesi olisi lepotilassa, tällöin keskimerenpinta olisi tarkasti sama kuin geoidi – joskaan näin ei asianlaita ole. Meriin kohdistuu monenlaisia voimia, jotka työntävät ja kääntävät vesimassoja eri suuntiin, ja näin ollen aiheuttavat meritopografian. Edellä mainittuja voimia aiheuttavat veden paikalliset lämpö- ja suolaisuusvaihtelut, ilmakehän painevaihtelut, tuulet sekä geostrofiset virtaukset (Coriolis-voima). (Vermeer 2011, s. 147)

Meritopografian määrittämistä tarvitsemme muun muassa merivirtauksien hahmottamiseen. Merivirtauksien avulla voimme havainnoida valtamerten vaikutuksia maapallon ilmastoon sekä ilmastonmuutokseen, sillä virtaukset kuljettavat mukanansa lämpöä, kemiallisia yhdisteitä (esimerkiksi hiilidioksidia), ravinteita, merten eliöstöä sekä liike-energiaa. (Lee ym. 2010, s. 71)

1.3 Meritopografian määrittäminen

Meritopografia voidaan ratkaista erilaisilla menetelmillä, joita ovat (Vermeer 2011, s. 151):

- altimetria ja gravimetrinen geoidimääritys
- mareografit ja gravimetrinen geoidimääritys
- tarkkavaaitus rannikkoa pitkin
- oseanografinen (fysikaalinen) mallinnus.

Tässä työssä tutustutaan meritopografiaan, joka lasketaan altimetriasta ja painovoimasatelliitti GOCEn (Gravity field and steady-state Ocean Circulation Explorer) tuottamasta geoidimallista. Saatuja ratkaisuja vertaillaan aikaisempien maanpäällisesti suoritettujen havaintojen kanssa. Meritopografia, *MDT*, voidaan määritellä geoidimallista seuraavasti:

$$MDT = MSS - N, \tag{1}$$

jossa *MSS* on keskimerenpinnan korkeus (the altimetric mean sea surface, *MSS*) vertausellipsoidiin nähden ja *N* on geoidikorkeus.

Jotta voisimme ratkaista *MDT*:n yllä olevasta yhtälöstä, meillä tulee olla määriteltyinä *MSS* sekä geoidi samaan koordinaattijärjestelmään, vertausellipsoidiin sekä vuorovesimalliin. *MSS*-malleja löytyy useita, joista tuorein on nimeltään ”*MSS* CNES CLS 11”, jota myös tässä työssä käytetään. Kyseinen *MSS*-malli on ratkaistu 16 vuotta kestäneistä altimetriahavainnoista, joita ovat eri aikoina tuottaneet seuraavat satelliittimissiot (Aviso 2012):

- TOPEX/Poseidon, 10 vuotta & TOPEX/Poseidon tandem, 3 vuotta
- ERS-1 & 2, 8 vuotta
- GFO, 7 vuotta
- Jason 1, 7 vuotta
- Envisat, 7 vuotta.

1.4 GOCE

GOCE on Euroopan avaruusjärjestön (European Space Agency, ESA) vuonna 2009 laukaisema painovoimasatelliitti, jonka tehtävänä on määrittää tarkka ja yksityiskohtainen kuvaus maapallon painovoimakentästä sekä geoidista (Rummel ym. 2011, s. 644). Kuten edellisessä luvussa todettiin, tarvitsemme geoidin tarkkaa määrittämistä, jotta saisimme ratkaistua meritopografian.

GOCE on ainutlaatuinen satelliitti (kuva 1) jo pelkän kokonsa, muotoilunsa sekä kiertoratansa vuoksi:

- paino 1200 kg, kiertorata 260 km, vrt. TOPEX/Poseidon (2402 kg, 1336 km).

GOCEn kiertorata on aurinkosynkroninen, tarkoittaen, että ratatason kiertymä pysyy Aurinkoon nähden paikoillaan. (Rummel ym. 2011, s. 646). Tämä johtaa siihen, että satelliitti ylittää saman maapallon paikan samaan vuorokaudenaikaan samanlaisissa valaistusolosuhteissa päivästä toiseen. Aurinkosynkroninen rata aiheuttaa lisäksi sen, että se laskostaa vuorovesi-ilmiöitä, eli vääristää signaaleita, jolloin tarvitaan koko maapallon kattava vuorovesimalli, jotta signaalien vääristymät saadaan korjatuiksi (Durand ym. 2010, s. 774).

GOCE kuljettaa mukanansa useita erilaisia instrumentteja, joita ovat:

- geodeettinen GPS-vastaanotin
- tähtisensorit (3 kpl)
- sähköstaattinen painovoimagradiometri
- magneettiset vääntimet (magnetic torquers)
- ionimoottorit.

GPS:llä (Global Positioning System) mitataan satelliitin paikka kiertoradallaan, joka saadaan lasketuksi GPS-vastaanottimen havaitsemista koodi- ja vaihe-eroista, joko geometrisesti tai redusoidulla dynaamisella ratamäärittelyllä (the method of reduced dynamic orbit determination). Määrittelyllä saadaan ratkaistuksi satelliitin lentorata 1–2 sentin tarkkuudella. (Rummel ym. 2011, s. 645–646)

Painovoimagradiometri koostuu kuudesta äärimmäisen tarkasta kiihtyvyysmittarista, jotka mittaavat Maan painovoimavektoreita, eli geopotentiaalin gradientteja, joiden avulla rekonstruoidaan Maan painovoimakenttä (Vermeer 2011, s. 167). Gradiometri on sijoitettu satelliitin massakeski-pisteeseen, siten että instrumentin *x*-akseli osoittaa lentosuuntaan, *y*-akseli lentoratatason normaaliin sekä *z*-akseli kohti Maata (Rummel ym. 2011, s. 645).

Painovoimagradiometrin akselien orientaatio suoritetaan kolmen tähtisensorin avulla. Satelliitin radan aiheuttama kiertoliike vääristää kiihtyvyysmittareiden havaitsemaa gravitaatiosignaalia, kulmanopeuden ja -kiihtyvyyden muodossa. Kulmanopeudet voidaan erottaa kiihtyvyysmittarien havainnoista tähtiseurantaa käyttäen. Matalan ratansa vuoksi satelliittiin kohdistuu ilmanvastusta, jota kompensoidaan ionimoottoreiden avulla. Lisäksi satelliitin orientointi pidetään stabiilina magneettisten vääntimien (magnetic torquers) avulla, jotka luovat satelliitin ympärille magneettikentän, joka vastavuoroisesti Maan magneettikentän kanssa luovat tarvittavan momentin, jotta satelliitti pitää asemansa ja liikkeensä. (Rummel ym. 2011, s. 645–646)

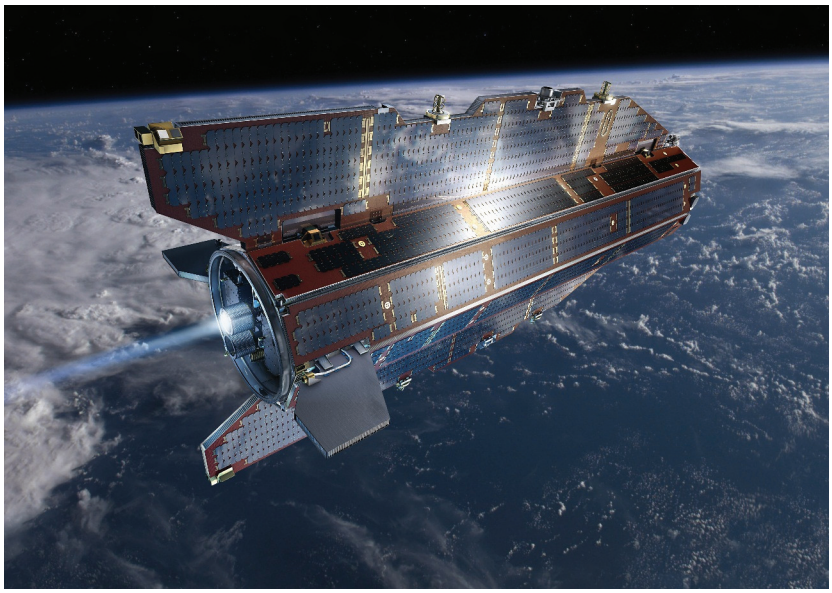

Kuva 1. Kuvaus GOCEsta kiertoradallansa (European Space Agency 2012a).

GOCEn tuottamia havaintoja käsitellään ESAn High-level Processing Facility (HPF) -projektissa, jonka päämääränä on tuottaa globaalisia painovoimakenttämalleja. Painovoimakenttämallien laskentaan on olemassa kolme erilaista menetelmää, joita ovat direct (DIR), time-wise (TIM) sekä space-wise (SPW). DIR-menetelmässä käytetään GOCE-datan tukena a priorisia -painovoima-kenttätietoja muiden painovoimasatelliittimissioiden ratkaisuista (GRACE), kun vastaavasti TIM-menetelmässä painovoimakenttä lasketaan pelkästään GOCE-datasta. SPW-menetelmä perustuu lähinnä avaruuteen, josta suoritetaan Wiener-suodatuksella ja pienimmän neliösumman kollokaatiolla painovoimakentän laskenta. Taulukkoon yksi on eriteltynä ominaisuuksia, joista edellä mainitut laskentamenetelmät muodostuvat. (Pail ym. 2011, s. 820–821)

2 Itämeren meritopografian ratkaisu GUT:lla

Luvussa esitellään GOCE User Toolboxin käyttöä meritopografian ratkaisemisessa. Esitetään ohjelman komentosarjoja ja annetaan niiden tuottamille ratkaisuille selitykset. Luvussa esitellään erilaisia komentoasetuksia, joilla määritellään ratkaisun kokoa, muotoa ja tarkkuutta, minkä lisäksi vertaillaan GOCEn kolmella eri painovoimakenttäratkaisulla (DIR, TIM ja SPW) tuotettuja tuloksia.

Taulukko 1. DIR-, TIM-, ja SPW-laskentamenetelmien ominaisuuksia (Pail ym. 2011, s. 833).

	DIR	TIM	SPW
Painovoimakenttä	GOCE-data + a priori -painovoimakenttämalli	Pelkkä GOCE-data	GOCE-datan hiloista tuotettu malli
A priori -informaatio	EIGEN-5C	-	EGM2008 (pienillä asteluvuilla + Quick-look malli)
Painovoimakentän laskentamenetelmä	Pienimmän neliösumman inversio-menetelmä	Pienimmän neliösumman inversio-menetelmä	Kiertoradan Wiener-suodatus + pienimmän neliösumman kollokaatio
Satellite-to-satellite tracking (SST)	Dynaaminen ratamäärittely (the method of reduced dynamic orbit determination)	Geometrinen ratamäärittely	Geometrinen ratamäärittely
Satellite gravity gradiometry (SGG)	Mittauksen kaistanleveyden ARMA (autoregressive moving-average) -suodatus	Koko spektrin ARMA-suodatus	Kovarianssi funktiot (kohinan aikakorrelaatio ja signaalin avaruuskorrelaatio)
Resoluutio (aste- ja järjestysluku, L)	240	224	210
Spatiaalinen mittakaava 20000/L	83 km	89 km	95 km

2.1 GOCE User Toolbox (GUT)

GOCE User Toolbox on Euroopan avaruusjärjestön (European Space Agency, ESA) kehittämä työkalu GOCEn (Gravity field and steady-state Ocean Circulation Explorer) tuottaman aineiston käsittelyyn, analysoimiseen sekä visualisoimiseen. GUT on käskypohjainen ohjelma, johon annetaan syötteeksi komentoja, joilla ohjelma laskee haluttuja kenttiä, joita ovat muun muassa geoidikorkeudet, MSS, MDT, merivirtaukset ynnä muut. Ohjelma sisältää useita erilaisia komentoja, jotka ovat havainnollistettuina kuvaan 2. Lisätietoja löytyy GUT:n Workflow Manualista.

Komentojen syötetiedostoina toimivat valmiina olevat havaintoaineistot, eli eri menetelmillä (DIR, TIM, SPW) tuotetut painovoimakenttämallit sekä a priori -tiedot, joita ohjelmasta löytyy kiitettävän paljon. Esimerkiksi pelkästään erilaisia MSS-malleja löytyy seitsemän kappaletta:

- CNES-CLS 2011 MSS 2min
- DNSC-DTU 2010 MSS 2min
- DNSC-DTU 2010 MSS 5min
- DNSC-DTU 2010 MSS 10min

```
* adapt           Regridding of a data set via interpolation.
* add             Logical addition of data sets.
* changeellipse   Transform a data set to a different ellipsoid.
* changetide      Transform a tidal data set to a new tide system.
* export          Write data in an external format (lossy).
* filter          Low-pass filtering.
* geoidheight     Computes the Geoid.
* gf2shf/shf2gf   Spatial/Spectral domain transformations.
* gravityanomaly  Compute free air anomaly on the terrain.
* gsveast         Eastward component of geostrophic velocity.
* gsvnorth        Northward component of geostrophic velocity.
* heightanomaly   Compute height of the terrain above the telluroid.
* import          Convert to GUT file format (to provide meta-data).
* landmask        Mask out land (sea) regions.
* scale           Multiplicative rescale of a data set.
* spatialmdt      Compute dynamic topography in the spatial domain.
* stats           Report simple statistics.
* subtract        Logical subtraction of data sets.
* surfacegrav     Evaluate geopotential on a surface.
* transect        Slice through a gridded data set.
* vertical        Compute deflection of the vertical at the terrain.
```

Kuva 2. GUT:n sisältämät komennot.

- SMO CLS 2001
- Danish National Space Center regional DNSC09 MSS 2min
- IBIROOS CLS regional mean sea surface 1min.

Ohjelma sisältää README-tiedostot kaikista syötetiedostoista, mistä löytyvät yksityiskohtaiset informaatiot sekä ominaisuudet syötteille. Yllä olevat MSS-mallit löytyvät README_MSS -tiedostosta. Ohjelma tulostaa laskennasta syntyneet Output-tiedostot nc-formaatissa, joita voidaan erikseen visualisoida BratDisplay-aliohjelman avulla. BratDisplayllä malleja voidaan visualisoida ja kohdentaa haluamallaan tavalla, muun muassa valitsemalla erilaisia projektioita sekä väriskaaloja, jotta malleista saadaan mahdollisimman helppolukuisia.

Ohjelmalla voidaan laskea kentät halutuilla tekijöillä (vertausellipsoidit, suodattimet ym.) sekä tarkkuuksilla (rasterin spatiaalinen koko) koko maapallon kattavasti, myös mantereille. Laskennassa rasterin koko täytyy miettiä tarkasti, sillä laskenta-aika kasvaa potenssilain mukaisesti rasteria pienennettäessä. Esimerkiksi laskettaessa MDT koko maapallolle rasterin ollessa $0{,}2 * 0{,}2$ astetta (kuva 3), laskentaan kului noin 1,5 h, mutta kun tarkkuus kasvatetaan $0{,}1 * 0{,}1$ asteeseen, laskentaan olisi kulunut noin vuorokausi.

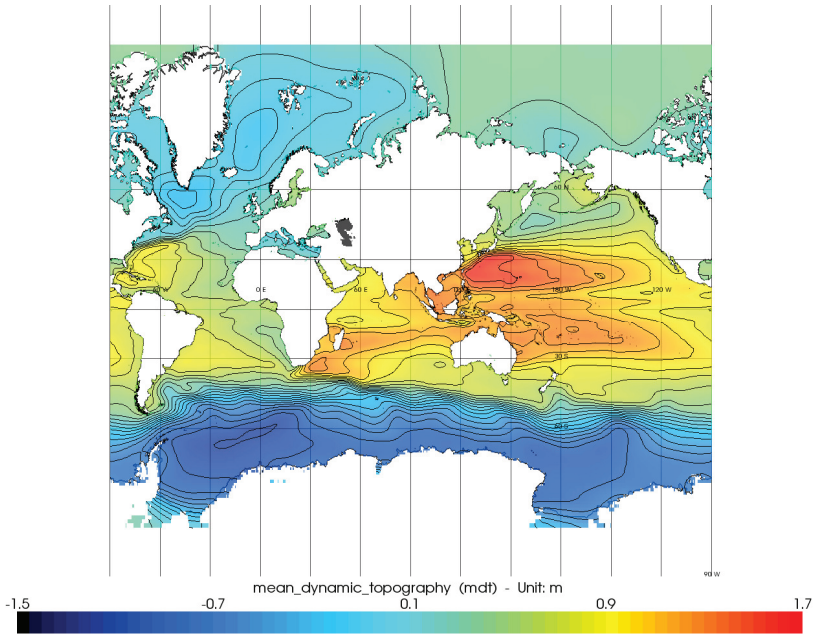

Kuva 3. Maapallon merialueiden meritopografia laskettuna DIR-menetelmällä vuoden 2009–2011 aineistoista (rasteri 0,2°×0,2°).

Tutkimuksen tulokset perustuvat GOCE level 2 dataan, jonka aineistot ovat kerättynä vuosilta 2009–2011. Ainoastaan SPW-painovoimaratkaisulle ei syystä tai toisesta ole tarjolla vuoden 2011 aineistoja. Painovoimakenttäratkaisun aste- ja järjestysluvun (L) arvo määrittää alimman mahdollisen raja-arvon gravitaatiomallin spatiaaliselle mittakaavalle, joka on suurin piirtein 20 000/L km. Tästä syystä DIR-menetelmällä saadaan lyhkäisin mahdollinen mittakaava, kun L:n arvo on 240, mikä antaa mittakaavaksi 83 km. Tästä syystä tässä työssä on valittu GOCEn painovoimakenttäratkaisuksi DIR-ratkaisu, jonka tuloksia tullaan vertaamaan muihin ratkaisuihin. (Pail ym. 2011. s, 820–821)

2.2 ”Step by step” -ratkaisu

Lasketaan seuraavaksi Itämeren alueelle meritopografia käyttämällä vuoden 2009–2011 DIR-havaintoaineistoja. GUT-työkalulla voidaan laskea MDT suoraan yhdellä komennolla ”spatialmdt_gf” ja rajata laskenta haluamalleen alueelle. Lasketaan kuitenkin seuraavassa Itämeren MDT askel askeleelta, jolloin myös nähdään, minkälaisista malleista kyseinen kenttä muodostuu.

Aloitetaan laskenta määrittelemällä ensiksi geoidikorkeudet valitulle vertausellipsoidille sekä vuorovesimallille. Tämän jälkeen rajataan

laskennan tarkkuus (rasterin koko) sekä kohteena oleva alue, käyttäen leveys- ja pituuspiirejä. Vertausellipsoidiksi valitaan TOPEX/Poseidon-ellipsoidi, sillä valittu MSS on määritelty samaan vertausellipsoidiin. Vuorovesimallina käytetään keski-arvoista laskettua vuorovesimallia (mean). Ratkaisun alueeksi rajataan Itämeren alue, pienine lisäyksineen, pituuspiireinä -5–52 itäistä pituutta, sekä leveyspiireinä 51–73 pohjoista leveyttä. Tarkkuudeksi eli rasterin suuruudeksi valitaan $0{,}1 * 0{,}1$ astetta. Komennoksi saadaan seuraava syöte, jonka tuottama malli on havainnollistettu kuvaan neljä:

"C:\Users\Timo>gut geoidheight_gf -InFile GOCE2011.DBL -Ellipse TOPEX -R 355:52,51:73 -I 0.1:0.1 -T mean-tide -OutFile GOCE_dir_MT_TP.nc".

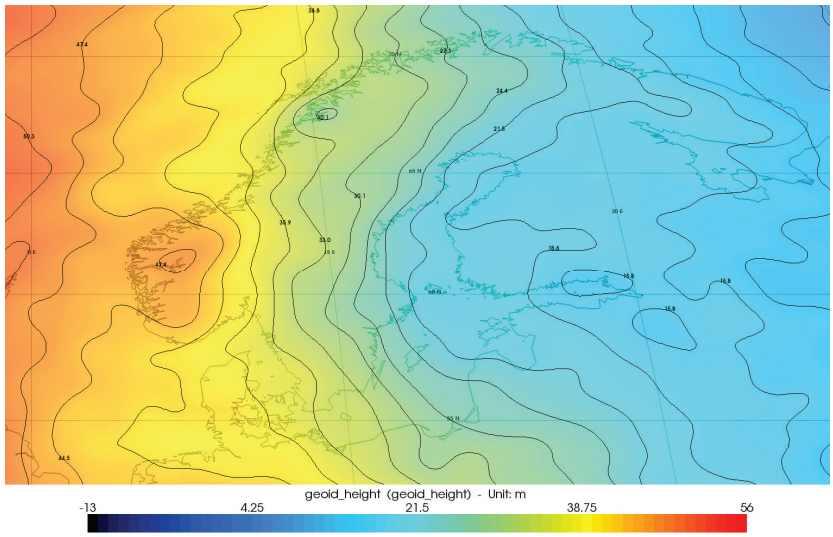

Kuva 4. Itämeren alueelle lasketut geoidikorkeudet.

Seuraavalla komennolla määritetään keskimerenpinnan keskikorkeus samaan vertausellipsoidiin, vuorovesimalliin sekä rasteriin kuin geoidikorkeudet:

"C:\Users\Timo>gut adapt_gf -InFile MSS_CNES_CLS_11_2M.nc -Gf GOCE_dir_MT_TP.nc -OutFile MSS_adapt.nc".

Tämän jälkeen vähennetään MSS- sekä geoidikentät toisistaan, kaavan yksi mukaisesti, joiden erotuksena saadaan meritopografia (kuva 5):

"C:\Users\Timo>gut subtract_gf -InFileLhs MSS_adapt.nc -InFileRhs GOCE_dir_MT_TP.nc -OutFile MSS_GOCE_dir.nc".

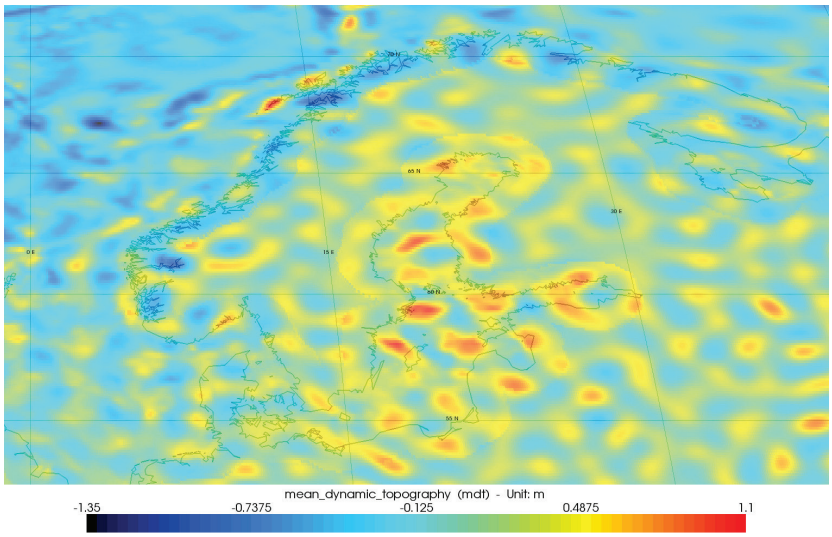

Kuva 5. Itämeren alueelle laskettu meritopografia (suodattamaton).

Kuten kuvasta viisi nähdään, meritopografia on ratkaistuna myös mantereiden yli, jotka tulisi luonnollisesti poistaa ratkaisusta. Mantereiden poistaminen suoritetaan tässä vaiheessa ennen suodattamista, sillä mikäli ne poistettaisiin suodattamisen jälkeen, aiheutuisi siitä virheitä rannikkohavaintojen tuloksiin (European Space Agency 2012b, s. 75). Poistetaan ratkaisusta mantereiden arvot komennolla:

> *"C:\Users\Timo>gut landmask_gf -InFile MSS_GOCE_dir.nc -InLsmFile GUT_LSM.nc -OutFile MSS_GOCE_dir_lmsk.nc".*

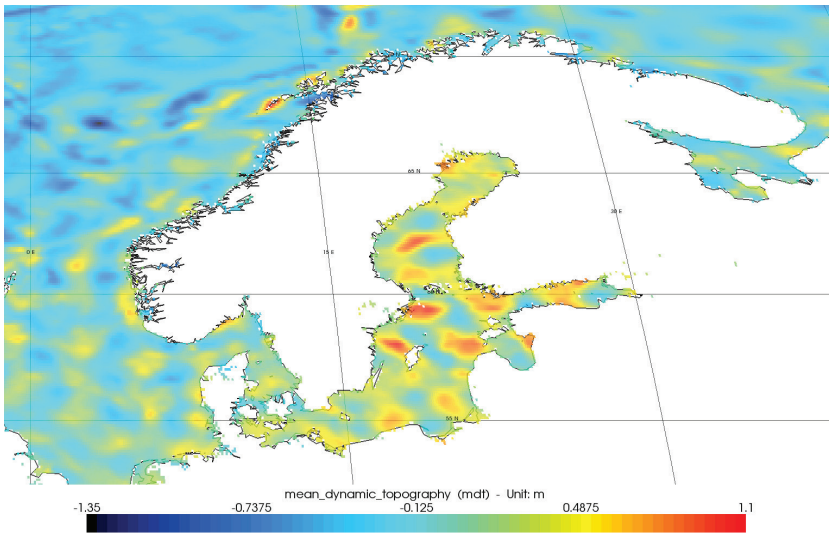

Kuva 6. Suodattamaton Itämeren MDT, josta poistettu mantereiden arvot.

Kuvassa kuusi havaitaan vielä useita täplämäisiä punertavia ja kellertäviä alueita, jotka ovat aineistossa esiintyviä virheitä. Virheet johtuvat GOCEn rajallisesta resoluutiosta, mistä johtuen lyhyiden aaltojen korkeat asteet sisältävät tallentuessaan virheitä. Mallissa esiintyvät virheet tulevat suodattaa pois jollakin optimaalisella suodattimella. Seuraava komento suodattaa aineiston keskiarvoisella Hanning-suodattimella:

"C:\Users\Timo>gut filter_gf -InFile MSS_GOCE_dir_lmsk.nc -Fhan 2,3 -OutFile MSS_GOCE_dir_lmsk_fhan23.nc".

Kuvaan seitsemän on havainnollistettuna lopullinen ratkaisu Itämeren alueen meritopografialle. GUT-työkalu ei itsessään visualisoi luotuja tiedostoja, vaan tiedostojen visualisointi suoritetaan aliohjelman BratDisplayn avulla. Kuvassa seitsemän esiintyvää ratkaisua on muokattu havainnollisemmaksi BratDisplaytä käyttäen siten, että projektioksi on valittu Robinson-projektio, joka mielestäni visualisoi aluetta kaikkein parhaiten. Lisäksi väriskaala ja arvojen rajaukset ovat valittuina mieleisiksi. Aliohjelman kutsu tapahtuu seuraavalla komennolla:

"C:\Users\Timo>BratDisplay MSS_GOCE_dir_lmsk_fhan23.nc".

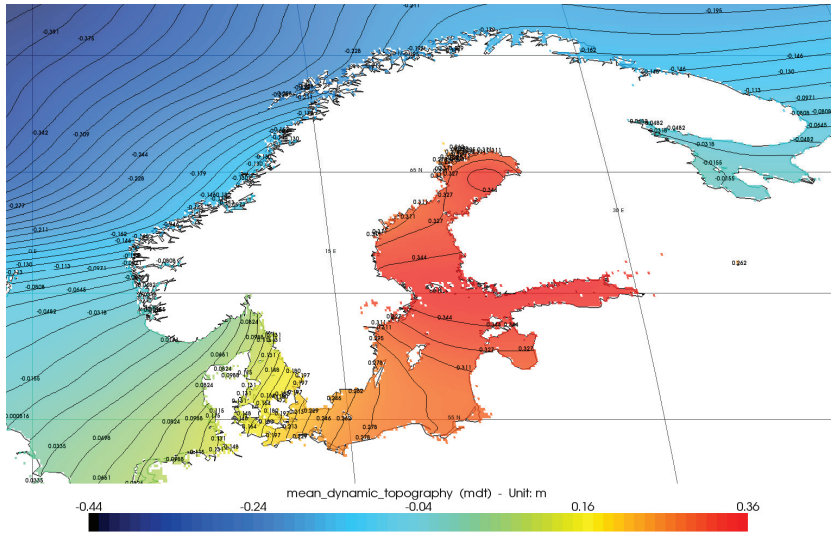

Kuva 7. Itämeren alueelle ratkaistu meritopografia ("step-by-step" ratkaisu).

Tulostetaan GUT-työkalulla vielä ratkaistun kokonaisuuden tilastotiedot, jotka sisältävät muun muassa ratkaisun minimi- ja maksimiarvot. Tämä suoritetaan komennolla stats_gf:

"C:\Users\Timo>gut stats_gf -InFile MSS_GOCE_dir_lmsk_fhan23.nc".

```
INFO:    Extracted 'mdt'
INFO:    (Stats) Bounds [51, 73] N,  [-5, 52] E

INFO:    (Stats) mdt
          Lon x Lat : 571 x 221
          Maximum   : 0.358949 m at (26.8 E, 60.4 N)
          Minimum   : -0.440511 m at (-5 E, 73 N)
          Mean      : -0.126215 m
          Variance  : 0.0434547  =>  RMS : 0.208458 m
          W-Mean    : -0.0928262 m
          W-Var     : 0.0469598  =>  RMS : 0.216702 m
          Valid     : 52892 / 126191  (41.9%)
```

2.3 Suora ratkaisu

Seuraavassa ratkaistaan Itämeren meritopografia samoilla parametreilla kuin edellä, mutta suoritetaan laskenta käyttäen vain yhtä komentoa. Tuloksena pitäisi olla likimain yhtäläinen ratkaisu edellisen luvun kanssa. Ratkaistaan meritopografia vuosien 2009–2011 DIR-aineistolla seuraavalla komennolla:

"C:\Users\Timo>gut spatialmdt_gf -InShpFile GOCE2011.DBL -InSshFile MSS_CNES_CLS_11_2M.nc -InLsmFile GUT_LSM.nc -Fhan 2,3 -Ellipse TOPEX -R 355:52,51:73 -I 0.1:0.1 -OutFile Itameri_ROB2011.nc".

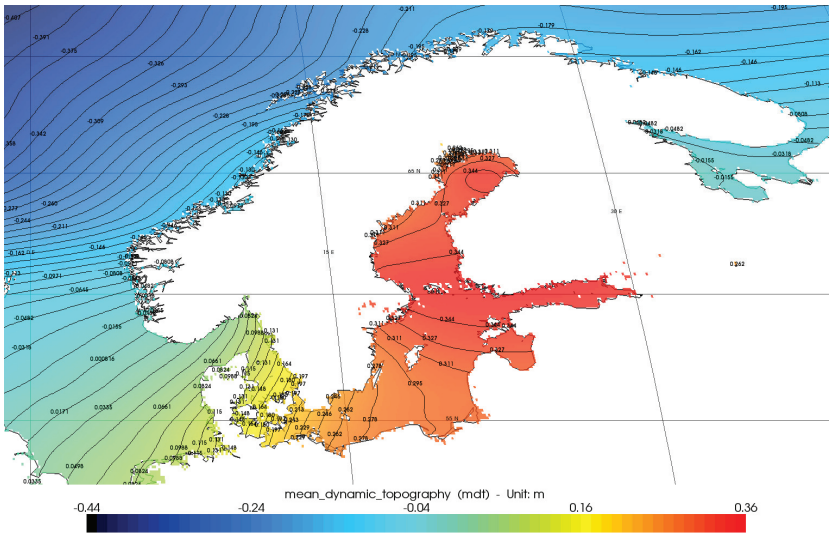

Kuva 8. DIR-menetelmällä (2009–2011) ratkaistu meritopografia (suora ratkaisu).

Kuvan kahdeksan ratkaisu vaikuttaa ainakin visuaalisesti yhtäläiseltä ”step by step” ratkaisun kanssa (kuva 7). Katsotaan seuraavaksi millaisia eroja ratkaisujen väliltä todellisuudessa löytyy. Eroavaisuudet ratkaisuille saadaan siten, että vähennetään edellä ratkaistu MDT sekä ”step by step”-MDT toisistaan. Vähennys suoritetaan komennolla:

”C:\Users\Timo>gut subtract_gf -InFileLhs MSS_GOCE_dir_lmsk_fhan23.nc -InFileRhs Itameri_ROB2011.nc -OutFile Diff_stepbystep_spatialmdt.nc”.

Ratkaisujen eroavaisuuksien arvoiksi saadaan seuraavat:

“C:\Users\Timo>gut stats_gf -InFile Diff_stepbystep_spatialmdt.nc”.

```
INFO:    Extracted 'mdt'
INFO:    (Stats) Bounds [51, 73] N,  [-5, 52] E

INFO:    (Stats) mdt
          Lon x Lat : 571 x 221
          Maximum   : 1.13179e-010 m at (-5 E, 51 N)
          Minimum   : -8.74353e-011 m at (45.5 E, 65.1 N)
          Mean      : -2.47688e-011 m
          Variance  : 5.46123e-022  =>  RMS : 2.33693e-011 m
          W-Mean    : -2.15109e-011 m
          W-Var     : 5.76184e-022  =>  RMS : 2.40038e-011 m
          Valid     : 52892 / 126191  (41.9%)
```

Yllä olevista tuloksista näemme, että ratkaisujen erot ovat häviävän pieniä, niin kuin olettaa saattoi.

2.4 Eriarvoisilla parametreilla laskettuja meritopografioita

Lasketaan seuraavassa Itämeren meritopografia käyttäen erilaisia laskentamenetelmiä sekä GOCE-aineistoja, jotka perustuvat joko level 1 tai level 2 dataan. Pyritään hahmottamaan mallien eroavaisuudet ja havaitsemaan, kuinka paljon mallit tarkentuvat, jos tarkentuvat, kun käytössä on pidempiaikaisia GOCE-havaintoaineistoja. Lisäksi vertaillaan, mikäli mallit tarkentuvat, kun lasketaan tiheämpää rasteria, eli saavutetaanko raskaammalla laskennalla ehostuksia malleihin. Seuraavien mallien laskentamenetelminä ja havaintoaineistoina ovat:

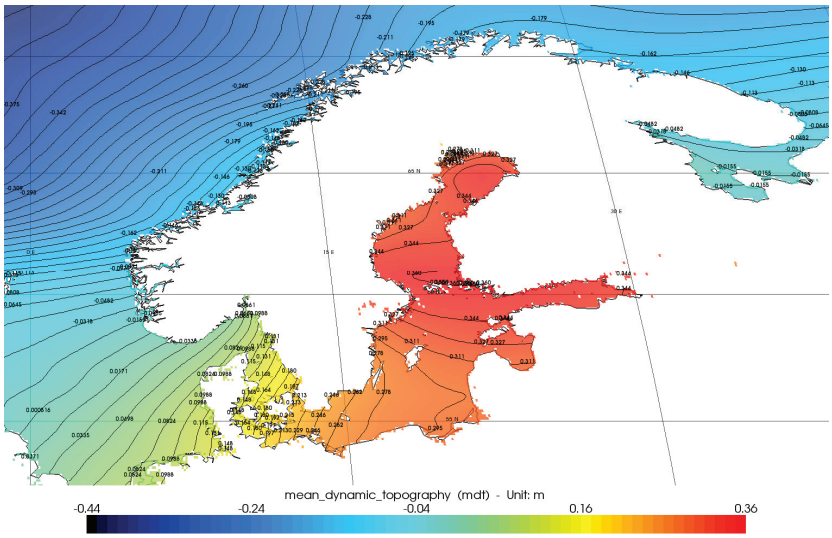

Kuva 9. DIR-menetelmällä (2009–2010) ratkaistu meritopografia (rasteri 0,1° × 0,1°).

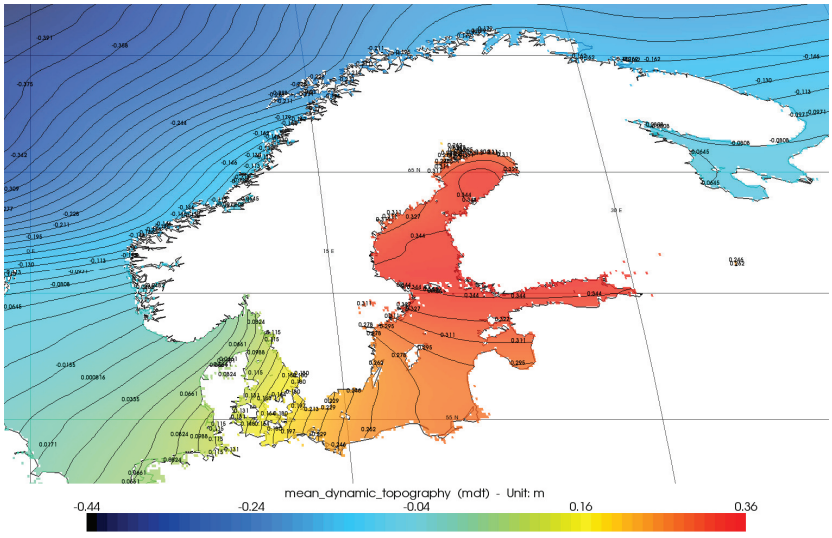

Kuva 10. SPW-menetelmällä (2009–2010) ratkaistu meritopografia (rasteri 0,1° × 0,1°).

- DIR-menetelmä vuoden 2009–2010 havainnoilla, rasterilla 0,1° ∗ 0,1° (kuva 9)
- SPW-menetelmä vuoden 2009–2010 havainnoilla, rasterilla 0,1° ∗ 0,1° (kuva 10)

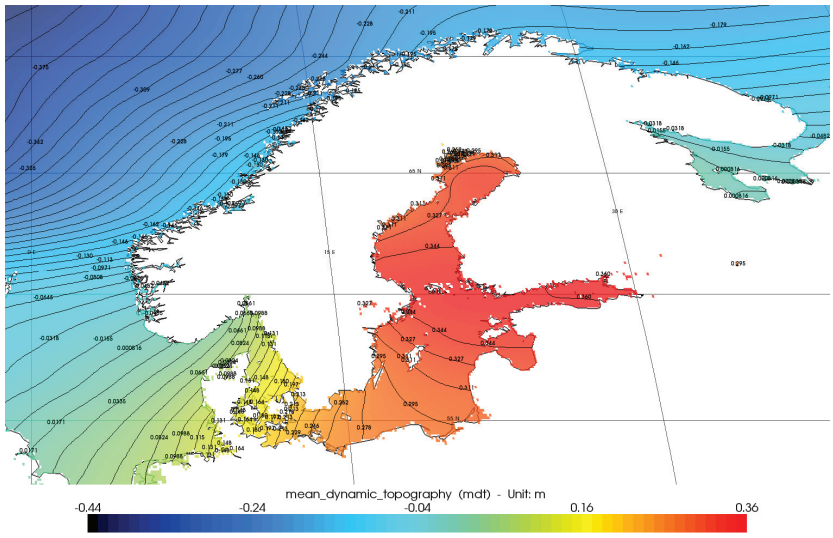

Kuva 11. TIM-menetelmällä (2009–2011) ratkaistu meritopografia (rasteri 0,1° × 0,1°).

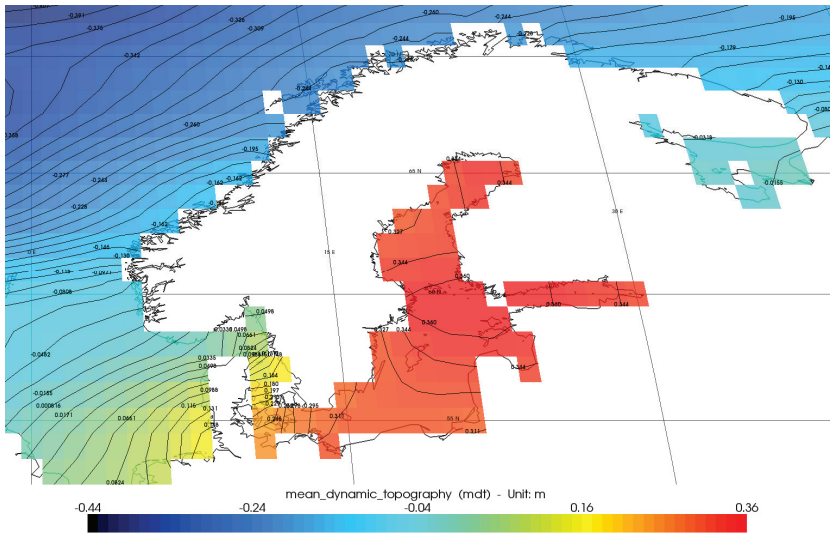

Kuva 12. Itämeren alueen meritopografia, DIR 2009–2011 (rasteri 1,0° × 1,0°).

- TIM-menetelmä vuoden 2009–2011 havainnoilla, rasterilla 0,1° ∗ 0,1° (kuva 11)
- DIR-menetelmä vuoden 2009–2011 havainnoilla, rasterilla 1,0° ∗ 1,0° (kuva 12)

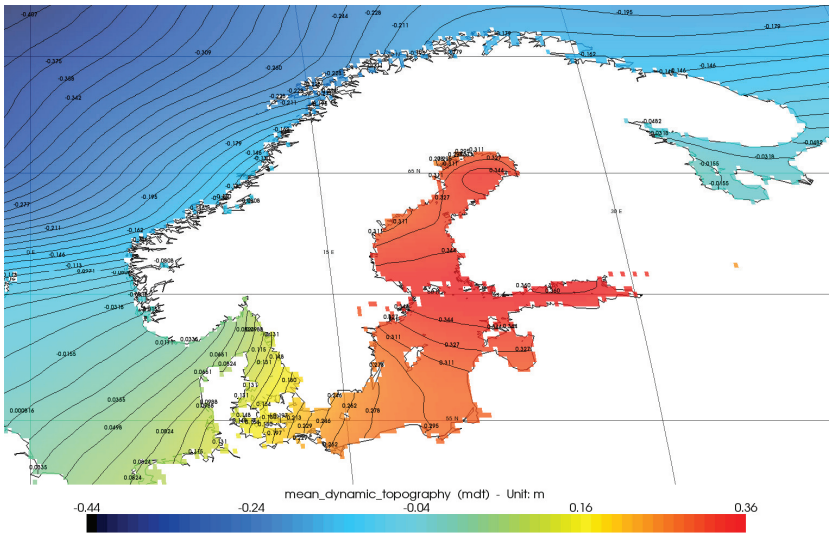

Kuva 13. Itämeren alueen meritopografia, DIR 2009–2011 (rasteri 0,2°×0,2°).

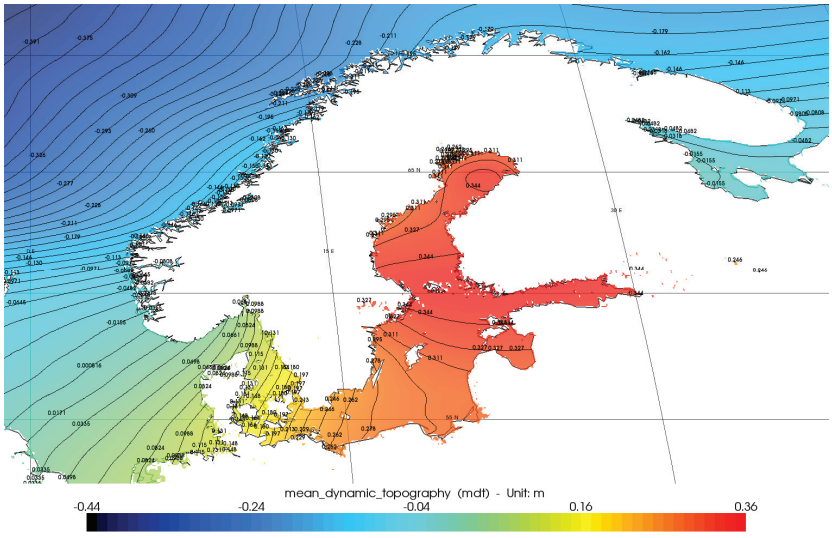

Kuva 14. Itämeren alueen meritopografia, DIR 2009–2011 (rasteri 0,05° × 0,05°).

- DIR-menetelmä vuoden 2009–2011 havainnoilla, rasterilla 0,2° ∗ 0,2° (kuva 13)
- DIR-menetelmä vuoden 2009–2011 havainnoilla, rasterilla 0,05° ∗ 0,05° (kuva 14).

Yllä olevien kuvien pohjalta on taulukoihin 2 ja 3 merkitty menetelmillä saatuja meritopografia-arvoja valituille alueille. Alueiksi on valittu Helsinki

(60°09’ N, 24°58’ E), Kemi (65°44’ N, 24°33’ E), Tukholma (59°19’ N, 18°05’ E) sekä Klagshamn (55°31’ N, 12°55’ E). Alueiden koordinaatit ovat kyseisillä alueilla sijaitsevien mareografien koordinaatteja, joille GUT-ohjelmalla laskettiin meritopografia-arvot. Alueet valittiin siten, että tuloksista nähtäisiin onko Itämeri kallellaan pohjoiseen mentäessä sekä millaisia eroavaisuuksia pääkaupunkien väliltä löytyy. Taulukoiden tuloksista saadaan seuraavat tulokset Klagshamn – Kemi välille sekä Tukholma – Helsinki välille:

- DIR 2009–2011 Klagshamn – Kemi 12,2 cm, Tukholma – Helsinki 2,1 cm
- DIR 2009–2010 Klagshamn – Kemi 12,3 cm, Tukholma – Helsinki 2,2 cm
- SPW 2009–2010 Klagshamn – Kemi 13,6 cm, Tukholma – Helsinki 2,6 cm
- TIM 2009–2011 Klagshamn – Kemi 10,1 cm, Tukholma – Helsinki 1,8 cm.

Taulukoiden tuloksista havaitaan huomattava harppaus tultaessa Pohjanmereltä Itämerelle. Hyvin lyhkäisellä matkalla Tanskan Frederikshavnilta Ruotsin Klagshamniin meritopografia kasvaa 10,2 cm (DIR 2009–2011) ja edelleen itään mentäessä Helsinkiin saavuttaessa, meritopografia on kasvanut 25,0 cm.

Erilaisilla laskentamenetelmillä saadut tulokset poikkeavat toisistaan melkoisen vähän. Taulukoissa olevista tuloksista voidaan DIR-menetelmän vuoden 2009–2011 havaintoaineistoja pitää lähinnä todellisuutta vastaavina, sillä menetelmässä on käytetty hyödyksi pitkäaikaisista GRACE-havainnoista tuotettua EIGEN-5C painovoimakenttämallia (Pail ym. 2011, s. 833). Pelkistä GOCE-havainnoista tuotettujen mallien (TIM) tulokset jäävät hieman DIR-malleista, kun vuorostaan SPW-mallien ratkaisut ovat hieman suurempia.

Laskennan aikatehokkuutta vertailtiin erikokoisten rasterien avulla, joiden tulokset ovat taulukossa 3. Toisesta sarakkeesta nähdään heti, että yhden asteen rasterilla lasketut tulokset ovat hieman kyseenalaisia, sillä rasterin kattama alue on todellisuudessa niin suuri (111 km $*$ 111 km), että nopeat muutokset kapeilla alueilla vääristyvät keskiarvon myötä (Frederikshavn 4,9 cm). 0,2 asteen rasterilla lasketut tulokset vaikuttavat jo melko hyviltä, varsinkin aavoilla alueilla. 0,2 asteella lasketut ratkaisut kärsivät kuitenkin samoista ongelmista kuin yhden asteen rasterit, sillä rasterin koko todellisuudessa on noin 22 km $*$ 22 km, jolloin kapeiden alueiden, joissa muutokset tapahtuvat äkkinäisesti, mallinnukset kärsivät. 0,05 asteen rasterilla saadaan ratkaistuksi todella yksityiskohtaisia alueita, joskin laskenta-aikaa kasvaa merkittävästi.

Taulukko 2. Erilaisilla laskentamenetelmillä ja havaintoaineistoilla ratkaistut MDT:n tulokset rasterin pysyessä samana $0{,}1° \times 0{,}1°$.

	DIR 2009–2011	DIR 2009–2010	SPW 2009–2010	TIM 2009–2011
Helsinki 60°09′ N, 24°58′ E	35,8 cm	35,7 cm	34,8 cm	35,9 cm
Kemi 65°44′ N, 24°33′ E	33,2 cm	34,1 cm	32,9 cm	32,1 cm
Tukholma 59°19′ N, 18°05′ E	33,7 cm	33,5 cm	32,2 cm	34,1 cm
Klagshamn 55°31′ N, 12°55′ E	21,0 cm	21,8 cm	19,3 cm	22,0 cm
Frederikshavn 57°26′ N, 10°34′ E	10,8 cm	11,4 cm	9,4 cm	11,4 cm

Taulukko 3. DIR-menetelmän vuosien 2009–2011 havaintoaineistojen ratkaisut erikokoisille rastereille.

	$\mathbf{1,0° \times 1,0°}$ **10 s**	$\mathbf{0,2° \times 0,2°}$ **1,5 min**	$\mathbf{0,1° \times 0,1°}$ **18 min**	$\mathbf{0,05° \times 0,05°}$ **4,5 h**
Helsinki 60°09′ N, 24°58′ E	36,3 cm	36,0 cm	35,8 cm	35,7 cm
Kemi 65°44′ N, 24°33′ E	34,4 cm	33,3 cm	33,2 cm	32,9 cm
Tukholma 59°19′ N, 18°05′ E	36,4 cm	33,3 cm	33,7 cm	33,7 cm
Klagshamn 55°31′ N, 12°55′ E	26,8 cm	20,8 cm	21,0 cm	21,1 cm
Frederikshavn 57°26′ N, 10°34′ E	4,9 cm	9,1 cm	10,8 cm	10,8 cm

Laskentaan kuluneet ajat olivat seuraavat:

- rasterin koko $1{,}0° * 1{,}0°$ 10 s
- rasterin koko $0{,}2° * 0{,}2°$ 1,5 min
- rasterin koko $0{,}1° * 0{,}1°$ 18 min
- rasterin koko $0{,}05° * 0{,}05°$ 4,5 h.

Laskenta-ajat kasvavat täten potenssilain mukaisesti rasteria pienentäessä. Vaikka 0,05 asteen rasteri tuottaa erittäin yksityiskohtaiset tulokset, ei menetelmä silti ole kovin käytännöllinen, sillä laskenta-aika on kovin pitkä. Käytännöllisimmät menetelmät ovatkin 0,2 ja 0,1 asteen rasterit, jotka molemmat tuottavat tarpeellisen tarkkoja tuloksia laskenta-aikaa oleellisesti pidentämättä.

3 Itämeren meritopografia

Luvussa esitetään kolme aikaisempaa maanpäällistä Itämeren merenkorkeuskampanjaa (Baltic sea level, BSL), joiden tuloksista laskettiin

meritopografiat Itämerelle. Meritopografiat laskettiin ensimmäisen ja toisen BSL-kampajan yhdistetyistä tuloksista, joiden tuloksia tarkennettiin myöhemmin kolmannen kampanjan tuloksilla. Lopullisia yhdistettyjä BSL-kampanjoiden tuloksia paranneltiin entisestään ERS-2:n tuottamilla altimetriahavainnoilla, jonka tulokset myös esitetään. Edellä mainittujen kampanjoiden tuloksia vertaillaan GOCE-datasta lasketun MDT:n kanssa, jonka laskenta esiteltiin luvussa kaksi.

3.1 Itämeren merenkorkeuskampanjat – mareografit

Markku Poutanen ja Juhani Kakkuri (1999, s. 289) määrittelivät tutkimuksessaan "The sea surface of the Baltic" Itämeren meritopografian, joka laskettiin kolmesta Itämeren merenkorkeus-kampanjasta, jotka suoritettiin 1990, 1993 ja 1997. Kampanjoissa olivat mukana kaikki Itämerta ympäröivät maat, joiden pitkäaikaisista mareografi-havainnoista saatiin laskettua keskimerenpinnan keskikorkeus.

Mareografeja ja GPS-asemia oli käytössä useita kymmeniä (BSL3:ssa yhteensä 60 kpl.). Mareografit mittaavat kuvan 15 mukaisesti meriveden korkeutta kaivossa kelluvan uimurin avulla, mikä tallentaa merivedenkorkeutta reaaliajassa. BSL-kampanjoissa käytetyt mareografit olivat yhdistettyinä kansallisiin vaaitusverkostoihin, jolloin saatiin ratkaistuiksi absoluuttiset merenpinnankorkeudet. (Kakkuri & Poutanen 1999, s. 289-290)

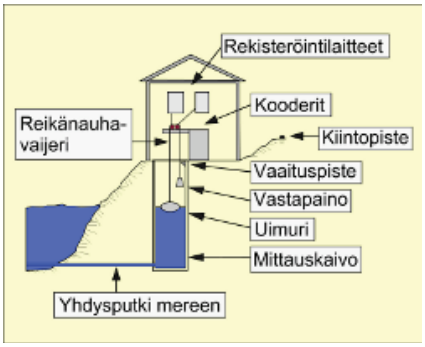

Kuva 15. Mareografin toiminta (Ilmatieteenlaitos 2012).

Ensimmäinen BSL-kampanja ei ollut valtaisa menestys, sillä Auringon aktiivisuudesta johtuen havainto-olosuhteet eivät olleet otollisimmat. Lisäksi ajankohta oli poliittisesti epävarmaa aikaa, mistä johtuen kampanjaan eivät osallistuneet Baltian maat eikä Venäjä. Toisessa BSL-kampanjassa olosuhteet olivat suotuisammat niin poliittisesti kuin sääilmiöidenkin suhteen. Keskimerenpinta laskettiin 35:n mareografin

voimin ja geoidikorkeudet laskettiin professori Martin Vermeerin luomasta geoidista, joka oli laskettuna Suomen, Viron, Latvian, Liettuan, Norjan, Puolan, Venäjän sekä Ruotsin painovoimatiedoista. Kampanjan tuloksista laskettiin Itämeren meritpografia kaavan yksi mukaisesti, mistä saadut tulokset ovat havainnollistettuna kuvaan 16. (Kakkuri & Poutanen 1997, s. 307, 311)

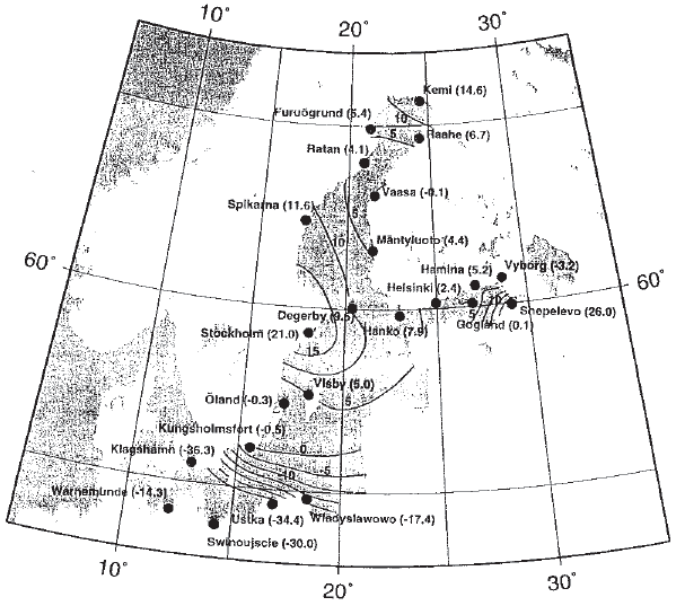

Kuva 16. Toisesta BSL-kampanjasta laskettu Itämeren meritopografia (Kakkuri & Poutanen 1997, s. 316).

Vuonna 1997 suoritettiin viimeisin BSL-kampanja, jonka tuloksia yhdisteltiin aikaisempien kampanjoiden kanssa. Kolmas BSL-kampanja järjestettiin samanaikaisesti EUVN:n (European Vertical GPS Reference Network) GPS-kampanjan kanssa, mikä nosti havaintoasemien määrän yhteensä kuuteenkymmeneen. Geoidimallina käytettiin NKG96-geoidia, joka on laskettu Skandinavian ylle. Yhdistetyistä BLS-kampanjoiden mareografi-, ja GPS-havainnoista sekä NKG96-geoidimallista laskettiin Itämeren MDT, jonka tulokset ovat esitettynä kuvassa 17, missä mustat pisteet maitten rannikoilla ovat nimenomaisia mareografeja. (Kakkuri & Poutanen, s. 290)

Toisen ja kolmannen BSL-kampanjan väliset erot ovat selvästi nähtävistä kuvista 16 ja 17. Toisessa BSL-kampanjassa määritellyn Itämeren meritopografian välinen ero, Puolan luoteis-rannikolta (Ustka) Perämerelle (Kemi), on ollut lähes 50 cm. Vastaavasti kolmannen BSL-kampanjan vastaava ero Ustkan ja Kemin mareografien välillä on ollut ”enää” vain 30 cm. Kuvista nähdään, että tulokset ovat hyvinkin rannikkomyönteisiä,

tarkoittaen että merialueiden arvoviivat ovat melko pelkistettyjä. Tämä johtuu siitä, että pelkillä maanpäällisillä menetelmillä ratkaistut meritopografiat voidaan ratkaista vain rannikoilla ja saarilla, joille on rakennettu mareografeja tai GPS-asemia. Tästä syystä avomerelle ei saada ratkaistuksi yksilöityä meritopografiaa, koska havaintoja avomereltä ei ole.

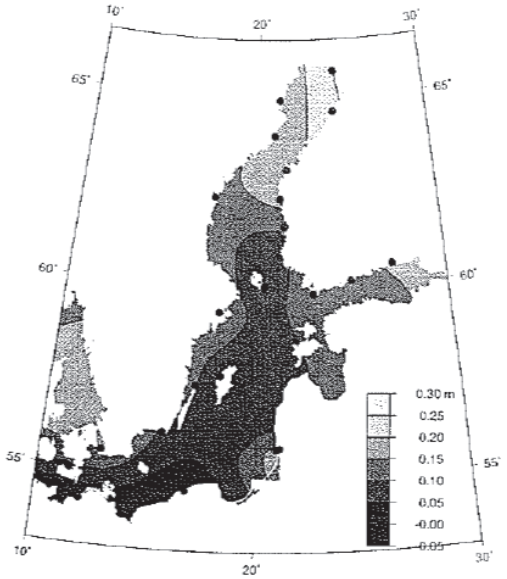

Kuva 17. BSL-kampanjoiden tuloksena ratkaistu Itämeren meritopografia (Kakkuri & Poutanen 1999, s. 291).

3.2 ERS-2 altimetriahavainnoilla paranneltu MDT

Avomeriltä saadaan tuotettuja havaintoja altimetriahavainnoilla, joita käytettiin kolmannen BSL-kampanjan lopullisten tuloksien parantamiseksi (Poutanen 2000). Vuoden 1997 altimetria-havaintoina käytettiin ESAn kaukokartoitussatelliitti ERS-2:sta, jonka tarkoituksena on ollut muun muassa merien, tuulien sekä ilmakehän tutkimus (European Space Agency 2012c). ERS-2 aineistolla parannettu Itämeren MDT on kuvattuna kuvaan 18, jossa vasemmalla on pelkällä ERS-2 aineistolla laskettu MDT, ja oikealla puolella ERS-2 + BSL-kampanjoista laskettu MDT.

3.3 GOCE MDT versus maanpäälliset MDT-kampanjat

Kuten edellä mainittiin, maanpäälliset kampanjat eivät tuota ratkaisuja avomereltä, jolloin voidaan olettaa GOCE-mallien olevan ainakin siinä suhteessa ylivertaisia. Pelkistä kuvista tehdyillä vertailuilla voidaan todeta, että riippumatta GOCE-mallin laskentamenetelmästä Itämeri näyttäisi nousevan Pohjanmeren suulta, Kattegatilta, Perämeren pohjukkaan noin

23–25 cm. Toisen BSL-kampanjan vastaava lukema on 35–40 cm ja kolmannen kampanjan vuorostaan noin 20 cm. ERS-2 parannuksilla nousua olisi 20–25 cm. Tulokset ovat esitettyinä taulukossa neljä.

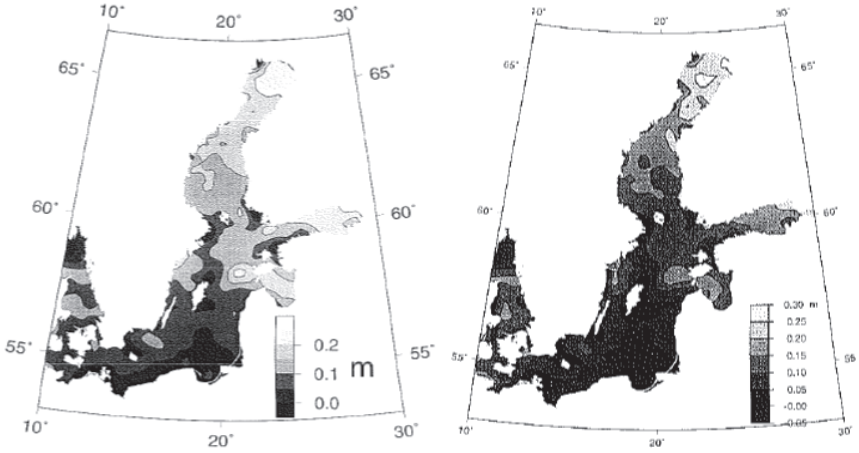

Kuva 18. Vasemmalla ERS-2:n altimetriahavainnoista laskettu Itämeren meritopografia, oikealla ERS-2 + BSL-kampanjoista laskettu meritopografia (Poutanen 2000, s. 27).

Vielä mielenkiintoisemmat eroavaisuudet mallien välillä ovat nähtävissä Itämeren etelä- ja pohjoisosien välillä – Puolan rannikolta Perämeren pohjukkaan. GOCE-mallit antavat nousuksi vain 6 cm, kun vuorostaan BSL2-kampanja antaa 25–30 cm. BSL3-kampanjasta saadaan hieman pienemmät lukemat nousulle 20–25 cm, jotka ERS-2 parannuksilla pienenevät vielä lukemiin 15–20 cm. Edellä mainitut tulokset ovat havainnollistettuina taulukkoon viisi.

Taulukko 4. Meritopografian välinen ero Kattegatin ja Perämeren välillä.

Malli	Tulokset
GOCE-mallit (DIR, TIM, SPW)	23–25 cm
BSL2-kampanja	35–40 cm
BSL3-kampanja	~20 cm
BSL-kampanjat + ERS-2	20–25 cm

Taulukko 5. Meritopografian välinen ero Puolan rannikkoalueiden sekä Perämeren välillä.

Malli	Tulokset
GOCE-mallit (DIR, TIM, SPW)	~6 cm
BSL2-kampanja	25–30 cm
BSL3-kampanja	20–25 cm
BSL-kampanjat + ERS-2	15–20 cm

Kakkuri ja Poutanen (1997, s. 315) ovat taulukoineet toisen BSL-kampanjan meritopografia-arvoja käytetyille mareografeille, joista vertailukohdiksi poimimme seuraavat Klagshamn (-36,3 cm), Tukholma

(22,2 cm), Kemi (14,6 cm) sekä Helsinki (2,4 cm). Näistä saadaan meritopografian suuruudeksi välille Klagshamn – Kemi (50,9 cm) sekä välille Tukholma – Helsinki (19.8 cm). Luvussa kaksi laskettiin GOCEn DIR-menetelmällä meritopografiat kyseisille väleille, jotka olivat Klagshamn – Kemi 12,17 cm ja Tukholma – Helsinki 2,10 cm.

Yllä olevat esimerkit käyvät hyvin ääriesimerkeistä, joiden mukaan vaikuttaisi siltä, että mallit ovat hyvin kaukana toisistaan, ainakin numeerisesti. Erot johtunevat kuitenkin moninaisista syistä. Ensinnäkin BSL-2 mallin tulokset ovat ensimmäisestä varsinaisesta onnistuneesta kampanjasta, jonka aineisto kerättiin noin yhden viikon aikana. Lisäksi meritopografian tulokset ovat mareografeilta, kun vuorostaan GOCE-mallien tulokset ovat laskettu koordinaattien mukaan mahdollisimman läheltä mareografien sijainteja. Merivesi saattaa käyttäytyä mareografin kohdalla hieman eritavalla kuin kilometrinkin päässä rannasta.

Kolmannen BSL-kampanjan tulokset ovat jo huomattavasti lähempänä GOCE-mallien tuloksia kuin toisen BSL-kampanjan tulokset. BSL3-kampanjakin kärsii avomerihavaintojen poissaolosta, sillä avomerelle interpoloidut arvot ovat melko summittaisia. Kun BSL3-kampanjaa parannellaan ERS-2 satelliitin altimetriahavainnoilla, mallin tulokset alkavat näyttämään hyviltä myös avomerelle. Parannellussakin mallissa ihmetystä aiheuttavat tulokset Puolan ja Saksan rannikoilla, joissa meritopografia vaikuttaisi olevan lähes 15 cm alempana, mitä GOCE-malleissa. Syynä tähän saattaisi olla eri maiden väliset eroavaisuudet kansallisissa vaaitus-arvoissaan.

4 Yhteenveto

Tutkimuksen tarkoituksena oli tutustua GUT-ohjelmiston käyttöön sekä luoda ohjelmalla erilaisia malleja Itämeren meritopografiasta. Luotuja meritopografiamalleja vertailtiin keskenään sekä erilaisten maanpäällisten kampanjoiden kanssa.

GUT on ESAn kehittämä työkalu GOCE-painovoimasatelliitin tuottaman aineiston käsittelyyn, analysoimiseen sekä visualisoimiseen. GUT on käskypohjainen ohjelma, johon annetaan syötteeksi komentoja, joilla ohjelma laskee haluttuja kenttiä, joita ovat muun muassa geoidikorkeudet, meritopografia sekä merivirtaukset. Lasketut tiedostot ovat nc-formaatissa.

GUT-ohjelmalla laskettuja nc-tiedostoja visualisoidaan BratDisplay-aliohjelmalla, jolla laskettuja malleja voidaan visualisoida ja kohdentaa haluamallaan tavalla, muun muassa valitsemalla erilaisia projektioita, joille

malli kuvastuu. BratDisplay-aliohjelmalla malleista saadaan helppolukuisia, jopa kauniita. GUT:n määrittelystä enemmän luvussa yksi.

GUT-ohjelmalla laskettiin meritopografiamalleja kaikilla erilaisilla GOCEn laskentamenetelmillä (DIR, TIM, SPW) sekä eriarvoisilla parametreilla, muun muassa ratkaistavien rasterien suuruuksilla. Rasterien suuruuksilla tutkittiin laskennan aikatehokkuutta, eli kuinka yksityiskohtaisia malleja on järkevää luoda laskenta-ajan kasvaessa. Tulokset malleista ja optimaalisista parametreista ovat esiteltyinä luvussa kaksi, jossa todetaan, että rasterin kokoluokaksi riittää vallan mainiosti jo $0{,}2° * 0{,}2°$ rasteri, joskin tässä työssä mallit laskettiin pääsääntöisesti $0{,}1° * 0{,}1°$ rastereilla, koska tutkimuksen kohteena oleva alue (Itämeri) on varsin pieni. Yksityiskohtaisempien mallien luonnissa ongelmaksi nousee laskenta-aika, joka kasvaa potenssilain mukaisesti, kun esimerkiksi $0{,}1° * 0{,}1°$ kokoisen mallin laskenta-aika oli 18 min, oli se vuorostaan $0{,}05° * 0{,}05°$ kokoiselle mallille jo 4,5 h.

GUT-ohjelmalla luotuja malleja vertailtiin kolmen merenkorkeuskampanjan (Baltic sea level, BSL) tuloksista saatujen mallien kanssa, jotka ovat laskettuina mareografi- ja GPS-asemien havainnoista käyttäen kulloinkin valittua geoidimallia. Maanpäällisin menetelmin tuotettujen meritopo-grafiamallien ongelmaksi muodostuvat avomeret, sillä asemat ovat sijoiteltuina ainoastaan rannikoille sekä saarille, eivätkä ne näin ollen tuota havaintoja merialueilta. Tämän takia vertailuun otettiin myös paranneltu BSL-malli, jonka tuloksia paranneltiin ERS-2 satelliitin altimetriahavainnoilla. Malleja ja niiden vertailuja on kuvailtu luvussa kolme, jossa eräänä vertailukohtana toimivat Pohjanmeren ja Perämeren välisen alueen meritopografian erot, jotka olivat malleilla seuraavat:

- GOCEn DIR-menetelmä 25 cm
- BSL2 (1993) 35–40 cm
- BSL3 (1997) 20 cm
- BSL-kampanjat + ERS-2 20–25 cm.

BSL-2 mallin tulokset olivat vasta ensimmäisestä varsinaisesta onnistuneesta kampanjasta, jonka aineisto kerättiin noin yhden viikon aikana. Tästä johtuen mallin ratkaisut jäivät melko suppeiksi. Kolmannen BSL-kampanjan tulokset olivat jo huomattavasti lähempänä GOCE-mallien tuloksia, vaikkakin avomeriongelma oli mallissa yhtäläinen BSL2-kampanjan kanssa. Altimetriahavainnoilla täydennetty malli näyttää jo huomattavasti paremmalta. Kyseisessä mallissa avomerihavainnot tuottavat aineistoon selkeän parannuksen, ratkaistessaan avomerelle yksilöllisiä arvoja. Parannellussakin mallissa ihmetystä aiheuttivat tulokset Puolan ja Saksan rannikoilla, joissa meritopografia vaikuttaisi olevan lähes 15 cm alempana, mitä GOCE-malleissa. Tähän voisi olla syynä BSL-

kampanjassa olevien maiden väliset eroavaisuudet kansallisissa vaaitusarvoissaan.

GOCE-mallit vaikuttavat kuitenkin erinomaisilta, kuten pitääkin, sillä GOCE on merkittävä kehitysaskel kaukokartoitussatelliittien aikakaudella, sillä sen tuottama painovoimakenttämalli on ennennäkemättömän tarkka. GOCE level 2 data sisältää jo vuosien 2009–2011 havainnot, jotka tuovat malleihin huomattavaa tarkkuutta.

GUT-ohjelma on erinomainen työkalu GOCE-datan käsittelyyn, sillä se on hyvin pelkistetty (komentoikkunapohjainen) ja melko helppokäyttöinen. Lisäksi ohjelma on kaikille avoin ja ohjelman mukana tulevat todella kattavat käyttöohjeet, jossa aloittelijalle kerrotaan pala palalta, mitä ohjelmalla voidaan tehdä. GOCE level 3 data julkaistaan alkuvuonna 2013, jolloin GUT-ohjelmalla lasketut mallit tulevat tarkentumaan entisestään.

Acknowledgements. *The topic of this work was developed in FGI with MSc Mirjam Bilker-Koivula, PhD Jenni Virtanen and Professor Jaakko Mäkinen. My advisor with this work was Mirjam who gave me many excellent ideas and comments during the working process. I owe my sincerest gratitudes to Mirjam for doing that.*

5 Lähteet

AVISO (2012). Mean Sea Surface description. [Viitattu 7.12.2012]. Saatavissa: http://www.aviso.oceanobs.com/en/data/products/auxiliary-products/mss/mss-description.html.

DURAND, M., FU, L., LETTENMAIER, D.P., ALSDORF, D.E., RODRIGUEZ, E. & ESTEBAN FERNANDEZ, D. (2010). The surface water and ocean topography mission: Observing terrestrial surface water and oceanic submesoscale eddies. Proceedings of the IEEE. Vol. 98:5. S. 766–779. DOI:10.1109/JPROC.2010.2043031.

EUROPEAN SPACE AGENCY (2012a). Article images. [Viitattu 2.12.2012]. Saatavissa: http://www.esa.int/SPECIALS/GOCE/SEMD304XQEF_1.html.

EUROPEAN SPACE AGENCY (2012B). GUT tutorial. [Viitattu 2.12.2012]. Saatavissa: https://earth.esa.int/c/document_library/get_file?uuid=cfedafbe-14f9-4014-8168-f888692a4e57&groupId=10174.

EUROPEAN SPACE AGENCY (2012C). ERS-2. [Viitattu 12.12.2012]. Saatavissa: http://www.esa.int/Our_Activities/Operations/ERS-2.

ILMATIETEENLAITOS (2012). Vedenkorkeuden mittaaminen. [Viitattu 2.12.2012] Saatavissa: http://ilmatieteenlaitos.fi/mareografi.

KAKKURI, J & POUTANEN, M. (1997). Geodetic determination of the surface topography of the Baltic Sea. Marine Geodesy. Vol. 20:4. S. 307–316. DOI:10.1080/01490419709388111.

KAKKURI, J & POUTANEN, M. (1999). The sea surface of the Baltic – a result from the Baltic Sea Level Project (IAG SSC 8.1). International Association of Geodesy Symposia. Vol. 121 Schwarz (ed.), Geodesy Beyond 2000 – The Challenges of the First Decade. S. 289–294. Heidelberg, Berlin, Germany: Springer-Verlag. ISBN 3-540-67002-5.

LEE, T., HAKKINEN, S., KELLY, K., QIU, B., BONEKAMP, H. & LINDSTROM, E.J. (2010). Satellite observations of ocean circulation changes associated with climate variability. Oceanography. Vol. 23:4. S. 70–81. DOI:10.5670/oceanog.2010.06.

PAIL, R., BRUINSMA, S., MIGLIACCIO, F., FÖRSTE, C., GOIGINGER, H., SCHUH, W., HÖCK, E., REGUZZONI, M., BROCKMANN, J.M., ABRIKOSOV, O., VEICHERTS, M., FECHER, T., MAYRHOFER, R., KRASBUTTER, I., SANSÒ, F. & TSCHERNING, C.C. (2011). First GOCE gravity field models derived by three different approaches. Journal of Geodesy. Vol. 85:11. S. 819–843. DOI:10.1007/s00190-011-0467-x.

POUTANEN, M. (2000). Sea surface topography and vertical datums using space geodetic techniques. Suomen Geodeettisen laitoksen julkaisuja. N:o 128. Helsinki: Hakapaino. ISBN 951-711-235-1.

RUMMEL, R., HORWATH, M., YI, W., ALBERTELLA, A., BOSCH, W. & HAAGMANS, R. (2011). GOCE, Satellite Gravimetry and Antarctic Mass Transports. Surveys in Geophysics. Vol. 32:4–5. S. 643–657. DOI:10.1007/s10712-011-9115-5.

VERMEER, M. (2011). Fysikaalinen geodesia. Aalto-yliopisto, Geomatiikan koulutusohjelma. [Viitattu 2.12.2012]. Saatavissa: http://users.tkk.fi/mvermeer/fys.pdf.

GNSS – Risks and threats

Iiro Kuusisto

Aalto University School of Engineering
Department of Real Estate, Planning and Geoinformatics
iiro.kuusisto@aalto.fi

Abstract

Global Navigation Satellite System has become very popular and easy to use. Unfortunately, people are not aware that it is not always reliable. There are several vulnerabilities that can cause errors and disruptions. Vulnerabilities can be divided in three sections: intentional, unintentional and system related. Intentional means that someone is trying to affect the solution with jamming, spoofing or meaconing. Jamming is the most common of these and it is usually done by sending noise like signals that disrupt receivers. Unintentional disruptions consist of natural and man-made phenomena. Good example of natural disruptions are solar flares and of man-made phenomena radio signal transmissions. There is a huge demand for radio frequency bandwidth and many signals easily interfere with weak GPS signals, which might cause errors. All three segments of GNSS have their own weaknesses and they are called system related vulnerabilities. This report gives a description of all these types of vulnerabilities, looks at various methods to mitigate their effects, and presents few examples from the real-world reported in the media.

1. GNSS overview

1.1 What is it?

The term Global Navigation Satellite System (GNSS) is used when speaking generally of space-based systems that send signals, which can be used to determine Position, Navigation and Timing (PNT). The best-known of these systems is US Global Positioning System (GPS) and because it is by far the only system that is ready and operative this paper will concentrate in it. In addition, these other systems work mainly the same way and that is why most of the things are also relevant when speaking of other GNSS systems like Russian GLONASS, European Galileo or Chinese Beidou. [14]

GPS consists of three segments: the space, ground and user segments (Fig. 1). Space segment's full constellation consists of 24 GPS satellites that are distributed in six different orbital planes. Each satellite sends a signal that has its own code, which is used to identify the satellite in the orbit. The ground segment is also known as the control segment. Its task is to upload the data to the satellites, synchronize the time across the constellation, and enable orbit and clock determination. The user segment consists of receivers and antennas that calculate the PNT from the received data. [14]

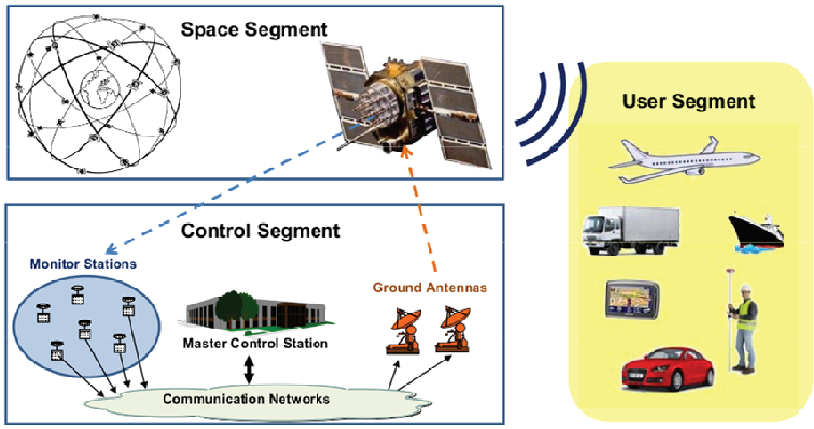

Figure 1. GNSS segments [6].

1.2. How does it work?

The GPS measurements are primarily done by measuring the traveling time Δt of the signal from the satellite to the receiver. This value is then multiplied by the speed of light and the result is a range between them. This range is called the pseudorange. It varies from the true range because of different system unknowns that must be either solved or estimated to get the true range. These unknowns can result for example from synchronism errors. Δt can be computed from the ranging code that is included to the carrier signal. The receiver determines the Δt by comparing the received code to the replica code that it generates by itself. When the maximum correlation is obtained, the Δt has been solved as depicted in Fig. 2. [13]

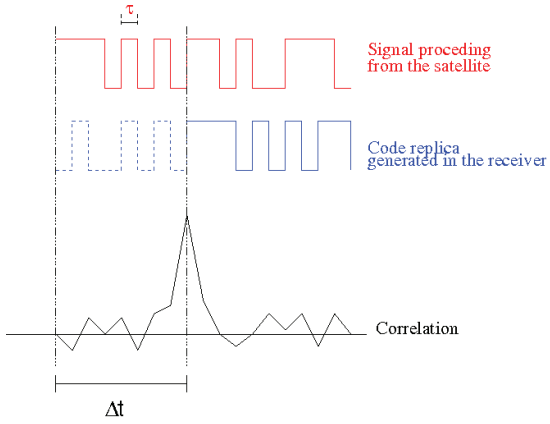

Figure 2. Comparing codes [13].

The travelling time can also be computed by the carrier phase. These carrier phase measurements are much more accurate than those relying on code but with natural ambiguity. These range measurements need at least four satellites to determine time and position and the ambiguity changes every time the receiver, for example, loses the lock on the signal. [13]

Every satellite sends a navigation message with its signal. This message contains the identifier, which was mentioned earlier, as well as information of satellites health, predicted range accuracy, ionospheric and clock correlation coefficients, and orbital ephemeris. The message also contains an almanac which has status, location and identifier information of all satellites in the constellation. [13, 14]

1.3. What is it used for?

GNSS is nowadays widely used in various areas of applications. Its free of charge signals and cheap receivers and chipsets has made it an easy solution. In this section a few applications are listed and some are described in more detail.

First, an obvious use for GNSS is surveying. A simple GNSS receiver might not have the required precision for every surveying measurement but with signal augmentation and receivers specifically build for surveying these requirements can be fulfilled. GNSS techniques have indeed revolutionized the way geodetic measurements are made and many countries and municipalities are using GNSS as a basis of their geodetic network. [12]

Second, GNSS is also used for example in transport, highways management, fisheries and agriculture, health services, telecommunications and tracking vehicles or valuable cargoes. Road transport applications are the major users of GNSS signals while they contain many everyday solutions such as in-car navigation, taxi services, public transport monitoring and emergency vehicle location. In addition to road transport, GNSS is also used in aviation, maritime and railway applications where in some situations the precision is vital. [14]

Finally, critical applications of GNSS are those that have a potential to cause harm for humans or environment. In these applications, GNSS misbehavior might be fatal. As mentioned before, emergency services are one of these applications but also in maritime and air navigation the system must be reliable. In addition, both maritime and aviation use GNSS for search and rescue missions and approaches. These applications need high accuracy and thus the vulnerabilities of GNSS systems must be known. [12, 14]

2. Vulnerabilities of GNSS

2.1. Intentional

Intentional interference is usually divided in three forms: jamming, spoofing and meaconing. Jamming is the most common form of these intentional interferences and it consists mainly of transmitting noise-like signals. Spoofing means sending false signals into the receiver, and meaconing is delaying and rebroadcasting of navigation signals. [2, 14]

A jamming device transmits noise signals across one or more GNSS frequencies and might cause a loss of lock. Because the GNSS systems and frequencies are known, it is rather easy to build a jammer and instructions are widely available on the internet. There are also a huge number of commercial jammers on the internet and some of them can be bought for approximately 20 €. Some of these jammers are designed to fit into a pocket and some into car lighter sockets. Very powerful jammers are also commercially available even though all jammers are illegal. One kind of a GPS jammer is in Fig. 3. [14]

Figure 3. GPS Jammer [1].

GNSS receivers behave unpredictably in areas where there is noise jamming. Trials have shown that receivers give false information rather than reporting an error. Sometimes, these errors are too large to be misleading, for example when a ship is sailing inland and the speed is tens of times too fast. The problems and hazardous incidents might happen in those situations when errors in position are only hundreds of meters and in speed only few knots. This combined with bad visibility and weather conditions and user's huge trust to the system's faultlessness might end up disastrously. [14]

GNSS jamming can be split into four areas: accidental, criminal, Blue Team deliberate, and Red Team deliberate, where Red Team means "terrorists" and Blue Team "friendly forces". Accidental jamming is mainly caused by other RF signals that interfere with the weak GNSS signals. Criminal jamming is mostly caused by people who don`t want to be tracked by GPS. This means for example car thieves. This form of jamming can be dynamic or static. These jammers are mainly low power just to defeat, for example a car from tracking but exceptions do occur when people are not concerned about the impact to the surrounding areas. Red Team jamming is indiscriminate but may be targeted at some specific areas. It will most probably be high power and have an effect on different locations simultaneously. The mission of Blue Team jamming is commonly to defeat tracking. Its impact might be similar to criminal jamming. [14]

GNSS spoofing is a harmful, intentional interference where receiver is fooled to track false GNSS signals. The targeted receiver cannot detect spoofing and hence cannot warn of false position or navigation. That is why spoofing is more dangerous than intentional jamming. Function of a portable spoofing device can be seen in Fig. 4. [8]

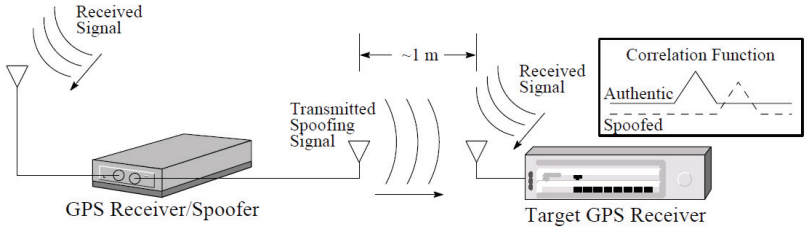

Figure 4. Portable spoofing device [8].

GNSS meaconing means interception and rebroadcasting of the navigation signals. Its aim is to confuse navigation. It delays the signals arrival to the receiver but does not modify the signal. There is also accidental meaconing, which may be caused by the proximity of a GPS antenna with poor impedance matching. [11, 14]

2.2. Unintentional

Unintentional disruptions consist of natural or man-made phenomena, such as solar flares and radio signal transmissions. Also, space weather, the changing environmental conditions in near-Earth space, for example in troposphere, has a remarkable effect on the signals. This section lists a few disruptions and describes what kind of problems they might cause. [1, 14]

Many man-made phenomena, for example television and personal electronic devices, can interfere with the GNSS signals. These interfering signals might cause a loss of lock if their frequency and magnitude are right. A shared use of finite radio spectrum could also be kept as a threat. As the amount of communication and broadcast services grow, grows the demand of bandwidth as well. This increases the risks to interfere with other signals. As mentioned before, also a GPS antenna might cause accidental jamming and meaconing and, thus, antennas should not be mounted very nearby each other. [1, 14]

To reach the GNSS receivers, signals must travel through the atmosphere. Atmosphere causes many variations to signals but a good number of them can be modeled and, thus, deleted or mitigated. However, atmosphere is

not invariant but actually highly variable over many temporal and spatial scales, which make it impossible to delete all the errors. [14]

Troposphere is the lowest and densest part of the atmosphere. It is the layer that contains our weather system, which causes variations in signal delay. These variations can be largely mitigated with a proper model. Ionosphere, instead, is the upper part of the atmosphere and while it is highly variable, it can be more problematic. If these variations are not corrected, they cause the largest errors in GNSS. Next few paragraphs highlight a couple of atmospheric GNSS vulnerabilities which mostly occur in the ionosphere. [14]

There are both slow and fast variations in total electron count in the ionosphere and both of them cause disruptions. These disruptions are proportional to the total electron count along the signal path. Slow variations are indirectly caused by the sun. Earth`s diurnal rotation, Sun`s 27 day rotation and Sun`s activity cycle of 11 years all have an effect to the total electron count. These slowly varying variations can be mitigated with a model or, for example, using a dual frequency receiver. Fast variations are indirectly a consequence of solar flares and Coronal Mass Ejections (CME). These variations are impossible to model but mitigation is possible again with a dual frequency receiver. [14]

GNSS signals can break up in the ionosphere due a small disruption and this might cause a signal multipath. This is called scintillation in ionosphere. Receivers notice a rapid variation in the signal amplitude and phase and this might cause a loss of lock. [14]

Solar storms, such as Carrington event could cause a major and long lasting impact on electronic infrastructure (Fig. 5). When huge amount of charged particles crash into Earth’s magnetic field, they induce electric currents that at least disrupt communications. In addition, nuclear explosions in the ionosphere, may cause somewhat similar propagation anomalies to solar storms. [14]

When a receiver picks up a signal from the satellite and a reflected signal it is called multipath. Signals can reflect off distant objects like buildings or very nearby objects. Errors caused by the reflection that happen near are more subtle than those of distant reflections because the original signal and the reflected signal may merge together. Multipath is very well known phenomenon and there are several ways to mitigate its effects, such as multipath rejecting antennas. Nevertheless, multipath still causes errors of tens to hundreds of meters every now and then especially to unprepared users. [1, 14]

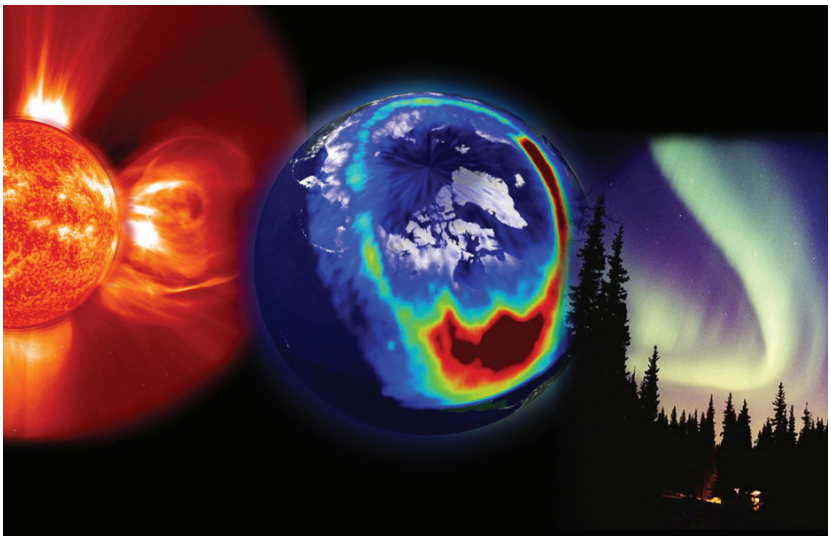

Figure 5. Carrington event (http://www.ancientdestructions.com/carrington-event-1859-royal-charter-storm/carrington-event-1859-solar-storm/).

2.3. System related

All the three segments of GNSS have vulnerabilities to failures and these are called system related vulnerabilities. Even though the space and ground segments are designed to be able to resist a military attack, they still have some weaknesses. [14]

One vulnerability of GPS-system is the reduced number of satellites. If the number of satellites, for one reason or another, drops to or below the specified minimum of 24, the users would experience a reduction in service, position outages and the accuracy would drop because of the satellite geometry. Another vulnerability is uploading erroneous navigation data to the satellite. The data consists of clock predictions and precise orbit predictions and its function is to enable achievement of full position accuracy. If an incorrect set of data is uploaded, it might cause an error in satellites clock and position knowledge. [14]

A jump or drifting of satellite´s clock is another potentially dangerous vulnerability. Every satellite has a precise atomic clock onboard but sometimes these clocks behave unpredictably. Because GNSS depends on time measurements, the operators should notice this kind of errors and mark the satellite unhealthy as fast as possible to avoid fatal consequences. Satellites might also send signals with bad structure that could cause unpredictable behavior in receivers. These bad signal structures can occur, for example, if there is a fault in signal modulation or generation process. [14]

The GPS user segment is wide and the receivers vary from decryption-capable military receivers to mass-product mobile phone receivers. User segment is not coordinated and even though every manufacturer has their own quality control and testing systems, some software bugs may still occur. [14]

UTC and GPS time has a relation that needs leap seconds every now and then. Even though it is described precisely how receivers should handle leap seconds correctly, some receivers still handle them wrong causing timing error. Another problem with the receivers can come up when there is a system upgrade in the GPS. Upgrades might cause unexpected behavior. For example, in 2007, a 32nd GPS satellite was launched and some receivers started to have problems because they were only designed for maximum of 31 satellites. As mentioned before, manufacturers have their own testing regimes but it is unlikely that a receiver would be totally free of software bugs. Such bugs can concern, for example, handling satellites that are marked unhealthy or behavior when signals are weaker or stronger than usually. All these may cause errors or affect the performance of the receiver. [14]

3. What can be done to prevent these?

3.1. System related and unintentional

Many of the problems mentioned above are possible to avoid or at least mitigate their effects. Choke ring antennas decrease power of signals at low elevations (Fig. 6). This type of antenna reduces the interference or can handle multipaths. Also receivers can be improved to handle multipaths better for example by using multiple-frequencies or receiver filtering or processing techniques. Integrating GNSS with some other measurement units like IMU makes the system more robust because when primary system fails another system takes over. [1, 14]

Many of the atmospherical problems can be mitigated by using a proper model. For example, tropospheric conditions can be modeled beforehand avoiding the measurement errors. Slow variations in ionosphere can also be modeled but these errors can as well be mitigated by using DGPS corrections or multi-frequency GNSS receivers. This is based on the fact that signal's change in traveling time is dependent to its frequency. Satellite Based Augmentation System (SBAS) is based on the correction signals send by extra satellites. Although SBAS signals can improve accuracy and

integrity, they are also disrupted by the atmosphere. In addition, SBAS is only limited to a regional area. [1, 3, 14]

Figure 6. Leica´s choke ring antenna. Choke ring antennas are designed to block signals from low elevations. (http://www.gecoengg.ae/products/gps-systems/at504.html)

3.2 Intentional

Noise jamming can be blocked by noise-jamming adaptive antennas and noise filtering in some degree but nowadays some jammers have switched to transmitting codes instead of noise. One way of countering jamming is n-element controlled reception pattern antennas. The idea is to steer the antenna gain null in the direction of jammer and some gain to the direction of desired signal. The more there are antenna elements, the more there are directions possible to be nulled and the greater is the gain that can be directed to signal. [14, 15, 19]

In addition to the method mentioned above, there are several overlay systems that can mitigate problems and errors. Many of these are also usable in avoiding unintentional errors. A few of these systems are described next.

Receiver Autonomous Integrity Receiver (RAIM) is incorporated in many receivers. It is an algorithm that compares smoothed pseudoranges that should be consistent. This way it determines the integrity of the GNSS solution. Algorithm determines the faulty satellite and eliminates its signal from the calculation. [4]

eLoran is an enhanced version of the old Loran-C system. eLoran is a terrestrial navigation system based on transmission stations that send radio pulses and it works much the same way as GPS. eLoran is, however, totally independent and complementary system that has no failure modes in common with satellite based systems. That is why some experts see this as a promising future solution alongside with the GNSS. [20]

Ground-Based Augmentation System (GBAS) improves accuracy and integrity of the GNSS. Its ground system consists of at least two GNSS receivers that collect pseudoranges and computes and broadcasts differential correction. It works much of the same way as SBAS but the main difference is that GBAS uses only ground infrastructure and it is more local service than SBAS. [5]

There is also a UK government funded project called GNSS Availability Accuracy Reliability anD Integrity Assessment for timing and Navigation (GAARDIAN). Its aim is to create mesh of interference detection and mitigation sensors that will be placed near PNT dependent infrastructure or applications. The system will monitor the integrity, reliability, continuity, and accuracy of the GNSS and eLoran signals and if it detects an anomalous condition (natural or intentional) users will be alerted. [21]

4. Real-world threats

4.1 Intentional

4.1.1 Example: Newark airport in New Jersey in 2009

In 2009, engineers at the Newark airport in New Jersey noticed that Federal Aviation Administration reference receivers were suffering short daily outages. Something was interfering with the GPS signals. It took months to solve what was behind this interference. Finally, it turned out that a driver who passed by on the nearby New Jersey turnpike every day had a jammer in his truck. The jammer prevents a tracking device from determining and reporting the speed and position of the car but it also disrupts other nearby GNSS applications. These jammers are illegal but have become popular among commercial drivers who do not want their employers track their every move. It is also possible to evade road tolls with these jammers. [18]

4.1.2 Example: North Korea is jamming GPS signals

South Korean government says that interference is causing troubles with GPS signals. They say that North Korea is behind this. On April 30th 2012 more than 250 commercial flights had to rely on other navigation methods because GPS had become unreliable. South Korean aviation authorities had to warn the pilots to “exercise extreme caution when using GPS”. This was

not the first time when interference occurred near the border. GPS communications had disruptions also in August 2010 and in March 2011 when jamming signals interfered with cell phone navigation. This second occasion was suspected to be caused by a mobile jamming unit and it happened during mutual U.S. and South Korean military exercises. [17]

4.1.3 Example: Tragedy of a 9-year-old boy

A mother claims that her nine-year-old boy died because an ambulance was delayed when its satnav was broken. On September 13th 2011, a boy had a severe asthma attack while he was having breakfast. Mom called an ambulance but only a car and a paramedic came instead. Finally, after 24 minutes, the ambulance came even though the nearest ambulance station is only a mile and a half away. Mom said that a social worker had later told that the ambulance took so long to arrive because their satnav was broken. West Midlands Ambulance Service confirmed that the satnav was broken but they say that the service does not only rely on it. Ambulances also have map books and Emergency Operation Centre can advise drivers with the use of GPS location systems. [16]

4.2 System-related

4.2.1 Phase jumps

The GPS L1 C/A-code signal has been examined several years. It is found that at times there are unexpected changes in the signal phase. It is also found that these phase jumps are dependent on the satellite. Some satellites tend to have them more often than the others. For example, on the period from mid-2009 until mid-August 2011 SVN48 had almost 2800 of these recorded jumps whereas SVN34 had only a bit more than 100. One observed case of a phase jump was SVN48 (PRN07) on September 15, 2010. There were three fast changes in the signal, all of them around 20° and they happened in less than 6 seconds. Their metric detections were three double-peaks of about 0.4 meters. [10]

4.2.2 Incorrect ephemeris

On 27th of April, 2012, there was an anomaly in the SVN58 (PRN12). In this example, two stations, DARW and STK2, were observed. DARW flagged the navigation message unhealthy but the other station had never paid attention to the healthy bits of the message. The anomaly in DARW lasted

from 3.02 to 3.26, when the unhealthy message was broadcast. DARW experienced a maximum error of -144.8 meters. Because the STK2 did not concern about the healthy bits, it experienced huge errors for almost three hours, the maximum being almost -3000 meters, before a new navigation message was issued. [7]

4.3 Unintentional

4.3.1 Atmospheric effects: ionospheric scintillation

Sun has its own activation cycles, end every 11 years it reaches its maximum, called solar maximum. Then its far ultraviolet portion of the spectrum increases, and that makes Earth's ionosphere thicker and denser. Ionospheric irregularities cause ionospheric scintillation. This scintillation can be classified as refraction and diffraction. The number of electrons the signal faces on its way to the receiver has an effect to the signal. If the number of electrons in a volume unit increases, the group velocity slows down and the phase speeds up. This is due to the physical fact that their product should be constant. In other words, the signal faces different layers and refracts from them. Refraction has a following effect: faster phase velocity causes phase shifts and slower group velocity causes ranging errors. When ionospheric irregularities reach certain length, they start to diffract GPS signals. This has an effect that the signal reaches the receiver through multiple paths. Every path has an effect to the signal phase and amplitude. [9]

5. Conclusions

GPS has become very convenient and popular and almost everyone is familiar with it. Still very few know its vulnerabilities and are aware of the fact that it does not always tell the truth. Partly that is why people do not have non-GPS-reliant back-ups for the occasions if GPS happens to fail. This is true mostly when speaking of non-professionals and in most cases it causes only inconvenience. Safety critical systems, on the other hand, seldom rely only on GNSS but the back-up system might also be reliant on GNSS, thus, they have a common point of failure. As in the case of 9-year-old boy, the primary system was satnav and one of the back-ups was Emergency Operation Centres aid with the help of GNSS location systems.

Unpredictable space weather events can affect performance of the GNSS. These space weather events can be rather low-power and happen quite often or they can be so called Carrington events that happen about once in 200 years. Their effects to GNSS systems are quite different. While small scale events might cause only a reduction in accuracy, the super-storms might disrupt GNSS signals and satellites either temporary or they might even cause a complete satellite failure.

Space weather events are not the only natural disruptions to GNSS systems. Signals travel 20 000 kilometers and through the atmosphere where they are very vulnerable to interference. Atmospheric models for troposphere and ionosphere can be made but they do not rule out all the possible sources of interference. Those cases can cause errors but it is rare that they cause a threat. Multipath can cause an error of hundreds of meters but this usually happens only for unprepared users while there are ways to mitigate multipath effects effectively.

The risk of jamming is increasing at the same time as the amount of applications that use GNSS is increasing. Jammers are easy to purchase or build because the internet is full of instructions. Criminals use jammers for car thefts to block tracking and for avoiding road tolls. These people seldom care about the effects they might cause to the nearby areas and depending on the power of the jammer, the area might not even be that small. Jamming might even be more intentional than this as we saw in the section 4.2. Unintentional jamming must not be forgotten either. Weak GNSS signals interfere with other RF signals in the atmosphere causing errors. This happens because there is a huge competition of limited frequencies.

Errors can be mitigated by using for example choke ring antennas, receiver filtering or integration with IMU. There are also many augmentation systems for GNSS but some of them use satellite signals as well as receivers and in case of a Space Weather event those are not able to tell whether there is an error or not. Most promising of augmentation systems might be the eLoran. eLoran is a ground-based system and totally independent from GNSS. They do not share common vulnerabilities and thus eLoran is a fine complementary system alongside with the GNSS.

References

[1] Dixon, C. S. & Hill, C. J. & Dumwille, M. & Lowe, D. 2012. GNSS vulnerabilities: Testing the Truth. http://mycoordinates.org/gnss-vulnerabilities-testing-the-truth/. [Cited 17.2.2013].

[2] Forssel, B. 2012. The Vulnerability of GNSS. Workshop on GNSS Interference and Jamming, Oslo, 24 May 2012. http://nornav.custompublish.com/getfile.php/1986430.753.fedbtwusex/GNSS%20vulnerability,%20Oslo%202012.pdf.

[3] GMW. 2011a. SBAS General Introduction. Navipedia. http://www.navipedia.net/index.php/SBAS_General_Introduction. [Cited 19.1.2013].

[4] GMV. 2011b. RAIM. Navipedia. http://www.navipedia.net/index.php/RAIM. [Cited 20.2.2013].

[5] GMV. 2011c. GNSS Augmentation. Navipedia. http://www.navipedia.net/index.php/GNSS_Augmentation. [Cited 20.2.2013].

[6] GMV. 2011d. GPS Architecture. Navipedia. . [Cited 20.2.2013].

[7] Heng, Liang. 2012. Safe satellite navigation with multiple constellations: Global monitoring of GPS and Glonass signal-in-space anomalies. http://waas.stanford.edu/~wwu/papers/gps/PDF/Thesis/LHengThesisFinalSignedSecured.pdf

[8] Humphreys Todd E. & Ledvina Brent M. & Psiaki Mark L. & O'Hanlon Brady W. & Kintner Jr, Paul M. 2008. Assessing the Spoofing Threat: Development of a Portable GPS Civilian Spoofer. Preprint of the 2008 ION GNSS Conference Savanna, GA, September 16-19, 2008. http://radionavlab.ae.utexas.edu/images/stories/files/papers/ion2008r01_for_distributionW.pdf

[9] Kintner Jr, Paul M & Humphreys, Todd & Hinks, Joanna. 2009. GNSS and Ionospheric Scintillation - How to Survive the Next Solar Maximum. Inside GNSS magazine, Vol. 4:4. 2009. http://www.insidegnss.com/node/1579

[10] Langley, Richard. 2012. Innovation: The Devil Is in the Details: Looking Closely at Received GPS Carrier Phase. http://www.gpsworld.com/gnss-systeminnovation-devil-details-13195/

[11] Marnach, D. & Mauw, S. & Martins, M. & Harpes C. Detecting meaconing attacks by analysing the clock bias of GNSS receivers. European Navigation Conference, April 25-27, 2012, Gdansk, Poland. http://www.itrust.lu/docs/A5-3.pdf.

[12] Pereira, R. B. 2011. GNSS Applications. Navipedia. http://www.navipedia.net/index.php/GNSS_Applications. [Cited 7.2.2013].

[13] Sanz Subirana, J. & Juan Zornoza, J.M. & Hernández-Pajares, M. 2011. GNSS Basic Observables. Navipedia. http://www.navipedia.net/index.php/GNSS_Basic_Observables. [Cited 7.2.2013].

[14] Thomas, M. & Norton, J. & Jones, A. & Hopper, A. & Ward, N. & Cannon, P. & Ackroyd, N. & Cruddace, P. & Unwin, M. 2011. Global

Navigation Space Systems: reliance and vulnerabilities. The Royal Academy of Engineering. 45 s. ISBN 1-903496-62-4.

(http://www.raeng.org.uk/news/publications/list/reports/RAoE_Global_Navigation_Systems_Report.pdf)

[15] Tseng, H.-W. & Atterberg, S. Small Controlled Reception Pattern Antenna (S-CRPA) Design and Test Results. Proceedings of 26th JSDE Conference, Ventura County, CA, October 2000. http://www.navsys.com/papers/0010001.pdf

[16] Did faulty satnav stop 999 crew from saving my son's life? Tragedy of boy, 9, who died after ambulance was delayed on way to hospital**.** Daily Mail. 2012. [Cited 21.2.2013]. http://www.dailymail.co.uk/health/article-2103330/Tragedy-boy-9-died-asthma-attack-ambulance-delayed-sat-nav-didnt-work.html

[17] DPRK jamming GPS signals, says Seoul. North Korea Tech. 2012. [Cited 21.2.2013]. http://www.northkoreatech.org/2012/05/03/dprk-jamming-gps-signals-says-seoul/

[18] GPS jamming – No jam tomorrow. The Economist. Mar 10th 2011. http://www.economist.com/node/18304246

[19] Interference & Jamming (Un)intended Consequences. Inside GNSS magazine, Vol. 7:4. 2012. http://www.insidegnss.com/node/3159

Internet references

[20] http://www.gla-rrnav.org/radionavigation/eloran/background_information.html [Cited 20.2.2013].

[21] http://www.gps-world.biz/index.php/en/gaardian [Cited 20.2.2013].

Global Navigation: Introduction to Satellite Based Augmentation System over Indian Region

Aditya Raju

Department of Radio Science and Engineering
Aalto University
Otakaari 5, 02150 Espoo, Finland
aditya.raju@aalto.fi

Abstract

Nowadays, the Global Navigation Satellite System (GNSS), a breakthrough in navigation system, caters to a large portion of civilian and military users to determine accurately their position, navigation and time (PNT) parameters. For more demanding applications like aviation sector, more reliable and highly accurate services are essential. Such services are implemented with additional system known as Satellite Based Augmentation System (SBAS), which improves the quality of service. This paper illustrates various issues responsible for inaccuracies in SBAS and methods to mitigate them. A detailed presentation of one such regional SBAS system developed for Indian subcontinent, also known as GPS Aided Geo Augmented Navigation (GAGAN) is presented.

1. Introduction to navigation and augmentation

In 1957, the launch of the first artificial satellite Sputnik, by the Soviet Union triggered great advances in space technology. Subsequently, came more challenges in satellite navigation like the determination of orbit of a satellite from the variations of the signal radiated by the orbiting satellite, received at a known position on earth. Within a short period, solutions to such challenges led to the development of inverse process where the position of the target receiver on earth could be located based on the signal received from an orbiting satellite, at a known orbit. This thought formed the basis for present day satellite navigation, where a system of satellites, referred as a constellation, provides autonomous geo-spatial positioning with a global coverage. It enables small electronic receivers to accurately determine their latitude, longitude and altitude based on the time signal sent from the radio of the visible satellite. This concept was validated with the launch of series of satellites such as Transit satellites and Timation satellites which provide accurate clock data, operated by the United States (US) armed forces. The main focus of these satellites was to provide the US forces with precise positioning capability. The newly experimented navigation system performed extremely well to sub-meter accuracy though they had some limitations in coverage, fast real-time position determination as the total orbiting satellites were limited. Eventually, the limitations were resolved and gave way to improved global system called the Global Navigation Satellite System (GNSS) with the introduction of US NAVigation System, Timing And Ranging Global Positioning System (NAVSTAR GPS) having more than 24 satellites in its constellation as on March 2013.[4]

Though the main objective of developing a global navigation was assumed to be for military applications, it was also realized that these systems were also capable of a lot of scientific and civil applications, like geodesic measurement, transport and disaster management among others. An important application that was soon envisioned was the use of GPS in spacecraft navigation. Soon, onboard receivers were flown first with Landsat satellite to demonstrate the precise positioning ability of the technology. Since then, many receivers were flown with subsequent launches and nowadays, they are used as a main operation means of navigation.

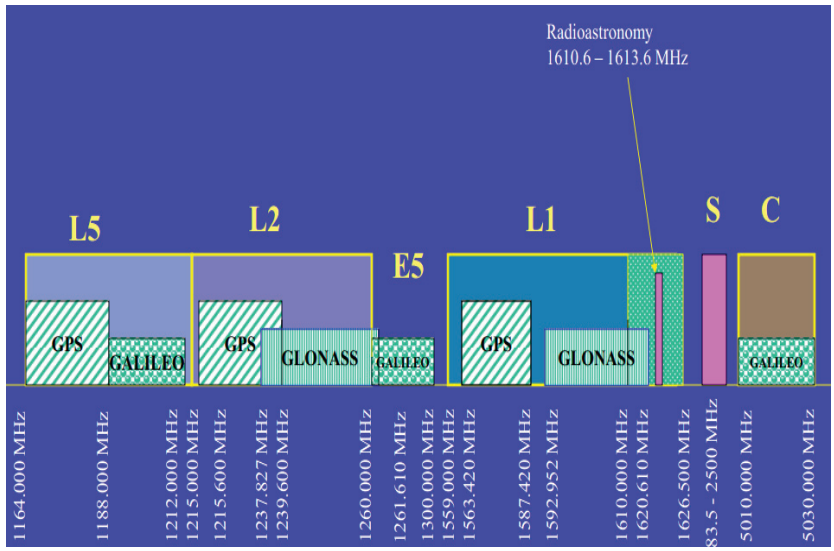

Figure 1. Spectral bands used by various Radio Navigation Satellite Systems. (Source: European Space Agency)

The GNSS employs three basic segments - space segment, control segment and user segment, to facilitate the navigation process. The space segment consists of a constellation of satellites in Medium Earth Orbit (MEO) that transmits signals, which can be received on the electronic receiver. Number of visible satellites at any point of time is very crucial parameter, as it enhances the accuracy of the estimated value. Signals that are sent by the satellite include ranging code, which consists of Coarse/Acquisition (C/A) code or the Precision (P) code that enables the receiver to compute the distance between the satellite and the receiver. They are also called as pseudo-random noise code (PRN). Additionally, they transmit navigation data, which is binary-coded message that provides information on the satellite ephemeris (Keplerian elements or satellite position and velocity), clock bias parameters, almanac, satellite health status, and other complementary information. They operate mostly on the L-band (1164 MHz to 1610 MHz) and Fig. 1 illustrates the spectrum used by various radio navigation systems operated by various countries. The second segment - control segment, tracks and monitors the signal from the space segment and estimates the orbits and clock behaviour of the satellites. This information is uploaded to the satellites so it can be transmitted to users. In the user segment, the main function is to extract the navigation information and to compute the position, using the incoming carrier wave. There are two measurement methods that are incorporated in the user segment - the first method is called Pseudo-ranging, where the incoming PRN code and locally generated copy are compared and the transmission delay between

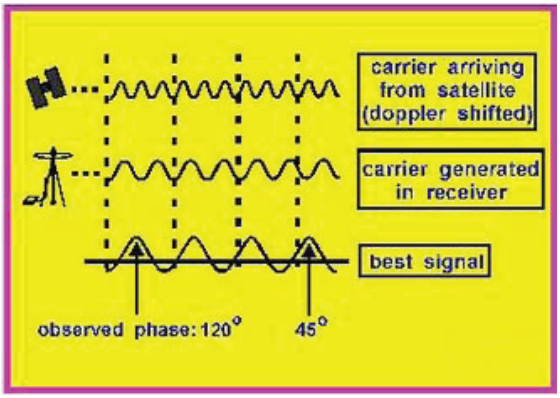

Figure 2. Career phase measurement. (Source: GPS tutorial, University of New South Wales)

the satellite and the receiver is computed. This method can efficiently calculate the user's position, when the signal is available from four or more satellites along with satellite position available in the ephemerides of the navigation message. Three satellites provide the position information in X, Y and Z coordinate while the fourth satellite is used for time error estimation, usually caused by errors in quarts oscillator in the receiver device. The second method is career phase observable. In this method the received carrier signal's phase is compared with a receiver generated signal at the same frequency. Fig. 2 explains the carrier phase measuring technique.

With the rising importance and utility of the GNSS, various countries have implemented their own navigation system. United State's Global Positioning System (GPS) and Russian GLobal Orbiting NAvigation Satellite System (GLONASS) are the only global systems that are fully operational at the moment. Other GNSS systems being developed are the Beidou and Galileo system of China and Europe, respectively.

Although, GNSS capability to provide navigation assistance is tremendous, still, it cannot meet the performance requirements for some applications like aircraft landing that requires extremely high accuracy and reliability. Such challenges led to the design of an overlay system, called as augmentation system, which complements the GNSS to improve performance. The augmentation system incorporates external information, captured from various external sources, in the calculation process to improve the accuracy, availability, continuity and integrity of the system. Thus, it assures the overall reliability of the navigation system in all weather conditions. Augmentation systems are classified based on how they capture external information transmitted to the receiver. With the growing potential of satellites, Satellite Based Augmentation System (SBAS) is

getting more common and many countries have already started operating them. Existing systems includes the Wide Area Augmentation System (WAAS), operated by the United States, the European Geostationary Navigation Overlay Service (EGNOS), operated by the European Space Agency, Multi-functional Satellite Augmentation System (MSAS), proposed by Japan and GPS Aided Geo Augmented Navigation (GAGAN) system, proposed and operated by India. The following sections will explain about various augmentation methods and more elaborately the GAGAN system developed by India.

2. Augmentation methods and operation

Augmentation system improves the accuracy of the GNSS, by providing corrections to mitigate the errors arising out of various sources. In order to provide such corrections, the system involves earth stations that were very carefully surveyed and whose exact locations are precisely known. These stations receive the GPS signals and compare them with the value they should actually receive, and their difference can be used to compute the correction value. These corrections are sent to the receiver either through space based system or a ground based system. Various augmentation methods and its operation are explained below.

2.1 Satellite based Augmentation System (SBAS)

The SBAS consists of carefully established ground segments that receive the GPS data. The ground segments have the capability to track dual frequency L1/L2 Coarse/Acquisition (C/A) code for civilian use and L2 Precision (P) code signals (military use) to determine the pseudo-range and career phase of the visible satellites [1]. The ground station send the measurement to a SBAS master facility, which calculates clock and ephemeris correction of each GPS satellite, ephemeris information for geo-stationary satellite and Ionosphere Grid Points (IGP). IGP are imaginary grids points which are considered to have constant value over each grid area. These grids are used to calculate error bounds due to ionospheric effects. This correction information is then sent to the Geo-stationary communication satellites that are visible to the master station, and from there, correction information are retransmitted to the user segment and necessary

corrections are made. Fig. 3 illustrates the method of space based and ground based augmentation systems.

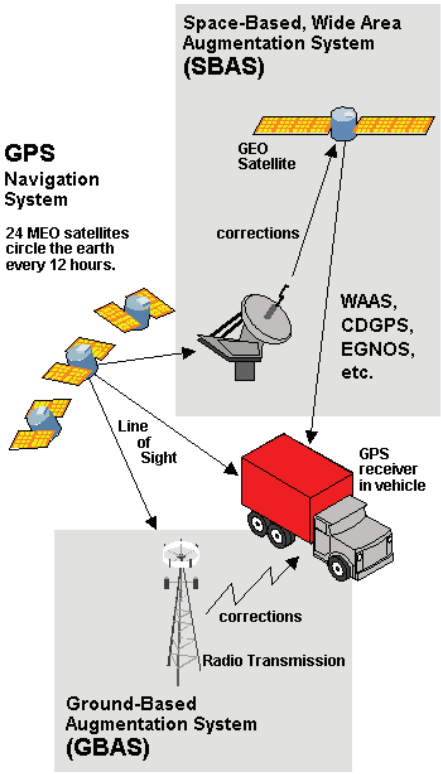

Figure 3. Space based and ground based augmentation. (Source: http://www.pcmag.com/encyclopedia/term/58917/gps-augmentation-system)

2.2 Ground-Based Augmentation System (GBAS)

In a ground based augmentation system, the pseudo-range measurement made by the ground based receiver system is essentially used to calculate the differential correction for each satellite. These corrections are sent to the airborne user via a data link and the airborne user applies the correction values to the pseudo-range, to calculate the position solution. This system is based on the assumption that the two receivers, ground-based receiver and airborne receiver that are within a short baseline separation, will have error sources common to both. GBAS mainly aims at providing navigation assistance at a terminal area like airport. Fig. 4 explains the GBAS system used in airport area. A typical GRAS consists of a space segment, ground segment and user segment. Space segment consists of GNSS satellites as well as ranging source that may provide optionally by a SBAS. The GBAS ground segment consists of a number of reference

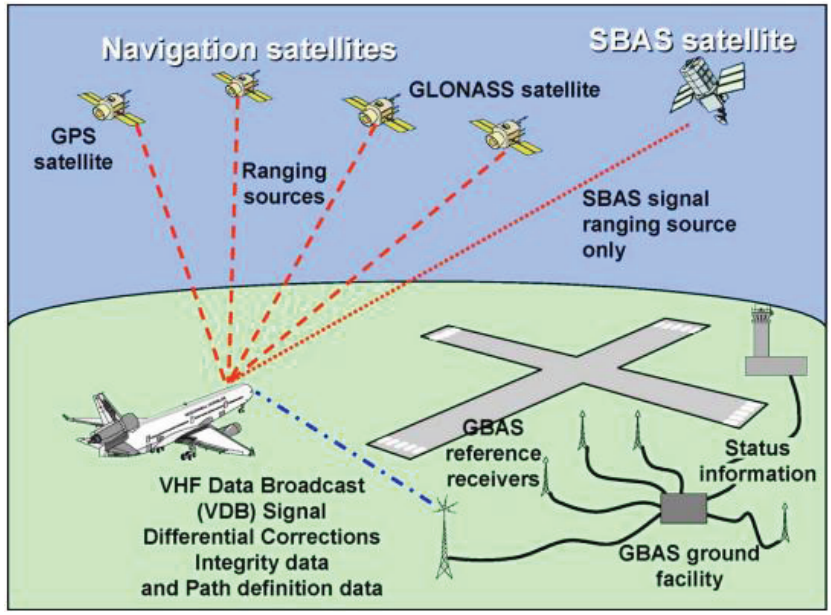

Figure 4. Architecture of ground based augmentation system [2]

receivers that are sited near the airstrip property. These reference receivers will tract the GNSS satellite and fetch the necessary pseudo-range values and other signal health and system parameters and send them to the centralized facility. The centralized facility will calculate the corrections from multiple, redundant observation of pseudo-range values and are broadcast to the user over a Very High Frequency (VHF) Data Broadcast (VDB) in the 108.0-117.975 MHz band. [2]

The 108–117.975 MHz band is currently also used by conventional landing systems such as VHF Omni-directional Ranging (VOR) systems and Instrument Landing Systems (ILSs). Consequently, the band is getting congested in some parts of the world. Since the VDB signal structure was designed to provide very high spectral efficiency, it offers significant flexibility over the conventional systems. For example, a single ILS frequency assignment provides only a single approach to a single runway end but with GBAS, the same 100 KHz band used by conventional system, can theoretically support up to 192 approaches with the capability for multiple approaches to the same runway end if desired. [2] Thus GBAS has enormous potential to replace conventional systems.

2.3 Ground-based Regional Augmentation System (GRAS)

GRAS blends the GBAS and SBAS concepts. GRAS architecture, shown in Fig. 5, consists of a GRAS Reference Station (GRS) that collects the GPS

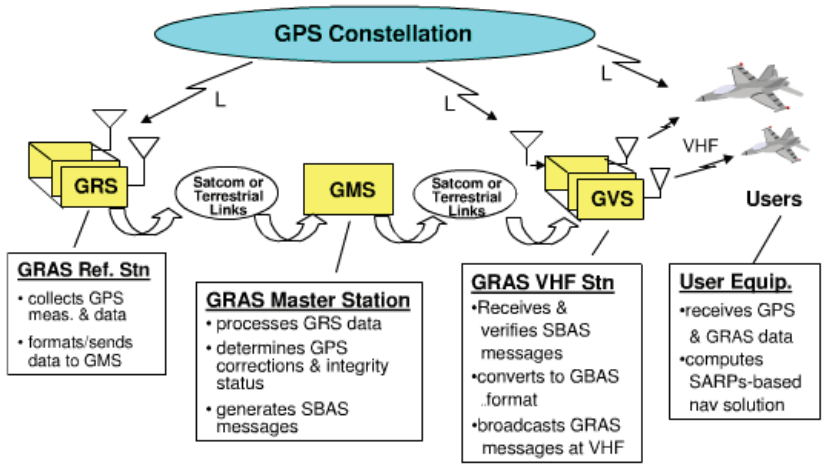

Figure 5. GRAS concept [3]

data and transmits them to centralized units to compute the correction information just like the SBAS. Information from the centralized facility is then sent to a ground based terrestrial stations that can transmit the correction information over a VHF data broadcasts (VDB) and a compatible receiver can receiver them. They are mostly used in regions such as Australia where a dedicated geo-stationary satellite is unavailable. [3]

2.4 Aircraft-Based Augmentation System (ABAS)

International Civil Aviation Organization (ICAO) defines a ABAS as “an augmentation system that augments and/or integrates the information obtained from the other GNSS elements with information available on board the aircraft”. ABAS includes methods to provide integrity monitoring through either the exploitation of redundant GNSS measurements referred to as Receiver Autonomous Integrity Monitoring (RAIM) (see Fig. 6a. and 6b and [4]) or through the use of onboard sensors (e.g., barometric altimeters, inertial navigation systems, other navigation systems to enhance continuity, availability, or accuracy over that provided by the other elements of GNSS [5].

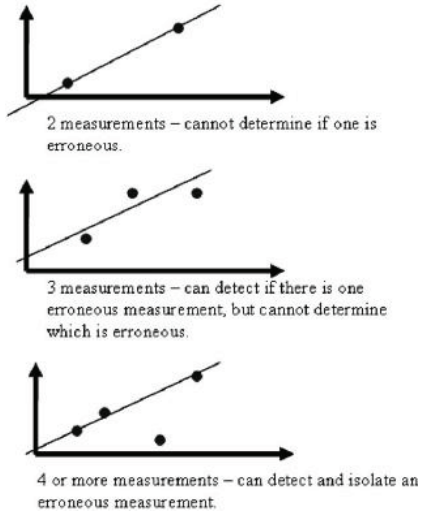

Figure 6a. Illustration of RAIM concept through an analogy of a two-dimensional problem involving noisy measure-ments of a linear relationship [4]

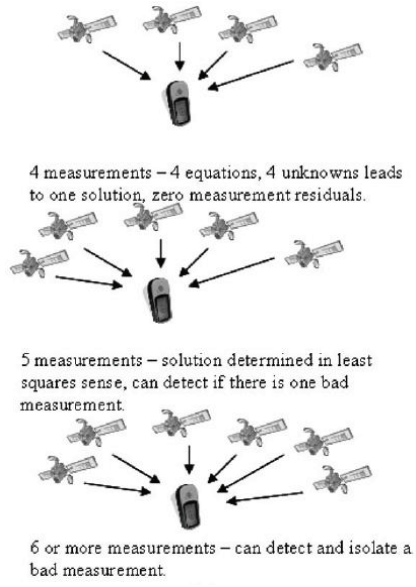

Figure 6b. Illustration of RAIM concept through an analogy the four-dimensional problem of solving user position and clock error in GNSS [4]

3. SBAS performance parameters

Numerous errors sources can degrade the quality of the augmentation process. To ensure the quality of the augmentation system is within acceptable limits, performance parameters are specified. The performance parameters of the SBAS system are listed below.

3.1 Accuracy

Accuracy is usually measured by a term called as Navigation System Error (NSE), which give the difference between the real position value and the position provided by the user's onboard equipment. Thus, SBAS provides compliance with respect to the accuracy requirements by providing the correction information for clock errors, satellite orbit errors and ionospheric propagation errors.

3.2 Integrity

International Civil Aviation Organization (ICAO) defines integrity as amount of trust that can be placed on the correctness of the information provided by the SBAS system. The SBAS assures integrity requirements by

- Providing the user with necessary alarms so that the user can reject the faulty correction information from a flawed satellite source in its calculation.
- Providing the user with Horizontal Protection Level and Vertical Protection Level (HPL/VPL) along with the corresponding alarm limit, to assess the health and availability of the system used. HPL and VPL define the radius of a circle in horizontal and vertical plane, respectively, which contains the true position at the centre and a good probability of finding the indicated position within the region. These are calculated based on the error estimates provided by the SBAS system.

3.3 Continuity

Continuity explains the probability that the system continues to provide the necessary performance as indicated in the performance specification throughout the phase of operation. A lack in continuity will hamper the operation to be aborted and relates to associated risks.

3.4 Availability

Availability refers to the probability that the navigation system is ready to provide service when any user operation starts. Normally, if other performance criteria such as accuracy, integrity and continuity are met along with the navigation service ready to use at any point of time, then availability parameter is satisfied.

Table 1 shows the acceptable performance ranges put forth for various operation phases in aviation industry.

The biggest disadvantage of SBAS systems is that, they are available only in certain regions in the world. Moreover, they have different framework in different countries and hence interoperability has been an important challenge. To standardize the system globally and for achieving interoperability, ICAO Standards And Recommended Practices (SARP) has specified standard specifications and SBAS Interoperability Working Group (IWG) coordinates the understanding between various service providers. [10]

Table 1. Performance requirements for different services in aviation sector. (Source: Navipedia)

Typical Operation	Horizontal Accuracy (95%)	Vertical Accuracy (95%)	Integrity	Time-To-Alert (TTA)	Continuity	Availability
En-route	3.7 km (2.0 NM)	N/A	1 – 1 × 10-7/h	5 min	1 – 1 × 10-4/h to 1 – 1 × 10-8/h	0.99 to 0.99999
En-route Terminal	0.74 km (0.4 NM)	N/A	1 – 1 × 10-7/h	15 s	1 – 1 × 10-4/h to 1 – 1 × 10-8/h	0.99 to 0.99999
Initial approach, Intermediate approach, Non-precision approach (NPA), Departure	220 m (720 ft)	N/A	1 –1x10-7/h	10 s	1 – 1x10-4/h to 1 – 1x10-8/h	0.99 to 0.99999
Approach operations with vertical guidance (APV-I)	16 m (52 ft)	20 m (66 ft)	1 – 2 × 10-7 per approach	10 s	1 – 8 × 10-6 in any 15 s	0.99 to 0.99999
Approach operations with vertical guidance (APV-II)	16 m (52 ft)	8 m (26 ft)	1 – 2 × 10-7 per approach	6 s	1 – 8 × 10-6 in any 15 s	0.99 to 0.99999
Category I precision Approach	16 m (52 ft)	6.0 m to 4.0 m (20 ft to 13 ft)	1 – 2 × 10-7 per approach	6 s	1 – 8 × 10-6 in any 15 s	0.99 to 0.99999

However, SBAS has benefited us in many ways. Their services can cover large land areas and provide assistance in areas where other systems cannot be deployed. Thus, increased capability, flexibility and cost effective solutions than the legacy systems are noteworthy benefits.

4. GAGAN - SBAS over Indian region

With rising necessity of accurate positioning systems, for Safety Of Life (SOL) applications such as aircraft take-off and landing and other aviation needs, Indian government proposed to set up a SBAS system for its region, called as GAGAN. This project is a joint effort of Indian Space Research Organisation (ISRO) and Airport Authority of India (AAI) and they are planned to be executed in two different phases- Technology Demonstration Phase (TDP) and Final Operation Phase (FOP). TDP phase consisted of studying the feasibility parameters and designing a system with necessary operation blocks, to demonstrate the capability of the design. In FOP, design are finalised after necessary modifications and complete operational goals are achieved.

4.1 GAGAN Functions and Architecture

The main function of GAGAN implementations are:

- Ranging: It provides additional ranging signals to improve availability typically using a Geo-Stationary link.
- Integrity Channel: It provides transmission of GPS and integrity data to navigators.

Fig. 7 illustrates the architecture of GAGAN. There are three basic segments in GAGAN- ground segment, space segment and the user segment. Major elements in SBAS ground segment are: (i) Reference Stations (RS); (ii) Mission Control Centre (MCC); (iii) Land Uplink Station (LUS) and space segment consists of GEO satellite with necessary payload. User segments are the end users like maritime vessels, airplanes and land based systems that are equipped with suitable receivers to receive geostationary satellite signals.

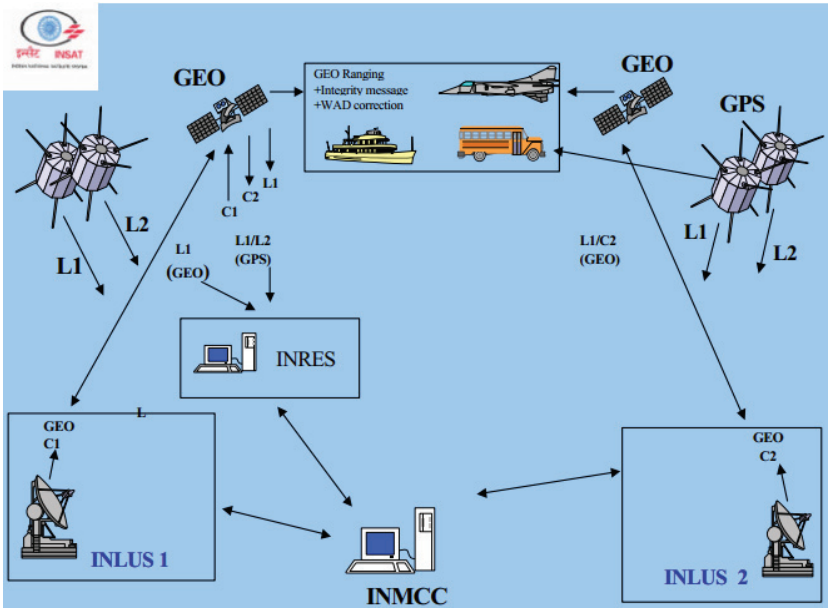

Figure 7. GAGAN architecture [6]

4.2 Ground segment

Various elements in the ground segment are used to collect the GPS data, perform necessary computations to determine correction value and to retransmit them to space segment so that users can apply necessary corrections. GAGAN ground segment consists of following elements:

4.2.1 Indian reference stations (INRESs)

These stations collect measurement data and broadcast messages from all the GPS and GEO satellites visible to it and forward it to the Indian Mission Control Centre (INMCC). These stations were carefully surveyed and selected at places where the multipath signal and other error source are least. Eight INRESs were initially proposed for technology demonstration phase. To improve performance, additional nine more stations were added later in the final operation phase. [11]

4.2.2 Indian Mission Control Centre (INMCC)

The main functions of the INMCC are: network management, integrity monitoring, iono-tropo model delay estimation, wide area corrections such as separation of errors, orbit determination, and command generation. The INMCC also consist of a main frame computer and a host of secondary computers connected to a network. Two INMCC have been planned and are operational now. [11]

4.2.3 Indian Navigation Land Uplink Station (INLUS)

INLUS communicates with the geostationary satellite. This segment consists of a signal generator and a Radio Frequency (RF) unit along with an 11 m antenna. This station receives correction messages, which contains User Differential Range Errors (UDREs) and iono-tropo grid models from the INRESs through the INMCC and formats it before retransmitting it to user through the Geo-link. The INLUS also provides GEO ranging information and corrections to the GEO satellite clocks. [11]

Fig. 8 describes the various signal flow in the SBAS GAGAN system.

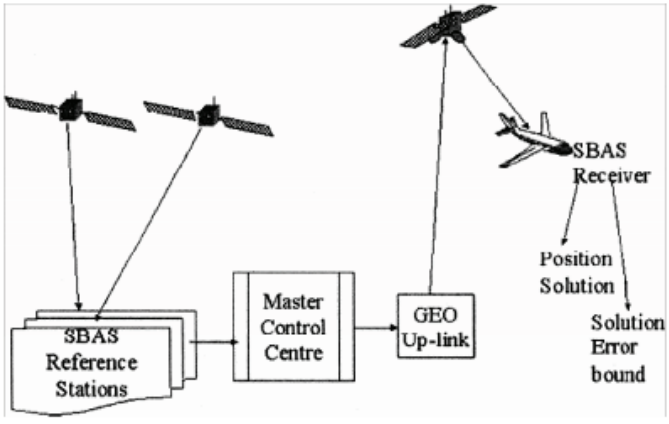

Figure 8. SBAS Data Flow [7]

4.3 Space segment

Space segment consists of geostationary satellites that can relay information to the user. For this augmentation purpose, 3 geostationary satellites have been proposed and two satellites: PRN127, GSAT-8 at 55° E and PRN128, GSAT-10 at 83°E are already operational. The third satellite is planned to be used as a backup satellite and is expected to be operational in near future. [12]

The geostationary satellite operates a navigation payload compatible with GPS L1 frequency and GPS L5 frequency [13]. Its main functions are to relay the geostationary signal to be received by the modified GPS receiver at the user segment.

Fig. 9 shows the coverage of GAGAN by GSAT-8 and GSAT-10 over the Indian subcontinent.

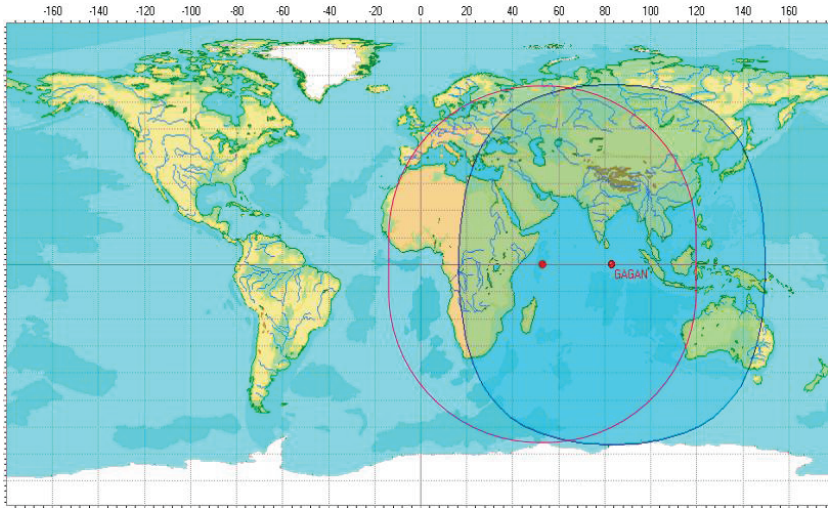

Figure 9. Planned GAGAN coverage.

4.4 User segment

The user segment consists of receiver device that can receive dual frequency at L1 and L5 bands that are downlink channels for geostationary satellites. They also have the capability to track the operational 7 IRNSS satellites and receive position information. Main users of this service include aviation sector for SOL applications and to assist other civil transport and maritime operations.

The initial phase of GAGAN will cover around 1500 Km around Indian subcontinent and a majority of the area lies around the mid and low latitude region and is worst affected by delays, large spatial and temporal gradients, equatorial anomaly, depletions (bubbles), scintillations etc.

Normal grid based methods often fail frequently and hence a need for different algorithm is extremely necessary to calculate the correction values. For this purpose, various ionospheric studies were carried out which analysed the ionosphere and its variations. A total of 18 Total Electron Content (TEC) reference stations were established in equally-spaced latitudes and longitudes in order to study the spatial variation of the TEC. It was found that the anomaly was highest in the equinoctial months of March, April, September and October followed by winter months and then summer [8]. To mitigate such anomaly, new methods such as region specific coefficient based model and ISRO GIVE MODEL- Multi Layer Data Fusion (IGM-MLDF) [9] have been developed. GM-MLDF computes the ionosphere corrections and confidences at pre-defined grid points at 350 km shell height. Ionosphere delays are computed at 250 and 450 km shell heights in order to capture the vertical movement and large scale irregularity of the Indian ionosphere and then employing data fusion for fusing the delays and confidences at 350 km shell height. A goodness of fit test is used by the ionosphere storm detection algorithm, to protect the user from uncertain behaviour of the ionosphere. Moreover, IGM-MLDF also models associated uncertainties to protect a GAGAN user from ionosphere effects.

Incorporating such distinct and improved algorithms, the performance of the GAGAN system looks extremely good during the validation phase. The Final System Acceptance Test (FSAT) was conducted on July 16, 2012 and the results are given in Table 2.

The applications of GAGAN are vast, ranging from civil aviation to non-aviation applications like surveying, maritime applications, cartography, and disaster management among others. The GAGAN system would greatly benefit the civil aviation in a number of ways - first, they would enable precision landing during bad weather condition, even in the remotest airport where the ground based systems are still unavailable. Also, the all weather operation would reduce flight delays and diversions, thereby reducing the airline operating cost and reducing emission. Secondly, they would improve the capacity of airline routes by reducing the safety spacing between aircrafts in the demanding traffic routes. The GAGAN system is designed to work with other augmentation systems like MSAS, EGNOS and WAAS and thus seamless augmentation service in international routes will also be made possible in future. Future commercial aspects also looks promising as the GAGAN footprint covers most South-Asian countries and augmentation to other countries could be provided with minimal expansion effort. However, GAGAN signals outside India has not been validated yet

Table 2. GAGAN FSAT results [14]

Service Level	Parameters	Requirement	Observed Performance/Results
RNP 0.1	1. Availability	>0.99 over the Indian FIR	99.8%
	2. Horizontal Accuracy	<72 m 95% bound	0.7m Average
	3. Vertical Accuracy	N/A	1.52m Average
	4. Time to Alarm	10 s	6.2S
	5. Vertical Alert Limit	N/A	-
	6. Horizontal Alert Limit	185.2m	Not Provided
APV1/1.5	1. Availability	99% over 76% of India	86.57 %
	2. Horizontal Accuracy	<7.6 m 95% bound	0.7m Average
	3. Vertical Accuracy	<7.6 m 95% bound	1.51m Average
	4. Time to Alarm	6.2 s	6.2s
	5. Vertical Alert Limit	50 m	VPL<50
	6. Horizontal Alert Limit	40 m	HPL<40

and hence more performance assessment is needed before commencing commercial services to other countries.

5. Conclusion

GNSS contribution to the ever-growing human needs is tremendous. Aviation sector is considered to be the most benefitted and noteworthy as it has considerably improved the safety of human life during air travel. With emerging technologies such as SBAS and GBAS, which supplements GNSS, navigation systems are getting more robust and fail-safe.

Though different augmentation techniques are available, due to the versatility and low cost of satellite operations, SBAS is making its way to be the mainstream augmentation system. Other areas, such as Australia, where geostationary satellite is either not available or very expensive due to political or technical reasons, newer augmentation methods such as GRAS which eliminates the need for geostationary satellite have been developed. These augmentation systems are carefully designed so that they can meet the high performance standards specified by SARP. However, the augmentation systems developed so far are regional and global interoperability is extremely essential to benefit the aviation sector. India's GAGAN implementation helps the augmentation cover the Indian subcontinent and helps to make more equatorial ionosphere studies possible. The implementation of GAGAN system would enable India to have sovereign means of enhancing GPS. They would also boost confidence in air travel and contribute greatly to the management of increasing air traffic. Further expansion of augmentation service to neighboring countries will help India on a commercial aspect, as well as greatly improve foreign relations.

References

[1] R. Gold, "*Optimal binary sequences for spread spectrum multiplexing*", IEEE Trans. Inf. Theory, vol. 13, pp. 619–621, Oct.1967.

[2] Murphy and T. Imrich, "*Implementation and operational use of ground-based augmentation systems (GBASs) VA component of the future air traffic management system*", Proc. IEEE, vol. 96,no. 12, pp. 1936–1957, Dec. 2008.

[3] G. Crosby, W. Ely, K. McPherson, J. Stewart, D. Kraus, T. Cashin, K. Bean, and B. Elrod, BA "*Ground-based Regional Augmentation System (GRAS) – The Australian proposal*", Proc. Inst. Navig. ION GPS 2000, Salt Lake City, UT, Sep. 2000.

[4] Global Positioning System: Papers Published in Navigation, vol. V, RAIM. Fairfax, VA:Institute of Navigation, 1998.

[5] T. Murphy, M. Harris, and M. Braasch,B, "*Availability of GPS/INS integration methods*", in Proc. Inst. Navig. ION GPS 2001, Salt Lake City, UT, Sep. 2001.

[6] S. V. Kibe, "*Indian plan for satellite-based navigation systems for civil aviation*", Current Science, vol. 84, no. 11, Jun. 2003

[7] K.N Rao, Suryanarayanan, "*GAGAN- The Indian Satellite based augmentation system*", proc. Indian Journal of Space and Radio Physics, pp293-302, vol. 36, Aug. 2007.

[8] S. Ray, A. DasGupta,"*Geostationary L-band signal scintillation observations near the crest of equatorial anomaly in the Indian zone*", Journal of Atmospheric and Solar-Terrestrial Physics, Volume 69, Issues 4–5, April 2007.

[9] Srinivasan, Nirmala, A. S. Ganeshan, and Saumyaketu Mishra. "*A New Grid based Ionosphere Algorithm for GAGAN using Data Fusion Technique (ISRO GIVE Model-Multi Layer Data Fusion)*" 39th COSPAR Scientific Assembly. Held 14-22 July 2012, in Mysore, India. Abstract F4. 3-8-12, p. 1876. Vol. 39. 2012.

[10] "*Global SBAS status*", IWG conference, Munich, Germany, Jan. 2012

[11] P Soma, K N Suryanarayana Rao, S V Kibe, K Sampath Kumar, Elango K, "*GAGAN: building block by block*", Coordinates, April 2012.

[12] Shivakumar,S.K , "*Views on GNSS*", Coordinates, Sep. 2012

[13] http://www.isro.org/satellites/gsat-10.aspx

[14] http://www.icao.int/Meetings/anconf12/WorkingPapers/

/ANConfWP90.1.1.en.pdf

Positioning Techniques of Modern Smartphones

Ross Snell

Aalto University School of Engineering
Department of Real Estate, Planning, and Geoinformatics
ross.snell@aalto.fi

Abstract

Smartphones have developed significantly over the past few years. With their development has come positioning technology. Positioning techniques of modern smartphones can be divided into network based and handset based methods. A test of these methods in an indoor and outdoor environment was conducted to examine their limitations and strengths. It was found that A-GPS works better than Integrated GPS methods, or network based methods. With regards to indoor testing, it seemed that the smartphone device is susceptible to error such as multipath, and signal complications, producing less accuracy than results conducted outdoors. The more modern smartphone, the Samsung Nexus produced better results than the older Nokia 5800.

1. Introduction and Background

The development of the basic mobile phone into the multi-faceted smartphone has introduced a number of new technologies to the smartphone user. Subsequently one of the standard features of many modern smartphones is positioning - the ability to geographically locate the position of the smartphone and then present this information to a variety of interested parties.

The different techniques that modern smartphones use to identify a position can be divided into those which are network based, which rely on mobile communication infrastructure, and those which are handset based, which depend upon the use of a positioning satellite system such as the Global Positioning System (GPS). Broadly speaking network based methods are cheaper to implement but lack the accuracy of handset based methods (Mallick, 2003)

Unsurprisingly, a wide range of applications have been developed, which take advantage of this relatively new technology. These include applications which provide route guidance and directions from one location to another, in addition to those applications which track sporting activities or identify friends or places of interest which happen to be nearby. Furthermore, a user's positioning information is of great interest to third parties such as advertisers who can alert the user of shops or restaurants that are in their vicinity, and emergency services who can quickly identify where a caller is located to speed up the dispatch of necessary services. Indeed the American Federal Communications Commission has set minimum requirements relating to positioning standards on mobile phones for this purpose.

Although the development of positioning in modern smartphones has undoubtedly proved a useful tool in day to day life, questions remain as to the accuracy and consistency of the ability to identify a precise location. The effectiveness of positioning technology is influenced by many factors, including the technique used to find a position, the environment the user is in, and the technology they are using. Therefore we must be aware of things like weather conditions, the type of buildings nearby, tree coverage, and the mobile device and positioning technique we might be using when finding our position with a smartphone.

The aim of this report is to try and gain a more comprehensive understanding of these different positioning techniques, and how the environmental conditions and available technology might influence upon the ability to accurately locate a smartphone. Ultimately it is hoped to

ascertain how effective these positioning techniques actually are. To achieve this, I conducted a variety of tests on modern smartphones, in both indoor and outdoor environments. I also compared the effectiveness of various positioning techniques. Testing took place in early spring 2012.

This report outlines in detail the theoretical background of positioning techniques, and further explains the plan and results of the tests conducted. Finally, conclusions will be drawn based on the available literature and experiences of the testing.

2. Theoretical background

In order to provide positioning information or develop a positioning based application a potential user needs to know the location (approximate or exact) of the smartphone and express this as x and y coordinates that can be displayed on a map. This is therefore the aim of any positioning technique (Huber, 2010). The accuracy of the location is heavily dependent on the technique used, and as may be expected the more accurate techniques are often more expensive.

As previously mentioned, the techniques can be divided into network based methods and handset based methods.

2.1 Network based methods

Network based methods are the cheapest to implement because they mainly rely on existing cellular infrastructure. The accuracy ranges from over a kilometre to just a few metres depending on the type of network based method in use, and other conditions.

2.1.1 Cellular Identity

In the simplest form, the mobile phone network can be thought of as being divided into cells. Each cell represents a geographical area within which a base station (usually located around the centre of the cell) sends and receives signals to mobile phones. When a base station picks up a signal from a phone, we can conclude that the phone is within the cell belonging to that particular base station.

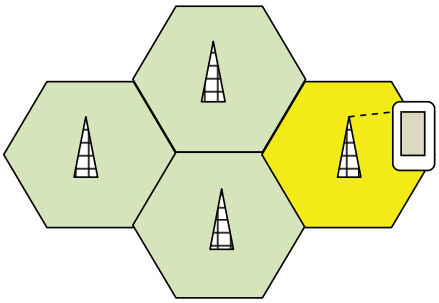

Figure 1. Positioning using Cellular Identity.

This process is further illustrated in Figure 1. The hexagons represent cells with a base station at the centre of each cell. The smartphone is sending and receiving signals from the base station on the right and so we know that the smartphone is located somewhere within that cell.

This technique is undoubtedly beneficial in terms of cost and availability. Every phone that uses a base station (i.e. all cellular phones!) can be located in this way without the need for additional technology. However, in practice the size of the cell can be so large as to prevent any useful location information being obtained. If the cell is divided into smaller sections (as often they are) the accuracy can be improved, but the position would still be somewhere within an area sized anything from 500 metres to 1 kilometre (Mallick, 2003). This level of accuracy may be useful for an ambulance dispatcher who can quickly send an ambulance in the right direction whilst obtaining more detailed address information. However, for route guidance and other applications, this level of accuracy is not sufficient.

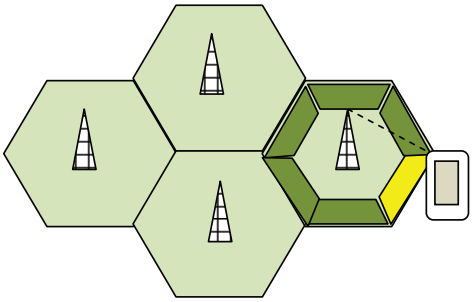

Figure 2. Cellular Identity with Timing Advance and Cell divided into sections.

To further improve the accuracy of positioning, a technique known as Timing Advance can be introduced. This calculates the time taken for a signal to reach a base station, and on the basis of this, a distance can be calculated. Therefore, we know that within the cell, the mobile phone is a

certain distance from the base station, and within that distance the phone must be located in a certain section of the cell. This is illustrated in Figure 2. This method represents an effective technique of further defining the precise location of the phone without demanding updates to the handset. However, the accuracy can still be improved upon.

2.1.2 Time of Arrival and Angle of Arrival

The cellular identity method uses only one cell of the mobile phone network. But often, in larger cities for example, a phone can be connected to a number of base stations and cells. When a phone is able to send and receive a signal from three base stations in three different cells, then we can use some form of triangulation to ascertain a more precise location.

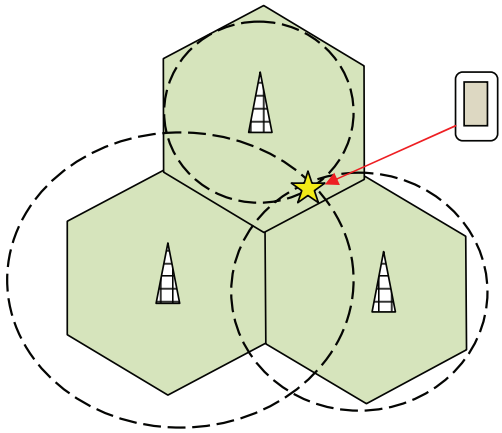

Figure 3. Time of Arrival using three base stations.

Figure 3 illustrates this process in more detail. A phone is located within a certain cell, but is sending and receiving signals to three base stations. When the distance is calculated (indicated by the dotted circle from each base station), we can identify a more accurate location based on where the three distances intersect. In Figure 3 this point is indicated by the star.

This method, called Time of Arrival or TOA, relies on accurate timekeeping and can produce more accurate results, from 50 metres in urban settings to 150 metres in rural environments (Mallick, 2003).

In addition to TOA a technique known as Angle of Arrival (AOA) can be used. This is similar to the TOA technique but calculates the position based upon the angle that a signal sent from a handset meets the base station. When three angles have been obtained from three separate base stations, we can then calculate where the phone sending the signals may be located.

2.2 Handset based methods

The development of mobile phones has been driven by the progression of computational power and ability. Most smartphones now have sufficient computational power to be able to perform the complicated mathematical calculations and triangulations needed in order to find a location, although this of course can be more efficient with outside help.

One example of a technique where the handset makes calculations is known as Enhanced Observed Time Difference (E-OTD). This uses the same principals of TOA but here the handset, and not the base station, makes triangulation calculations to find a position.

As mentioned, the disadvantage of these handset based methods is that they often require more equipment in the phone and thus are more expensive. The advantage is that the techniques available are usually far more accurate.

2.2.1 Global Positioning System

One of the most common methods used for obtaining location is the satellite based system. The American Global Positioning System (GPS) is one of the most well-known, although now similar projects are being launched by other countries and organisations.

The principle of GPS is based on triangulation. The mobile phone with the GPS receiver connects to a satellite. The time taken for the signal to reach the satellite is calculated and when measurements are taken from three or more satellites a location can be ascertained. Figure 4 shows this process in more detail.

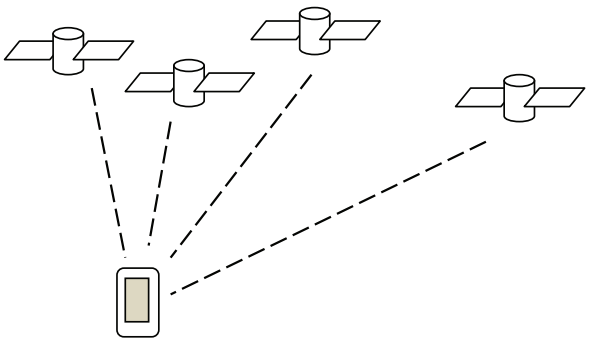

Figure 4. GPS positioning.

Whilst it is possible to get a two dimensional (x and y) based position with three satellites, a fourth satellite can provide measurements of the third dimension providing a position with x, y, and z coordinates. This is in addition to the two satellites providing the x and y coordinates, and the one satellite working as the clock to ensure accurate timings.

Although GPS is accurate, it requires very precise calculations. Considering the distances involved, any small mistake in timing can lead to huge discrepancies in providing a coordinate (Mallick, 2003). Furthermore, the system works best when there is a line of sight from the phone to the satellite. Therefore indoor based methods are not so accurate, unless they rely upon assistance from other sources to get the position.

The accuracy of GPS can range from 5 metres to 40 metres (Mallick, 2003).

2.2.2 Assisted Global Positioning System

To overcome the limitations of GPS, different techniques and technologies can be incorporated in order to improve the reliability and accuracy of the position that is identified. When there is not a line of sight to a satellite, then alternative techniques can be used to supplement the information. Such techniques may include the cellular identity method that has been previously mentioned.

A further problem with the basic GPS method is that it might take a long time to get a fix on a position. When someone's position is changing rapidly, for example when they are travelling in a car, then the GPS may not be able to keep up.

Assisted GPS or A-GPS is a technique which provides accurate information in a quicker time. It works by including a number of receivers attached to base stations, which can collect and decode satellite information to be used by the handset. Figure 5 illustrates this process.

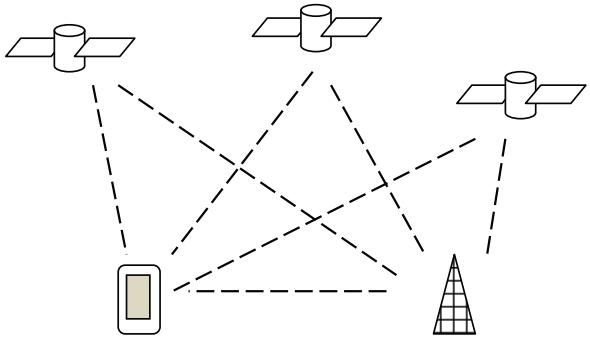

Figure 5. Positioning with A-GPS.

With this assistance, the speed to get a fix on a satellite and to make a calculation on the position of the smartphone is faster, and the calculation can take into account external environmental factors such as whether the user is indoors or not. A-GPS takes the strain out of the handset and provides opportunity to get a quicker fix on the location of a smartphone.

2.3 Indoor and outdoor environments

Ultimately, the technology behind positioning methods is limited by external environmental factors, as well as technical limitations of the phone. A phone might have excellent technical capabilities and a fast connection to the Internet but the accuracy of results will suffer if the device is in an unsuitable environment. In the case of GPS based techniques a line of sight to a satellite is usually required. Therefore, results are better in an outside environment. However even here, there are limitations which can distort the final positioning result.

2.3.1 Limitations of outdoor environments

The outdoor environment varies significantly. An urban environment for example, may involve low level housing or densely packed high rise buildings. Outdoor environments can also include deserts, fields, dense forests, broad leaved forests and coastal areas. In addition to the type of environment, the weather conditions can also impact upon the accuracy of different positioning methods. Here is a brief summary of some of the phenomena that can affect the accuracy of GPS outdoors.

Multipath
Multipath occurs when a signal from one satellite reaches a receiver twice because it has deflected off another object such as a tall building. Figure 6 shows this in more detail:

Because the signal has arrived twice the distance calculations become confused and accuracy suffers (Bajaj et al. 2002).

Forests
Forests are also diverse in their nature. In Finland a typical forest is made up of spruce trees which have pine needle shaped leaves, whereas elsewhere in Europe forests have trees with broad leaves. It should also be taken into account that forests may only have leaf cover for a small part of the year. This is important, because it has been found that leaf cover is one of the main factors in influencing positioning in forests. Where there is significant

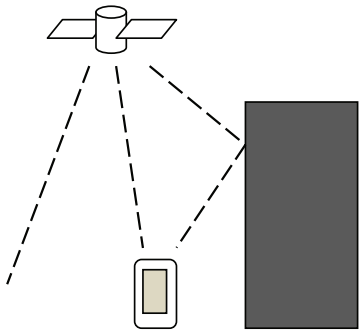

Figure 6. The effect of Multipath.

leaf cover, the accuracy falls. Furthermore, broad leaves create more disruption to accuracy than pine needle leaves (Sigrist et al. 1999).

Climatic conditions
The climate is another significant factor on the accuracy of GPS. As GPS depends on the speed of signals being measured as they reach the mobile device it is important that the signals travel at a dependable speed. However, climatic conditions that are heavy with water vapour can cause propagation error where the signal slows down as it moves through a humid atmosphere. The slower signal creates an error when measuring the distance based on timings and therefore calculating the position of the device (Bajaj et al. 2002).

Solar activity
As the GPS depend upon measurements made outside of the earth's atmosphere, the distances are affected by minute changes in gravitational fields and satellite orbits. Therefore, when solar activity is high, the measurements can be adversely affected. A-GPS techniques can alleviate errors from such atmospheric conditions as the calculating power provided from the support stations can take these factors into account to a certain extent (Dedes and Dempster, 2005).

2.3.2 Limitations of indoor environments

Whilst indoor environment has the obvious disadvantage of not having a line of sight to the sky, it must be remembered that the indoor environment also suffers from many of the problems of outdoor environments. A signal may have been sent at a time when solar activity is high, and it may have travelled through dense atmospheric conditions causing propagation error even before it contends with the problem of finding a receiver in an indoor environment. Furthermore, multipath errors are accentuated.

Signal strength

The obvious problem of indoor environments is that of the satellite signal penetrating the roof obstacle. The signal strength impacts upon accuracy and also upon the ability of the smartphone to calculate based on satellite information. A-GPS techniques are assisted in calculations from the support stations, which somewhat alleviate this error indoors (van Diggelen, 2001).

Multipath indoors

In an indoor environment, the problem of multipath is increased to the extent that the reflected signal can be stronger than the direct signal. In worse cases, the direct signal may not register at all and so the smartphone makes calculations solely on a reflected signal. Obviously, in these instances, the accuracy suffers significantly (Dedes and Demspter, 2005).

3. Testing plan

The aim of the testing is to ascertain the effectiveness of the different positioning methods of modern smartphones.

Owing to the range of different positioning techniques available, as well as the variety of different factors that influence positioning accuracy when identifying a position, the scope of possible testing is very broad. Taking time constraints into account, it was therefore not feasible to test every possible environmental condition, with every positioning technique. Instead it was felt sufficient to test the different techniques separately in different locations and record the conditions during testing.

Positioning techniques would be tested in an outdoor environment and an indoor environment. In addition, the outdoor environment tests would take place at two different lines of latitude.

Both indoor and outdoor testing involved the use of the “Sports Tracker” application (http://www.sports-tracker.com/). Sports Tracker uses the positioning capabilities of a smartphone to track the movement of the smartphone over a certain time period. It can be used for tracking sports or activities such as jogging, walking, or cycling for example. The application plots the route that the smartphone has taken on a map of the area. It is possible to restrict the positioning techniques available to Sports Tracker by altering the settings of the smartphone.

3.1 Outdoor testing

Outdoor testing took place in April 2012. The initial testing plan was to test three positioning techniques – network based, GPS, and A-GPS in both the southern and northern location.

3.1.1 Outdoor testing tools used - smartphone

The Nokia 5800 was used as the smartphone to test the different positioning techniques. The Nokia 5800 uses the Symbian architecture and had all the positioning techniques required to undertake the testing.

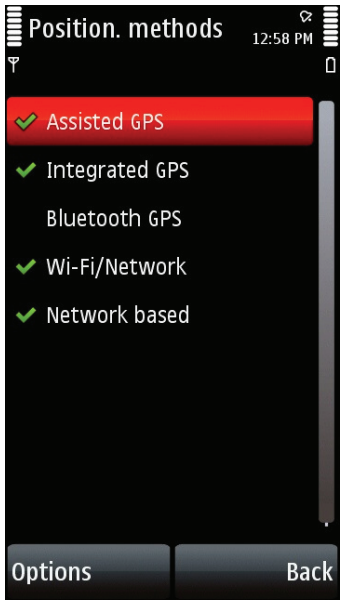

Figure 7. Screenshot of the N5800 Positioning Methods.

As can be seen in Figure 7, the positioning methods available were: Assisted GPS, Integrated GPS, Bluetooth GPS, Wi-Fi/Network, and Network based. Each of these methods could be enabled or disabled accordingly. The Bluetooth GPS and Wi-Fi/Network methods were not used in this testing. Bluetooth GPS involves a Bluetooth connection to an external GPS device, whilst the Wi-Fi/Network method relies upon accessibility to a Wi-Fi Network. The testing route involved forest areas where it was unlikely to connect to, or locate a Wi-Fi network.

3.1.2 Outdoor testing tools used – software

The Sports Tracker application was installed on the smartphone and used for testing.

3.1.3 Testing locations – Helsinki and Rovaniemi

Outdoor testing took place in two quite different locations within the country of Finland. The first location was in the city of Helsinki. This is the capital city and so it can be expected that there is good infrastructure in terms of the cellular network and other communications. Helsinki is a northern city located at latitude of 60 degrees.

The second location was in Saarenkylä, a suburb in the city of Rovaniemi. Rovaniemi is situated approximately 700 kilometres directly north of Helsinki and lies on the Arctic Circle, at a latitude of 66 degrees. Although it is a much smaller city than Helsinki, it has good infrastructure to serve the many tourists who visit the city every year.

Both locations are indicated in Figure 8.

Figure 8. Helsinki at Position 1 and Rovaniemi at Position 2 (Map Source: Bing Maps).

It was felt that the opportunity to test the same positioning methods at different latitudes and in slightly different environments would provide interesting clues as to their effectiveness and to the impact of different environmental conditions. Helsinki was expected to have had a better communication infrastructure than Rovaniemi, thus it can be expected that

Network based methods are more accurate in Helsinki. In addition, it may be that connections to satellites in northern latitudes are more problematic, which would mean that GPS and A-GPS might also be more effective in Helsinki.

3.1.4 Testing routes

In Helsinki, the route taken with the smartphone was approximately 8 kilometres long. The route was in a fairly central location, passing important landmarks such as the Meilahti Hospital, and the Presidential Residence at Mäntyniemi. The environment included forest areas, open parks, coastal routes and more urban areas. Figure 9 shows the route in more detail with the start and finish indicated by the red spot and the red line indicating the route taken.

Figure 9. The route in Helsinki (Map Source: Open Street Map).

The route followed the following streets: Mäntytie – Paciuksenkatu – Seurasaarentie – Tamminiementie – Meilahdentie – Ramsaynranta – Saunalahdentie – Munkkiniemenranta – Ritokallionpolku – Munkkiniemenpuisto – Munkkiniemenpuistotie – Paciuksenkatu – Paciuksenkaari - Kallionportaankatu – Mäntytie.

The speed of movement across the route in Helsinki was, according to Sports Tracker, approximately 12.5 kilometres per hour. This was consistent with a running pace.

In Rovaniemi, it was not possible to follow a route of similar length. Instead a shorter route was planned around a local street, named Jahtipolku. The circuit is indicated in Figure 10.

The speed of movement along the route in Jahtipolku was approximately 5 kilometres per hour according to Sports Tracker. This pace is consistent with a walking pace.

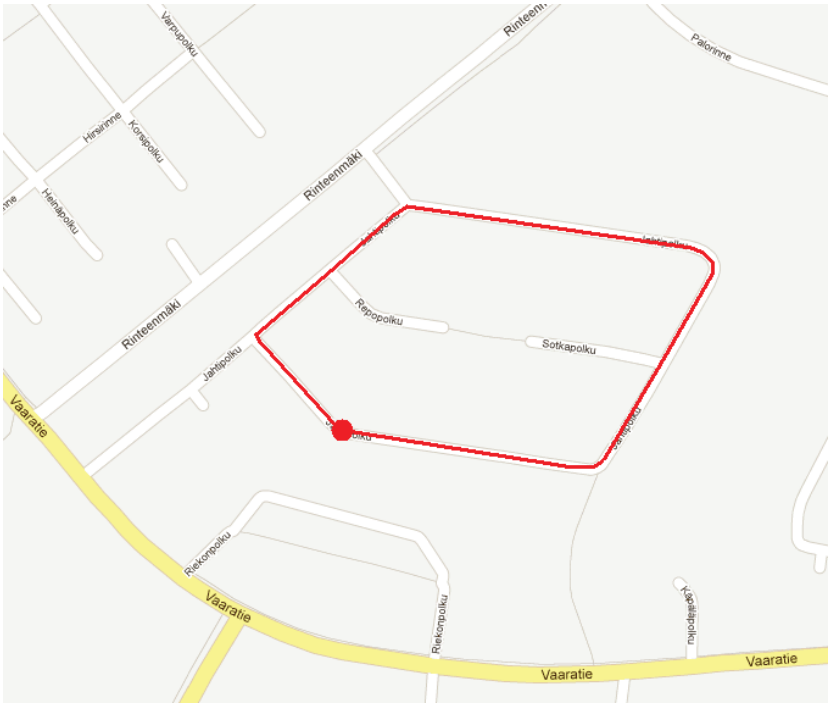

Figure 10. The route in Rovaniemi (Map source: Google Maps).

Jahtipolku is a residential street with low rise (one storey) houses and some tree coverage. The street is located in a fairly urban area between the centre of Rovaniemi and Rovaniemi airport.

It is expected that a slower pace of movement results in more accurate results. This is because there is more time to carry out calculations and to get a fix on a position.

3.2 Indoor testing

Indoor testing aimed to test the same positioning techniques under the constraints of an indoor environment. It was expected that the positioning accuracy would not be as accurate as the positioning accuracy experienced in outdoor environments, mainly because of the building infrastructure blocking a view to the sky.

3.2.1 Indoor testing tools used – smartphones

For the indoor test two smartphone devices were used. They were the Nokia 5800 with Symbian software, and the Samsung Galaxy Nexus with Android software.

Using two devices would also test the technical capabilities of the different phones to locate accurately whilst being constrained by the indoor environment. Each device had the same positioning techniques enabled.

3.2.2 Indoor testing tools used – software

As with the outdoor testing, the indoor testing routes would be tracked using the Sports Tracker application.

3.2.3 Indoor location and route

Testing took place at just one location, a sports hall in Otaniemi, in the greater Helsinki area. The sports hall has a small oval shaped running circuit measuring 158 metres (source www.otahalli.fi). Figure 11 shows a photo of the sports hall.

Figure 11. A view from inside Otahalli.

The testing route would follow the running track as close as possible. The hall is large and has three external walls. There are no floors above the

sports hall meaning that the ceiling is part of the external roof.

4. Test results

Altogether there were ten separate tests of different conditions and different methods. This section will present these results and comment on the conditions for each.

4.1 Outdoor testing in Helsinki

There were three tests of positioning techniques in an outdoor environment in Helsinki. They were with Integrated GPS, A-GPS and Network Based methods.

4.1.1 Helsinki with Integrated GPS

The first test was conducted on 31 March 2012 and used the Integrated GPS method of the Nokia 5800. This was the phone's internal GPS system.

On this day there was still snow on the ground and some points, although the sky was mostly clear with some clouds.

An overview of the route tracked according to Sports Tracker is indicated in Figure 12.

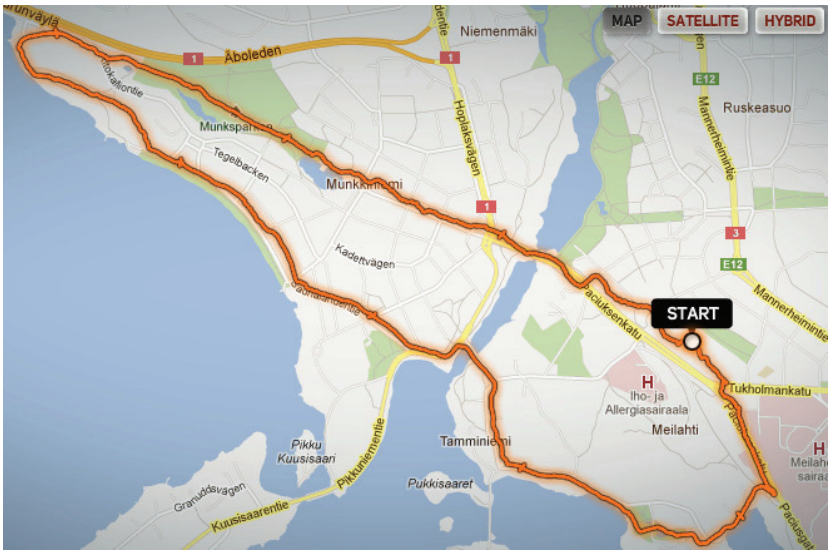

Figure 12. Helsinki with Integrated GPS.

For visualisation purposes, I have included the map in the background. It is important to consider the limitations and accuracy of the map however when conducting the analysis.

At the level of zoom indicated in Figure 12, the route seems to be fairly accurate, indeed it is fair to say that as expected the representation is accurate to within a few metres. On closer inspection however, there are some interesting sections which deserve further investigation.

Munkkineimen puistotie

Munkkiniemen puistotie is an urban area. The road itself can be described as a boulevard, with a tree lined tram route running down the centre of the road. Either side of the road, there are high rise buildings which are used for a variety of purposes, residential, retail, and commercial.

The movement down Munkkiniemenpuistotie was mostly in a straight line. It was therefore expected that the representation would also be a similar straight line. The actual representation is indicated in Figure 13.

Figure 13. Integrated GPS at Munkkiniemenpustiotie.

It can clearly be seen that the actual representation is not in a straight line. Instead it diverts significantly from the more direct line expected.

Munkkiniemen puisto

Munkkiniemen puisto is an open park with forest cover only in a small corner of the park. The movement here was also in a straight line. The representation is indicated in Figure 14.

As a comparison with Munkkiniemenpuistotie the line presented in Munkkiniemen puisto is more accurate, it is a straighter line which is more representative of the movement which took place.

Start and Finish

The start and finish point was at the same location on Mäntytie. This point is an urban residential area with fairly high rise buildings (four storeys) on

each side of the road. The representation of the start and finish point is indicated in Figure 15.

Figure 14. Integrated GPS at Munkkiniemen puisto.

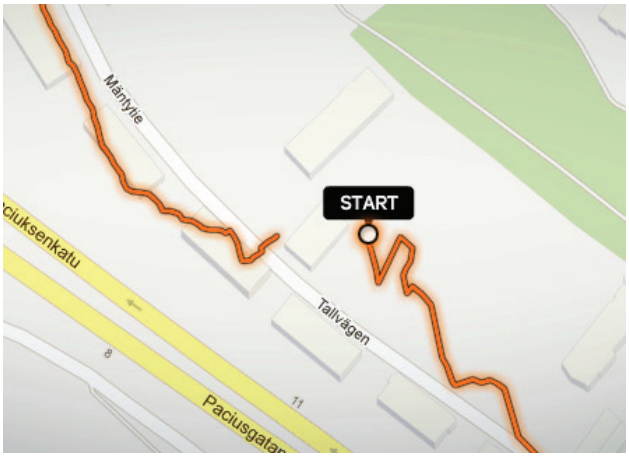

Figure 15. Integrated GPS Start and Finish points.

As can be seen in Figure 15, rather than indicate the start and finish points at the same location, there is a significant distance between them. We can draw some conclusions regarding the accuracy based on this fact.

Distance travelled

According to the Sports Tracker application, the distance travelled along this route was 7.95 kilometres.

4.1.2 Helsinki with A-GPS

The second test was conducted on 14 April 2012 and used the Assisted GPS method of the Nokia 5800. The phone therefore used a connection to base stations to achieve a quicker fix. Accordingly, more accurate results were expected.

On this day there was less snow on the ground, although snow had not completely melted away. The weather was dry, however the sky was overcast with light cloud cover.

An overview of the route tracked according to Sports Tracker is indicated in Figure 16.

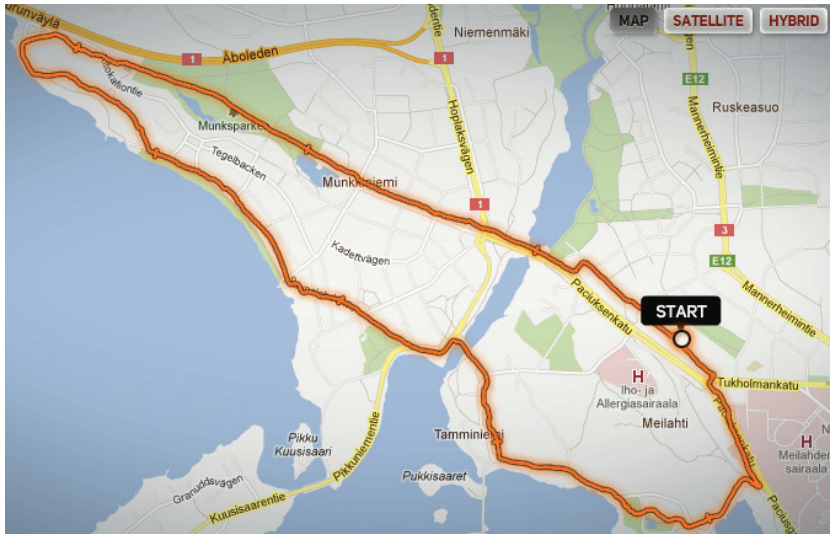

Figure 16. Helsinki with A-GPS.

Upon initial comparison with the results of the Integrated GPS test, the route plotted appears to be smoother and therefore more accurate. At this zoom level, the overall accuracy appears to be as expected, within a few metres of accuracy. It is still worth looking at some details to obtain better analysis.

Munkkiniemenpuistotie

Figure 17 shows the results of the GPS projection along Munkkiniemenpuistotie with A-GPS.

Figure 17. A-GPS at Munkkiniemenpustiotie.

The line produced is more direct and straighter than the line produced under the same conditions with Integrated GPS enabled.

Nevertheless, the outcome is not perfect and there are still deviations which are not likely to represent the actual situation that occurred during the run.

Start and Finish

The start and finish point was at the same location in Mäntytie. The projected start and finish is indicated in Figure 18.

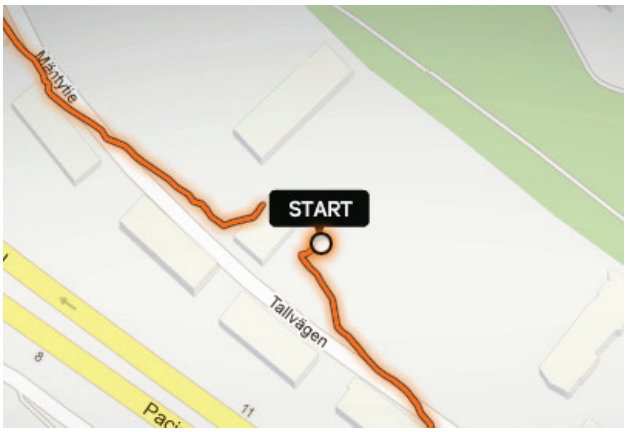

Figure 18. A-GPS Start and Finish points.

As with the GPS test, the start and finish points are recorded as being some metres apart. In reality they were at the exact same point on the ground. When comparing with the results of Integrated GPS however, these

points do seem to be slightly closer together and therefore more accurate to some degree.

Distance travelled
According to Sports Tracker, the distance travelled with A-GPS was 7.71 kilometres. This is 240 metres shorter than the same distance recorded with Integrated GPS. The explanation for this, is that the route recorded with Integrated GPS had more bends and deviations than the A-GPS route recorded – even though these routes were the same travelled. This suggests that the A-GPS is more accurate as it plots straighter lines of movement.

4.1.3 Helsinki with Network based methods

It was not possible to use the Sports Tracker service with Network based methods. Instead a location application, in this instance Google maps, was used to see whether the phone could identify a position using Network based methods only.

Figure 19 shows a screenshot of the results.

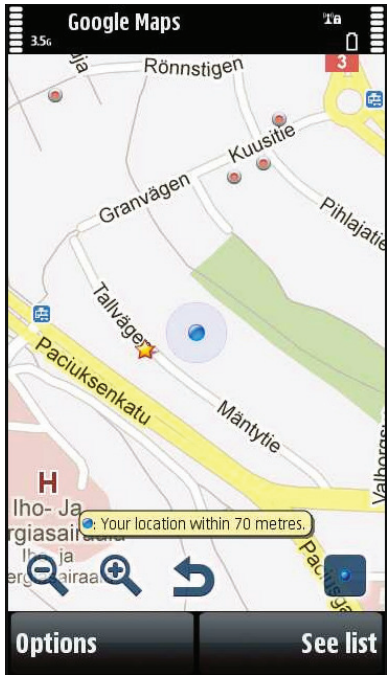

Figure 19. Screenshot of Google Maps with Network Based positioning.

With Network based positioning methods, the Google maps application was able to locate the position of the smartphone to within an accuracy of 70 metres. It took approximately 30 seconds to achieve this result.

4.2 Rovaniemi

As with Helsinki, there were three tests of positioning techniques in an outdoor environment in Rovaniemi. They were with Integrated GPS, A-GPS and Network Based methods. Testing took place on the same day on the 6 April 2012. There was snow on the ground and the temperature was close to freezing point. The sky was clear.

4.2.1 Rovaniemi with Integrated GPS

The first test used the Integrated GPS method of the Nokia 5800. This was the smartphone's internal GPS system.

An overview of the route tracked according to Sports Tracker is indicated in Figure 20.

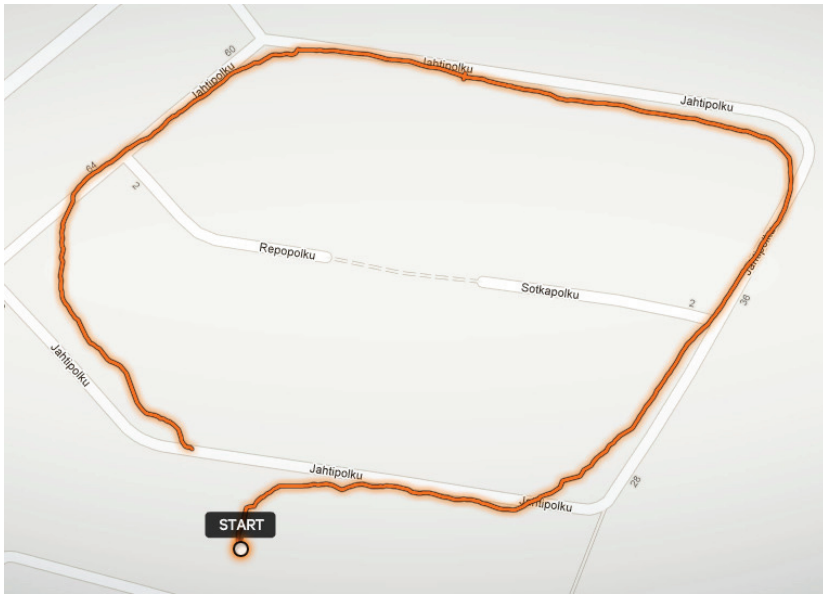

Figure 20. Rovaniemi with Integrated GPS.

As can be seen in Figure 20, the route recorded was again accurate to within a few metres. However, there are some points where accuracy seemed to suffer more than others and these deserve closer examination.

Corners

The route is shaped roughly like an unequal pentagon with 5 corners. Some of these corners have more acute angles and others have quite open, obtuse angles. It seems that the route tracked with GPS has had difficulty with some of these corners, in particular the corner to the left of the picture. It

could be explained by the fact that GPS takes longer to fix a new position, which means that some interpolation is involved between the fixes that have been recorded.

Straight sections
The actual route travelled involved long straight sections before turning at the corners. It is expected therefore, that the route projected is made up of more direct, straight lines. There are points however such as the final straight section where the projected route is wavy and deviates from the true route that was walked during the testing.

Start and Finish
During testing the start and finish point was at the same location. The projected route however indicates a significant gap between the start and finish.

Distance Travelled
The distance travelled according to the Sports Tracker route tracked with Integrated GPS was approximately 0.84 kilometres.

4.2.2 Rovaniemi with A-GPS

The second test used the Assisted GPS method of the Nokia 5800. The phone therefore used a connection to base stations to achieve a quicker fix. Accordingly more accurate results were expected.

An overview of the route projected with A-GPS is indicated in Figure 21.

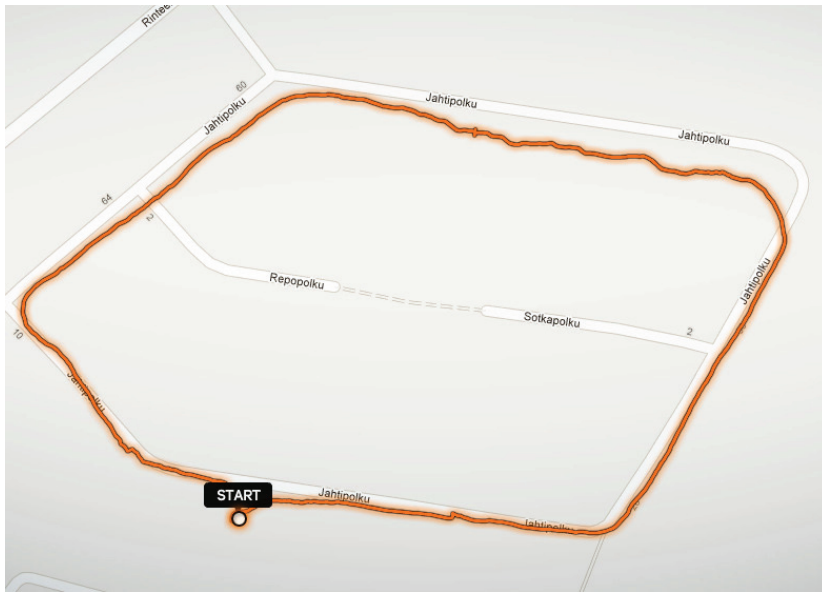

Figure 21. Rovaniemi with A-GPS.

According to Figure 17, the route recording has a similar level of accuracy to other GPS tests, in that it appeared to accurately indicate the correct position within a few metres. When comparing with the Integrated GPS test however, the results clearly seem to be more accurate here.

Corners
With A-GPS, the corners are more accurate as they have not been rounded off like they had been in the Integrated GPS test. Subsequently, the approximate unequal pentagon shape of the route can be discerned. There is one point on the right hand side where the accuracy level seems to have slipped and the corner has been rounded. In fact, at this point it seems that the Integrated GPS method performed better.

Straight sections
For the majority of the route, straight sections have been more accurately depicted. Movement was in a straight direct line and this is indicated especially well on the right section. The northern section however has not performed so well and the accuracy level has slipped here. With Integrated GPS route projection, this northern section achieved better results.

Start and Finish
The route projected with A-GPS seems to indicate a more accurate start and finish point. Whilst they may not be the exact same location (as they were in real life), they are still much closer than depicted using the Integrated GPS technique.

Distance Travelled
According to the Sports Tracker website, the distance travelled with the A-GPS positioning enabled was 0.88 kilometres. This was 40 metres more than was recorded with Integrated GPS.

Interestingly, the increased distance recorded is because the GPS device more accurately recorded the movement of the smartphone at corners and did not cut the corners off as it did with the Integrated GPS method. From experience in Helsinki, however, the Integrated GPS method produced longer distance because more deviations were recorded on the straight sections of the route.

4.2.3 Rovaniemi with Network based

Because it was not possible to use Network based methods with Sports Tracker service, the Nokia Location application was used to show whether a fix on the position of the smartphone could be obtained. A screenshot of the result is displayed below in Figure 22.

Figure 22. Screenshot of Location.

As can be seen in Figure 22, the application was not able to get a fix on the position when restricted to Network based methods only. It can be assumed therefore, that the accuracy was of insufficient quality to be displayed on a map with this application.

4.3 Indoor testing

Indoor testing consisted of four tests of positioning techniques. They were with Integrated GPS, and A-GPS on Samsung (Android), and Nokia (Symbian) devices. Network based testing did not take place. All tests were conducted on the 24 April 2012. The original plan was constrained by other activities in the sports hall, which meant that it was not possible to follow the running track exactly. Rather, the route followed the running track as close as reasonably possible.

4.3.1 Indoor with Nokia 5800 and Integrated GPS

The first indoor test involved the Nokia 5800 with the A-GPS function disabled. The smartphone was therefore forced to use the Integrated GPS function in the tracking. An overview of the route can be seen in Figure 23.

Figure 23. Overview of route tracked indoor with Integrated GPS, Nokia 5800.

Movement was always smooth and in straight lines. The start and finish locations were at the same point, and movement around the circuit was in an anticlockwise direction. The route tracked in Figure 23 immediately appears to have inaccuracies, which we will examine further.

Start / Finish points

In reality the start and finish point was at the same location. However, the route tracked shows a significant distance between the two points. This suggests that there was a both delay in calculating the location and that the calculation was susceptible to error. Indoors, this error may have been caused by a factor such as multipath.

Altitude
The route was always on the same level, however the route tracked (not indicated in Figure 23) indicates a change in level varying between 5 metres. Although this is not a significant error we can measure with some certainty that there is a 5 metre error in terms of altitude accuracy. This may have been caused by weak signals or multipath error.

Corners and straight sections
The straight section to the west (left of the image) has been measured as being fairly straight, indicating some degree of accuracy, however it does not appear to match direction of the route travelled, which was more of a direct north – south movement. The eastern straight section, which included the start and finish point has not been accurately measured at all. Indeed, the initial movement recorded goes east, south, and west, before moving in a remotely accurate northern direction. This suggests some difficulty in finding a start location and matching this to the true direction of movement.

The corner sections are comprised of bends which more closely resemble right angles rather than the smooth bends that were walked in reality.

Distance travelled
The measured distance was 0.18 kilometres.

Overall accuracy
A rough estimation would suggest that the overall accuracy varies between 0 – 15 metres.

4.3.2 Indoor with Nokia 5800 and A-GPS + Integrated GPS

The second indoor test involved the Nokia 5800 with all positioning techniques available. The sports tracker application could use A-GPS (and Integrated GPS) in the positioning. The results of the route tracked can be seen in Figure 24.

With regards to movement in reality, the same conditions apply to previous testing. Movement around the track was anticlockwise and movement was in straight lines. The start and finish point was at the same location. At first glance the results appear to be slightly better than those achieved with Integrated GPS.

Start / Finish points
Again, the start and finish points are not at the same location. However it does seem that they are somewhat closer together than were recorded under Integrated GPS conditions.

Figure 24. Overview of route tracked indoor with A-GPS, Nokia 5800.

Altitude
Interestingly, the altitude recorded varies more than that recorded with Integrated GPS. Here, the altitude varies from between 0 to 20 metres of accuracy.

Corners and straight sections.
Whilst the overall shape of the route is accurate, the reflection of the movement is not. The tracked route is not smooth. It turns and deviates in unusual directions but within a certain level of accuracy. Certainly, the additional computing power provided by A-GPS appears to have helped, particularly at the beginning of the route, however, the accuracy is still not a true reflection of the route travelled.

Distance travelled
According to the measurements, the distance travelled was 0.17 kilometres.

Overall accuracy
The overall accuracy appears to vary from between 0 – 10 metres. This is more accurate than that provided with Integrated GPS only.

4.3.3 Indoor with Samsung Android (two tests)

The Samsung Android smartphone had all positioning techniques enabled. Again movement was smooth and in a clockwise direction around the track. The same test was repeated twice and the results are visible in Figure 25 below.

Test 1 Test 2

Figure 25. Indoor with Samsung Nexus (Android software). Test 1 on left and test 2 on right.

It is interesting to see that the two tests produced quite different results despite being conducted under the same conditions.

Start / Finish points
The first test produced the most accurate start and finish position in that they were both recorded in almost the same location. The second test was unable to repeat this level of accuracy. We can conclude from this therefore, that positioning accuracy varies over time. This may be due to limitations with calculations or other external factors which limit accuracy.

Altitude
In both cases, the altitude varies between 0 – 12 metres.

Corners and straight sections
In terms of corners and straight sections it seems that test 1 produced more accurate results than test 2. However, it does seem that the overall accuracy is good and the straight sections and corners are represented fairly closely to how they were travelled in real life. Test 2 does seem to struggle more at the start section and the straight section to the west (left) of the track seems to have some accuracy problems. Overall though, the path is smooth.

In test 2, there is an interesting point on the eastern section where the route tracked indicates a small circle. This is an interesting error because it is unlikely to have been caused by a failure to find a fix on a position, but is more indicative of error due to external factors such as multipath.

Overall accuracy
Overall the accuracy recorded in both tests is far more accurate than that recorded with the Nokia 5800 with A-GPS enabled. Although the level of accuracy is around the same, at between 0-10 metres, the consistency is far greater and the result is more accurate, more often.

5. Commentary and Conclusions

Whilst the tests that were conducted were comprehensive in that all methods were experimented with, it was not possible to repeat the tests several times and under several different conditions to identify any real patterns. We must take this into account when drawing conclusions from the results.

The testing and the results obtained can however, be used to give us a very general picture of the effectiveness of different positioning techniques. This can be further supplemented by previous investigations, reports and literature on the subject.

This section of the report will look at and analyse the results. It is hoped to provide explanations as to why certain methods have performed a certain way at a certain point, and to draw conclusions based on what we have learnt.

5.1 Outdoor positioning with Network Based methods

As anticipated, the accuracy of Network based methods was not as good as the handset based methods such as GPS. At best, it has been reported that Network based positioning can identify the position of a smartphone within an accuracy of 5 metres. This entails using a combination of complex calculations such as triangulation based on time of arrival and angle of arrival, which further requires the smartphone to be within signal of three or more base stations.

The Nokia 5800 and the Sports Tracker application were not able to use Network based methods to record a path in the same way that the handset based methods could do. This may be for several reasons, including the

time taken to get a signal and make calculations when moving, as well as the range of accuracy being insufficient to produce interpolation.

It seemed that Network based methods worked best when the smartphone was not moving. In this respect it is good for emergency situations if a person carrying a phone is injured and in need of help. For tracing a route, however, Network based methods were not effective.

In terms of location, there was a difference between Helsinki and Rovaniemi. In Rovaniemi, the smartphone using the Nokia Location application was unable to find a location in a suburban area. Whilst the cellular identity method could have been used because it needs only one base station, it may be that the accuracy was insufficient for the application to even attempt to identify or present the position of the smartphone. More accurate results may have been produced had there been more base stations within reach.

In Helsinki, the smartphone was able to identify position within 70 metres. It is difficult to speculate what Network based method was used to achieve this result, although it is suggested that a range of 50 metres to 100 metres (Mallick, 2003) can be achieved by cellular identity using a cell divided into sections. It took approximately 30 seconds to achieve this result. Assuming that three or more base stations were within signal, perhaps a longer time would have been required to calculate based on time of arrival and triangulation.

It can be concluded on the basis of this brief study, that Network based methods are of limited effectiveness when used on the Nokia 5800. In particular, this method did not prove to be effective when trying to track the position of a moving target.

5.2 Outdoor positioning with Integrated GPS

Both Integrated GPS and A-GPS performed better than Network based methods in terms of tracking a moving target and accuracy of a stationary target.

Considering the complexity of the calculations required to identify the position of a smartphone, the results of Integrated GPS on the Nokia 5800 were quite satisfactory. The path drawn using the Sports Tracker application ranged from approximately 0 – 10 metres distance from the true path that was travelled.

It seemed that the environment had an impact on the accuracy of the route that was traced. In Helsinki, where the environment was more diverse it was easy to see the influence of different areas and environments with Integrated GPS enabled.

One clear example was the change from the open park land of Munkkiniemen puisto, to the high density urban environment of Munkkiniemenpuistotie. The actual route travelled was more or less a straight, direct line. There are no sharp turns or bends during these sections. Accordingly, the line reported by Sports Tracker indicated a line which was more or less straight, but only when the movement was through the open park where there were no nearby trees or buildings to disrupt the signal. In Munkkiniemenpustiotie, there was potential disruption from the tall buildings that lined the street, as well as the trees which ran down the centre of the road. The accuracy of the line drawn by Sports Tracker at this point was not so effective, deviating significantly from the true route travelled. We can therefore conclude based on this evidence, that Integrated GPS works better in open spaces than in dense, urban environments.

The impact of buildings upon the effectiveness of Integrated GPS can also be witnessed on Paciuksenkatu where the movement was next to tall buildings and the route reported was approximately 10 metres away from the true route.

The drop in accuracy next to buildings can be attributed to multipath, where one GPS signal arrives at the receiver many times because it reflected off nearby buildings and objects

In addition to the impact of buildings, there is also the potential for error because of the proximity of trees. The route in Helsinki travelled through a forest area and it was reasonable to expect some disruption to accuracy at this point. Surprisingly, however, the accuracy and effectiveness of the equipment at this point was quite good. This could be due to a number of reasons, firstly there had been some trees cut down in the forest recently so the forest was not particularly dense. Secondly, the types of trees were Spruce trees with thin pine needle leaves. It has been found that trees with broader leaves have more of an impact on GPS accuracy than the trees themselves (Sigrist et. al, 1999).

In Rovaniemi, there were no high rise buildings or instances of dense forestry in the area where the testing took place. Furthermore, the pace of movement was slower. Accordingly, it is noticeable that the straight lines have been more accurately represented in this area, and there is not such a great deviation from the true line travelled. Instead, the time taken to get a signal is perhaps more noticeable in Rovaniemi where the corners have become rounded possibly due to the need to interpolate between points where accurate positions were identified.

We can conclude from these tests that Integrated GPS is effective in finding an approximate position. The reliability of the results however, is

adversely affected by the presence of buildings and forests, and the time taken to get a fix on a position can distort results at corners and bends.

5.3 Outdoor Positioning with A-GPS

Of all the methods, A-GPS seemed to be the most effective and most accurate. The ability to share the burden of calculation with other base stations improved accuracy and seemed to mitigate against the effect of potential multipath disruption from buildings and forest for example.

This can be seen most clearly in Munkkiniemenpuistotie where the Integrated GPS had difficulty in identifying a true position because of the effect of multipath. The line produced with A-GPS is straighter, and therefore more accurate.

In addition, the speed taken to get a fix on a position is also more effective. In Rovaniemi, the sharp corners of the route were more accurately represented by the Sports Tracker application when using A-GPS possibly because the device was able to identify the position more regularly and so the interpolation needed was not so great.

There were points however when A-GPS did not prove as accurate. Figure 26 compares the GPS route recorded with Integrated GPS in red with the A-GPS route in green recorded in Rovaniemi.

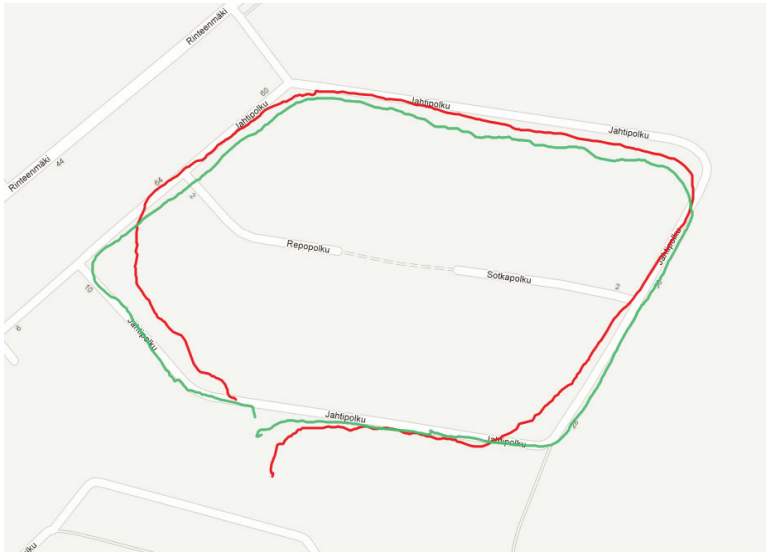

Figure 26. Integrated GPS route (red) A-GPS route (green).

Whilst in the main the green line representing A-GPS appears to be more accurate, with tighter corners and straighter lines, the northern section seems to be more accurate for the Integrated GPS method. There are

several explanations for this behaviour. There could be noise within the device, or maybe the device lost network connection. In any case, this shows that although A-GPS is usually more effective than Integrated GPS, there are instances when the accuracy does drop.

Based on the tests performed, the accuracy of A-GPS was similar to that of Integrated GPS at about 0-10 metres. However, the consistency of A-GPS was higher, and so it was more accurate more often.

5.4 Indoor based methods

The indoor testing, whilst limited, did provide interesting results. Particularly in the case of the older smartphone, the Nokia 5800, the outdoor tests proved far more accurate than the indoor tests. There are a number of possible factors for this. Indoor testing is more susceptible to error from multipath and signal complications, not to mention the other errors that might occur from the external environment.

We have seen in the outdoor testing that the Integrated GPS needs longer to get a fix on a position. In the indoor testing, this is combined with the inaccuracies from external factors. This may explain why in the Internal GPS test indoors, the start of the route was particularly ridden with errors, going in strange directions before it started to follow more accurately the true route travelled.

The indoor test with the A-GPS setting of the Nokia 5800 proved slightly more accurate, showing the influence of assistance with the calculations. However, the influence of the external error was evident, with the route being still not close to the true route followed.

The more recent and more powerful smartphone, the Samsung Nexus with Android software proved far more accurate in the testing. A comparison of the indoor tests is shown in Figure 27.

The differences between the results of the Samsung Nexus and the Nokia 5800 are fairly clear. Furthermore, the results produced by the Samsung Nexus were more consistent.

An explanation for this consistency and improved set of results might be that the Samsung Nexus has capabilities to receive a broader range of signals. In addition, the superior computing power enables quicker calculations and can take into account some of the factors that cause error in the positioning analysis.

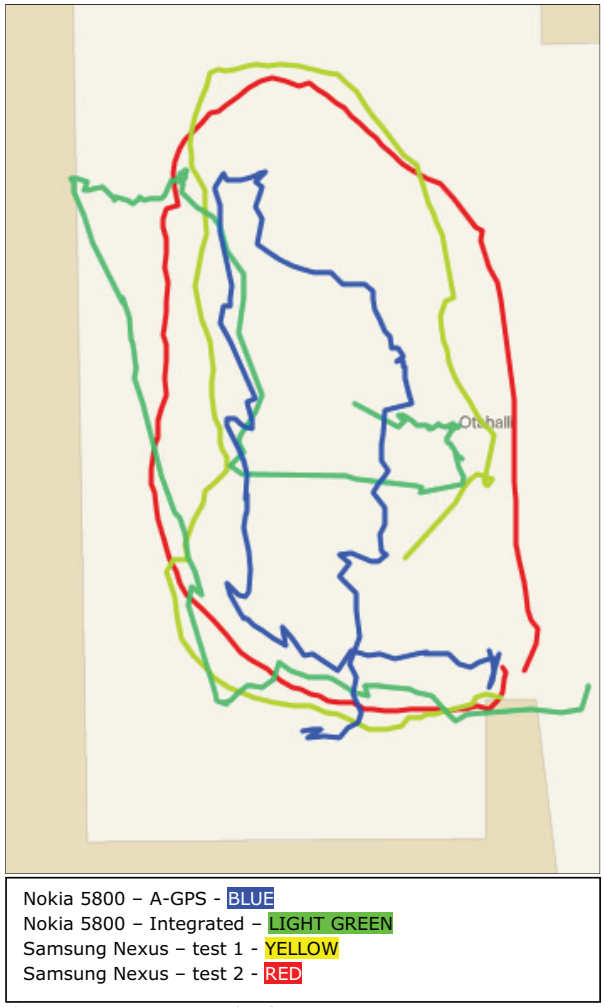

Figure 27. Comparison of Indoor testing routes.

5.5 Overall conclusions

Overall A-GPS was the most effective positioning technique. For modern purposes, this method together with Intergrated GPS produces a level of accuracy to within 10 metres. This is sufficient for navigation and meeting people for example. Applications can further improve the accuracy of GPS positioning. A car navigation application for example, knows that a car will be on a road and therefore it can restrict the positions identified to those which are on the road. This technique is known as a map-matching algorithm, where a position can be matched to a point on a map. In this way the impact of multipath distortion and other errors can be alleviated.

Network based proved to be fairly ineffective in this testing, although it does have potential for the future. Network based methods may prove to be more effective in indoor environments for example, and the network itself is improving with complexity and accuracy all the time. It may be that Network based methods are soon able to provide a level of accuracy and consistency to compete with modern existing handset based methods

Most of all it seems that now the environment could have an even bigger impact on the effectiveness of positioning techniques of modern smartphones. In this short testing round, we saw how multipath errors caused by high rise buildings can significantly affect the accuracy of the route recorded.

In addition, it is worth recalling how errors can affect the reporting of the length of a route travelled. A less accurate method might record a path which deviates from a straight line, elongating the true length of the path. On the other hand, the less accurate method could also round off corners, which would reduce the length of the true route travelled. Distance is therefore not a useful parameter with which to measure accuracy of a route. This is particularly significant when we consider that many governments are investigating means of road taxation based on the distance travelled along certain roads. With current technologies, there is potential for inaccuracies within such a system.

With regards to indoor testing, we can conclude that more modern smartphones can produce more accurate results. In addition, it seems that although indoor GPS is clearly a challenge, there is potential to produce results to an acceptable level of accuracy.

As the technology behind positioning develops the future will undoubtedly see more accurate positioning, regardless of environmental factors.

References

BAJAJ, R., RANAWEERA, S. L., & AGWARAL, D. P. (2002). GPS: Location Tracking Techology, IEEE Computer 35(4): 92-94. Available at: https://ece.uwaterloo.ca/~ndpbucha/MSCI442/GPS%20Location%20Tracking%20Technology.pdf.

BILL, R., CAP, C., KOFAHL, M., & MUNDT, T., (2004). Indoor and Outdoor Positioning in Mobile Environments – A Review and some Investigations on WLAN-Positioning. University of Rostock. Available at: http://www2.auf.uni-rostock.de/doc/publikationen/2004_GG_1508313137.pdf.

DEDES, G. & DEMPSTER, A. G. (2005). Indoor GPS Positioning – Challenges and Opportunities, IEEE 62nd Vehicular Technology Conference, 1: 412-415. Available at: http://www.gmat.unsw.edu.au/snap/publications/dedes%26dempster_2005.pdf.

VAN DIGGELEN, F. & ABRAHAM, C., (2001). Indoor GPS technology presented at CTIA Wireless Agenda, Dallas, pp. 1-10. Available at: http://www.ed-china.com/ARTICLES/2006JUN/5/2006JUN30_IC_RFD_TS_11.PDF.

HUBER, D. (2010). Background Positioning for Mobile Devices – Android vs. iPhone, School of Electrical and Computer Engineering, Technical University Berlin. Available at: http://www.snet.tu-berlin.de/fileadmin/fg220/courses/WS1011/snet-project/background-positioning_huber.pdf.

MALLICK, M. (2003). Mobile and Wireless Design Essentials, Indiana: Wiley Publishing. Available at: http://etutorials.org/Mobile+devices/mobile+wireless+design/Mobile+and+Wireless+Design+Essentials/.

RAY, M. (2008). Cell-based positioning for improving LBS, Coordinates, IV(5). Available at: http://mycoordinates.org/cell-based-positioning-for-improving-lbs/

SIGRIST, P., COPPIN P., & HERMY, M. (1999). Impact of forest canopy on quality and accuracy of GPS measurement, International Journal or Remote Sensing, 20(18): 3595-3610.

ZEIMPEKIS, V., (2003). A Taxonomy of Indoor and Outdoor Positioning Techniques for Mobile Location Services, ACM SIGecom Exchanges 3(4): 19-27. Available at: http://eden.dei.uc.pt/~jjlp/ubicomp/papers/p19-zeimpekis.pdf

Hybrid Positioning with a Smartphone

Tuomas Keränen

Aalto University School of Engineering
Department of Real Estate, Planning and Geoinformatics
tuomas.keranen@aalto.fi

Abstract

This paper explains general ideas used in ubiquitous positioning with smartphones. The purpose is to provide smooth and seamless positioning solution across indoor and outdoor environments. This is usually achieved through a hybrid positioning scheme that integrates multiple positioning technologies. Additionally, this paper presents various field tests that were carried out. The accuracy and reliability of digital compass and accelerometer in smartphones were analysed in more depth using Matlab.

1. Introduction

Nowadays, there is a notable growth of capabilities in handheld devices. Various technologies are applied into smartphones, such as GPS, WLAN, Bluetooth, accelerometer, digital compass, camera, gyroscope, etc. Positioning capability is becoming one of the standard features in smartphones, thus more people are getting used to the location-enabled life.

Employing the Global Navigation Satellite System (GNSS), the applications in the devices greatly enrich the end users' outdoor activities. However, given the nature of GNSS, it is clearly not suited for applications in urban canyons and especially indoors. Satellite based technologies continue to struggle indoors due to well known issues such as the weak signal or non-line-of-sight conditions between the mobile user and satellites. Smartphones contain the potential for indoor navigation and positioning utilizing the mentioned technologies already available in the devices. (PEI et al., 2011)

2. Methodology

2.1 Hidden Markov Model (HMM)

In general, hybrid positioning solutions are nowadays based on Hidden Markov Models. HMM is considered the most effective among all methods as it provides a probabilistic framework. With this framework, it is easy to integrate multiple types of observations to implement a hybrid positioning solution. (JINGBIN LIU, 2012)

In probability theory, a stochastic process is called a Markov process if it assumes Markov property. The Markov property suggests that the conditional probability distribution of future states only depends upon the present state. In other words, given the present, the future does not depend on the past. In a discrete-time finite state space, a Markov process is represented with a Markov chain, as the discrete-time states transit from one to another in a chain-like manner. (JINGBIN LIU, 2012)

An observable Markov model requires that all states themselves can be directly observed. However, this requirement is too restrictive for many problems of interest as in hybrid positioning. Therefore, the concept of Markov models is extended to the case of hidden Markov models. In HMM,

hidden states are not directly observable, but they can be observed in a Bayesian sense through an observation sequence. The observations are a probabilistic function of hidden states. (JINGBIN LIU, 2012)

2.2 Pedestrian Dead Reckoning

Dead Reckoning (DR) is a long-standing method of navigation. It is based on a position determined previously, DR is used to estimate the current position of a particular object in an iterative process by projecting its course and speed over elapsed time. However, this approach is limited by accuracy for smartphone pedestrian positioning. (CHEN et al., 2011, II)

Therefore Pedestrian Dead Reckoning (PDR) technologies are introduced. These technologies are mathematically based on the traditional DR, but movement distance is not calculated by integration of acceleration. Instead, the technologies make use of human physiologic characteristics of a pedestrian to propagate a user's position. The procedures of PDR positioning typically include step detection, step length estimation, and heading updates. (CHEN et al., 2011, II)

2.3 Positioning with WLAN

WLAN provides wireless communication over short distances using radio signals. A WLAN is installed in an area where a wireless Internet access is needed, for example in airports, hotels, shopping centers and offices. WLANs are built by attaching devices called Access Points (APs). WLAN signals are becoming an important positioning data source. (JINGBIN LIU, 2012)

In this approach, the positioning is usually based on a technique called fingerprinting. Prior to positioning using WLAN, a fingerprint database needs to be created. The positioning area is divided into Reference Points (RPs). Signal strengths from APs are measured in every reference point. After collecting RSSI (Received Signal Strength Indication) data on each RP, a fingerprint database is created. The accuracy of this method depends on how closely the RPs are situated from each other. (CHEN et al., 2011, I)

2.4 Experimental set-up

To study the accuracy and the reliability of different sensors in smartphones, various field tests were carried out. These test were WLAN radio map generation test, pedestrian step detection test, static accuracy of

a GPS performance of smartphones test, digital compass test and static accelerometer test. Furthermore, the results from digital compass test and static accelerometer test were analyzed with Matlab.

3. Field tests

3.1 WLAN radio map generation

The aim was to create a fingerprint database for inside the Finnish Geodetic Institute building using Nokia 6710 devices. First, a reference point network (about 3 by 3 meters) was created by taping small pieces of papers with identifiable numbers on the floor. Next, the signal strength levels were measured by standing with the smartphone above every reference point, in two different positions, for two minutes in total. Always making 180 degree turns after the first minute. (CHEN et al., 2011, I)

3.2 Pedestrian step detection test

This test was conducted by walking between reference points with a smartphone in hand (Nokia N8), and calculating the actual number of steps taken during the walking, for reference. In this case, the phone's accelerometer was used to detect periodic acceleration patterns to count the number of steps afterwards. The N8 consistently failed to detect about 5% of the steps regardless of the person testing. (JINGBIN LIU, 2012)

3.3 Testing the static accuracy of a GPS performance of smartphones

This test was carried out on the roof of the Finnish Geodetic Institute building. The testing was done with Nokia N8 and Samsung Galaxy S smartphones. A GPS device called u-blox was used as reference (the device connected to the laptop in Picture 1). The test lasted for about one hour.

3.4 Digital compass test

The accuracy and reliability of the digital compasses inside smartphones (Nokia N8 and Nokia 6710) were tested in two different scenarios, with a wooden trolley and in general handheld pedestrian scenarios. All the tests

were done inside the Finnish Geodetic Institute building on the corridors of the third floor (Picture 2). The handheld tests were repeated two times.

Picture 1. GPS testing on the roof of the FGI building.

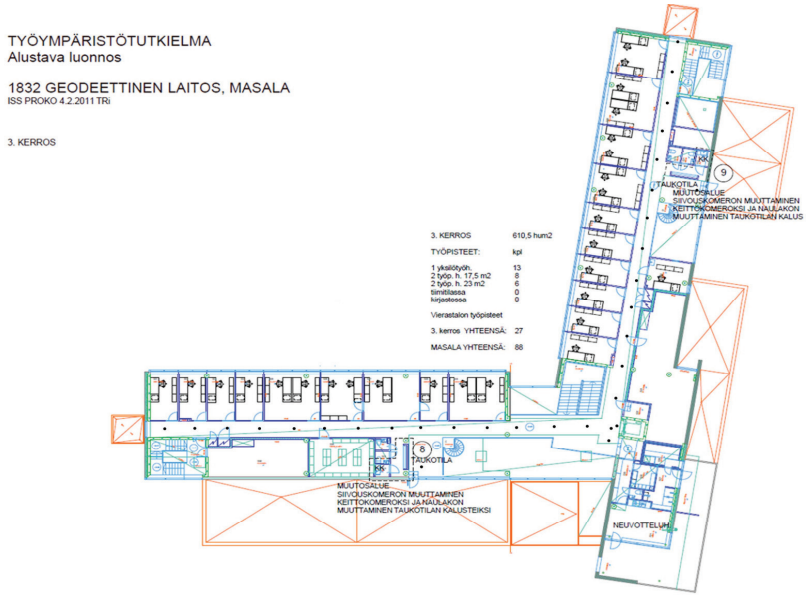

Picture 2. Layout of the 3rd floor of the FGI building.

The testing was done with a help of three RPs marked by tape on the floor (Picture 3, under the wooden trolley). The device was carried handheld (or

pushed with the trolley) between the reference points in a straight line (maintaining the heading as precisely as possible). The smartphones were held stationary on each reference point for about one minute before continuing to the next RP. A time-log (Appendix A) was created from every test to identify two different stages (stationary and moving).

The smartphones collect the heading data about 10 times a second. Thus, there were about 5000 – 7000 measured headings from every individual test.

Picture 3. Testing with a wooden trolley.

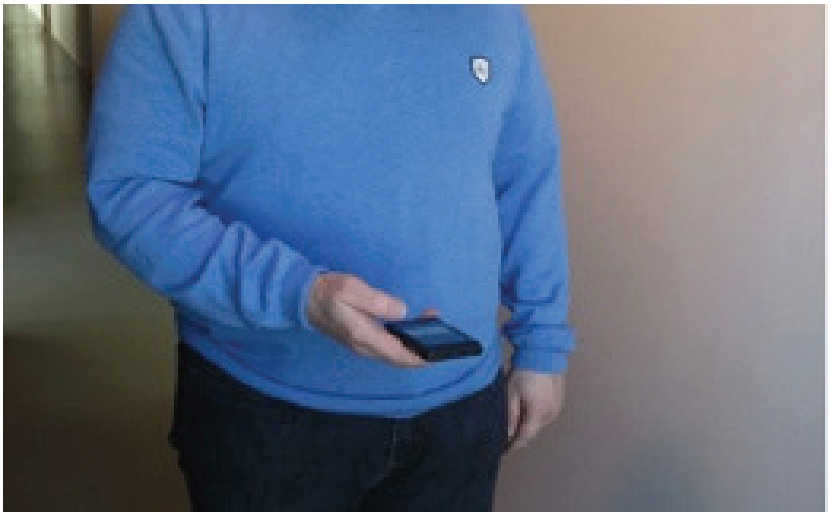

Picture 4. Handheld testing.

3.5 Static accelerometer test

The accuracy of the accelerometer in Nokia N8 smartphone was also tested is static circumstances. The device was left on a table untouched for about one and half hours.

4. Analysis and results

4.1 Digital compass test

The data was analyzed using Matlab (example of the code can be found on Appendix B). Furthermore, an Excel table was also created. The RPs coordinates were known in WGS84 system. By transforming the coordinates in to a local coordinate system, a reference heading (with respect to true north) was calculated. Magnetic north was obtained by correcting the heading by +7.7 degrees.

The results were plotted with Matlab (Figure 1) with regards to the reference heading. Stationary and moving sections were identified by different line styles.

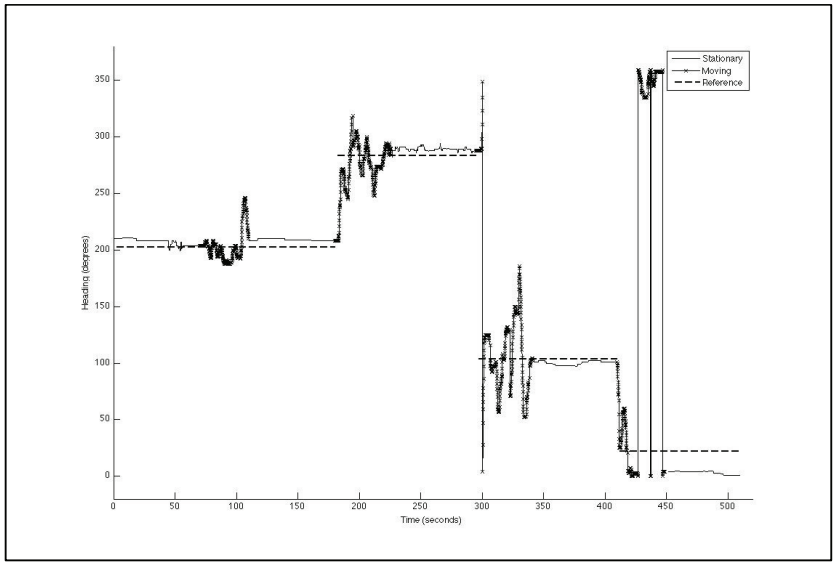

Figure 1. Digital Compass test graph.

Some statistical numbers were also calculated and put to an Excel table (Table 1). Moving and stationary errors were calculated separately.

Table 1. Digital compass test (degrees).

	Stationary RMSE	Moving RMSE	Avg error stationary	Avg error moving	MAX stationary error	MAX moving error
Tuomas N8	9.4962	27.2545	-0.3273	-5.723	21.177	174.295
Jingbin N8	12.2437	26.5938	-6.0169	-5.0587	35.823	165.705
Woodcar N8	15.7	25.7396	6.0091	1.635	74.823	169.295
Woodcar 6710	31.7457	23.2501	8.5254	-3.1447	75.705	98.295

4.2 Static accelerometer test

The results were analyzed using Matlab (example of the code can be found on Appendix C). Furthermore, an Excel table (Table 2) was also created. The purpose was to find how much "drifting" had happened during the testing. (JINGBIN LIU, 2012).

Table 2. Static accelerometer test N8 (m/s2).

	Avg acc. (x-axis)	Avg acc. (y-axis)	Avg acc. (z-axis)	RMS (x-axis)	RMS (y-axis)	RMS (z-axis)
N8 (2s gravity)	0.0124	-0.0821	-0.0602	0.0544	0.1159	0.1037
N8 (all gravity)	-7.1136E-13	-1.06E-13	6.5499E-12	0.0529	0.0818	0.0845

The Nokia N8 has a three-axis (three dimensional) accelerometer and the measurement data is in SI-system (m/s^2) (http://doc.qt.nokia.com/qtmobility/sensors-api.html, 2012). First, the gravity has to be removed from the measurements. This can be done by calculating the average value from the measurements with respect to every axis and subtracting the corresponding value from the axis measurement. Gravity was first removed by using 2 seconds of measurements from the beginning to calculate the average value. Second method was to use all the measurements to remove the gravity. Figures 2 and 3 were generated by the latter method.

Next, the cumulative velocity (equivalent to integration) was calculated (Figure 2) by multiplying the accelerometer data with the corresponding time intervals. From this data the cumulative distance (equivalent to double integration) was calculated by multiplying the velocity data with the corresponding time intervals (Figure 3).

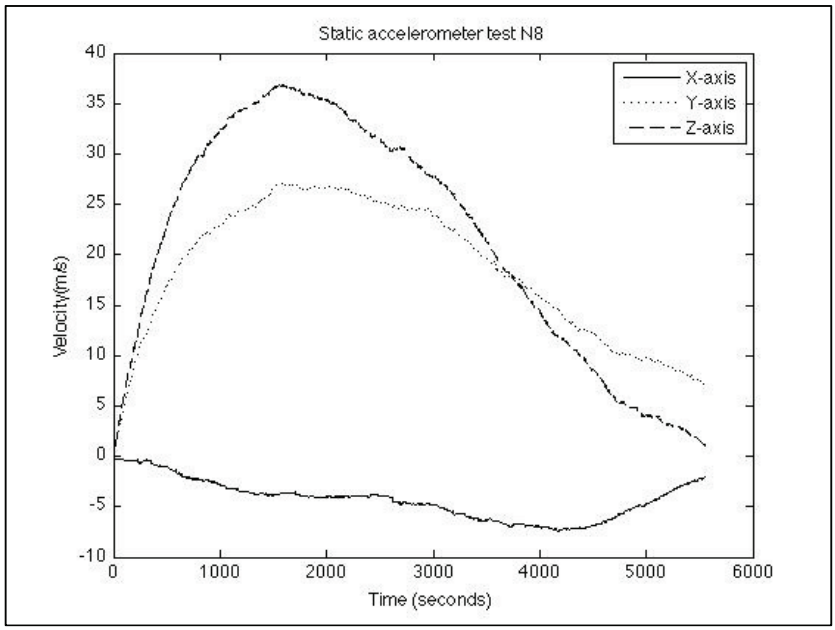

Figure 2. Static accelerometer test N8 (velocity).

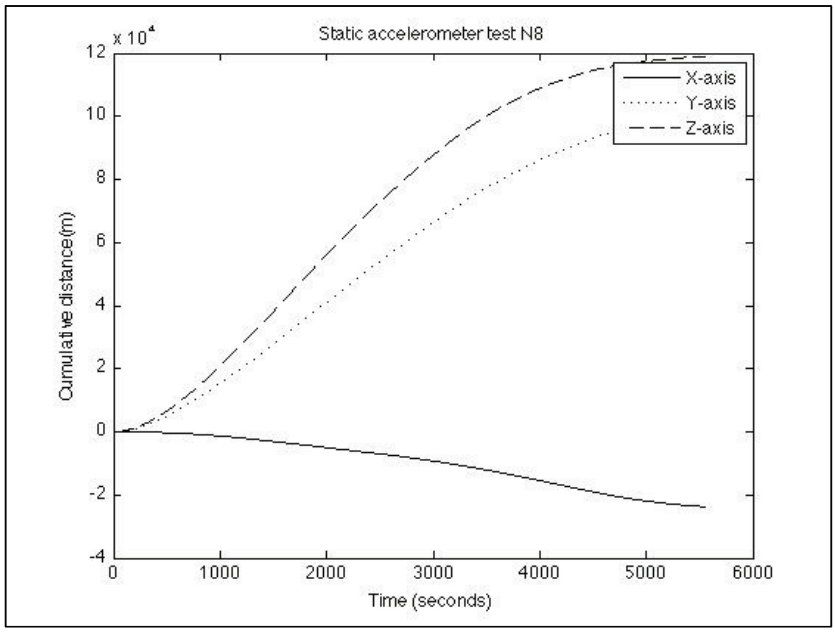

Figure 3. Static accelerometer test N8 (distance).

5. Conclusions

5.1 Digital compass test

The conclusions are that when the smartphone is held stationary, the accuracy is surprisingly good. However, when the device is moving and especially during turns the errors were quite big (tens of degrees). For positioning purposes, the digital compass is useful for correcting the absolute heading (drifting) from time to time, but not continuously. Thus integration with other position techniques requires careful implementation. Otherwise the errors can be too big for the purpose.

Heading accuracy with the wooden trolley is very similar to the handheld tests. The additional stability does not have any advantages. The handheld results were a bit different between different testers, as expected.

Another interesting result is that there was negligible interference from large metallic objects to the digital compass. One of the reference points was situated right next to an elevator on purpose (circa 150 seconds on the Figure 1). No effects on accuracy were found.

5.2 Static accelerometer test

As said, Figures 2 and 3 were generated with removing the gravity by using all the measurements. With 2 seconds gravity removal the results were even worse.

Based on this test, the accuracy of the Nokia N8 accelerometer is very poor and sensor must be of low quality. Obviously, the accelerometer is not designed to be used in positioning applications. However, for short periods of time accelerometer data can be useful.

Acknowledgements. *This work was part of the project iSpace (Indoor/outdoor Seamless Positioning and Application for City Ecosystems) in Finnish Geodetic Institute, Department of Navigation and Positioning.*

6. References

LING PEI, RUIZHI CHEN, JINGBIN LIU, HEIDI KUUSNIEMI, YUWEI CHEN, TOMI TENHUNEN (2011). Using Motion-Awareness for the 3D Indoor Personal Navigation on a Smartphone. In 24th International Technical Meeting of the Satellite Division of the Institute of Navigation, Portland OR, September 19-23, 2011.

JINGBIN LIU (2012). Hybrid Positioning with Smartphones.

RUIZHI CHEN, LING PEI AND JINGBIN LIU, HELENA LEPPÄKOSKI (2011). WLAN and Bluetooth Positioning in Smart Phones.

RUIZHI CHEN, LING PEI, YUWEI CHEN (2011). A Smart Phone Based PDR Solution for Indoor Navigation. . In 24th International Technical Meeting of the Satellite Division of the Institute of Navigation, Portland OR, September 19-23, 2011.

http://doc.qt.nokia.com/qtmobility/sensors-api.html 27.4.2012

APPENDIX A: Example of a test log in digital compass testing

With the wooden trolley

08:44:30 start static on RP1
08:46:40 start walking
08:48:20 stay on RP15
08:51:40 turning and walking
08:52:30 stay on RP30
08:54:45 turning
08:55:00 walking
08:55:55 stay on RP15
08:57:00 turning
08:57:08 walking
08:58:03 stay on RP1
08:59:30 end

Tester Jingbin with N8

09:39:30 start static on RP1
09:40:30 start walking
09:41:02 stay on RP15
09:42:02 turning and walking
09:42:42 stay on RP30
09:43:42 turning and walking
09:44:20 stay on RP15
09:45:25 turning and walking
09:46:10 stay on RP1
09:47:10 end

Tester Tuomas with N8

09:29:30 start static on RP1
09:30:40 start walking
09:31:20 stay on RP15
09:32:30 turning and walking
09:33:16 stay on RP30
09:34:25 turning and walking
09:35:11 stay on RP15
09:36:20 turning and walking
09:36:59 stay on RP1
09:38:00 end

APPENDIX B: Example of a Matlab code for analyzing digital compass tests

```
function N8compassT()
datafile = 'HandheldN8Tuomas.txt'
data = load(datafile);


transData = zeros(length(data(:,5)), 2);
transData(1,1) = 0;
transData(1,2) = data(1,5);
for i= 2:length(data(:,5))
    transData(i,1)                                                                    =
GetInterval(data(1,1),data(1,2),data(1,3)+data(1,4)/1000,data(i,1),data(i,2),data(i
,3)+data(i,4)/1000);
    transData(i,2) = data(i,5);
end


f1t15(1:1536) = 202.177;
f15t30(1:2528-1536) = 283.295;
f30t15(1:3529-2528) = 103.295;
f15t1(1:4400-3529) = 22.177;


% tuomasS1 = tuomas(1:602);
% tuomasW1t15 = tuomas(1:950);
% tuomasS15 = tuomas(1:1536);
% tuomasW15t30 = tuomas(1:1939);
% tuomasS30 = tuomas(1:2529);
% tuomasW30t15 = tuomas(1:2930);
% tuomasS152 = tuomas(1:3529);
% tuomasW15t1 = tuomas(1:3869);
% tuomasS12= tuomas(1:4400);


set(0,'DefaultAxesColorOrder',[0 0 0]);


hold on;
plot(transData(1:602,1),transData(1:602,2),'-','LineWidth',1.5);


hold on;
plot(transData(603:950,1),transData(603:950,2),'-x');


hold on;
plot (transData(1:1536,1),f1t15,'--','LineWidth',2);


hold on;
plot(transData(951:1536,1),transData(951:1536,2),'-','LineWidth',1.5);
```

```
hold on;
plot(transData(1537:1939,1),transData(1537:1939,2),'-x');

hold on;
plot(transData(1940:2529,1),transData(1940:2529,2),'-','LineWidth',1.5);

hold on;
plot(transData(2530:2930,1),transData(2530:2930,2),'-x');

hold on;
plot(transData(2931:3529,1),transData(2931:3529,2),'-','LineWidth',1.5);

hold on;
plot(transData(3530:3869,1),transData(3530:3869,2),'-x');

hold on;
plot(transData(3890:4400,1),transData(3890:4400,2),'-','LineWidth',1.5);




hold on;
plot (transData(1537:2528,1),f15t30,'--','LineWidth',2);
hold on;
plot (transData(2529:3529,1),f30t15,'--','LineWidth',2);
hold on;
plot (transData(3530:4400,1),f15t1,'--','LineWidth',2);


axis([0 520 -20 380]);
%title('Pedestrian Digital Compass test (Tuomas N8)');
xlabel('Time (seconds)');
ylabel('Heading (degrees)');
legend('Stationary','Moving','Reference');

t = load(datafile);
tuomas = t(:,5);

% Stationary errors
tuomas3869t4400error = tuomas(3869:4400)-22.177;
tuomas2930t3529error = tuomas(2930:3529)-103.295;
tuomas1939t2529error = tuomas(1939:2571)-283.295;
tuomas951t1536error = tuomas(951:1567)-202.177;
tuomas1t602error = tuomas(1:602)-202.177;
stationaryerrors                                                    =
vertcat(tuomas3869t4400error,tuomas2930t3529error,tuomas1939t2529error,tuomas951t15
36error,tuomas1t602error);
```

```
stationaryRMS = sqrt(mean(stationaryerrors.^2))
lenghthSE = length(stationaryerrors)


% Moving errors
%tuomas15t1error = tuomas(3529:3869)-22.177;
%tuomas30t15error = tuomas(2529:2930)-103.295;
%tuomas15t30error = tuomas(1537:1939)-283.295;
%tuomas1t15error = tuomas(603:950)-202.177;

tuomas15t1error = tuomas(3529:3869)-22.177;
tuomas30t15error = tuomas(2572:2930)-103.295;
tuomas15t30error = tuomas(1568:1939)-283.295;
tuomas1t15error = tuomas(603:950)-202.177;

movingerrors                                                                    =
vertcat(tuomas15t1error,tuomas30t15error,tuomas15t30error,tuomas1t15error);

for i = 1:length(movingerrors)
    if movingerrors(i) > 180
        movingerrorsC(i) = movingerrors(i) - 360;
    else
        movingerrorsC(i) = movingerrors(i);
    end
end
movingerrorsC = movingerrorsC';
movingRMS = sqrt(mean(movingerrorsC.^2))
lenghthME = length(movingerrorsC)

averagestationaryerror = mean(stationaryerrors)
averagemovingerror = mean(movingerrorsC)

maxstationaryerror = max(abs(stationaryerrors))
absmovingerror = abs(movingerrorsC);

sabsme = sort(absmovingerror);
maxmovingerror = max(sabsme)

return;

function [dSec] = GetInterval(hour1, min1, sec1, hour2, min2,sec2)
    dSec = (hour2-hour1)*3600+(min2-min1)*60+sec2-sec1;
return;
```

APPENDIX C: Example of a Matlab code for analyzing the accelerometer accuracy

```
function staticaccN8gravall()
datafile = 'saN8.txt';
data = load(datafile);


close all;


transData = zeros(length(data(:,5)), 2);
transData(1,1) = 0;
transData(1,2) = data(1,5);
for i= 2:length(data(:,5))
    transData(i,1)                                                                    =
GetInterval(data(1,1),data(1,2),data(1,3)+data(1,4)/1000,data(i,1),data(i,2),data(i
,3)+data(i,4)/1000);
    transData(i,2) = data(i,5);
    transData(i,3) = data(i,6);
    transData(i,4) = data(i,7);
end


% Removing gravity
xg = mean(transData(:,2));

yg = mean(transData(:,3));
zg = mean(transData(:,4));


xc = transData(:,2) - xg;
yc = transData(:,3) - yg;
zc = transData(:,4) - zg;


% Average acceleration
xaverage = mean(xc)
yaverage = mean(yc)
zaverage = mean(zc)


% RMS of acceleration
xRMS = sqrt(mean(xc.^2))
yRMS = sqrt(mean(yc.^2))
zRMS = sqrt(mean(zc.^2))



% Time intervals
timeda = zeros(length(transData(:,1)),1);
for j = 2 : length(transData(:,1))
    timeda(j) = transData(j,1) - transData(j-1,1);
end
```

```
timed = timeda;

% Velocities for every axis
velocityx = zeros(length(transData(:,1)),1);
for k = 2 : length(transData(:,1))
    velocityx(k) = timed(k)*xc(k);
end
cumulativeVx = cumsum(velocityx);

velocityy = zeros(length(transData(:,1)),1);
for k = 2 : length(transData(:,1))
    velocityy(k) = timed(k)*yc(k);
end
cumulativeVy = cumsum(velocityy);



velocityz = zeros(length(transData(:,1)),1);
for k = 2 : length(transData(:,1))
    velocityz(k) = timed(k)*zc(k);
end
cumulativeVz = cumsum(velocityz);

set(0,'DefaultAxesColorOrder',[0 0 0]);

% Plotting velocity vs time
figure(1);
plot(transData(:,1),cumulativeVx,'-','LineWidth',1.4);
hold on;
plot(transData(:,1),cumulativeVy,':','LineWidth',1.4);
hold on;
plot(transData(:,1),cumulativeVz,'--','LineWidth',1.4);

title('Static accelerometer test N8');
xlabel('Time (seconds)');
ylabel('Velocity(m/s)');
legend('X-axis','Y-axis','Z-axis');

% Distance in each interval
xs = timed.*cumulativeVx;
ys = timed.*cumulativeVy;
zs = timed.*cumulativeVz;

% Cumulative distance
xtotaldistance = cumsum(xs);
ytotaldistance = cumsum(ys);
ztotaldistance = cumsum(zs);
```

```
% Plotting the cumulative distance

figure(2);

plot(transData(:,1),xtotaldistance,'-','LineWidth',1.4);

hold on;

plot(transData(:,1),ytotaldistance,':','LineWidth',1.4);

hold on;

plot(transData(:,1),ztotaldistance,'--','LineWidth',1.4);



title('Static accelerometer test N8');

xlabel('Time (seconds)');

ylabel('Cumulative distance(m)');

legend('X-axis','Y-axis','Z-axis');




return;



function [dSec] = GetInterval(hour1, min1, sec1, hour2, min2,sec2)

    dSec = (hour2-hour1)*3600+(min2-min1)*60+sec2-sec1;

return;
```

Dexter Industries GPS sensor for Lego Mindstorms NXT

Henri Turto and Niko Kareinen

Department of Real Estate, Planning and Geoinformatics
Vaisalantie 8, FI-00076, AALTO
henri.turto@aalto.fi
niko.kareinen@aalto.fi

Abstract

Lego Mindstorms NXT 2.0 is not a toy but an education tool as well. Many teachers around the word uses NXT to teach students various subjects such as robotics. The standard package comes with touch, sound, light and utrasonic sensors. Although these sensors may provide certain navigation capabilities, third-party sensors have been developed by various manufacturers to enhance the navigation capabilities. In this project, we researched the navigation and positioning properties of the NXT standard package in combination with the GPS sensor provided by Dexter Industries. Three different tests were carried out: static, navigation, and tracking tests. The static tests demonstrated accuracies within the values reported by the manufacturer. On the other hand, the accuracy was barely good enough for the practical navigation. Furthermore, the vehicle tracking test showed that the route could be tracked with good accuracy while the velocity outputs were relatively stable.

1 Introduction

This is a report about Lego Mindstorms Robotic Invention System NXT 2.0 project that was done for Aalto University School of Engineering Department of Real Estate, Planning and Geoinformatics course Maa-6.3255 Seminar on Geodesy, Navigation and Positioning. In this project, we have researched navigation and positioning possibilities of Lego Mindstorms Robotic Invention System NXT 2.0 (for now on Lego NXT 2.0) with Dexter Industries DGPS sensor and HiTechnic NXT Compass Sensor. The Lego NXT 2.0 has other sensor that could be used for navigation but we chose these two to delimit the project. The Lego NXT 2.0 is a toy and an educational tool. With it, you can build your own robots from Lego blocks. The heart of the Lego NXT 2.0 package is the intelligent NXT brick that has a microprocessor. To the NXT brick, one can upload programs to control the robot. The Lego NXT 2.0 package comes with NXT-G 2.0 programming tool that has a visual block diagrams that are easy to use. In Verkkokauppa.com shop the age recommendation for the LegoNXT 2.0 is 10+ years and in November 2012 the price is set to 264,90 EUR a package.

For the research, three different tests were concluded. First test was done with the $GPSstat$ data logging program to log measurements while the robot was kept static on a known point referred as GNSS3 located in Espoo's Otaniemi near Falcon Gentti building. The purpose of this test was to evaluate the accuracy and the precision of the Dexter Industries DGPS sensor. The manufacturer informed accuracy should be three meters in horizontal plane and more than ten meters in the vertical plane [4].

The second test done was navigation test made with the $GPSNav$ program to navigate the robot to coordinates that were uploaded to the robot. GPSNav calculates the robot position from the GPS satellite signals that the Dexter Industries DGPS sensor receives and from that solution it calculates the heading and distance to the uploaded goal coordinates. The HiTechnic NXT Compass Sensor measures the Earth's magnetic field and from it the sensor can calculate its direction. The $GPSNav$ also logs the coordinate solutions along the way and calculates new heading from them to get better navigation result. The navigation test was done on a tennis court in Otaniemi, Espoo.

The third test was vehicle tracking and velocity test. This test was done with $GPSstat\_vel$ program that logs the location of the robot as well as its

velocity. This test was done to see how accurately the Dexter Industries DGPS sensor can measure velocity and locate its position in a larger scale of road. This test was done along a highway in Espoo.

Expectations for the setup were low because of the price of the robot as well as it is a Lego toy. In the Dexter Industries DGPS sensor manufacturers webpage, there are video files of navigation tests that were concluded in a big parking lot. In these files the robot reached its goal.

In our test results, it is shown that the accuracy of the Dexter Industries DGPS sensor that the manufacturer informs is possible to reach in static measurements and a 10 minute interval but in the navigation test the calculated positions were inaccurate for several meters. The vehicle tracking test showed that the route could be tracked with surprisingly good accuracy. The velocity output was relatively stable.

2 Lego Mindstorms NXT 2.0 robotics kit

With Lego Mindstorms Robotic Invention System NXT 2.0 package, you can build your own programmable robot. Lego Mindstorms is a product of the Lego Group and was developed with MIT Media Lab (research lab part of Massachusetts Institute of Technology). The first Lego robot product of this line was introduced in 1998 and it was called Lego Mindstorm RCX. The next version introduced in 2006 was called Lego Mindstorms NXT. The product we are using is the latest model Lego Mindstorms NXT 2.0 and it was introduced in fall 2009. The product with its predecessors is used by thousands of teachers around the world to teach robotics (Carnegie Mellon Robotics Academy). For now on, we use a shortened name Lego NXT 2.0 for Lego Mindstorms Robotic Invention System NXT 2.0, which is enough to differ it from the previous generations of Lego robot products.

Lego NXT 2.0 package comes with the NXT intelligent brick, servo motors, and various sensors. The contents and descriptions of the retail NXT package are listed in Table 1 [7].

3 Lego NXT 2.0 third-party sensors

There are several companies that manufacture sensors for Lego Mindstorms. In the project, two third party sensor were used in the navigation

Table 1. Original Lego NXT 2.0 package

Product (quantity)	**Detailed description**
The NXT Brick (1)	Two processors: first one is 32-bit, 48 MHz Atmel AT91SAM7S256 ARM, with 64 kB RAM + 256 kB Flash-memory. The second processor is 8-bit, 8 MHz Atmel ATmega48 AVR-processor, with 512 B RAM + 4 kB Flash-memory LCD display with resolution of 100x64 pixels Loud speaker for 8-bit sound Four buttons 3 output ports for servo motors 4 Input ports 1 USB 2.0 port Bluetooth support (Bluetooth chip sold separately) For power supply it takes 6 AA batteries 1,5 V or a rechargeable battery
Servo motors (3)	Motor with a two way angle recognition, the angles can be read from the motor or to give commands to reach the preferred angle approximately in 1 degree precision Adjustable speed and direction of rotation Built-in tachometer Overheating protection
Touch sensor (2)	Touch sensor is a button that gives you basic true/false feedback
Ultrasonic sensor (1)	Ultrasonic sensor can measure distance and locate objects. It can measure distance in centimetres from 0-254. It can also be used to detect motion. Sensor generates sound waves and it detects the echoes it receives back and then calculates the distance from the time interval of sending/receiving the signal.
Colour sensor (1)	Colour sensor detects light and different colors. It has a red led light as a lamp. To work properly the sensor needs a light from the environment. To detect colours the differences in contrasts need to be quite big for it to work properly.

tests the Dexter industries DGPS sensor and HiTechnic digital compass sensor. The DGPS sensor alone was also used in the static measurement test. The two used third party sensors are introduced in a Table 2. The sensors that are made especially for Lego Mindstorms have in common that they connect directly in to the Lego NXT ports. Most third party products are sensors, they measure something, but some products add

Table 2. DexterIndustries dGPS and HiTechnic compass sensor specifications.

Sensor/ Manufacturer	**Description**
Dexter industries DGPS Sensor	The sensor can be used to log positional data or to navigate to a point. Information that can be read from the sensor: Positional data: Time (UTC), latitude, longitude, velocity (cm/s), heading (degrees) Navigational data: Distance and angle to destination from the start and along the way from the last call. Reported horizontal accuracy of 3 m. Reported vertical accuracy of 10 m or less. The output data is in integers. Sensor has a GPS chip manufactured by Sky Traq chipset
HiTechnic Compass Sensor	The Compass sensor measures Earth's magnetic field digitally and outputs heading in one degree accuracy. The magnetic heading is calculated to and the sensor outputs an integer between 0-359. The heading is updated 100 times in one second. The Sensor can be calibrated in addition, so that near by external magnetic fields such as the robot batteries and servos can be compensated out from the heading results.

different features to the NXT series. Besides sensors, the wireless connections are common features in third party products. Available wireless connection methods are at least WiFi and a few different radio frequencies as well as the Lego supported product Bluetooth Dongle. Also if for projects that need more input ports, there are several different products that can do that. HiTechnic has two different products for such use that they call multiplexers. HiTechnic Sensor Multiplexer for example allows you to connect four sensors for only using one port. The HiTechnics multiplexer may not work with all the third party sensors as in the manufacturers webpage it is stated what sensors it does support and it lists only Legos own and the HiTechnics own sensors. For controlling the NXT brick there several products that connect Lego Mindstorms with the game console pads. One of these products is the Dexter industries manufactured the NXTChuck, which connects the Nintendo Wii's Nunchuck controller to NXT brick. The Nunchuck control pad has accelerometer, joystick and two buttons. There is also a product that can directly connect to the wireless Microsoft Xbox pad. [1, 2, 3]

4 NXT in teaching

Lego Mindstorms Robotic Invention System NXT 2.0 was designed with learning in mind. The product with its predecessors is used by thousands of teachers around the world to teach robotics [5]. The Lego Mindstorms is quite open system and in that way full of possibilities for further projects.

The NXT-G programming platform is very easy to use. Its visual programming language is quite easy to manipulate even if the person does not have programming skills. For more complicated programs, there are third party programming platforms that are more suitable for people with programming experience. The software developer kit (SDK) allows you to create even your own programming environments. The third party sensors make possible to use the robot in various projects in different fields. For navigation teaching, there is gyroscopes and different sensors for distance measuring available for projects that could use several sensor to get better navigation results. In addition, the possibility to make your own sensor might be interesting for engineering students. The open source hardware developer kit (HDK) gives possibilities to use better GPS receivers to navigate robots more accurately.

There are several robotics competitions that are based in using Lego NXT 2.0. Lego lists a few completions on their webpage [6]. These competitions are meant for people with young age. The youngest age limit is 6 to 9 years old and the oldest level being from 7 to 19 years old. From these competitions, the participants can win college scholarships.

5 NXT programming platforms

There are multiple options available to program and making programs for the Lego NXT Intelligent Brick. The most stripped-down option is to use the NXT Program option available in NXT menu. However, this is only adequate for extremely simple programs. The standard Lego NXT robotics kit comes bundled with NXT-G programming environment, which is based on the graphical programming environment LabVIEW by National Instruments. Additionally, National Instruments has released its own toolkit for the NXT. NI LabVIEW for Lego Mindstorms allows more advanced graphical programming for the NXT.

In 2006, with the launching of the first Lego Mindstorms NXT robotics

kit, Lego released the firmware for the NXT Intelligent Brick as open source for the first time. In addition to the firmware source code developer kits for software, hardware, and bluetooth were also released.

SDK includes driver interface specifications and tools, which can be used to create third-party programming environments. HDK includes schematics for the NXT 6-wire digital connector system. The bluetooth developer kit (BDK) enables developers to use the NXT block bluetooth protocol. BDK makes it possible to program the NXT block to communicate with any bluetooth device.

The decision to make Lego Mindstorms an open source system has had great benefits. Developers have utilized the SDK to create a wide variety of third-party programming environments based on high level programming languages. The HDK has made it possible to develop third-party sensors, which are able to interact with the NXT Intelligent Brick. This has created a small industry within the Lego NXT community, which produces components designed specifically for the NXT. With the BDK, the NXT Intelligent Brick can also interact with devices not specifically designed for the system. The bluetooth interface also makes it possible to transmit code directly to the NXT unit, enabling interactive control and real time code interpretation.

The following sections will discuss the bundled NXT-G and various available third-party environments. NXT-G language, used in the field testing of the project, is covered in more detail.

5.1 NXT-G 2.0

The NXT-G bundled with retail Lego Mindstorms NXT, both the original and 2.0 versions, is a visual programming language (VPL) for the NXT Intelligent Brick. The original NXT-G 1.0 and 2.0 versions are functionally very similar. Compared to version 1.0 the 2.0 includes new tools and features. Programs are created by constructing program elements in a visual environment, instead of specifying the elements in text form. The basic structure of programs created in VPL consists of elements and their relations, expressed as boxes and lines, arranged in flowcharts. NXT-G is based on NI LabVIEW 7.1. The high-level block diagrams implemented in NXT-G are based on lower-level LabVIEW block diagrams.

The basic elements in NXT-G are blocks and data wires. The blocks are connected to sequence beams. Blocks are read from left to right, which defines to execution order for the program. Data between blocks in a se-

quence beam is transferred using data wires. The direction of the data flow is the same as the execution order: data moves from left to right. Parallel threads are implemented as parallel sequence beams. Data in sequence beams can be stored in variables, which can be read from parallel sequence beams. This makes NXT-G very straightforward in creating programs which do e.g. data logging parallel to main program.

Standard blocks

NXT-G 2.0 comes with a number of standard blocks, which can be used to control and program the sensors and motors of the retail NXT Intelligent Brick. The blocks are as per default separated into six categories: common, action, sensor, flow, data, and advanced blocks.

For many purposes, one of the most essential tasks is to get the robot moving. The **common and action blocks** includes the blocks for controlling the servo motors either individually or by a move-block. A motor-block can be used to control a single connected servo motor by adjusting the direction, motor power, and cycle duration. The move-block can control all of the connected servo motors simultaneously. The choice to use either motor- or move-blocks depends on the nature of the task needed to perform. Motor block is more suited for simple explicit tasks. Because the movement is controlled explicitly by turning each motor, it is straightforward to use the motor block configuration with different sensors, which can e.g. control the input for the motors. However, for more complex movement instructions the motor approach requires a large number of individual motor-blocks. This uses a considerable amount of memory space, which is very limited in the NXT Intelligent Brick. Additionally, there are no built-in smart features in the motor-block: the cycle counters must be manually reset after each iteration. Furthermore, a small drift in one of the motors in e.g. two-motor setup can cause the direction to veer off course. The move-block is designed to be a more convenient alternative to motor-blocks. Because the block can control multiple motors at once, movement forwards or backwards can be executed by a single block. Furthermore, it can be used to steer the robot based on just one directional input. Unlike motor-block, move-block can reset cycle sensors automatically. The move-block can also correct automatically for motor drift. For example, in case the move-block is programmed to steer forward and it detects one of the motors drifting, it will automatically correct the steering. Since the movements can be programmed using less blocks, using move-

blocks also reduce the required memory space. This will in turn permit the creation of more complex programs.

The **flow-blocks** include basic selection of control mechanisms. Iteration and control flow statements can be programmed using the loop-block, which can be set to run either indefinitely or to terminate on a given condition. This enables easy programming of basic *for*- and *while*-loop structures. Flow-blocks also include wait and termination blocks. Selection statements can be programmed using a switch-block, i.e. a switch-case structure.

The **data-blocks** include various mathematical operations. Math-block can perform elementary arithmetic operations as well as absolute value and square root functions. Also included are blocks for relation-statements, range, and Boolean logic (AND, OR, NOT, XOR). The variables, random variables, and constants are also included in data-blocks. These blocks are used to store initial parameters and values computed during the execution. As mentioned earlier, variable-blocks can be used to transfer data between parallel sequences.

The **advanced-blocks** contain blocks for altering data types, string handling, file access, calibration, bluetooth connection, and motor reset functions. The data type, string handling, and file access blocks are especially important when logging the data with NXT. Since NXT-G does not support dynamic typing, in order to format the data, the number types must be converted to text prior string concatenation. File access block can read, write, close, and delete a file specified by a filename. A good approach to data logging with NXT is to close and delete any existing data log of the same filename before the main program. This will prevent the build up of the data in single file between different measurement sessions (unless this behaviour is wanted, naturally). With this approach, the data must be uploaded to a computer between each measurement session. However, the small memory space of NXT limits the size of the data logs substantially, thus preventing long data logging sessions in any case.

The sensors connected to the NXT Intelligent Brick are programmed by **sensors blocks**. The standard blocks include touch, sound, light, ultrasonic, rotation, NXT buttons, clock, bluetooth, and RGB color sensors. The NXT-G language supports most third party sensors. In this study two such third-party sensors were used: the Dexter Industries NXT GPS-sensor and HiTechnic NXT compass sensor. The bring the sensors into use in NXT-G, they have to be imported manually to the programming en-

vironment. The required blocks for both compass and GPS are available for download in the respective manufacturers websites. Once downloaded and extracted, the blocks can be imported using the built-in block import feature in NXT-G.

Third-party sensor blocks

HiTechnic NXT compass sensor block The compass block for HiTechnic NXT Compass Sensor, provided by HiTechnic, supports all compass features. The compass can output both absolute and relative heading. The absolute heading corresponds to the current magnetic heading, and is given in degrees, ranging from 0 to 359. The relative heading options compares the absolute heading to a set target and returns the difference. The target heading can be set either as a data input or manually in the block. Additionally, the block can be configured to check if the current heading is either inside or outside a given angle range and return a yes/no logical value. The compass block also includes a calibration function, which computes the compass deviation offsets. However, HiTechnic states that for normal operation the calibration is not usually required, if the compass sensor is placed 10-15 cm from the NXT Intelligent Brick and motors. [2]

Dexter Industries GPS sensor blocks To control the Dexter Industries GPS sensor three separate blocks, provided by Dexter Industries, were imported. The blocks included: GPSRead, GPSNavigation, and GPS-X -blocks. *The GPSRead block* is used to read positioning information from the GPS sensor. The block has six output types: time, latitude, longitude, heading, velocity, and signal data. Due to the limitations in NXT all output data is in integer format. The time output is UTC in *hhmmss*-format. Latitude and longitude output are represented in integer decimal degree format by 8- and 9-digit integers, respectively. Positive latitude and longitude correspond to northern and eastern hemispheres, negative values to southern and western hemispheres. Heading is output between 0 to 359 degrees, with north as the reference heading and values increasing clockwise. Velocity output is given as cm/s. Signal status returns 1 for valid and 0 zero for invalid GPS signal. *The GPSNavigation block* can be used to compute data in order to navigate to a target destination. The block takes the target latitude and longitude as input values. As with GPSRead, the format for the input values is integer decimal degree. Using the target coordinates the navigation block computes two output values: the distance to target in meters and the angle to the destination in de-

grees. The angle is between 0 and 359 degrees. *The GPS-X block* takes advantage of the latest extended firmware for the Dexter Industries GPS sensors as of June 2012. The block provides additional information which can be used to assess the quality of the measurements, namely HDOP value and the number of satellites in view. Additionally, the block can read the altitude data from the sensor. The altitude output is in meters. [4]

5.2 Third-party programming platforms

There are several different programming platforms for Lego Mindstorms. When choosing a third-party programming language be prepared that there might be bugs in the implementation. Also some may not support all the features for Lego NXT that are available in the original programming language. One that has been developed a lot is lejOS programming environment which allows you to code JAVA. The lejOS is an open source code and stated as easy to use. For using the leJOS, the NTbrick needs a new firmware. Downloading the new firmware to the NXTbrick ends the guarantee of the product. LejOS offers most possibilities the JAVA language has but there might come restrictions because of the amount of NXTbrick's inner memory. [7]

Another interesting programming environment could be the nxtOSEK platform which allows programming with C/C++ languages. The nxtOSEK also demands a new firmware and ends the guarantee of the device. There are programming enviroments for Matlab and Python lovers as well. For Matlab there is a third party toolbox Mindstorms NXT Toolbox for MATLAB which was created mainly as a student work in RWTH Aachen University's student project - MATLAB meets LEGO Mindstorms. This toolbox allows the use of the Matlab mathematical operations to create artificial intelligence to the robot and allows the many possibilities to plot and process the sensor recorded data. For the students of Aalto University, the nxt-python platform might be interesting because in Aalto School of Engineering mandatory programming courses python is the teaching language. [7, 8, 9]

6 Field test setup

In order to test the capabilities of the Dexter Industries GPS sensor for the Lego Mindstorms NXT robot, a number of field tests were carried out. The main purpose of the tests was to determine the basic performance level of the GPS sensor and its capabilities both in static measurements as well as navigation. Based on the tests, it is possible to assess possible realistic practical uses for the Lego Mindstorms NXT equipped with the Dexter Industries GPS sensor.

The GPS was attached to the NXT programmable robot unit and the system was programmed using the graphical NXT-G programming environment. As mentioned in Section 5, there are multiple programming environments of variable complexity available for the NXT. The choice of using NXT-G was motivated by a number of reasons.

Simplicity Since the NXT-G environment is bundled with and wholly supported by the NXT, this enabled us to concentrate more on the actual GPS performance. No custom firmware is needed to program the robot with NXT-G.

Initial testing As first testers of the GPS sensor, one of the aims was to provide initial test results, on which further development could be done. By using the NXT-G environment, we can in a sense provide an out of the box testing for the sensor to determine the standard performance level of the sensor. By testing with NXT-G, we can assess whether the simple environment is adequate for simple positioning or of more advanced programming languages are needed for practical applications.

Existing support Dexter Industries provides support and multiple programming blocks for the NXT-G environment.

6.1 Build setup

The field testing setup of the robot consisted of both standard NXT components and third party sensors. The basic layout for the robot was a four-wheeled platform, on which the main NXT computer unit was attached. The unit was encased in a supporting structure, which provided a base for other sensors. The robot was powered by two standard Lego interactive servo motors, which powered one front wheel each. Additionally, a third servo motor was situated in the front part of the robot between the two driving motors. The computer unit, and especially the battery,

contributed the most of the weight of the robot. The main mass component was thus resting on top of the middle of the wheel base, making the structure adequately robust even for faster movements.

In addition to motors, the robot was equipped with sensors for compass, color sensor and GPS. The GPS sensor was attached to the supporting structure on top of the main NXT unit in order to minimize any obstructions to the signal by the structure. The compass sensor was attached to a boom, which was in turn mounted on the right hand side of the supporting structure. During preliminary testing, the compass was found to be somewhat sensitive to outside interference. The boom was used to place the compass sensor as far as was practically possible from other sensors, servo motors and the NXT unit to minimize disturbances to the compass reading. The RGB color sensor was attached to the left hand side of the robot in front of the servo motor. The sensor was directed towards the ground with a clearance of approximately 1 cm.

Furthermore, the orientation of the servo motors in relation to the main NXT unit had to be taken into account. The forward direction is defined by the wheel attachment points. When the input ports of the servo motors are above the wheels, the forward direction is towards the attachment points. The motors are connected to the NXT output ports labelled A, B and C. To use the default steering configuration in NXT-G, each of the motors should be connected to the output port on that side. If an alternative order or motor orientation is used, the steering has to be adjusted accordingly in the move block. The setup used in the field testing is illustrated in Figures 1, 2, and 3.

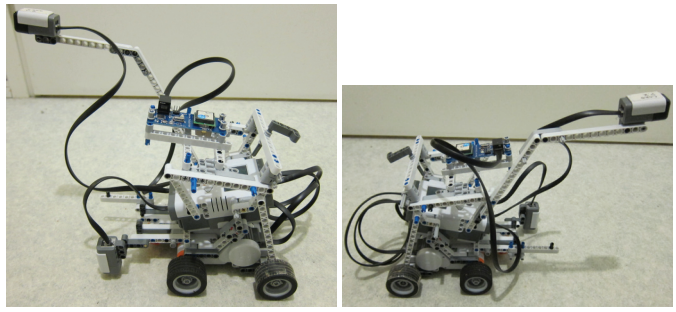

(a) Left side of the robot **(b)** Right side of the robot

Figure 1. Robot from the sides

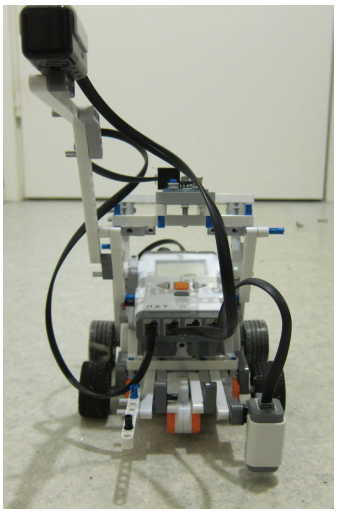

(a) Front side of the robot

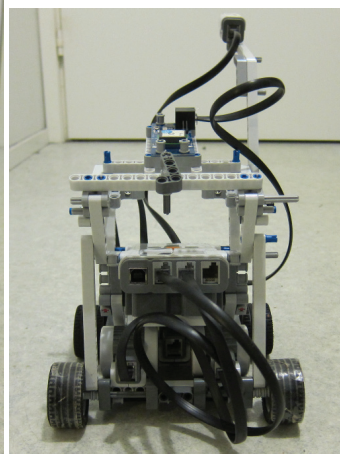

(b) Back side of the robot

Figure 2. Robot from the front and back

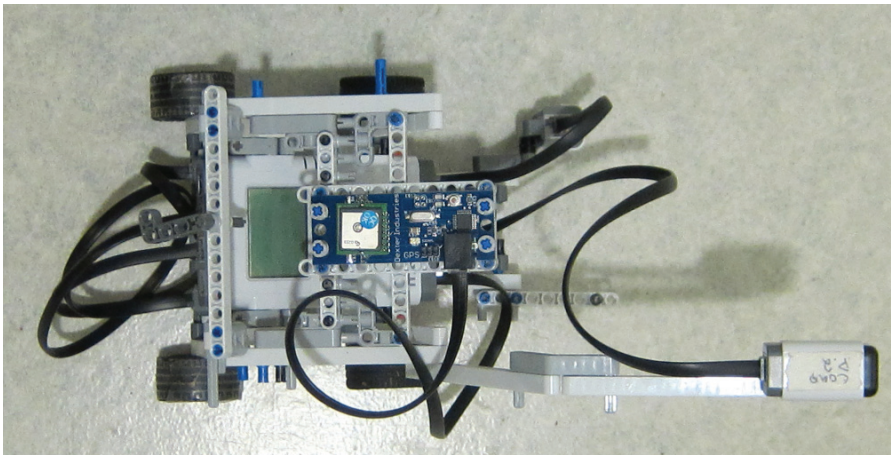

Figure 3. Upside of the robot

6.2 Test programs

To test the performance of the Dexter Industries GPS sensor various testing programs were created. The tests were designed to investigate the functionality of the GPS sensor in both position logging measurements and in a real-time navigation application. The GPSRead block was used to generate position information both in static measurements and while travelling with the robot. The navigation application was implemented using the GPSRead, GPSNavigation, and Compass blocks. Additionally, a program utilizing the output from the GPS-X block was created to log and

assess satellite visibility, altitude, and HDOP data.

In addition to the actual data logging programs, a few utility tools were created. These tools give direct output to the NXT screen without any data logging. The tools included for example a real-time position display showing current latitude and longitude as well as a navigation tool displaying the angle and distance to a predefined target destination. The latter was particularly useful since the target destinations for the navigation application were determined using Google Maps. By using the same target destination as with the actual navigation application test run, an estimate for the physical location (i.e. robot goal area) according to the GPS sensor could be quickly determined on-site.

GPS data logging programs

To record the coordinate solution from the GPS sensor, a data logging program, $GPSstat$, was created with NXT-G 2.0. This program serves as a general purpose data logging tool, which can be used to record the robot position both in static measurements and while on the move with robot. Because of the limited memory space of NXT, three versions of the program were created.

The first version records the robot position, two time parameters, robot orientation, and signal status once per second. The two time parameters are UTC time from the GPSRead block and program duration time from a Timer block.

The second version, $GPSstat\_vel$, additionally reads and logs the velocity output from the GPSRead block. Because the velocity output is not of special interest while making static measurements, the velocity logging was omitted in the first $GPSstat$ version to help reduce the size of the data logs, thus enabling longer continuous measurements.

Because $GPSstat$ works as a standalone GPS logging program as is, it can be easily implemented as a general purpose GPS data logging feature in other NXT-G programs. The $GPSstat$ program scheme is illustrated in Figure 4. First, the program closes and deletes any existing log files. Then a loop is started in which the GPS and time data is read, formatted to a string, and saved in a log file. The loop runs until terminated by the enter button.

The third version is $GPSsats$, which in addition to UTC, position, and signal status, logs the output of the GPS-X block: visible satellites, HDOP, and altitude.

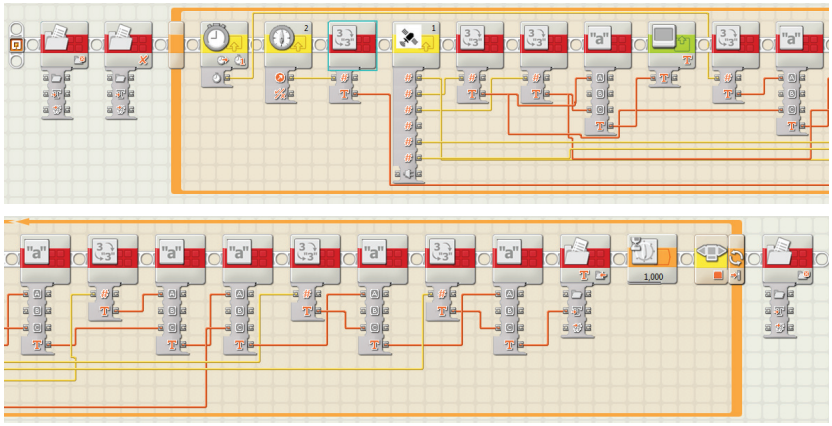

Figure 4. GPSstat NXT-G layout.

Naturally, all of these functionalities could be combined into a single program. However, during the testing it was found more convenient to have smaller programs generating smaller log files and to have automatically separate log files for each measurement based on the desired focus, e.g. position only, velocity, satellite visibility.

GPS navigation program

A destination seeking program, $GPSstat$, was created to test the navigation capabilities of the GPS sensor. The program consists of two parallel sequence beams. In the first sequence beam, the destination latitude and longitude are stored in as constant values. The values are connected to the corresponding target ports in the GPSNavigation block. The block then calculates the angle and distance to destination. The distance to destination is connected to a Compare block, which checks if the value is less than a preset threshold and returns a corresponding yes/no logical value. The logical value is connected to a Stop block, which halts the program when the distance is below the arrival limit. In the tests a threshold of 10 m was used. The angle to destination is stored as a variable. The sequence (excluding initial log file reset as with $GPSstat$) is inside a loop, which will run until the program is halted by the Stop block. The loop also includes a slightly altered version of $GPSstat$ for which writes the position, angle to destination and distance to target into a log file.

As the first sequence beam, the second is a run in a while loop. Two direction parameters are used to compute steering input for the robot. The direction parameters are the absolute magnetic heading from the Compass block and the angle to destination variable computed in the first se-

quence beam. The values are connected to a Math block which subtracts the angle to destination from the absolute heading. The difference is used as a steering input value for a Move block. The Move block is set to power level of 50 (out of 100) and the duration is set to unlimited. The unlimited duration will give the best response time for the steering, as the motors will not wait to complete a set amount of rotations/degrees/time, but will adjust the steering on every iteration instead. The latency is thus limited only by the execution speed of the loop.

The scheme for $GPSstat$ is illustrated in Figure 5.

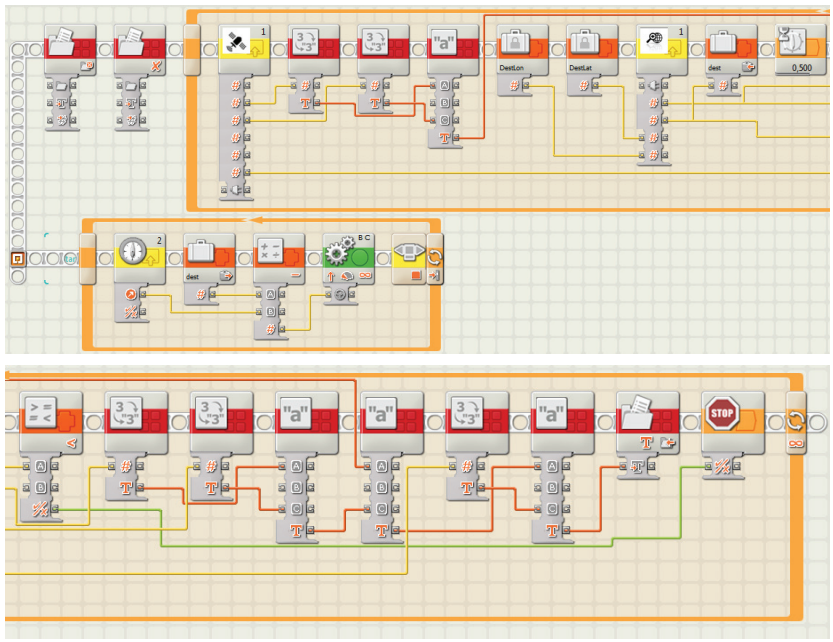

Figure 5. GPSnav NXT-G layout.

7 Field tests

The field tests consisted of various types of measurements, which were for the most part carried out at Otaniemi. Some initial field testing was also done around Espoo, particularly in Perkkaa and Leppävaara region. Furthermore, the GPS sensor was driven around by car in Espoo and Kirkkonummi.

The tests can be grouped in three categories: static tests, tests while moving, and navigation tests. Additionally, the initial signal acquisition time was observed during the start of each measurement session.

7.1 Static measurements

To assess the performance of the GPS sensor, a number of static measurements were conducted. The static measurement data logging was done with the $GPSstat$ program. Before logging any position data, the GPS sensor was allowed to acquire a valid signal, and the position output was monitored in real-time using on of the tools discussed in Section 6.2. At first, initial short proof-of-concept static measurements were carried out to make sure the $GPSstat$ program was working properly. These relatively short tests were carried out both in Perkkaa and Otaniemi. The duration of the initial tests was from approximately 3 to 5 minutes. Based on these tests, the later measurement times were set to be approximately 10 minutes.

The longer static measurements was carried out on a point GNSS3 near Falcon office building complex. The position of the GNSS3 had been determined during Engineering Geodesy course. The point is marked to the ground with a nail. This point was considered an accurate reference point in these field tests. The visibility on the point is relatively obstruction free, except for the Tinnu office building, which blocks a part of the Northwest view of the sky. The robot was placed on the point by fixing the nail to the middle of a simple targeting scope attached to the robot. By placing the robot on a know reference point, it was possible to compare location reading acquired with the GPS sensor to the location of the robot obtained with. GNSS3 point and the nearby Tinnu office building are illustrated in Figure 6a. Figure 6b shows the aerial view of the point.

A second location measured slightly more extensively was a point, which was used as the main starting location for the robot navigation tests. The point was located on a large tennis court complex near the Otaniemi sports field. Out of the tests locations, the tennis court was the most obstruction free. There were no major obstructions in any direction, apart from a few trees. The reference position of the point was determined using a Trimble GeoExplorer XH 6000 handheld GPS device. This way it was possible realize the starting point with relatively high accuracy.

In addition to robot position, the satellite visibility, HDOP and altitude was measured on GNSS3. Visibility measurements were taken both in conjunction with the static measurement and independently. The results allowed to compare the observed visibility to the visibility computed by Trimble Planning Software.

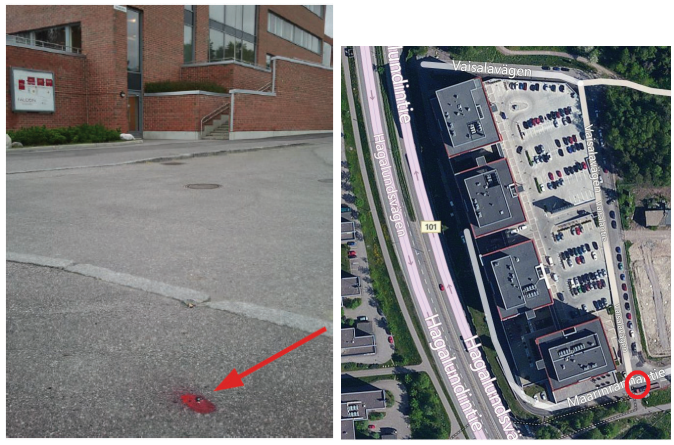

(a) GNSS3 point and Tinnu office building. **(b)** Aerial view of GNSS3 location.

Figure 6. GNSS3 point and surroundings.

7.2 Navigation tests

The $GPSNav$ program was used to test the navigation capabilites of the robot. The basic procedure for the initial navigation tests were to determine a goal point with Google Maps, locate the point on ground using the real-time navigation program discussed in Section 6.2, and then set the robot to travel to the goal zone from a adequate distance (i.e. approximately 30-50 m). Initial tests were carried out on parking lots in Perkkaa and near Maarintalo, Otaniemi. It soon became evident that an even more open space was necessary to test the navigation. The robot could not reach the goal destination unaided due to obstacles and errors in the GPS position. A few navigation tests were tried on the sports field tarmack. However, the track was deemed to be too narrow. Additionally, although the sports field was a relatively open space, there were apparently some visibility issues due to the track being located next to a hill. During test runs on the track, the signal was lost approximately every 3 minutes. Eventually, the tennis court next to the sports field was selected to serve as the main testing location. It had good visibility and a large unobstructed surface for the robot to manoeuvre on. The starting point for the navigation (tennis1) runs was set near the edge of the court. The goal destination was determined with Google Maps and it was approximately in the middle of the field. As with the earlier locations, initial testing with real-time navigation and test runs were carried out also on the tennis court. Even on the extremely spacious tennis court, the robot

would at times weer over the edge and get stuck in the soil. However, on the tennis court multiple succesful runs, where the robot reached the destination (according to the navigation data) were achived. The true end location of the robot was determined with the Trimble handheld GPS on two of such runs.

7.3 Vehicle tracking and velocity tests

Due to the slow speed of the robot, the track data from the navigation tests was concentrated on a very small area. The small physical movement of the robot tends to create very cluttered ground tracks, which will be further investigated in Section 8. To test the quality of GPS track data, while the sensor is on board a much faster moving vehicle, the robot was placed in a car. In addition to position, the velocity of the car was logged. The test was done with $GPSstat\_vel$. The car was driven with a constant target velocity of 100 km/h for approximately 15 - 20 km from Lommila to Veikkola and back to Perkkaa. The speed of the car was maintained as steady as possible by using cruise control set to 100 km/h. The route used is almost straight highway with constant speed limit and little variation in elevation, making it practical in maintaining the desired speed.

8 Analysis and results

After gathering data during the field tests, it was analysed using Matlab. A number of Matlab tools were written to read the generated log files and to visualize the results in a meaningful way. The data was analysed during and after the field tests to make possible corrections in the NXT-G programs. The general performance of the GPS sensor posed some difficulties in visualizing the data in practice. Almost every session contained clearly erroneous data points (e.g. location moved to North America), which had to be manually removed from the data. Furthermore, the frequency in which the GPS sensor would compute a new navigation solution seemed at times lag or even halt. In static measurements, a typical data set consisted of a few different constant coordinate pair solutions for hundreds of iterations, and a far smaller number of solutions with variation. This posed a problem when plotting the coordinate pairs, since the majority of data points would stack onto a single value. Directly plotting these results would give a false sense of variation in the data.

8.1 Data processing scripts

Log processing

Since each of the programs used in the fields tests generates slightly differently formatted logs, a Matlab script was written for each log type. For further development, it is possible to streamline and automate the data extraction process by combining the programs into a single file reading interface. By adding an identifier header (e.g. a different number for each log type) in the NXT-G program before generating the log, it would be possible to easily identify each log type. However, for the purpose of this project, separate read scripts were adequate.

KML file generation

The acquired data can be then further analysed and processed with Matlab. To visualize the data on a map, a Matlab script generating Google Earth compatible kml-files from the latitude-longitude. Two versions of the script was created: one generates a yellow line connecting the measured points, the other draws numbered red dots on each measured point. The points are numbered based on the data log line, thus giving a temporal representation of the data as well. The generated kml-files can be stacked in Google Earth to get a numbered route representation of the data. Separate scripts were created for $GPSstat$ and $GPSstat$ log types.

Coordinate frequency plot

As mentioned earlier in Section 8, the data had multiple duplicate data entries, which complicated the visualization. To give a representation of the frequency of the measured positions a Matlab script (statplot), generating a scatter plot of the data, was created. The script takes coordinate pairs (in any system), a possible reference point, and centering parameter as input. A weight based on the frequency of occurrence is given to each coordinate pair. The unique coordinate pairs are coloured logarithmically based on these weights. The colouring scale can be adjusted to suit the data, but in this case a logarithmic scale was most suitable in order to create desired dynamics. If coordinates for a reference point are provided, the script computes the offsets to this point. The mean value for the position is also computed and plotted. This script is extremely useful when estimating the level of scattering visually from the data.

Coordinate transformations

To assess the measurement accuracy in meters, the geodetic coordinates from the GPS sensor have to be converted to an Earth-Centered Earth-Fixed (ECEF) system. Although there are numerous conversion services online, it is more practical to make the transformations during the Matlab analysis. This way it is easy to process practically an arbitrarily large amount of data. The transformation formula from geodetic to ECEF system is computed according to equations in (1).

$$\begin{aligned} X &= (N(\phi) + h)\cos\phi\cos\lambda \\ Y &= (N(\phi) + h)\cos\phi\sin\lambda \\ Z &= (N(\phi)(1 - e^2) + h)\sin\phi \end{aligned} \tag{1}$$

where (ϕ, λ, h) are the geodetic latitude, longitude and ellipsoidal height, (X, Y, Z) are the ECEF coordinates, N is the radius of curvature in prime vertical, and e^2 is the square of the first eccentricity. N is a function of the geodetic latitude and it is given by (2)

$$N = \frac{a}{\sqrt{1 - e^2\sin^2\phi}}, \tag{2}$$

where a is the semi-major axis of the reference ellipsoid.

The conversion was implemented by writing two Matlab functions, geo2xyz and curvature, corresponding to (1) and (2), respectively. Minimal input for the geo2xyz is geodetic latitude and longitude. If no height from the reference ellipsoid is provided, it is set to 0 for each coordinate pair. The reference ellipsoid parameters are specified as input parameters to the curvature function. In case no parameters are specified, the default reference ellipsoid is WGS84.

To better assess the variation in the position with respect to a local reference point, the ECEF coordinates have to be transformed to a local coordinate system. This is done by translating the origin of the ECEF coordinate system to the local reference point and rotating the XY coordinate plane parallel to the local tangent. The coordinate transformation from ECEF to local East-North-Up (ENU) system specified by the reference point R is given by (3)

$$\begin{bmatrix} \Delta E \\ \Delta N \\ \Delta U \end{bmatrix} = \begin{bmatrix} -\sin\lambda_R & \cos\lambda_R & 0 \\ -\sin\phi_R\cos\lambda_R & -\sin\phi_R\sin\lambda_R & \cos\phi_R \\ \cos\phi_R\cos\lambda_R & \cos\phi_R\sin\lambda_R & \sin\phi_R \end{bmatrix} \begin{bmatrix} X - X_R \\ Y - Y_R \\ Z - Z_R \end{bmatrix}. \tag{3}$$

8.2 Static measurements results

The results gathered from the static measurements in the field tests were varied. During testing there were some problems with the GPS sensor losing signal sporadically and the some of results containing a large number of crude errors. In this section, the results of the static measurements made on GNSS3 are studied in more detail. Based on the Engineering Geodesy course results, the coordinates of the GNSS3 point were known to a centimetre level of accuracy. This precision is more than adequate since, as mentioned in Section 3, the accuracy of the GPS sensor was stated to be 3 m. The tennis1 point was used as a starting point for the navigation tests and was measured with the Trimble handheld device.

GNSS3 point

A static measurement of approximately 10 minutes using $GPSstat$ was carried out on the GNSS3 point. The reference coordinates for GNSS3 both in geodetic (WGS84) and ECEF coordinates are listed in Table 3.

Table 3. Geodetic (WGS84) and ECEF coordinates of GNSS3

X (m)	Y (m)	Z (m)
2885604.951	1333969.106	5510902.816
ϕ	λ	h (m)
60° 11′ 14.40244″	24° 48′ 37.24973″	22.412

To guarantee a good fix as well as to use all of the memory space for actual observations, the GPS signal was acquired approximately 20 minutes prior to the actual measurement. After the first static measurement the log file was exported and the robot kept in the same location to additionally measure satellite visibility, HDOP, and altitude.

During the 10 minute static measurement period a total of 487 solutions were obtained for GNSS3. The data did not contain any crude outliers and the signal was available for the whole observation period. Kml-files generated from the data, viewed with Google Earth, are illustrated in Figure 7. The GNSS3 point is also marked on the map with a labeled yellow pin.

At a visual inspection, the position fixes seems to vary around the GNSS3 point. When the data is plotted with respect to time, it is evident that a large number of points have identical coordinate solution with each other. The coordinates with respect to time are illustrated in Figure 8

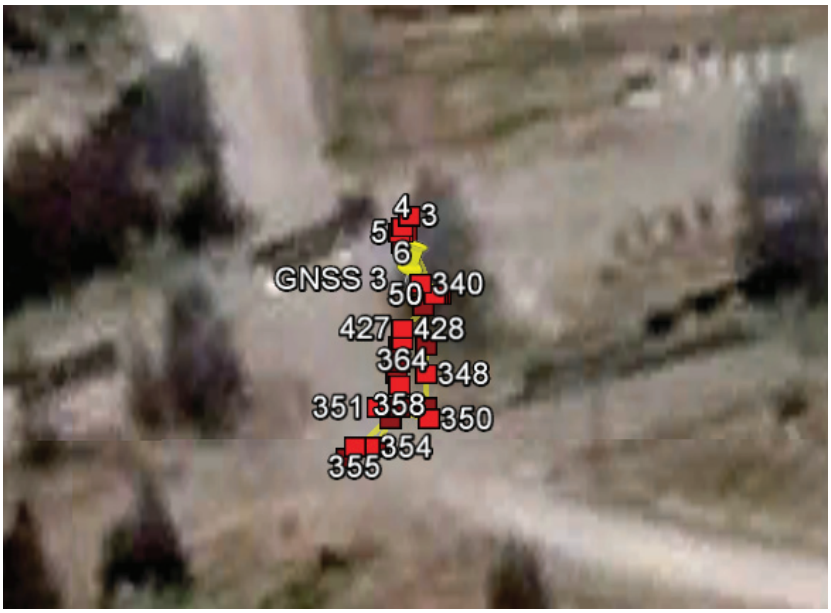

Figure 7. GNSS3 static measurement results kml-file in Google Earth.

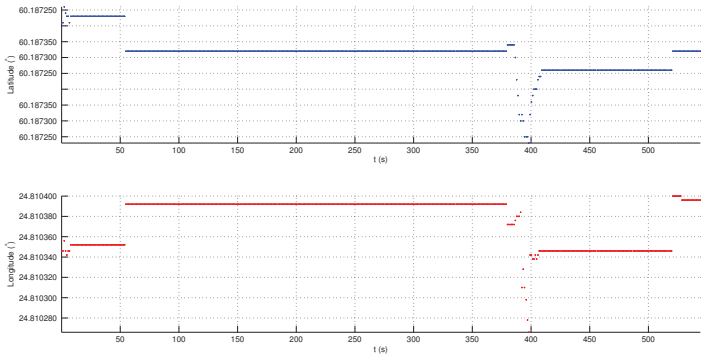

Figure 8. GNSS3 latitude and longitude as a function of the robot clock.

To examine the obtained latitude and longitude in local ENU system, the height of the GNSS3 point was used for all of the observations. The geodetic coordinates were transformed to ECEF coordinates, which were in turn transformed to ENU system with GNSS3 as the local reference. The subsequent frequency plot for the data is illustrated in Figure 9. GNSS3 point is marked with a red star and the mean of the observations with a green star.

The standard deviations and RMS differences to GNSS3 point for the coordinates are computed according to (4) and (5), respectively.

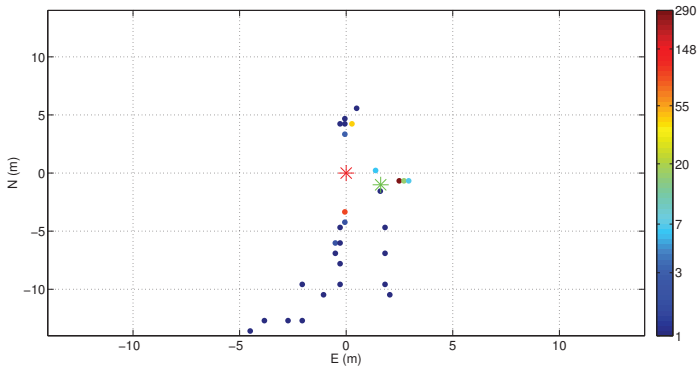

Figure 9. GNSS3 static measurement in East-North coordinates. The coloured bar shows the frequency of each solution. GNSS3 point is marked with a red star. The green star is the mean position.

$$\sigma = \sqrt{\frac{(\sum_{i=1}^{n}(x_i - \overline{x})^2}{n}}, \tag{4}$$

where x_i are the observed coordinates and $\overline{x}$ is the observed mean.

$$RMS_{diff} = \sqrt{\frac{(\sum_{i=1}^{n}(x_i - X_{GNSS3})^2}{n}}, \tag{5}$$

where x_i are the observed coordinates and X_{GNSS3} is the corresponding GNSS3 reference coordinate. In the case of ENU, the coordinates are already references to GNSS3, and the RMS difference is just the RMS sum of the residuals to this value. The values are listed in Table 4.

Table 4. Mean, standard deviation, and RMS of residuals to GNSS3 point of E and U coordinates.

	E (m)	N (m)
Mean	1.62	-1.01
Std. dev.	1.27	2.54
RMS	2.06	2.73

The figures and values show, that there is some bias in the observations, which show as larger RMS values with relation to standard deviations. The mean position is relatively close to the true position of the robot. Based on these results, the precision reported by the manufacturer is achieved.

The measurement was carried out on 1st of November at approximately 18:30 local time. The measurement conditions regarding satellite visibility and HDOP were examined with Trimble Planning Software and

Figure 10. Satellite visibility on 2012-01-11 18:10-19:10 at GNSS3 point computed with Trimble Planning Software.

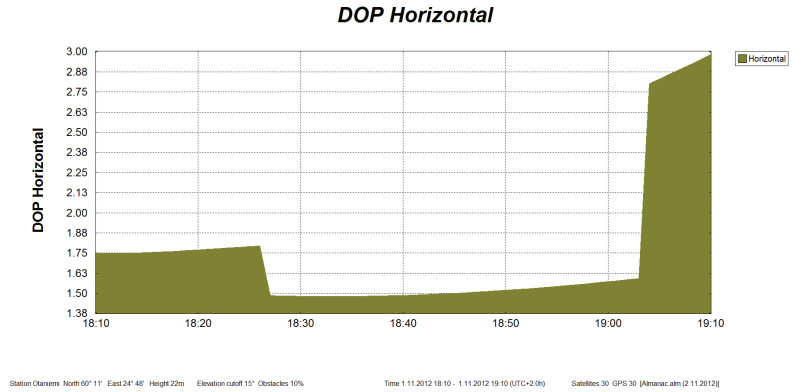

Figure 11. HDOP on 2012-01-11 18:10-19:10 at GNSS3 point computed with Trimble Plannig Software.

measured with the GPS sensor using $GPSsats$. The visibility graph from Trimble Planning software is illustrated in Figure 10. The obstruction from Tinnu office building was approximated in the software with a blocking mask, which was visually added using the skyplot tool.

The HDOP graph from Trimble Planning Software during the measurement is shown in Figure 11. The computed HDOP values indicate fairly good conditions, especially in the beginning of the period, when the static measurements were made.

The satellite visibility and HDOP values measured at GNSS3 with the GPS sensor are illustrated in Figures 12 and 13, respectively.

The satellite visibility is in a relatively good agreement with the Trimble Planning Software. The blocking mask estimation for the Tinnu building might be too big, which could cause some of the visible satellites to be left out from the graph. The HDOP values from the GPS sensor are mostly 1 with a larger values, probably due to a momentary reduction in satel-

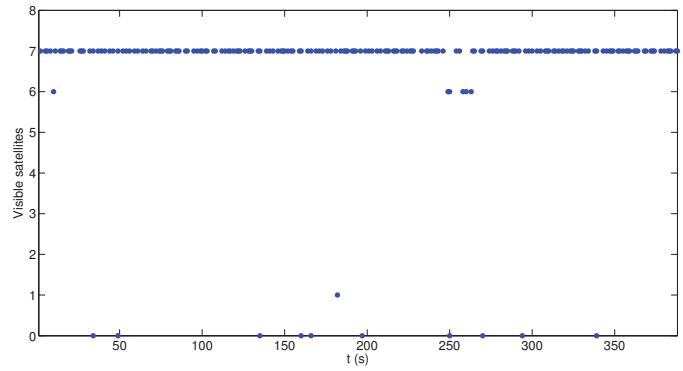

Figure 12. Visible satellites during approximately 18:40-18:48 at GNSS3 measured with GPS sensor.

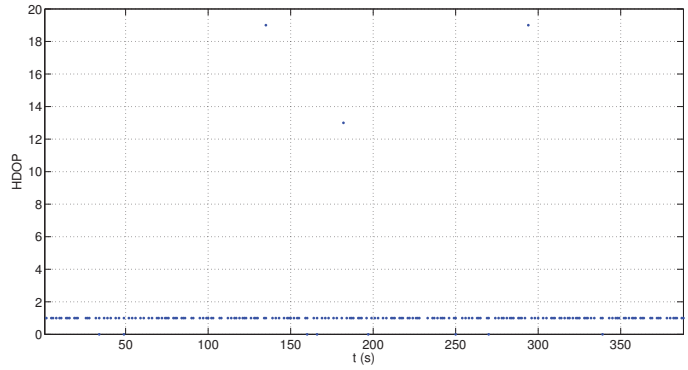

Figure 13. HDOP during approximately 18:40-18:48 at GNSS3 measured with GPS sensor.

lite visibility, which can be seen in Figure 12. However, since the HDOP values output by the GPS sensor seem to have reduced accuracy, it is questionable whether these values have any merit estimating the true HDOP. A better knowledge of the computation algorithm inside the GPS-X block is needed to evaluate these values further.

8.3 Navigation test results

The results from the navigation tests, carried out on the tennis court, were greatly influenced by the accuracy of the GPS sensor. Approximately 60% of the total test runs ended with the robot finding an end point within the tennis court. Most issues were seemingly caused either by some offset error, where the actual position observed by the robot would differ so much with the true position, that the dimensions of the court were not

adequate, and the test run would end when the robot drove out of the field. The same clustering of positions as observed with the static measurements is also evident in the position data gathered during the navigation tests. This would indicate, that the robot could not accurately and fast enough determine the position in order to always reliably navigate to the target destination. For most of the successful test runs, the true position of the robot overshot the target destination, even though the arrival threshold was set to be as large as 10 meters. However, the robot seemed to be reasonably capable of determining the direction in which it would have to travel. During testing, it would take approximately 5 to 10 seconds for the robot the determine the travelling direction with seemingly good accuracy. The initial orientation had no visible effect in the travelling direction determination. Two of the successful navigation test runs are examined in more detail.

Test run A

Figure 14 illustrates the position observed by the GPS sensor during test run A. The start (tennis1), destination (dest), and true end location of the robot (end1) are marked with yellow pins.

Figure 14. Test run A.

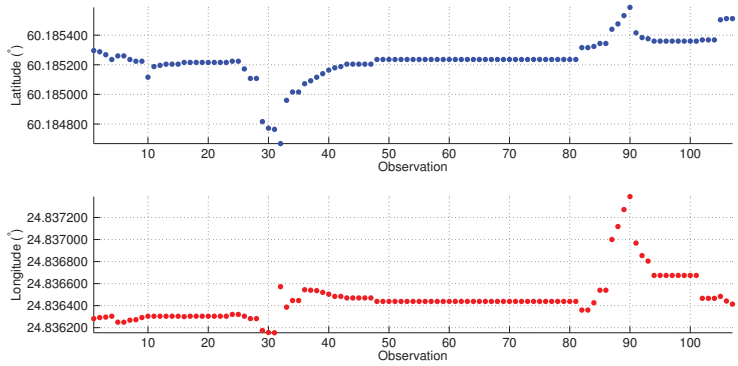

Figure 15. Latitude and longitude during test run A.

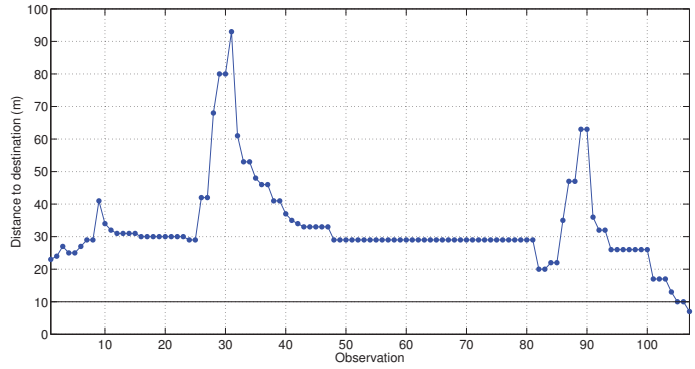

Figure 16. Distance to destination during test run A.

Visually the position seems to have a large variation, but as with the static measurements, there are relatively long periods where the observed latitude and longitude remain constant. Figure 15 show the development of observed position during the test run. Figure 16 shows the distance to destination during the test run. The target distance is marked with a black horizontal line.

Figure 16 shows the slow and sporadic change in the distance to destination computed by the navigation block. There are two distinct peaks in both position and distance graphs, which correspond to the GPS sensor observing clearly faulty readings. With relation to the destination position, the true end position was approximately 12 meters off the target. This is almost within the target area. The last observed robot position was approximately 17 meters off the true end position. The last observed robot position was approximately 8 meters off the target destination, which is very close to the last distance to destination (7 m) computed by the navi-

gation block, which indicates that the halting condition for the navigation module worked properly, but the error in observed position caused the robot to end up in erroneous location.

Test run B

Figures 17, 18, and 19 show similar graphs for test run B. The graphs show similar patterns as with test run A. In the beginning of the test run, there is a period where the position solution varies significantly in a short period of time, affecting the distance to target as well. However, after the initial erroneous movement, the position and distance patterns stabilise and change logically while the robot navigates towards the destination. With relation to the destination position, the true position of the robot was 17 m off the target. The last observed robot position was over 31 meters off the true end position, which is much larger than with testn run A. The last observed position with relation to the destination was off by 14 m. It is likely, that the last position did not have time to update before the navigation application halted, because the Figure 19 show, that the distance to destination was for a long time approximately 14 meters to the target before the last observed distance of 5 meters. Most likely the navigation block functioned correctly and the difference between last observed position and distance to target was caused by the halting of the program.

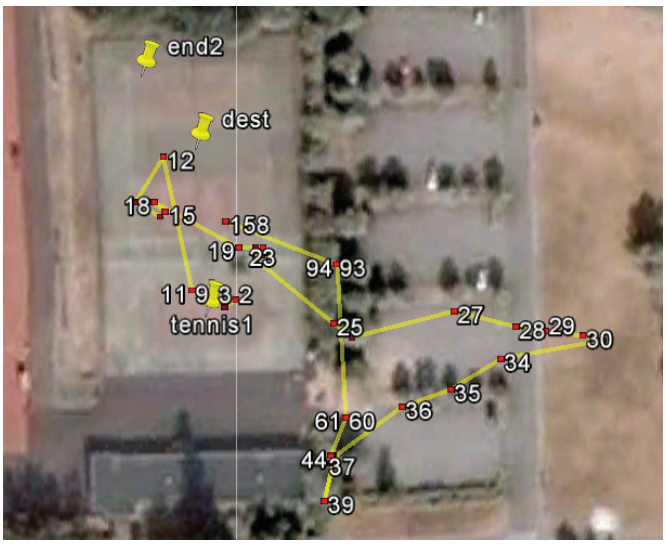

Figure 17. Test run B.

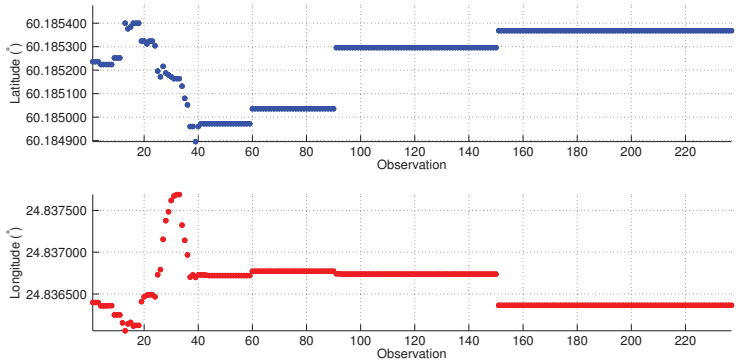

Figure 18. Latitude and longitude during test run B.

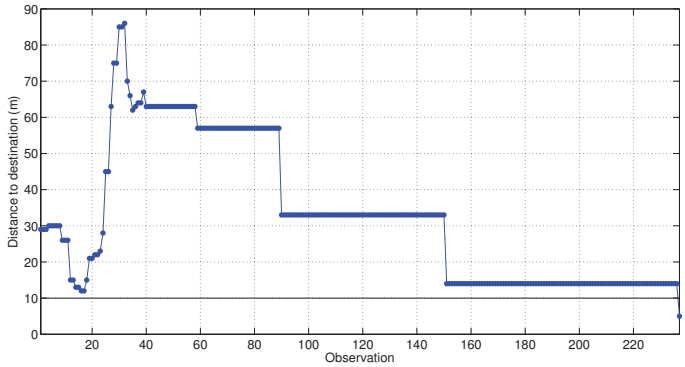

Figure 19. Distance to destination during test run B.

8.4 Vehicle tracking and velocity test

Compared to the navigation tests, when the GPS sensor was driven by a car with a much higher velocity, the resulting ground track was visually much more consistent. There were no significant outliers in the data and the ground track in general follows the road quite well. Figure 20 shows the logged route from Lommila to Veikkola, and from Veikkola to Perkkaa. Figure 21 shows the point, where the logging first starts at Lommila. The route from the return trip is also visible. Based on visual interpretation, the quality of the data is surprisingly good. The routes to and from Veikkola follow the road quite well and are clearly on separate lanes with correct orientation.

Figure 22 illustrates the velocity reading from a section on Turunväylä taken from the trip to and from Veikkola. The black line represents the mean velocity going to Veikkola, and the green line the mean velocity

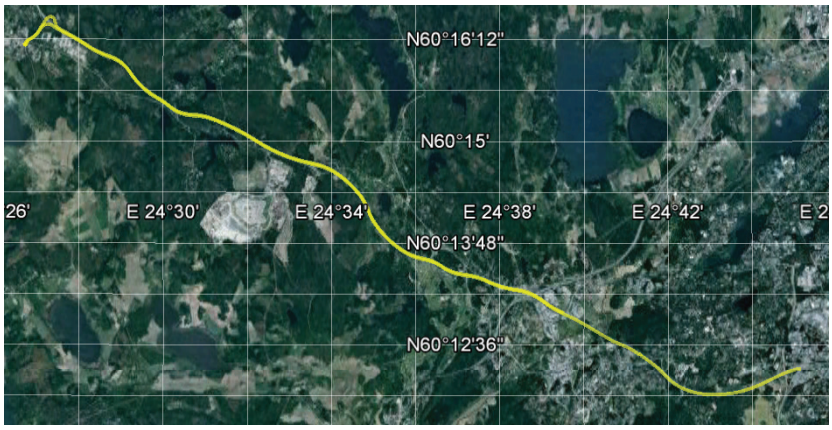

Figure 20. Lommila-Veikkola-Perkkaa route.

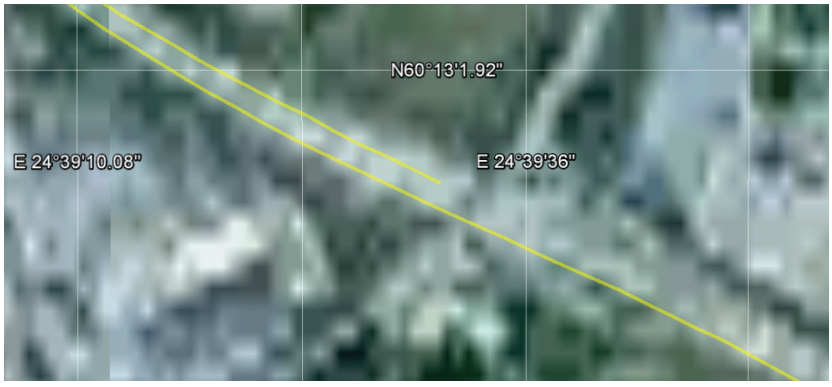

Figure 21. Route of the car following the road and visibly on correct separate lanes.

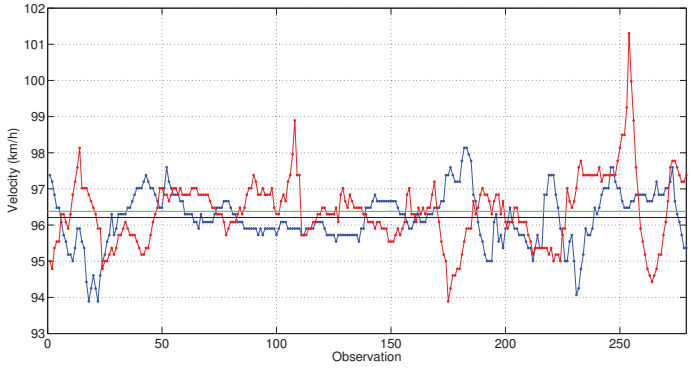

Figure 22. Velocity reading on a section of Turunväylä going to and from Veikkola. Black line is the mean velocity goign to Veikkola, and the green line the mean velocity coming from Veikkola.

coming from Veikkola. The velocity readings are taken on the same part of the road going both ways.

The mean values are listed in Table 5.

Table 5. Mean velocity and std. dev. of velocity to and from Veikkola.

	To Veikkola	From Veikkola
Mean velocity (km/h)	96.21	96.38
Standard deviation (km/h)	0.73	0.92

The results from the velocity tests seem to be relatively accurate. Based on the data, it is likely that the indicator error of the car is approximately 3-5 km/h.

9 Conclusions

Based on the tests the GPS sensor programmed with NXT-G performed moderately well. The accuracy achieved in the static measurement was within the accuracy reported by the manufacturer. However, the accuracy was barely good enough for practical navigation. The amount of room needed to even test the navigation and the subsequent poor performance really limits the application possibilities of the setup. The NXT-G programming language has its advantages, having moderately low learning curve. However, the limits of NXT-G soon become evident. Even simple programs require a lot of blocks and wires, which clutters the programming view considerably and consequently require a large amount of memory space. Furthermore, especially with the third-party sensor blocks for the GPS it would be useful to be able to access the GPS data directly. The GPSRead and GPSNavigation blocks perform a number computations to produce the position data and navigation data. The computation procedures are not directly available, and thus there is a level of uncertainty in assessing the reasons for the behaviour of the GPS sensor. This was especially evident in the update frequency of the solutions, in which the solutions for e.g. position and distance to destination seemed to stall to a constant value for multiple iterations. For a more inclusive approach it could be beneficial to use some custom firmware and program the sensors with one of the third-party conventional programming languages, instead of a visual programming language.

Bibliography

[1] DexterIndustries manufactures page.
URL: www.dexterindustries.com. [Accessed: 2012-11-27]

[2] HiTechnic manufacturer page.
URL: www.hitechnic.com. [Accessed: 2012-11-27]

[3] Official Lego third-party partners.
URL: http://education.lego.com/en-us/preschool-and-school/secondary/11plus-mindstorms-education/partners/. [Accessed: 2012-11-27]

[4] DexterIndustries wikipage for dGPS.
URL: http://dexterindustries.com/manual/dgps-2/. [Accessed: 2012-11-27]

[5] Carnegie Mellon Robotics Academy webpage.
URL: http://www.education.rec.ri.cmu.edu/content/lego/index.htm. [Accessed: 2012-11-27]

[6] Lego education competitions.
URL: http://education.lego.com/en-us/preschool-and-school/secondary/11plus-mindstorms-education/competitions/. [Accessed: 2012-11-27]

[7] Helsingin yliopiston robottiohjelmointikurssin luentokalvo.
URL: http://www.cs.helsinki.fi/u/strommer/jyu-luennot/kalvot/jyu-robottiohjelmointi-luento1.pdf. [Accessed: 2012-11-27]

[8] RWTH - Mindstorms NXT Toolbox for MATLAB.
URL: http://www.mindstorms.rwth-aachen.de/. [Accessed: 2012-11-27]

[9] Google code project webpage for nxt-python:
URL: http://code.google.com/p/nxt-python/. [Accessed: 2012-11-27]

GPS Wildlife Tracking

Tanja Kantola

Aalto University School of Engineering
Department of Surveying and Planning
tanja.kantola@tkk.fi

Abstract

The increased environmental awareness among societies calls for studies of impacts of various commercially driven projects on wildlife and their habitats. Researchers can equip animals with global positioning system (GPS) technology to obtain accurate (less than or equal to 30 m) locations that can be combined with sensor data to study animal behaviour and ecology. This report provides an overview of the state of the art of GPS wildlife tracking. The report reviews various wildlife tracking methods and how they are being used in con-junction with the modern GPS techniques – and how GPS has been integrated into functional wildlife tracking systems with data storage, data transfer, power supplies, packaging and sensor technologies. The report presents alternatives for retrieving GPS data from the tags carried by free-ranging animals by using dataloggers, radio-frequency download systems (e.g. very high frequency), integration of GPS with other satellite systems (e.g. Argos) and potential new data recovery technologies. Finally, the report presents case studies of how commercial GPS wildlife tracking applications are being used in ongoing projects.

1 Introduction

In the 1960s, the Craighead brothers pioneered the first use of radiocollars to study terrestrial wildlife when they radiocollared the first grizzly bears and elk as part of their ground-breaking studies in Yellowstone National Park [4]. Today, with the advent of animal-borne satellite collars, tags and transponders, ecologists and even ordinary internet users sitting at their desk can check the movements of many previously impossible to study animals, such as ocean-going fish, migratory songbirds and long-distance migratory mammals on Google Earth.

GPS wildlife tracking or GPS telemetry allows for a profound study of relatively fine-scale movement or migratory patterns of wild and free-ranging animals. It is a process whereby researchers, natural resource managers, conservationists and other interest groups can remotely observe an animal using the Global Positioning System and optional environmental sensors or automated data-retrieval technologies such as Argos satellite uplink, mobile data telephony or GPRS and a range of analytical software tools.

Traditionally, the study of wildlife has been, to a large extent, the remit of biological re-search with pure objective of furthering mankind's knowledge [5]. Originally the tracking data remained largely in use of the research community. The modern web service technologies, however, have enabled publishing some of the data also for the large audience. Currently there are public web services all over the world promoting the educative purposes of wildlife tracking. Such examples are the web map services of the Finnish Museum of Natural History, where anyone may follow the tracks of various satellite-tracked birds of prey. Links to maps and project descriptions can be found on the museum's web site[1].

Today, environmental awareness and new regulations are pushing decision makers and societies at large to address issues such as conservation of biodiversity and habitat fragmentation. This has raised the interest of the commercial sector in wildlife tracking technologies. Large-scale alterations of the landscape such as hydroelectric development, expansion of agriculture and settlements and the cumulative effects of timber extraction over many years, have continued the demand for high-quality studies of impacts on wildlife and their habitats. Increasing human populations around the world force many species in-to unfamiliar environments

[1] http://www.luomus.fi/english/

due to land use change and wildlife management actions (e.g. reintroductions and translocations). Traffic and infrastructure planners often have to carry out a study into the effects that projects could have on the local wildlife frequenting the proposed location and may even have to modify their plans to suit the resident wildlife. Some years ago, there was a debate of such a case in Espoo, Finland, where the occurrence of an endangered flying squirrel led to change in construction plans. Another example of commercial interest is the study of behaviour of birds around airports and the runway [5]. This is due to concerns over possible "birdstrike" causing considerable aircraft downtime and possibly even danger to passengers.

Habitat conservation and restoration efforts and the design of wildlife corridors are often supported by data on animal movements. Movement data of species commonly causing traffic accidents, such as moose and deer, may help design corridors for the animals to move between areas without danger to traffic and themselves. The Finnish Game and Fisheries Institute provides a web service for everyone to follow the movements of satellite-tracked moose[2]. The data is published with a four-week delay for the protection of the animals. This data is needed for game management and protection plans. As another ex-ample, GPS data from pronghorn antelope in Wyoming highlighted movement corridors that were threatened by oil and gas development in a narrow migratory pinch-point [4]. GPS tracking has also been applied in reindeer farming to track the animals and reveal knowledge of their pasture use and other behaviour patterns. Tracking of wolves, bears and other predators provides knowledge of the behaviour and movements of these species for example close to human settlements increasing insights into mechanisms governing human-wildlife encounters and conflict.

Knowledge of animal movements from GPS technology will also enable researchers to understand mechanisms of climate impacts on populations [4]. A compelling conservation example that harnesses the power of GPS technology is a study of the effects of climate change on predicted distribution of polar bears in the next 50 years. As well as allowing in-depth study of animal behaviour and migration, the high-resolution tracks available from a GPS-enabled system can potentially allow for tighter control of animal-borne communicable diseases such as the H5N1 strain of avian

[2] http://www.rktl.fi/riista/hirvielaimet/hirvielainten_satelliittiseuranta/pannoitetut_hirvet_kartalla.html

influenza.

A GPS-enabled device will normally record and store location data at a pre-determined interval or on interrupt by an environmental sensor. These data may be stored pending recovery of the device or relayed to a central data store or internet-connected computer using an embedded cellular (GPRS), radio, or satellite modem. The animal's location can then be plotted against a map or chart in near real-time or, when analysing the track later, using a GIS package or custom software. While tracking devices may also be attached to domestic animals such as pets, pedigree livestock and working dogs, wildlife tracking can place additional constraints on size and weight and may not allow for post-deployment recharging or replacement of batteries or correction of attachment.

This paper seeks to present an overview of the state of the art in the area of GPS wildlife tracking. Section 2 describes background of wildlife tracking techniques starting in traditional radio-telemetry. Section 3 concentrates in satellite tracking technologies - Argos and GPS. Section 4 discusses general issues of wildlife tagging, such as tag attachment to animals. Section 5 focuses on integration of GPS and data retrieval systems. Section 6 lists some commercial applications and describes two case studies, where they are being used in ongoing research projects. Section 7 wraps up the report in the conclusion summary reflecting the main issues discussed in the paper.

2 Wildlife Tracking Technologies

This section discusses the background of wildlife tracking as well as various technologies used in the field. Most of the described technologies may currently be combined or integrated with GPS tracking, i.e. usage of GPS tags, or at least there have been attempts to do so in the research community. All technologies have their advantages and disadvantages in certain application areas. GPS is becoming the state-of-the-art technology in wildlife tracking, but it's application still presents problems, for example related to data retrieval or GPS signal acquisition in harsh or exceptional environments, such as under-water. These shortcomings may, in some cases, be alleviated by using the GPS tag in conjunction with other technologies. These technologies may also be combined with each other.

2.1 Radio-Telemetry

The beginnings of modern animal tracking technology were founded in the late 1950s [5]. The first form of electronic positional animal tracking is usually now referred to as "radio-telemetry" (also VHF-telemetry). It describes a system whereby the animal is tagged with a transmitting device and it is up to trained personnel to work out where the signal is coming from. This is achieved by following the strength of the tag's signal until the animal is seen. Radio tags constantly transmit a radio signal at a set frequency in the very high frequency (VHF) range (142 - 230 MHz) [6]. Each tag transmits a unique radio frequency (e.g., 150.020, 148.800 MHz) used for distinguishing between different tagged individuals; these signals are detected using a receiver. Both tag and receiver are equipped with antennas, the size of which will determine the distance from which the tag can be detected. Receivers can tune into different frequencies either manually or automatically (using a programmable receiver).

The crudest systems emit an audible tone which changes depending on how strong the signal is [5]. This method is not always feasible because the animal may hear the observer approaching and move away, or the terrain may be impassable. In addition, this tracking method is likely to disturb and alter the tagged animal's behaviour. Thus, re-searchers may choose to obtain the location of a tagged animal indirectly, using triangulation. Triangulation requires at least two directional bearings toward a tag from known lo-cations [6]. The estimated location of the tagged animal is based on the intersection of the bearings and determined through estimation of the angle and distance to the transmitting tag. The distance is a relative measurement referenced to the receiver(s) position. Bearings are obtained using a handheld antenna, vehicle-mounted antenna, or antennas on fixed towers. The simplest way to obtain a bearing is to rotate the antenna 360°and record the direction in which the signal is the strongest, using a compass. Just two intersecting bearings are needed to generate an estimated location, but at least three bearings are needed to estimate the associated location error (Fig. 1).

Radio-telemetry accuracy is highly dependent on the user, i.e. how well trained the field personnel are [5]. It is also very much dependent on the distance between transmitter and receiver. Researchers usually, therefore, have to conduct field trials in order to estimate the accuracy of their chosen system in the environment in question (environmental conditions

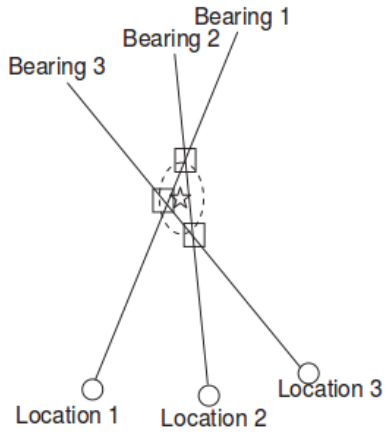

Figure 1. Triangulation to VHF tags. Two bearings might be enough for obtaining an estimate of the animal's location, but notice that different bearing pairs may produce different locations (squares). Therefore, at least three bearings are needed for estimating a more accurate location and its measurement error (star -location and oval - error). [6]

will affect the signals and therefore the system's accuracy). The tests may also be required to find out what range can be expected. The tests should also be done using the same personnel who are expected to be undertaking the data gathering for real as they are part of the system themselves.

When animals move large distances, are in inaccessible terrain, or many animals need to be tracked at once, aerial tracking may be used [6]. With small highly mobile animals, an ability to track from the air is often essential as terrain greatly reduces the ability to follow them for long periods.

The radio-telemetry tag devices are relatively simple and were therefore easily reduced in size over the years, which has enabled tracking of ever smaller species [5]. This is the biggest advantage of radio-telemetry over the other systems: the transmitter that is attached to the animal can be as little as 0.3 g - little enough to track small passerine birds, frogs, bats and insects. Radio tracking has fairly recently been used to test theories of how the magnetic compass is used in thrushes, to demonstrate the presence of a magnetic compass in homing bats and to track migrating dragonflies. In these experiments, animals were captured and fitted with radio transmitters. Upon release they were tracked with a combination of ground and aerial tracking in order to follow their paths.

Radio-telemetry technology is what the scientific community has grown used to over the decades, and there is a great deal of information about radio tracking in the scientific literature [2]. However, the range requirements make the process of tracking an animal a very difficult and often

prohibitively expensive business. A few automated radio-telemetry systems have been developed, but, even for automated systems, VHF technology requires receivers to be close enough to the animals to triangulate animal positions and therefore is not considered appropriate for global tracking. Also, use of RF spectrum may be problematic in terms of licensing. The physical size of the antenna required for optimal RF transmission can be relatively large and optimum positioning of an antenna on the animal is often not practical.

The tracking equipment itself is relatively inexpensive, but tracking in the field may be-come very costly in terms of researcher time and fuel costs, especially if aerial tracking is needed. Aerial tracking also includes risks. In addition, if triangulation is used, locations might be inaccurate. Terrain and vegetation cover can greatly influence signal accuracy because VHF signals may bounce off from hills, disappear in valleys, or be absorbed by heavy forest cover. Nowadays, ecologists may combine GPS and VHF units, and use the VHF units to validate the resource selection, survival or movement models developed with more fine-scale GPS data. Integration of VHF technology with satellite tracking technologies will be discussed more in the later sections.

2.2 Ultrasonic Tracking

In aquatic environments, radio frequencies (VHF) can be greatly distorted and are hard to detect [6]. Therefore, tags for tracking aquatic animals utilize ultrasonic frequencies (30-80 kHz, 75 kHz being the most popular). These frequencies can be used only in fresh water environments. Tracking ultrasonic tags is similar to radio tracking, with the primary difference being that tracking is conducted by boat, or by using fixed underwater receiver stations, because the tagged animal is underwater. Water-submerged antennas are often used to avoid signal distortion arising from the transition between water and air. In addition, homing in on the tagged animal, as described for radio tracking, can be used to position a boat or an aircraft directly above the tagged animal. The ad-vantages and disadvantages of ultrasonic telemetry are similar to the ones mentioned for radio tracking.

2.3 RFID and PIT Tags

Radio frequency identification (RFID) tags are some of the smallest tags currently available [6]. These tags encode information electronically (e.g., tag ID) and transmit it via radio waves. RFIDs utilize a wide range of frequencies (LF: 30-300 kHz; HF: 3-30 MHz; UHF: 300 MHz-3 GHz). Higher frequencies allow the information on the RFID to travel further using smaller tag antennas. Two types of RFIDs exist: active and passive. Active tags contain a battery that allows a constant transmission of the information onboard the RFID. Passive tags do not contain a battery and the information on them is transmitted only when in proximity to a reader that "wakes up" the tag by sending an electronic pulse to charge-up the tag. Because passive tags do not contain a battery, they can be very small, but this small size comes at the expense of reading range. Passive RFID chips can be as small as 0.3 mm^2; however, the read range of such a chip without an antenna is only 2-3 mm, connecting an antenna to the RFID chip increases its size (to several square centimetres) and read range (depending on antenna structure).

Passive Interrogated Transponders (PIT) tags are glass-encapsulated passive RFID tags that often utilize the low frequency range and can be as small as 8 mm (read range of 20 cm) [6]. These tags are now widely used in wildlife studies, especially when studying small mammals, fish, amphibians, reptiles, and insects. The tag is usually injected into the animal (except for insects), thus enhancing its durability in the field. Because the read range of PIT tags is relatively short, the animal has to pass very close to the reader for data to be gathered. This often allows studies only on the presence/absence of an animal at a certain location (e.g., a nest site or feeding station). Thus, animals that routinely use certain locations, and study questions that rely on these locations would be good systems for deploying PIT tags. Certain tracking systems can provide spatial information as well. For example, a series of readers along a river enables researchers to record the movements of fish up and down the river.

The advantages of RFIDs and PIT tags are their small size and low price [6]. These features increase the range of species that can be remotely studied and reduces the financial burden of tagging large numbers of individuals. Furthermore, the injection of PIT tags into to animal's body eliminates the need to attach external, potentially disturbing tags. However, the small size of these tags comes at the cost of read range. In ad-

dition, while the tags are cheap, tag readers are expensive, and obtaining many of them might not be feasible, thus limiting the number of reading points available. In addition to field use, RFIDs and PIT tags may be implemented for tracking small animals in controlled lab environments.

Figure 2. A paper wasp tagged with a passive RFID. The tag shown is an insert of a PIT tag, without the outer glass casing. [6]

2.4 Harmonic Radar

For tracking the flight path of insects, some researchers have used radar technology [6]. The insects are tagged with very small and lightweight tags emitting super high frequencies (SHF) (3-30 GHz) that allow a radar detector to distinguish the flying insect from the background noise of moving objects (e.g., plants moving in the wind). These tags are extremely light and small but the radar detectors are large, bulky, expensive, and difficult to move. Furthermore, tagged insects cannot be individually identified, and radar error can be up to 7 m. Tracking insects using radar is uncommon and little information is available about it.

Bird flocks, flying bat groups, and very large insect swarms can also be detected using radar [6]. In these cases, the animals are not tagged and the flight patterns of the entire group are detected by radars used for weather forecasting. This technique is used for tracking movements of large animal groups at large geographical scales. Radar technology does not allow distinguishing between individual animals or even between species. It can often be difficult to differentiate the signal of moving animals from background noise (e.g., clouds and vegetation).

2.5 Sensor Networks

Animals can be tracked in their habitat by a sensor network. In general, sensor networks are systems in which numerous compute and sensing devices are distributed within an environment to be studied. While some

sensor networks have static sensor positions, other, dynamic sensor networks consist of mobile nodes and wireless communication between them. It is possible to configure each of the deployed devices (e.g. large-mammal collar) as a separate node in a mobile network [8]. The nodes then communicate with each other as links that are available on a specific schedule, resulting in each device having stored location data from all other devices current as of the last set of communications. When the behaviour of the animals brings the devices into proximity with each other, remote retrieval of data from all marked animals depends only on querying one device rather than all the network nodes. This approach has been used on a limited basis with zebras in a pioneer ZebraNet project by the Princetown University[3]. ZebraNet consists of sensor nodes built into collars on zebras which take positional readings using a GPS unit and propagate them from zebra to zebra until infrequent communications percolate data to base stations. Hereby the collars operate as a peer-to-peer network to deliver logged data back to researchers.

[3] present a distributed wireless sensor network system designed to monitor European badgers and environmental conditions in a dense woodland environment. GPS receivers function poorly in densely wooded areas. Therefore information on badgers' movements and social interactions is usually gathered by on-site, night time observation, VHF radiotelemetry, and by remote video surveillance. All these methods are labour intensive and expensive. E.g. VHF tracking requires at least two people to get accurate location information on the animal, and it is not often practical to track multiple animals simultaneously.

This wildlife tracking installation was made up of three components. The first consists of active RFID transmitter tags embedded within a small light-weight collar designed to have minimal impact on badger behaviour. They are monitored by a second component consisting of a collection of fixed RFID receivers, referred to as detection nodes that are distributed throughout the woods at key locations close to known badger setts and latrines. The third component further complements the assembly by providing a bed of fixed sensor nodes that are deployed within badger foraging areas to monitor micro-climatic conditions - temperature and humidity in the same area - and their effect on species migration and mobility patterns. Sensor nodes and detection nodes were all connected through the same network. The network also included a single solar pow-

[3] http://www.princeton.edu/~mrm/zebranet.html

ered gateway with cellular connectivity, which was located conveniently for 3G coverage and for its own maintenance. As it had cellular connectivity, it could relay data instantaneously to the end users. Sensor networks require the tracked animals to move within fairly strictly defined boundaries and won't be discussed in more detail in this report.

3 Satellite Tracking

In the 1980s a breakthrough was made in animal tracking technology with the emergence of satellite tracking systems such as Argos [5]. A great advantage of satellite tracking is that animals can be tracked under all weather conditions, and at all times of day. Furthermore, once the tag is attached, there is no need to follow the animals in the field, thus greatly reducing the expenses of field work. This point is particularly important for long-ranging animals, such as migrants that can travel from pole to pole. This section introduces the application of Argos and GPS in wildlife tracking. New global navigation satellite systems (GNSS) are emerging, with the potential to be used in animal positioning. However, at the time of writing this report, no published scientific articles on their usage seemed to be available.

3.1 Argos

The Argos satellite system has been operational since 1978. The Argos DCLS (Data Collection and Location System) is carried onboard the National Oceanographic and Atmospheric Administration (NOAA) low-earth-orbit (LEO) satellites and the European Organization for the Exploitation of Meteorological Satellites (EUMETSAT) MetOp-A satellite, and will be carried on other LEO satellites to be launched by other countries [8]. Argos system used to be the state-of-the-art technology in the animal tracking field before GPS and it has been used extensively for scientific research involving wildlife tracking [5]. It may now be a thing of the past in some other application fields, but in wildlife tracking Argos still remains in use parallel and in conjunction with GPS. The most important reason for this is the data retrieval issue of using GPS tags: archival tracking units utilizing GPS geolocation usually need to be retrieved either by removal at recapture of the animal or by recovery of a self-release collar/harness bearing the tag. This may be fine for a homing

pigeon, which returns to its loft, or seabirds, which return to a nest after foraging (although the occasional non-appearance of an animal at the end of an experiment may explain a certain reluctance to use these expensive devices), but it is not fine for a small migrating bird which would have to be re-caught at the end of its journey.

Argos presents many advantages as a data transfer system, including worldwide coverage. A key advantage Argos offers is the capability for sending data from the device directly to the user on a global basis. The Argos system can provide supplemental sensor data (e.g. temperature, activity) and positions based on Doppler measurements of the Argos transmitter's uplink frequency. Although these positions are often less accurate (hundreds of metres to kilometres), they provide a backup to GPS positioning. Argos is therefore used as a data transfer system for animal-borne GPS, which has resulted in the development of Argos tags carrying GPS receivers. This kind of hardware interfaces GPS quality estimates of location and the data-relay capabilities of the Argos System. Argos-use in GPS data transfer is discussed in more detail in Section 5.2. The general Argos system functionality is summarized below[4]:

1. **Platforms (Platform Transmitter Terminals, PTT) send signals to satellites**. A platform refers to any equipment - device or tag - integrating an Argos-certified transmitter. Each platform is characterized by an identification number specific to its transmission electronics, which enables distinguishing individual animals. A platform transmits periodic messages characterized by the following parameters:

   - transmission frequency (401.650 MHz $\pm$ 30 kHz), which must be stable as the location is computed on the basis of Doppler effect measurement,

   - repetition period, which is the interval of time between two consecutive mes-sage dispatches, varying between 90 and 200 seconds according to the use of the platform,

   - platform identification number,

   - all collected data, which may include data recorded by other devices

[4] http://www.argos-system.org/html/system/how_it_works_en.html

attached to the Argos-tag such as a GPS, pressure sensor and others.

The transmission duration of each message is less than one second.

2. **Polar orbiting satellites collect data**. Polar orbiting satellites flying at an orbit of 850 km above the earth pick up the signals and store them onboard and relay them in real-time back to earth.

3. **Receiving stations relay data from satellites to processing centres**. Over 40 antennas located at all points of the globe collect the data from satellites. Data are either received in real-time by a regional antenna in the satellites' path or stored onboard and relayed to the nearest global antennas. Today, most of the globe is covered by the real-time antenna network.

4. **Processing centres collect all incoming data, process them and distribute them to users**. The satellites transmit the data to a receiving station on the ground which in turn sends the information to a processing center [6]. There are two global Argos processing centres, one in France and one in the USA. Once the data arrive at a processing center, locations are automatically calculated and information made available to users. The processing center consolidates the data and prepares them for presentation to the end user.

5. **Argos users around the world receive data**. Argos users around the world receive data directly in their office or on-site, depending on their choice (email, fax, web, cd-rom, or directly on mapping software).

Argos tags are often deployed on marine and migrating animals [5]. Also large birds (over 300 g weight) such as albatross have been Argos-tracked on their migratory journeys and the data remotely downloaded via the satellite. Argos-tracked marine species include loggerhead turtle, manatees, Pacific walruses and Greenland sharks. When aquatic animals are deep in the ocean, the satellites cannot receive the UHF signal [6]. Therefore, PTTs for aquatic animals are often equipped with a device that activates them only when the animal surfaces, thus preserving battery power. This may reduce the number of locations per day that can be obtained for these animals.

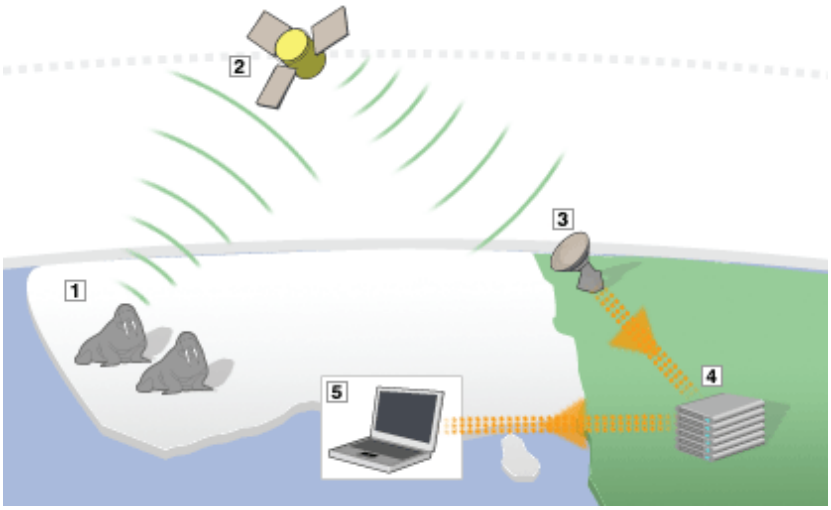

Figure 3. Argos system: 1. Transmitters on animals or objects relay pulses of data; 2. Passing satellite collects data and measures signals' frequencies; 3. Satellite relays data to terrestrial receiving stations; 4. Processing centre processes data and determines positions; 5. Researchers view information via email, website or 'virtual globe'. [Source: `http://news.bbc.co.uk/2/hi/science/nature/6701221.stm`]

Drawbacks of Argos include its inefficient use of electrical power due to the PTT transmitting without knowledge of whether there is an Argos satellite in view. The Argos system is expensive to operate for the user. Because PTTs use a very specific frequency, manufacturers are under stringent technical constraints. As a result, PTT tags are larger and more expensive than VHF tags [6]. On top of the purchase of the PTT it-self, there are service charges which were typically around $20 per day in 2009. Argos location accuracy varies (from 250 m to 1.5 km error) depending on the number of fixes the satellite obtained when passing over the tagged animal. In addition, the number of locations obtained per animal depends on its position around the world. At the poles, a tag can be detected up to 14 times a day, but this number declines at lower latitudes.

Collecte Localisation Satellites (CLS), who manage the Argos system (http://www.argos-system.org), is currently upgrading its satellites to the new Argos-3 standard, which is capable of two-way communication with tags and floats [1]. The two-way in-formation will allow the Argos system to inform tags when a location has successfully been collected. More importantly, tags will be able to passively listen for satellites over-head and only transmit when they detect a satellite. This should allow much more rapid location observations as a fixed repetition rate will be unnec-

essary, decreasing for example the time marine animals need to remain on the surface for successful location acquisition. Presently, the two-way receiver is too large and consumes too much power to be practical for animal tracking. However, technology advances might make some two-way applications possible for future wildlife studies, thus enabling further transmission and battery life efficiencies.

3.2 GPS

GPS is becoming more and more prevalent in the bio-tracking community [5]. It has become the de-facto standard method for determining position in so many applications due to its accuracy and near constant availability. The major benefit of GPS is that it offers truly global coverage. There are, however, major challenges to getting GPS tagging technology to operate in many animal tracking environments. Many wildlife species live in extreme environments and expose instruments to levels of shock and extreme temperatures beyond the range of conditions typically experienced by electronics carried by humans [8]. Applying GPS to wildlife tracking applications requires many innovations. Marine species spend their lives in salt water that blocks VHF and UHF transmissions and GPS downlink signals, only exposing a receiver or transmitting antenna for a short time when the antenna is above the surface. The requirement for unattended long operational life of 6 months to several years is critical to wildlife applications and seldom a commercial requirement. Under ideal conditions, GPS tags could collect hundreds of locations per day and high-quality data on animal-habitat interactions anywhere, but this must be balanced with power consumption and/or satellite bandwidth [1].

GPS units automatically record the animal's location at fixed, predetermined, time intervals and store the data onboard the unit [6]. The frequency at which locations are obtained will determine the battery life of the unit and therefore the tracking duration. Efforts to conserve battery power and memory space and offer new data streams have led some manufacturers to default their units so that they collect locations during only a fraction of the day [1]. However, as demonstrated in several surveys, this can result in significant signal loss and otherwise observable and potentially important behaviours become undetectable. There have been several attempts to solve the issue of battery power, including tags that integrate solar cells to enable the recharging of a battery.

By its nature, GPS technology does not perform well in harsh environ-

ments [6]. GPS units must have a clear view of the sky to enable communication with the GPS satellites. Heavy vegetation cover (e.g., thick forests) and aquatic environments may distort or disable the use of a GPS unit. Conventional GPS processing often relies on the reception of uninterrupted signal for many seconds before a position fix can be determined. Minimizing time to first fix (TTFF) has been critical for animal tracking be-cause the receiver is usually turned on and off over time to minimize current consumption and extend system life [8]. Today, TTFF after start-up is typically 30 s or less with a good antenna and clear view of the sky. This still presents major problems in areas such as marine environment where wave wash over the antenna poses a significant hurdle to continuity of received signal [6]. Occasional breaks in the signal due to wave wash make the decoding of signals very difficult. A team at the Dunstaffnage Marine Laboratory, Scotland, devised an algorithm for piecing together the fragments of the signal, as they were acquired, in order to obtain the signal length required for a position fix. Although this proved to be successful through some simulation tests, it does involve some intensive processing and relies on relatively long signal acquisition times due to the receiver having to wait to receive sufficient fragments. Diving animals also spend variable amounts of time underwater. This requires using wet-dry sensors to prevent underwater transmissions that would waste battery power [1]. In addition, power can be saved by programming tags to transmit only during certain periods of the day, shut down completely, or transmit less frequently at the "slow rate".

A number of other sources of signal disturbance may influence GPS data quality [2]. These errors may concern the satellite clock or the effects of the terrestrial atmosphere (particularly the ionosphere and troposphere), which slows down and deviates the satellite signal. Satellite constellation is also important because too few satellites or grouping of satellites in the same sector can lead to erroneous fix locations. The immediate environment of the receiver (habitat, topography, weather) can also affect data quality by generating screen or multipath effects. Finally, it is supposed that the behaviour of the target animal (e.g., locomotion, feeding, hiding) may influence the probability of obtaining a fix, as well as its quality. Hence, each fix has an associated, but unknown, level of error, which may be predictable to a certain degree, given the appropriate information. Another type of error that plagues GPS telemetry in addition to spatial inaccuracy of the locations acquired are missing data in the form of failed

location attempts. The combined effect can lead to mistaken inferences on animal spatial behaviour, especially those involving movement paths and habitat selection.

GPS technology was pioneered on large vertebrates, such as GPS-collared elephants, moose and bears carrying fairly large receivers [2]. The size of the de-vices is decreasing, however, and each decrease in size increases the range of animal species for which they are available. A US company Telemetry Solutions is even advertising GPS data loggers starting at just 2 grams that are already being produced in large quantities just for bats[5]. The reality is, however, that majority of the GPS, like Argos tracking technology, is still too large to track bats, small birds and insects [6]. Advances in GPS have been commercially and military driven and wildlife biology is apparently not a productive enough avenue. Another problem is that if fix-success rates (the ratio of observed fixes to the number attempted) and the accuracy and precision of location estimates are dependent on the surface area of GPS antennae, collars with much smaller antennae may exhibit substantially poorer performance. Furthermore, in areas where vegetation or terrain obstruct reception of satellite signals, the behaviour and movements of smaller animals may also reduce GPS performance. Smaller animals may have greater tendencies or opportunities to enter tree cavities or other places where reception of transmissions from GPS satellites is impossible.

A significant drawback to the GPS system is that locations are calculated by the tag rather than the satellite system, and each GPS location collected requires a fair amount of data [5]. Processing these data onboard requires considerable battery power, although these data can be stored and processed later. This is still problematic, because tags must be physically recovered to collect the track or data from which locations are calculated must be sent via limited satellite bandwidth. Thus, collecting high resolution GPS tracks is limited to situations where tags can be recovered and logged data downloaded from recovered tags.

In addition to a GPS unit, other sensors can also be attached to tags for collecting information about the environment and the animal's physiology [6]. Sensors may record water salinity, pressure, air and body temperature, heart rate, and activity. Having constant availability of the position data is essential in order to study biotelemetry as a correlation between physiology and position (and perhaps velocity) is a time-

[5] http://www.telemetrysolutions.com/track-wildlife/gps-for-bat.php

critical task. There was some research done that involved integrating EEG (electroencephalography) with GPS on pigeons. Marine animals are often equipped with pressure sensors to provide information on the animal's swimming depth, which is an additional spatial measure. The study of social behaviour can also benefit from these devices. For example, microphones attached to tags record vocalizations, and recently developed proximity loggers record instances and duration of social interactions between tagged individuals. These sensors provide additional useful and interesting data on the tagged individuals and by collecting data automatically, they can reduce the time required for behavioural observations [6]. However, the more sensors placed on the tag, the heavier and larger it will be. These additional datasets can also often add to the problem that there has to be a method for extracting the data from the tag.

Despite the great challenges, no other currently available technique can match the accuracy and efficiency of GPS telemetry in environments where it is suitable, especially for description of movements at fine spatial and temporal scales. Numerous studies have concluded that GPS telemetry is cost-effective due to its low operational expenses. It must be kept in mind, however, that wildlife tracking always includes a risk of loss of devices or failure due to other causes such as death of the tracked animal. Sections 4-6 of this report will concentrate in discussing issues of GPS wildlife tracking in further detail.

4 Wildlife Tagging

There are many methods for gathering tracking data remotely. All methods reviewed in this report involve affixing a tag to an animal and tracking the signals emitted from the tag, or downloading data stored on a tag. A tag may contain more than one type of tracking mechanism [6]. For example, a GPS recording tag can also be equipped with a VHF transmitter. The suitability of each tag type will depend on the study species, habitat, and the study aims.

The study objectives will guide how many animals and which individuals should be tagged, at what time of year they should be tagged, and the duration of the study [6]. It is important to carefully design a tracking study to ensure that the data collected will actually address the study questions. Animals must be captured and sometimes anaesthetized to allow the attachment of a tag. Capture equipment and anaesthesia can

be costly. Capturing an animal can be difficult and time consuming; it might take several days or even weeks to locate and capture an appropriate individual. Anaesthetization can be risky for the animal and should be conducted in consultation with a veterinarian or other experts. For some animals, anaesthesia could be more risky than the stress of being tagged while awake. A variety of local, national, and institutional regulations and laws will apply to most capture and tagging procedures.

The rule of thumb used by most researchers allows for tracking devices that weigh less than 5% of a terrestrial mammal's body weight and less than 2% of body weight for birds and bats [6]. Aquatic animals can carry slightly heavier weights, but the tag's effect on their hydrodynamics is usually the confounding factor. Battery weight usually contributes the most to device weight, and is positively correlated with the tag's life span and thus with the study duration. GPS and PTT fixes require considerable battery power, leading to a negative correlation between the number of GPS or PTT fixes and the tag's life expectancy. The development of solar-powered PTT and GPS units may increase tag life span. It is also important to match the battery life with the longevity of the attachment method. It makes little sense to invest in a large tag that can last for 2 years if the animal can remove it after 1 week.

Finally, once the study is completed, the tags should be removed to ensure the animal's well-being [6]. Tags are often deployed for short periods of time, but may adversely affect the animal if left on for too long. Drop-off mechanisms and pop-off units are one way to achieve tag removal, but animals may need to be recaptured and even anaesthetized for removing their tag. It may not always be possible to remove the tag at the end of the study, but every effort should be made to do so. As a practical consideration, many tags can be refurbished and reused, thus reducing the cost of tracking in future studies.

4.1 Tag Attachment

There are many ways to attach tracking units to study animals [6]. Researchers seek attachment methods that minimize interference to an animal's activities but ensure that the units remain on until the end of the study.

Collars are the mostly used attachment method for tracking terrestrial mammals [6]. They attach the tag around the animal's neck. Collars should be loose enough to allow an animal to swallow but not so loose

that it gets hung on vegetation. The space left between the collar and an animal's neck usually follows some rule of thumb specific to the species. Animals whose necks are larger than their heads (including many birds, reptiles, and amphibians) cannot be fitted with collars and are instead fitted with harnesses [6]. A harness is mounted on the animal's body like a backpack. Tags can also be sewn into the shaft of a bird's tail feathers. The tag then falls off with the feather when it molts; therefore, this attachment method is usually for a short time period.

When collars and harnesses will not work, because of the animal's body shape, or the environment, glues such as epoxy, cyanoacrylate (superglue), or eyelash glue may be used [6]. It is important to ensure the glue does not cause skin irritation. Glues are commonly used to attach tags to aquatic animals, crustaceans, reptiles, in-sects, and some birds. PIT tags and very small radio tags can be implanted in the animal [6]. Implantation can be carried out through injection, ingestion, or incision. An incision will require anaesthetizing the animal and keeping it under supervision for a few days after the surgery. Ear tags and leg mounts are two additional less commonly used attachment techniques.

5 Integrating GPS and Data Retrieval Systems

Animal-borne GPS systems are not simple hand-held GPS receivers that are strapped on to the animal. The manufacturers of biotelemetry devices integrate the GPS receiver as they would any other sensor into a complete system for deployment on wildlife [8]. The workhorse of all wildlife GPS systems is the micro-power data acquisition/controller (MDAC; Fig. 4). The MDAC manages the entire application to achieve a functional system by controlling numerous individual tasks, which may include:

- Turning on and off the GPS receiver, sensors and data transfer components to manage the energy budget and acquire positions at sampling times appropriate for the research goals. Often samples are taken under complex scheduling regimes (sometimes termed duty cycles) that can be programmed to change over the course of the year or study.
- Interfacing via signal processing with onboard sensors, collecting and storing data to memory (e.g. activity, temperature, dive data).
- Providing an interface so the user can program parameters and down-

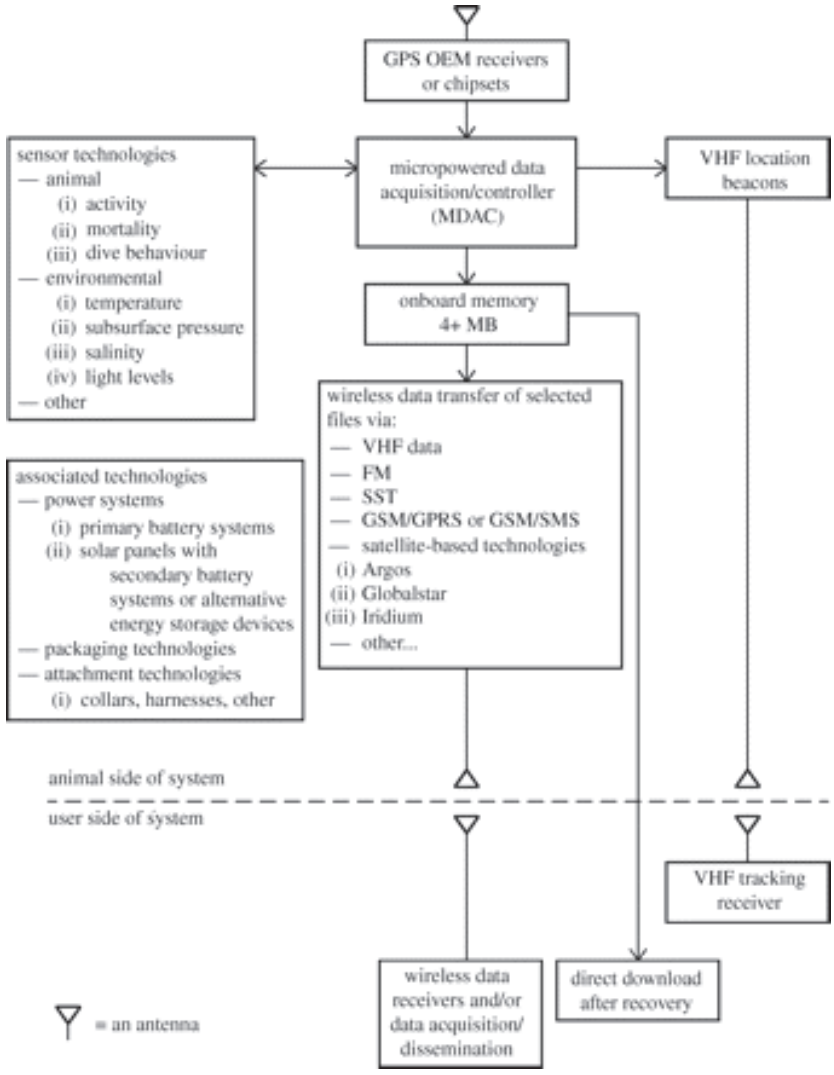

Figure 4. Block diagram showing the components of a GPS positioning and data collection system suitable for deployment on animals [8]. Note that many of these components were designed specifically for these applications.

load stored data.

- Controlling a VHF beacon that transmits a pulse rate (not GPS-based location data), which indicates that the GPS unit is operating correctly.

- Controlling a VHF beacon to report mortality events.

- Controlling the seasonal duty cycling of the VHF beacon and the means to relocate the collar for recovery and refurbishment.

- Managing the VHF beacon to avoid interference with GPS signals.

- Managing the wireless data transfer in those units equipped with that technology.

System and information management by the MDAC allow for the gathering, organization and storage of data. The next step is conveying the data to the user. Many data retrieval systems have been developed to meet various study circumstances, including reducing the potential disturbance to animals.

5.1 Store Onboard Systems – Manual Retrieval

In some applications, GPS data can be acquired and stored in the unit and then downloaded from the memory when the unit is recovered [8]. These systems can store GPS-based locations, pseudoranges or digitized GPS signals along with other sensor data (e.g. activity, dive information, temperature) and are often called store onboard (SOB) systems or 'archival tags' [5]. This kind of units do not offer any technical solution to data retrieval, but are suitable for certain species. For example, many species have an element of predictable behaviour, such as nesting, where the biologists can be confident of being able to re-capture the animal to retrieve the tag.

Historically, systems developed for terrestrial animals stored GPS-based locations and over time added sensor data, whereas systems developed for marine applications stored sensor data (e.g. dive information) and have over time integrated GPS-based locations. Both disciplines have benefited from obtaining both sensor and positional data to provide a deeper understanding of the biology of the animal. SOB units can be in the field several years before any data are recovered. SOB is less expensive than incorporating a wireless data transfer system, but there is the risk that the unit is not recovered and the data are lost. The development of accessory devices, such as programmable release mechanisms and the integration of VHF-tracking beacons, has increased the likelihood of recovering SOB units. The drop-off device is scheduled to detach a tag at a predetermined time, and the researcher is left to find it [6]. Having a VHF unit on such tags is useful for successfully locating them. After detaching from aquatic animals, tags float to the surface and can either be retrieved by the researcher or the data can be remotely downloaded through a satellite link.

In the mid-1990s, the first SOB units stored only about 1000 positions

in their limited memory [8]. Now, inexpensive, highly dense non-volatile memory in micro-miniature packages allows saving greater amounts of GPS and sensor data. User-friendly programming software allows independent duty-cycling of sensors and complex sensor-sampling schedules. The large capacity of datalog memory enables some sensor sampling rates near 1 Hz. Generally, current GPS-SOB systems can store about 12 000 GPS-based locations in 0.33 MB of memory powered by a single D-cell-sized primary lithium battery [8]. It is not uncommon for GPS subsystems to have 8-16 MB of memory, and much more could be added. In fact, most GPS systems are not memory-limited at all; the operational life is limited by the battery capacity, which is largely used to collect GPS position data, sensor data and housekeeping functions. Very little energy is used to download data as this occurs only after the unit is recovered, making SOB most efficient for maximizing GPS location and sensor data collection.

Another advantage of this approach is that it is not restricted by the bandwidth of any communications channel [5]. It can also be efficient in terms of power as there is no requirement for transmission over distance. No real-time updates are possible either and therefore you could have the case where researchers have tagged animals for a trip duration exceeding a year (or more) and they will have no idea where the animal has gone (and whether it is even still alive) until they successfully re-capture the animal after a very long period of time. This problem is often addressed by adding another simple radio-telemetry-style beacon to enable the researcher to periodically estimate the animal's position. That is only an option, of course, if weight constraints allow for it.

Some potential problems with manual data downloading in addition to inability to recapture the animal, include failure of the drop-off mechanism, inaccessibility to the drop-off location, or inability to find the tag [6]. For these reasons, GPS units should be deployed along with VHF / PPT / Ultrasonic units to allow tag retrieval. These other tracking devices can also be used for obtaining spatial data at a lower temporal resolution, as backup for GPS failures.

5.2 Remote Data Retrieval

Remote download permits multiple data downloads throughout the study period, allow-ing adaptive management decisions and troubleshooting of data acquisition rate [6]. Furthermore, remote downloading eliminates

the need for recapturing an animal or depending on unreliable drop-off mechanisms. It also eliminates the challenge of finding a dropped tag in dense vegetation. In fact, several countries are developing ethical regulations to ensure that the interference with animals will result in actual data reception by researchers [8].

Remote data transfer techniques can be incorporated to send data at regular intervals or near-real-time, especially for some applications that use recent data as a basis for implementing additional fieldwork such as finding a nest, den or predation site, or for adaptive management when animals begin using a certain area. Most GPS systems with data transfer technology also retain location and sensor data as an SOB, so that data can be down-loaded if the unit is recovered. This provides a backup dataset should the remote transfer become inoperable while on the animal.

VHF Beacon Data Transmitter

A special version of the conventional VHF beacon is used to encode GPS-based location data on the VHF beacon data transmission [8]. This data transfer method has the advantage of using a beacon, which normally is used for locating the animal, already onboard the system. Small amounts of data can be continually transmitted during 'on periods' of the VHF beacon data with little additional current consumption. However, power source restrictions do limit the VHF beacon data transmission to a narrow bandwidth and thus a very limited data rate. Systems using this approach can take upwards of 7 s to transfer a single GPS-based location and 45 min to transfer approximately 180 positions. Long upload sessions and the possible requirements for re-establishing communication if the link is disrupted might result in excessive disturbance and disruption of normal behaviour of the subject animal. Furthermore, with ever-increasing volumes of data from GPS systems, this approach is limiting when compared with other data transfer technologies and highly subject to noise interference. This VHF system is suited for situations in which small amounts of the GPS data are required in real time, while the remaining data can await downloading from the recovered units.

Radio Modem Technology

Modems MODulate and DEModulate data, and can use different segments of the radio-frequency spectrum and modulation technologies [8]. Among these technologies is single-channel narrow-band frequency mod-

ulation (FM). FM transceivers are commonly used to recover data from remote-fixed site instruments. In animal applications, single-channel FM modems are subject to problems such as interference on a selected channel. Also, unrestricted movement of instrumented animals means they must be classified as mobile systems, limiting the number of systems that can be deployed in a given area. Additionally, single-channel FM data modems require individual frequency allocation and licensing. Nevertheless, single-channel modem technology has proven useful for some wildlife applications.

A solution to minimize interference is found in spread spectrum technology (SST) [8]. SST allows data packets to be spread over many frequencies either through a technique called direct sequence coding or through frequency hopping. Using frequency hopping, the data packets are transferred on different frequencies in a pseudorandom manner. Packets transmitted on a frequency that experiences noise or interference are noted as damaged or missing and then retransmitted on another frequency that is probably free of the interference. Many SST units can successfully transfer data in an area, and even areas that contain single-channel narrowband FM units. SST is well suited for mobile applications like animal tracking, where chance encounters with other devices are expected. This technology also allows the user to operate unlicensed at power levels up to 1 W, which makes long-range data recovery from the ground or to aircraft possible.

Current SST systems optimize bandwidth and modulation to achieve high-speed data transmission and long-range performance (e.g. recovering 15-30 GPS-based locations per second) [8]. The download sequence is initiated by an SST transceiver connected to the researcher's laptop computer. However, the animal-borne radio modems cannot be in the receiving mode continuously; they must be duty-cycled to minimize current consumption. Typically, there are preprogrammed schedules at times when the re-searcher can be present to download the data. The line-of-sight range of the system is typically 1.5 km ground-to-ground and approximately 6-10 km to a transceiver in an aircraft.

The GPS-SST system uses substantially less power (typically less than 5% of the power budget is used for data transfer) than some other alternatives like Argos when large amounts of data must be transferred [8]. The protocol effectively and automatically recovers missing data packets to form a complete dataset over the specified time frame. The SST system

also has the advantage that in addition to downloading data on command, the two-way link can be used to adjust the duty cycle, sampling rates or other functionality of the GPS-SST system.

Argos DCLS

Sometimes the data extraction problem is addressed by use of Argos (see Section 3.1). Even though Argos is less capable than GPS in terms of accuracy and availability, it does offer one major advantage: the ability for the tag to transmit its position back to the user. This could be either the relatively poor quality Argos estimate or the payload data that is sent back could contain GPS position data. Figure 5 illustrates the approach for sending GPS positions via Argos. GPS positions are recorded in the transmitter and sent via the Argos system. Using GPS in addition to Argos allows users to:

- Have two location systems in one,
- Acquire positions as often as wanted,
- Obtain highest accuracy (10 meters) without influence from transmitter quality,
- Spread positions evenly throughout the day.

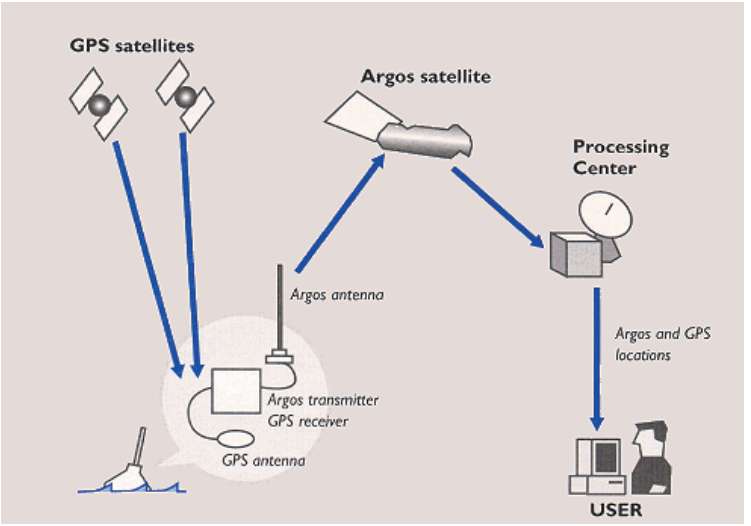

Figure 5. Sending GPS positions via Argos. [Source: `http://www.argos-system.org/html/system/how_it_works_en.html`]

Argos system allows the use of low-power transmitters (100 mW to 1 W) with small omni-directional antennas [8]. Current Argos systems specification and sophisticated data compression in the animal-borne units enable transferring about 24-48 GPS-based locations per day from collar-mounted units on medium- to large-sized animals, and up to 6-10 GPS-based locations from smaller avian units. Number of possible position transmissions is small, because the Argos bandwidth is very restrictive. Data can be recovered as frequently as daily; however, intensive use of the transmitter is a significant drain from the limited energy budget of an animal-borne unit, and thus limits the number of GPS-based locations that can be acquired. A well-planned data recovery schedule must be established to balance data collection and data recovery operational life. The Argos transmitter also requires significant power which places more demand on the battery and could therefore also impact size and weight.

The GPS reception and Argos transmission schedule is especially important when radio-marking birds, for which the mass of the unit is usually restricted to 3 to 5 per cent of the bird's body mass [8]. Recent developments allow the GPS data in the animal-borne Argos-GPS unit to be used with onboard orbital prediction programs enabling transmissions only during satellite overpasses. This increases data transfer and power efficiency for the system. When GPS transfer via Argos is applied to birds, solar charging often is used to prolong unit operation life. Many factors can affect the regularity and extent of solar charging (e.g. hours of light, cloud cover), and thus the performance of the unit.

A geographical limitation with Argos is that noise in the environment in Europe and Mongolia-Pakistan disrupts data transfer on the Argos uplink frequency [8]. To mitigate this, authorities are using international agreements to protect satellite uplink frequencies and technological solutions that include using high-power Argos transmitters or more exposed or modified antenna designs to achieve higher radiated power for a functional satellite link. Increased power will affect operation schedules and lifetime, and modified antenna designs increase antenna exposure and are subject to fatigue and breakage on the animal.

GSM/GPRS

Some GPS systems deployed on animals use GSM telephone data services [8]. Two GSM technologies are used in animal-borne systems. GSM/SMS services al-low the transfer and regular updating of GPS-based locations

and some limited data (e.g. mortality events) as an SMS message to a cell phone (six to eight positions per GSM per SMS message). Text message lengths are short. Larger datasets (e.g. activity data) use General Packet Radio System (GSM/GPRS) services when available. GSM services are widely available in Europe and Asia. Unfortunately, there are many vast areas throughout the world (e.g. much of North America, Australia and sparsely populated Africa) without GSM services; thus, neither GSM/SMS nor GSM/GPRS are an option. The most severe limitation is that animals might not encounter receiving towers, and therefore data collection can be intermittent or lost. Some systems now have 'failsafe modes' that allow older data to be data transferred when the animal returns to coverage. GSM/GPRS data transfer systems continue to evolve, but typical data rates are in the range of 21.4-171 kbps. The system can also be used in a two-way manner, allowing the change of onboard collar parameters.

One example of innovation here was done at SMRU (Sea Mammal Research Unit) at St Andrews University [5]. A conventional GPS unit was integrated with a GSM chipset for use on tags for Seals in the North Sea. When the phone network was available, the GSM enabled tags automatically used SMS messaging to send blocks of data back to the team once every two days. Haul-out data and coastal location data were incorporated into the messages. Data was presented for a three-month period. Although only a small fraction of the deployments successfully sent the data back at the expected times it did show the technology was feasible. [7] have reported a method combining the GPS and GSM technologies in bear research in Finland. A GPS-GSM collar on a bear locates itself with the help of a GPS module, while the GSM module sends the location information to the researcher as SMS message. The collar is interactive and can receive SMS commands, for instance, to adjust the interval at which location in-formation is transmitted. There are a couple of major disadvantages of this approach in addition to the limited coverage zones when considering it for wildlife tracking in general: 1) It is a heavy solution. The SMRU tags, for example, weigh around 450 grams. 2) The power requirements and cost of the devices are high.

LEO satellite telephone data services

Because there are many regions of the world without GSM coverage, commercial businesses provide satellite-based telephone systems [8]. Two

such systems, Iridium and Globalstar, include data services that are potentially useful for data transfer from animal applications. Both services are on LEO satellite systems and offer ad-vantages over Geosynchronous (GEO) systems for delivering mobile satellite services (MSS). These advantages result from orbits that enhance the quality of services to low-power mobile hand-held and vehicle-mounted equipment. GEO satellite systems, at altitudes of 35 800 km, are best suited for high-speed data. Unless the GEO satellite has high-gain directional antennas, it is unable to receive from small handsets with omnidirectional antennas.

Commercial off-the-shelf hand-held satellite telephones are not suitable for deployment on animals. Biotelemetry manufacturers must procure certified modules from large-scale manufacturers and access to the system must be contracted. It is often difficult to integrate data transfer in animal-borne applications, given the limitations in hardware and firmware designs that are optimized for non-animal applications, especially deploying and maintaining an antenna on an animal. The integration process is not trivial.

Iridium Satellites

The Iridium constellation currently provides mobile two-way data links for tracking and monitoring [8]. Iridium Satellite LLC is a privately owned company providing worldwide, two-way, near-continuous coverage for voice and data communications. A short burst data (SBD) service, analogous to text messaging, is also available. Iridium's current constellation is 66 LEO, cross-linked satellites, plus replacement spares. The satellites are in a near-polar orbit at an altitude of 780 km in six orbital planes, evenly spaced around the Earth. Each plane has 11 satellites equally spaced and a single satellite circles the Earth every 100 min, at 16832 miles h^{-1}. A satellite is visible to a stationary ground terminal for about 10 min, and, as it goes over the horizon, a call is transferred to the next satellite. Each Iridium satellite is cross-linked to four others to create a dynamic network in space.

Iridium is used in oceanographic applications in dial-up and in short-burst mode. Iridium has small low-profile antennas associated with the 1.5 GHz frequency communications link and the two-way link either via a command in dial-up or simple handshaking mode in SBD. Current technology is suitable for larger terrestrial species such as caribou. There are

at least two manufacturers[6] offering data transfer and animal unit reprogramming capability via Iridium.

Globalstar Satellites

Globalstar is a phone system suitable for mobile applications, consisting of more than 40 LEO satellites [8]. Handsets operate with hand-held, vehicle-mounted telephone devices using omnidirectional antennas. Calls and data links are passed from one satellite to another, enabling the Globalstar system to provide service to locations including some with signal blockage from buildings, terrain or other natural features. The greatest limitation is that there are areas in the world without coverage. From the satellite, data are transmitted to land-based receiving stations called Gateways, where further data management occurs and information is prepared for distribution to the user. The location of Gateways determines where the Globalstar system provides geographical coverage.

The Simplex data and asset tracking services section of the Globalstar system is used for wildlife telemetry [8]. Globalstar Simplex sends data at a speed of 100 bps and allows limited messaging. Globalstar uses code division multiple access (CDMA) technology. User terminals share time and frequency allocations and access to the network. Signals are separated at the receiver by a correlator that accepts a signal from a single terminal, while excluding other signals. Wildlife telemetry manufacturers program the GPS-Globalstar units to transmit the same GPS-based location message to the satellites up to four times to increase the probability that the message has been received at the satellite.

GPS-Globalstar collars can transmit every GPS location acquired in real time from the field to the internet, or log and store location estimates for later retrieval [8]. For example, a unit could be programmed to acquire a GPS location eight times per day and to transmit one GPS location per day or per week, thus conserving battery power and costing less for data delivery via the satellite system. The Globalstar Simplex services are designed to work with the second-generation satellite constellation to provide users with service into the next decade. Wildlife collars using a GPS-receiving antenna and a Global-star patch-transmitting antenna have recently become available and are being used on many projects, but no significant published results were available at the time of writing this report.

[6] `www.vectronic-aerospace.com` and `www.lotek.com`

6 GPS Wildlife Tracking Case Studies

GPS wildlife tracking systems are now available for almost all mammals and even for the bigger birds. One of the oldest manufacturers in the field is Lotek (www.lotek.com), which specializes in GPS collars for small to large mammals. Other well known manufacturers include Telemetry Solutions (http://telemetrysolutions.com), Vectronic-Aerospace (www.vectronic-aerospace.com), BlueSky Telemetry (www.blueskytelemetry.co.uk), Telonics (www.telonics.com), Sirtrack (www.sirtrack.com), Advanced Telemetry Systems (www.atstrack.com), North Star (www.northstarst.com) and Microwave Telemetry (www.microwavetelemetry.com), which advertises itself as the leading manufacturer of bird and fish tracking solutions. Description of their products and devices may be found on the companies' web sites, and there are other competitors on the market as well. This section describes two case studies, where commercial products are being used in research projects for tracking of birds of prey.

6.1 Case 1: Finnish White-tailed sea-eagles in satellite tracking

The White-tailed sea-eagle working group within WWF Finland decided in early 2009 to start a joint project with the Finnish Museum of Natural History (University of Helsinki, www.luomus.fi). The aim is to collect detailed data of the movements of White-tailed sea-eagles as they move around in the coastal areas of Finland through the year from the south-western archipelago and the Åland Islands to the corners of the Gulf of Bothnia and the Gulf of Finland. There are many ongoing plans to build wind farms in different parts of the Finnish sea coasts and archipelagos. Thus it is very important to collect exact data to point out areas that should be left untouched, being important for the protection of White-tailed eagles. The final impulse for the long planned satellite project was the threat of raising a vast wind farm in the Quarken area in the Vaasa region, namely Raippaluoto/Replot Island. This archipelago is one of the main breeding areas of the Sea-eagle in Finland. It is very clear that from the very beginning of the planning of the wind farm all the risks that may affect the local White-tailed sea-eagles should be eliminated beforehand. In spring 2009 WWF Finland sponsored the purchasing of four transmitters (70 gram Argos/GPS Solar PTT) made by Microwave Telemetry. These trackers may work 'forever' as they are equipped with solar cell chargers. Most of the Finnish White-tailed sea-eagles stay within Fin-

land over winter and thus during the darkest weeks solar cells may not get enough sunlight for charging the batteries. That is why the transmitters were equipped with an extra 16 gram battery. The final weight of the transmitters with its harness is about 100 grams.

During the first study year the researchers wanted to collect data of the transmitter functions in Finnish circumstances. The programming of the transmitters differs somewhat due to season and individual transmitter. During the bright season (May 16th - July 15th), tracking is recorded either every second hour day and night or once every hour between 5 to 19 o'clock. In the autumn (July 16th - Nov 15th) and in spring (Feb 16th - May 15th), tracking activity is limited to every hour between 7 to 18 o'clock. In winter (Nov 16th - Feb 15th), tracking records are collected only ten times between 8 to 17 o'clock to save the batteries.

The transmitters save the tracking records and send the data via satellite every fourth day as a data package to the main computer of Argos in France. From that computer, the researchers may download the data to their own computers. Currently, there are 5 tracked eagles, whose movements may be publicly followed on maps on the museum's web site, though most tracking spots are not included because of protection and clarity reasons. One of the tracked eagles is called Ivar. Between Jun 25th and Nov 19th 2009, there were 1526 GPS-locations of Ivar. According to the programming, there should have been 1813 locations, so the amount of successful locations of that period was 84%. In Aug-Oct, the successful locations varied from 89 to 94%, but in the beginning of Nov only 49%. After the 19th of Nov, the amount of day light was not enough to charge the battery to required level for GPS-locations. During the end of Nov and beginning of Dec, Ivan's movements could only be followed with a varying accuracy by Doppler-signals. They were received every 3rd day along with information packages.

There has been a similar seasonal variation in the amount of successful locations of other tracked eagles. Another tracked eagle, Tuuli, for example, stayed in the Björköby-Raippaluoto area until Boxing Day. Until then altogether 1716 GPS-locations were received. According to the programming, there should have been 2120 locations. Thus there were 81% successful locations. The amount of sunlight to recharge the battery diminished clearly. In Aug-Sep, the amount of successful locations was 95-96% and in Oct 89%, but in Nov-Dec only 55-57%. Also, other international studies have illustrated that Global Positioning System error may

vary across seasons for a reason or another.

6.2 Case 2: Satellite Honey Buzzard "Lasse"

A breeding Honey Buzzard male was equipped with a satellite transmitter in Kokemäki (western Finland) the 9th of August, 2010. He was named "Lasse". Lasse is the first satellite-tracked Honey Buzzard in Finland. The aim of this project is to follow autumn migration, find out the wintering area and, if the duration of battery will allow it, to follow the spring migration back to Finland. The few Finnish ring recoveries suggest that the Finnish Honey Buzzards spend their winter in tropical Africa. The size of the Finnish Honey Buzzard population is 3000-4000 pairs. The species has decreased considerably during the last few years. In Finland, the biggest threat for the Honey Buzzard is intense forestry which destroys breeding sites and increases competition for them with other bird of prey species. During the migration Honey Buzzards are still illegally killed by hunters, especially in the Mediterranean region.

Figure 6. a) Autumn migration 2010 of Honey Buzzard "Lasse" [Source `www.luomus.fi`]. b) Spring migration 18.-28.4.2011.

Lasse's transmitter is a traditional Argos battery-powered model (made by NorthStar). The weight of the unit is 20 g. The duty cycle of the transmitter is programmed so that it is 8 hours ON and then 108 hours OFF, which means that locations are obtained on average at 4,5-day intervals. The expected duration of the battery is approximately 550 hours (i.e., 9-10

months). The figure 6a shows Lasse's autumn migration from Finland to Gabon in 2010. At the time of writing this report (28.4.2011), Lasse is in Algeria on his way back to Finland (fig. 6b). Sadly, the researchers are expecting the battery of the transmitter to run out soon, before Lasse will reach Finland.

For clarity, only accurate locations have been shown in Finland, but in abroad all locations are shown. By clicking the dots in the map it is possible to see additional information on location data (date, GMT-time, coordinates, accuracy of location).

7 Conclusions and Discussion

GPS positioning and data collection for animal research developed as commercial GPS and other diverse technologies matured. The success of animal-borne systems depended on experience with earlier tracking technologies (e.g. conventional VHF and Argos). Similarly, future advances will draw on the technology described in this report and on the new developments. Changes in GPS technology are ongoing and accompanied by changes in the GPS OEM manufacturing community. New global navigation satellite systems (GNSS) including GLONASS, Galileo and Compass are emerging, with the potential to be used for animal positioning. Telemetry designers and manufacturers must select the appropriate technologies available from commercial and military sources, and integrate them into specialized instruments with rigorous performance requirements specific to an ever-increasing number of species, environments and researchers' objectives. Researchers must evaluate these offerings from a cost-benefit perspective. Widely varying study designs re-quire specific attributes from sensors and the GPS and data transfer systems. Surveying the specifications allows the user to choose the most efficient system in terms of operational life, unit size and cost per data point.

Animal research continues to benefit from the large commercial market driving GPS development. There are significant advances in receiver technology with trends for GPS receivers getting smaller, operating at lower voltages, consuming less power and exhibiting reduced TTFFs. Advances like these will contribute to methods to study smaller terrestrial, marine and avian species. At a time when over a million species are under threat from climate change, unless we can work out where they go

and how they get there, there is no hope of assessing the full impact of human activity on the billions of animals that move thousands of miles every year. Being able to track all size of small animals over large spatial scales is also vital for assessing the impact of animal movement on such commercially important issues as agriculture and disease transmission.

Vast amounts of scientific literature and articles have been published on GPS wildlife tracking during the last few years. Research has focused on many technical and algorithmic issues, such as the weak signal acquisition under dense canopies and filling the gaps between GPS fixes with various methods and algorithms. Another branch of research deals with application of these technologies in real-life studies - requirements, best practices and study design regarding the required data granularity, sampling rate, etc. Plenty of tracking case studies have been published in the field of biological and ecological sciences. The enormous quantities of data generated by the tracking systems clearly present a challenge to data management and analytical procedures, which again provide interdisciplinary research topics for GIS analysis and other related fields.

New opportunities are huge and shining, but there have been critical and warning tones as well reminding that everything is not yet perfect. Field work and real-life observation of wildlife is still required in order to interpret the data: researchers must not become estranged from the field study in the thrill of the new technical opportunities. GPS units are still expensive. It has been stressed that the high cost of GPS units should not lead to underestimated sample sizes due to the trade-off between the number and cost of GPS units. Managers and researchers need to be aware that if they use these new devices, they are basically also performing a field test of equipment. Standardized tests almost certainly overestimate performance compared with performance of units on free-ranging animals, when additional variation can be expected. Researchers should plan the number of animals to be marked based on an expectation of some loss of data caused by the death of animals and equipment failure. Consequently, success cannot be taken for granted and the logistic burden and final costs are subject to a certain degree of uncertainty. Although it is arguable that researchers could take this into account by marking a greater number of animals, tight research budgets, the high conservation value of especially individuals of a threatened species, and animal welfare issues do not easily allow for increased sample sizes beyond the absolute minimum. In addition, many conservation projects receive staggered funding -

they have to start small and if successful may receive further funds. Furthermore, in a management context information on a specific individual is often requested (e.g. a nuisance animal or a re-introduced animal). Due to the small sample sizes and the focus on single individuals, collar failures in such projects are a particularly hard blow.

To sum up, newly emerging wildlife tracking devices claim to be promising tools for the advancement of wildlife research and management. GPS can provide accurate, regular and frequent estimates of locations for movement ecology research into many species of animals. For the promise of new GPS, emerging GNSS and associated technologies to be fulfilled, engineers and biologists will need to work in partnership, share needs, under-stand limitations and be aware of emerging opportunities.

Bibliography

[1] Breed, G. A., Costa, D. P., Goebel, M. E., and Robinson, P. W. (2011). Electronic tracking tag programming is critical to data collection for behavioral time-series analysis. *Ecosphere*, 2(1):art10. doi: 10.1890/ES10-00021.1.

[2] Cagnacci, F., Boitani, L., Powell, R. A., and Boyce, M. S. (2010). Animal ecology meets GPS-based radiotelemetry: a perfect storm of opportunities and challenges. *Philosophical Transactions of the Royal Society B: Biological Sciences*, 365(1550):2157–2162.

[3] Dyo, V., Ellwood, S. A., Macdonald, D. W., Markham, A., Mascolo, C., Pásztor, B., Scellato, S., Trigoni, N., Wohlers, R., and Yousef, K. (2010). Evolution and sustainability of a wildlife monitoring sensor network. In *Proceedings of the 8th ACM Conference on Embedded Networked Sensor Systems*, SenSys '10, pages 127–140, New York, NY, USA. ACM.

[4] Hebblewhite, M. and Haydon, D. T. (2010). Distinguishing technology from biology: a critical review of the use of GPS telemetry data in ecology. *Philosophical Transactions of the Royal Society B: Biological Sciences*, 365(1550):2303–2312.

[5] MacLean, G. (2009). *Development of a miniature, long-duration GPS tag*. PhD thesis, Heriot-Watt University.

[6] Pinter-Wollman, N. and Mabry, K.E. (2010). Remote-Sensing of Behavior. In Breed, M. and Moore, J., editors, *Encyclopedia of Animal Behavior*, volume 3, pages 33–40. Oxford: Academic Press.

[7] Sundell, J., Kojola, I., and Hanski, I. (2006). A New GPS—GSM-Based Method to Study Behavior of Brown Bears. *Wildlife Society Bulletin*, 34(2):446–450.

[8] Tomkiewicz, S. M., Fuller, M. R., Kie, J. G., and Bates, K. K. (2010). Global positioning system and associated technologies in animal behaviour and ecological research. *Philosophical Transactions of the Royal Society B: Biological Sciences*, 365(1550):2163–2176.

Modern geodesy may be defined as *"the science of precise georeferencing and change monitoring on or above the Earth's surface"*. Modern geodesy relies on space technology and integrates complex Earth observation systems and modelling of geospatial data at higher accuracy in order to understand and predict how the solid Earth, atmosphere, and oceans work as a system. Modern geodesy applications include precise determination of position and velocity of points on the surface of the Earth, precise determination of the shape and changes of the Earth's ocean and land surfaces, or precise mapping of the spatial and temporal features of the gravity field.

ISBN 978-952-60-5214-4 (pdf)
ISSN-L 1799-4896
ISSN 1799-4896
ISSN 1799-490X (pdf)

Aalto University
School of Engineering
Department of Real Estate, Planning and Geoinformatics
www.aalto.fi

BUSINESS + ECONOMY

ART + DESIGN + ARCHITECTURE

SCIENCE + TECHNOLOGY

CROSSOVER

DOCTORAL DISSERTATIONS

Aalto-ST 12/2013